Binuclear late transition metal complexes with pyrazole based compartmental ligands: Scaffolds for cooperative organometallic transformations

Dissertation

for the award of the degree

"Doctor of Philosophy" Ph.D. Division of Mathematics and Natural Sciences

of the Georg-August-Universität Göttingen

within the doctoral program Catalysis for Sustainable Synthesis (CaSuS)

of the Georg-August University School of Science (GAUSS)

submitted by

Michael Kojo Ainooson

from Accra, Ghana

Göttingen 2014

D7

i. Prof. Dr. F. Meyer
ii. Prof. Dr. P. Vana
iii. Prof. Dr. D. Stalke

Date of the oral examination: 25/07/2014

I hereby declare that the dissertation, "*Binuclear late transition metal complexes with pyrazole based compartmental ligands; Scaffolds for cooperative organometallic transformations*" is my original research work and has not been submitted to any other university for the award of a degree. This work was undertaken from 2010-2014 under the supervision of Prof. Dr. Franc Meyer, in the Institute of Inorganic Chemistry, Georg-August-Universität Göttingen, Germany.

Göttingen 2014.

Table of Contents

Table of Contents

Table of Contents

1 Introduction

A number of catalysts used in organometallic chemistry require two adjacent accessible coordination sites at a single catalytically active metal ion for activating two substrates (**X** and **Y**) and bringing them in close spatial proximity (**I)**. In addition, in instances where two sites between two adjacent metal ions have tunable metal-metal separation, some other possibilities exist. One possibility is the activation two substrates **X** and **Y** on each respective metal and bringing them in close proximity (**II**); or the possibility of a multisite covalent or non-covalent interactions with a single substrate (**III**). The prospect also exists from the use of two different metal ions in a heterobimetallic system where each metal adjusts to a specific substrate or plays a defined role in the catalytic cycle.

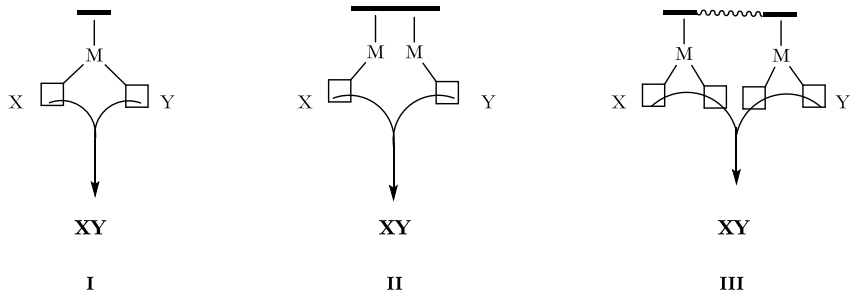

In nature, enzymes make use of synergetic effect of two or more proximate metal ions to achieve very efficient one-pot tandem catalysis.[1,2,3] Recent years have seen efforts in the development of catalysts that make use of cooperative interactions between metals with proximate centres.[4] Examples of such cooperative effects have been explored in bi-functional catalysis, double substrate activation and cascade reactions.[5,6,7] Bimetallic catalysts most especially, have been explored as a means of enhancing catalyst efficiency.

2 Bimetallic catalysts for enhancing efficiency in olefin polymerization

Bimetallic catalysts have been shown to sometimes lead to greater activity and selectivity usually not obtained with the respective mononuclear analogues.[8,9,10,11] The range of catalytic reactions

which explore metal cooperativity in bimetallic complexes are diverse, a few of which include, hydroformylation,[12,13] olefin polymerization[14,15] olefin-metathesis[16,17,18,19] and other reactions.[20,21,22]

Olefin polymerization

Monometallic olefin polymerization catalysts can generally be classed into early or late transition metal catalysts precursors. The early transition metal catalysts precursors have general subclasses as metallocenes,[23,24] and *ansa*-metallocenes (**I**),[25,26] constrained geometry catalysts (**II**)[27] and phenoxyimine catalysts (**III**).[28,29]

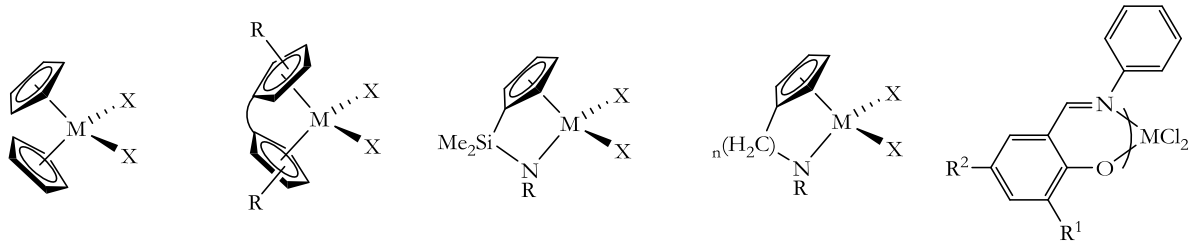

Metallocenes and *ansa*-metallocenes
M = (Ti), Zr

I

Constraint Geometry
M = Ti, (Zr)

II

Phenoxyimines
M = Ti, (Zr)

III

The field of olefin polymerization has seen a lot of research geared towards the use of ligand scaffolds capable of hosting metal ions in close proximity, and exploring electronic coupling and cooperativity between the metal centres in bimetallic complexes.

The bimetallic catalyst precursors usually are extensions of the monometallic precursors bridged by alkyl or aryl functionalities.[30,31,32,33,34,35] One such prominent example of homobimetallic early transition metal polymerization precatalyst that make use of cooperative interactions between two proximate centers (**A**), is the binuclear constrained geometry catalyst (**IV**) reported by Marks and co-workers.[30,36]

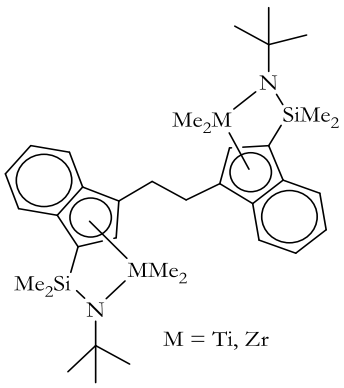

IV

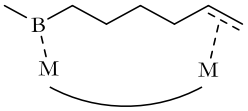

B = Weakly basic functionality

A

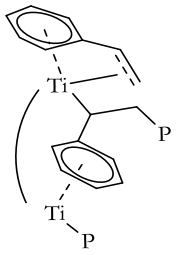

B

This binuclear catalyst shows cooperative Ti···arene interactions which significantly enhances homopolymerization rates, modifies enchainment regioselectivity and also greatly increases comonomer enchainment selectivity (eg. **B**).[36] Other reports of heterobimetallic metallocenes that make use of two distinct active sites working in concert have been reported Barnhart et.al.[37] Green and co-workers have reported the use of a bridged metallocene (**V**), used in ethylene polymerization reactions. The complex gives an activity of 8.72 x 10^2 kg PE/(mol_M·h), which is intermediate between that of the mononuclear complexes Cp_2ZrCl_2 (3.57 x 10^3 kg PE/(mol_{Zr}·h)) and $CpTiCl_3$ (2.52 x 10^2 kg PE/(mol_{Ti}·h)). This activity is attributed to the ability of the two sites to act independently, thus giving the combined effect of an averaged activity.

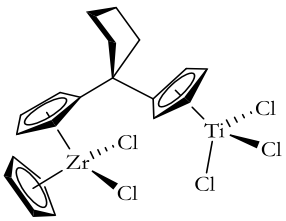

V

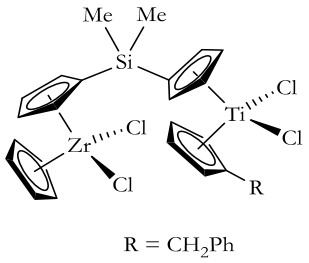

VI

The heterobimetallic complex (**VI**) is active in the polymerization of ethylene with activities up to 8.15 x 10^2 kg PE/(mol_M·h).[38] Molecular weight and molecular weight distributions of polymers generated from the bimetallic complex were much higher (with PDI = 2.0 – 3.0) than those obtained from the mononuclear Cp_2ZrCl_2 complex (PDI = 1.7) under similar conditions. This difference was attributed to interactions between the two different metal centers, but no mechanistic insight was reported.

On the other part of the spectrum, late transition metal complexes for olefin oligomerization and polymerization have been the subject of various investigations,[39,40,41,42,43,44,45] notably due to their less oxophilic nature and their ability to catalyze the copolymerization of olefins with polar comonomers. Late transition metal complexes are usually prepared from a combination of soft and hard donor groups with N^N/N^N^N,[46,47] P^N/P^P[48,49] P^O,[50,51] and O^N^N or O^N[40] chelates in a neutral or anionic ligand environment. Late transition metal catalysts, which involve neutral or monoanionic ligands, can generally be classed into *a*-diimine (**VII**),[52,53,54] bis(imino)pyridine (**VIII**),[55,56,57] phenoxyimine[58,59,60,61] (**IX**) catalysts and the more recent arylsulfonate type catalysts (**X**).[62]

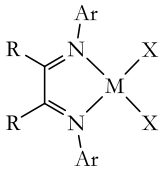

α-diimine

M = Ni, (Pd)
X = Cl

VII

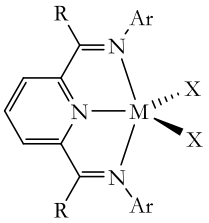

Bis(imino)pyridine

M = Fe, (Co)
X = Cl

VIII

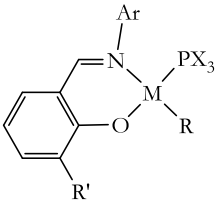

Phenoxyimine

M = Ni
R =Me, Ph
X = Me, Ph

IX

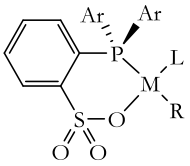

Arylsulfonate

M = Ni, (Pd)
R = Ph, Me
L = PPh_3, DMSO

X

A number of bimetallic systems, which mimic these pre-existing mononuclear complexes, have since been reported.[63,64,65,66,67,68,69,70,71,72] An example of a bimetallic system with an N^N donor is complex **(XI)** developed by Luo et. al.[73]

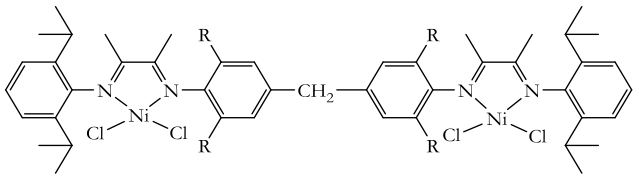

R = Me, Et, ^{i}Pr

XI

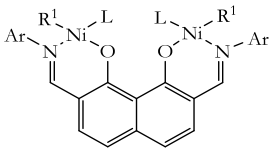

R^1 = CH_3, $C_{10}H_7$, R = CH_3, C_6H_5
L = PMe_3, PPh_3
Ar = 2,6-(^{i}Pr)$_2$-C_6H_3

XII

In this complex, the binuclear catalyst exhibits relatively higher activities (R = $CH(CH_3)_2$; 1.84 kg/(g Ni h), R = CH_2CH_3; 1.66 kg/(g Ni h) in the polymerization of ethylene, a marked departure from that of the mononuclear complexes which gives activities of (R = $CH(CH_3)_2$;

0.70 kg/(g Ni h), R = CH_2CH_3) 1.42 kg/(g Ni h). They attribute structural differences between the various complexes as being responsible for significant increase in activity of the bi- and multinuclear catalysts.

Also, the binuclear naphthylimine nickel(II) catalysts (**XII)**, which has a rigid ligation is shown to have twice the activity for homo polymerization of ethylene and also introduces more alkyl branches than the corresponding mononuclear analogues.[74] Ethylene copolymerization with unresponsive acrylates with this catalyst gives up to 11% comonomer incorporation. Although there is decreased activity in the presence of additives, the catalyst remains three times more active than the mononuclear analogues.

What is clear in all these approaches is that having ligands capable of hosting two different metals in a binucleating scaffold at an appropriate distance is vital for cooperative metal interactions. Most especially when the ligands have two adjacent donor atoms capable of acting as a bridging functionality as found in nitrogen heterocycles such as 1,2,4-triazoles,[75,76] pyridazines,[77,78] 1,2,4,5-tetrazines[79] and pyrazoles.[80] It has been proposed that the optimum separation between two metal centres; for one-step catalysis or the close binding of two reactants to the adjoining metal centres should be between 3.5-6.0 Å even when there is no direct interaction between the metal centres.[81] Pyrazoles, remain one of such versatile ligands, found to hold metals units at an appropriate distance (2.4-4.6 Å)[82,83] to direct metal-metal interactions; but close enough for cooperativity and allowing for some degree of electronic coupling through the ligand system.

3 Pyrazole as a ligand:

The chemistry of ligands bearing the pyrazole motif has been extensively studied in literature in the past decades and has been the subject of several reviews.[84,85,86,87,88,89] The pyrazole ring due it its ease of synthesis, can be prepared with various substituent on different positions on the pyrazole ring. Pyrazole derivatives have the ability to span adjacent metals at a favourable distance.[90,91] This has made the pyrazole motif one of the most versatile heterocycles, with the ability to incorporate various groups such as amino alkyls,[92,93,94,95] aromatics,[96,97,98] borates[99,100,101] and polydentate groups.[102,103,104] The 1*H* pyrazole is usually the starting point of most pyrazole based ligands.

Coordination modes of 1H pyrazole ligands

Upon deprotonation of the 1*H* pyrazole ligand, the pyrazolate anion is known to coordinate to metals in diverse coordination modes through the two nitrogens or its π-system[105,106,107,108,109] to elements in the s-block,[110,111] p-block,[112,113] d-block[114,115,116,117,118] as well as lanthanides.[113,119] Some of the diverse coordination modes adopted by the pyrazole motif are shown in Scheme 3. 1.

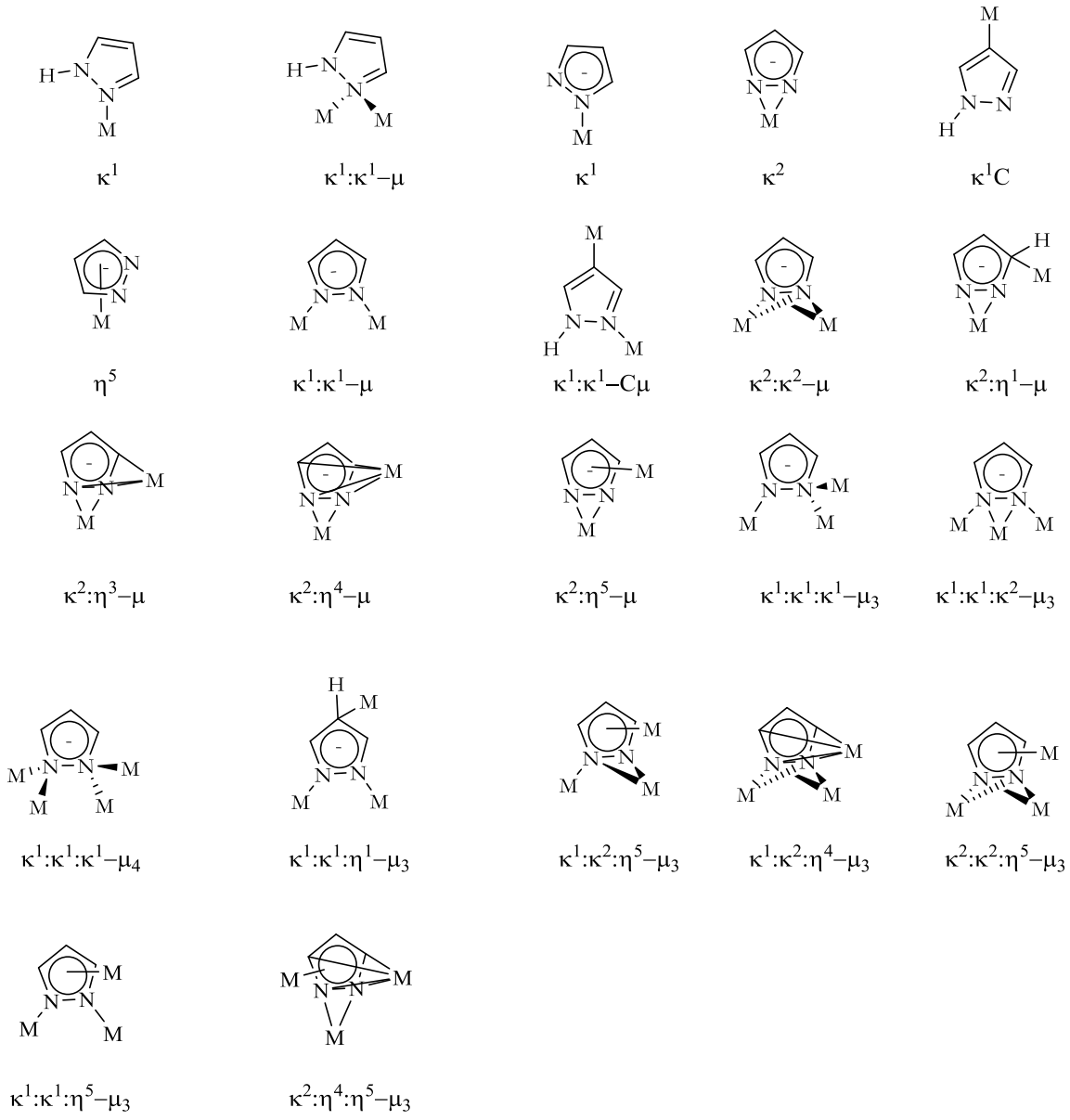

Scheme 3. 1: Various coordination modes of 1*H*-pyrazolyl ligand.[120]

3. 1 Compartmentalized 3,5-bridging pyrazole scaffolds

The use of 3,5-disubstituted pyrazolate ligands has been one of the widely explored strategies for controlling coordination behaviour.[121,122,123,124] By introducing substituents with additional donor groups, stability is enhanced due to the chelating effect of the multidentate binding sites. One of the widely explored synthetic routes to pyrazoles is mostly through the condensation of hydrazines with 1,3-diketones or using an acyl precursor.[125,126,127] (Scheme 3.1. 1)

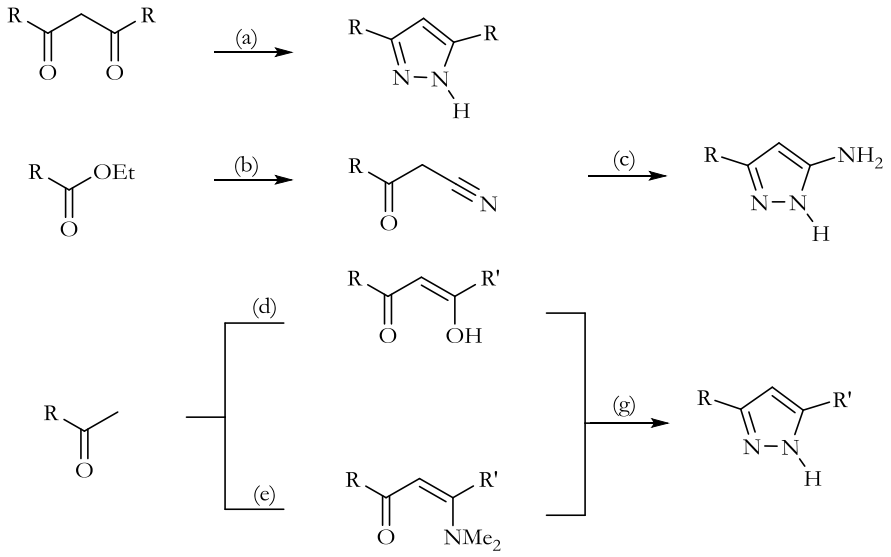

Scheme 3.1. 1: Conditions: (a) $N_2H_4 \cdot H_20$, reflux, ethanol (b) R'CHO, THF, reflux (c) $N_2H_4 \cdot H_2O$, ethanol, reflux (d) $R'CO_2Me$, NaOMe, toluene, reflux (e) $R'C(OMe)_2NMe_2$, reflux (g) $N_2H_4 \cdot H_20$, reflux, ethanol

The 3,5-disubstituted pyrazole bridges can take the form of a symmetrical environment, where both substituents on the 3,5-positions are identical, or an unsymmetrical environment where the ligand substituents in the 3,5-positions have different donor functionalities.

3.1. 1 Unsymmetric 3,5-substituted bridging environments

Pyrazolate based ligands with 3,5-substituted side arms on the heterocycle have been established as one of the valuable synthons for the preparation of highly compartmentalized bi- and oligonuclear metal complexes.[124] More especially when the aim is to have a heteroleptic ligand environment that is capable of discriminating between two different metal ions.

Although the use of unsymmetrical ligands usually poses a problem with the formation of positional isomers, it is not in case in **XIII**. The unsymmetric ligand **XIII** which features a soft P^N site and an adjacent N_2S_2 donor site was reported by Konrad et. al.[128] This ligand in the heterobimetallic NiPd complex houses the palladium(II) centre in the P^N compartment. The unsymmetric complex (**XIV**) which features a soft P^N site and an adjacent N^N donor site reported by Akita and co-workers[129] on the other hand has the ability to undergo switched metal arrangements.

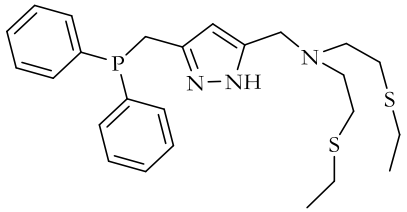

XIII

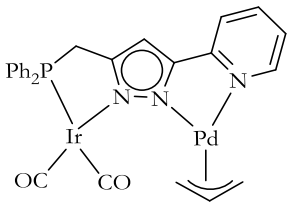

XIV

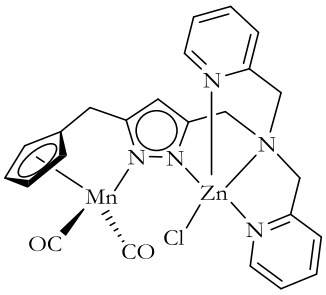

XV

In addition, a highly preorganized bimetallic complex (**XV**) combines an organometallic fragment and Werner type coordination environment in a heterobimetallic MnZn system and shows interesting redox properties as has been reported by Röder et. al.[130] The pyrazole moiety due to its versatile nature can also feature symmetric bridging ligand environments.

3.1. 2 Symmetric 3,5-substituted bridging environments

The use of such a symmetrical ligand system does not pose much of a challenge concerning the formation of positional isomers, but can pose a major challenge in the preparation of heterobimetallic complexes. A number of symmetrical bridging pyrazolate ligand environments, which have the potential to provide two *cis* vacant coordination sites for effective cooperation of activation of substrates have been investigated. Various groups such as alkyl amino groups[131,132,133,134] phosphane,[135,136,137] NHC carbenes,[138,139,140] cyclopentadienyl groups,[141] phenoxyimines,[142] etc. can append to the 3,5-positions.

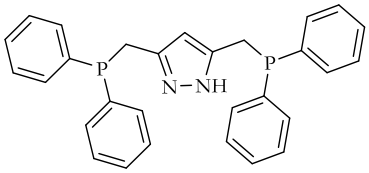

XVI

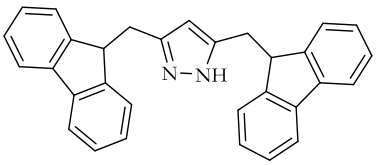

XVII

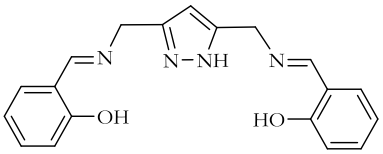

XVIII

For instance, bimetallic palladium(II) and rhodium(I) complexes of the binucleating PNNHP ligand (**XVI**) were prepared using metal transfer or by direct reactions. An early example is the dirhodium carbonyl adduct $[(\mu\text{-}\kappa^2\text{:}\kappa^2\text{-PNNP}^{Py})\{Rh(CO)_2\}]BF_4$ reported by Bosnich et. al.[143] The ligand forms rigid complexes with the metals within cooperative distance but also preventing metal-metal bond formation. Akita and co-workers[144] have also reported heterobimetallic complexes of the PNNP ligands ($[(COD)Ir^{I}(PNNP)Rh^{I}(COD)](BF_4)$). Carbon monoxide easily substitutes the COD ligands and the resulting catalysts precursors used in alkyne hydrogenation and alkene hydroformylation reactions.

Cyclopentadienyl substituted pyrazolyl ligands (**XVII**) have been prepared and its binuclear manganese(I) complex isolated and structurally characterized.[141] Likewise, their indenyl and fluorenyl lithium salt analogues have been isolated and characterized by Röder et. al.[145] Tetranuclear Mn complexes of the ligand (**XVIII**) reported by Okawa and co-workers[142] feature two phenoxyimine units on the 3,5-positions of the pyrazole. Important variations in the nature of the side arm (**XIX**, **XX** and **XXI**) allow for fine-tuning of the metal-metal distance in binuclear complexes.

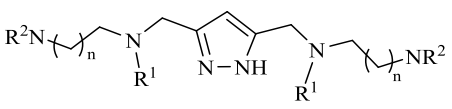

R^1 = H, Me
R^2 = Me, Et
n = 1, 2

XIX

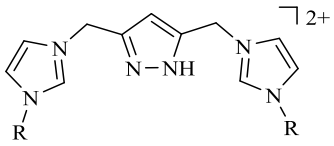

R = alkyl, aryl

XX

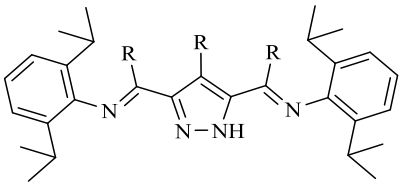

R = H, Me, Ph

XXI

For example, complexes bearing alkyl amino appendages (**XXII**) and (**XXIII**) model the urea amino hydrolase (E.C.3.5.1.5), which contains two proximate nickel(II) ions within the active site.

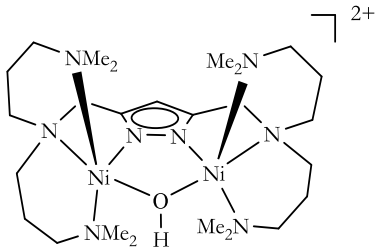

XXII

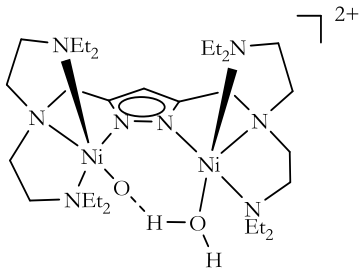

XXIII

Complex **XXII,** with its longer side arms forms six-membered chelate rings with Ni···Ni separation of approximately 3.5 Å, while **XXIII** with its shorter arms give five membered chelate rings with Ni···Ni separation > 4.0 Å.[146] Analogous copper(II) complexes with bridging hydroxide and acetate groups with metal-metal separation of 3.54 and 4.09 Å respectively have been reported.[147] The use of N-heterocyclic carbene (NHC) substituted pyrazole derivatives have also been reported.[148,149] Meyer et. al.[150] have reported on tetrasilver(I) complexes of pyrazolate-bridged compartmental NHC ligands (**XXIV**-**XXV**). These ligands provide two binding pockets and gives rise to unique multinuclear Ag(I)-NHC complexes.

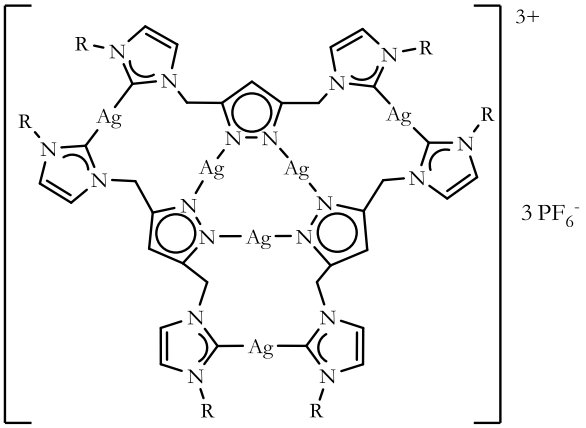

XXIV

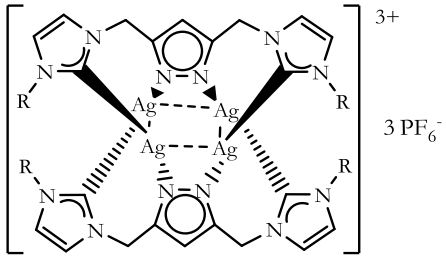

XXV

The pyrazole NHC ligands are able to form different interactions ranging from ionic to covalent interactions, and in the past few years research has shown the ability of NHC ligands to react and stabilize elements across the periodic table. Similar pyrazole bridged dinuclear complexes of ruthenium(II) and rhodium(III) with NHC have been reported by Reindl et. al.,[138] the metal-metal distances reported are in the range of 3.85-3.92 Å and no electronic coupling between the metal centres was observed.

A series of pyrazole-based ligands that possess appended imine donor sidearm and two adjacent binding compartments (**XXI**) akin to the *a*-diimine type have been explored by Meyer[151] and other investigators.[152]

Bi- and oligonuclear nickel(II) and palladium(II) complexes (Scheme 3.1.2. 1) after activation with MAO are active catalysts in olefin polymerization, with the nickel(II) complexes generally more active than the palladium(II) complexes. These catalysts also produce high molecular weight polyethylene with M_n values to the tune of 3.5 x10^5 and polydispersity around 2.5. In addition, the nickel(II) complex (**XXI**^{a}) after activation with MAO serves as highly active catalysts for the polymerization of norbornene.[153]

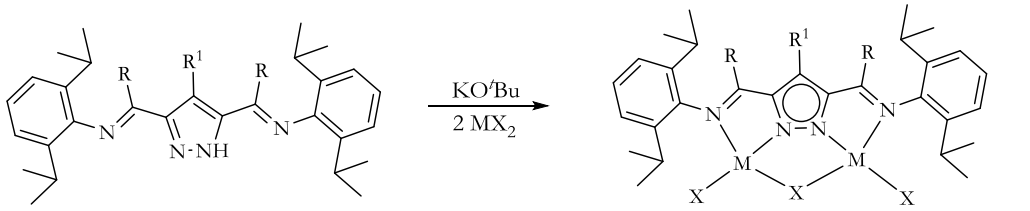

XXI

M = Ni (**XXI**^{a}), Pd (**XXI**^{b})
X = Cl, R = H, Me, R^1= H, Me, Ph

Scheme 3.1.2. 1: Bimetallic variants of *α*-diimine type catalysts used in olefin polymerization reactions

When treated with $SnMe_4$, **XXI**^{b}; (R = R^1 = Me) forms an unusual tetrametallic complex (**XXI**^{c}) which features terminal CH_3 and bridging μ-CH_2 groups, the first of its kind.[154]

The authors proposed a stepwise mechanism leading to the formation of (**XXI**^{c}) based on data obtained from NMR time scale experiments. In the proposed scheme, treating **XXI**^{b} with approximately 30 mol equivalent $SnMe_4$, the authors were able to detect the formation of two intermediates, a C_s (**1**) and a C_{2v} intermediate (**2**) leading to the formation of **XXI**^{c} (Scheme 3.1.2. 2). They also reported that the build up and decay of the different intermediates reach their maxima after 6 and 10 h respectively.[154]

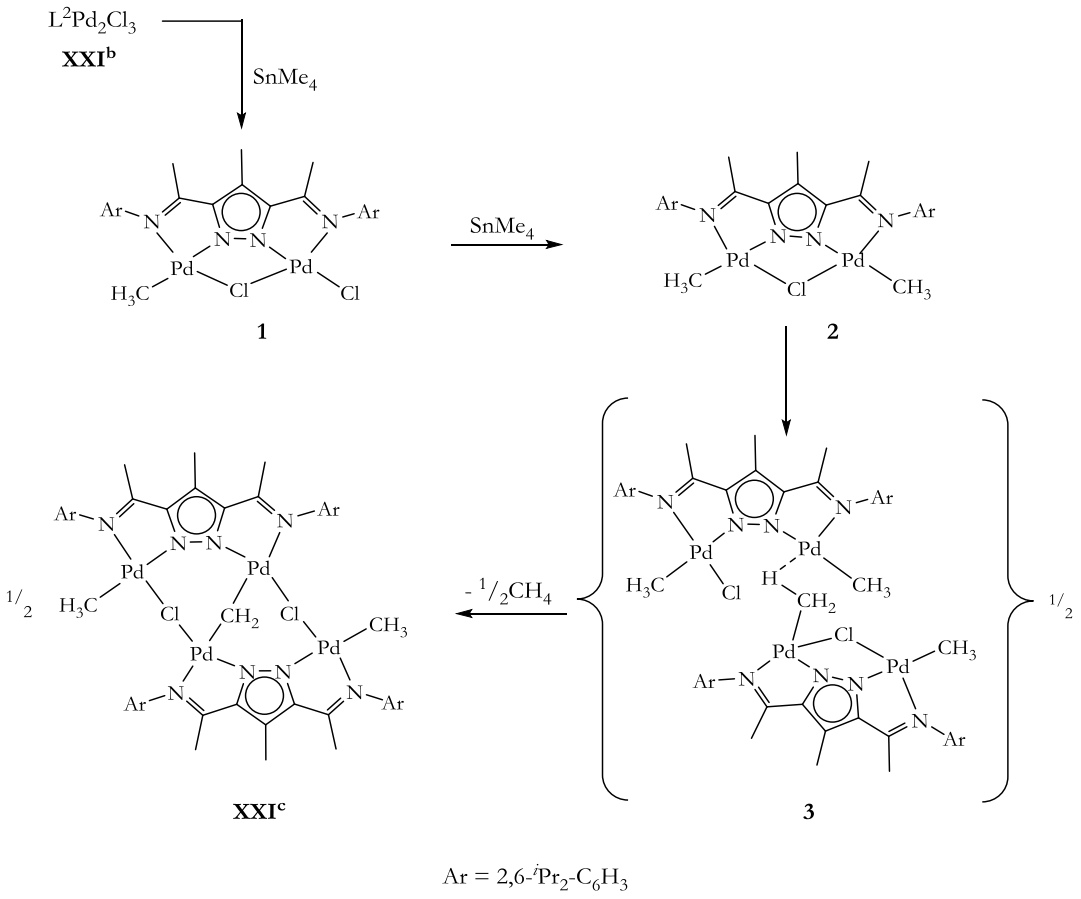

Scheme 3.1.2. 2: Proposed scheme leading to the formation of XXI[c][154]

Although the formation of a C_s and C_{2v} symmetric products leading to the formation of the tetrapalladium core were proposed based on ^{1}H NMR spectroscopic data, not much attempts were made at trapping and isolating these intermediates. Due to the transient nature of these intermediates, they react further to give other reaction products. In addition, the authors did note the formation of a second but unidentified product, which is formed with excess $SnMe_4$.[154]

This unique tetrapalladium complex **XXI[c]** also shows intriguing reactivity with simple olefins like ethylene to form mostly C_3 and C_4 products. In order to determine the origin of C atoms in the C_3 and C_4 products, ^{13}C ethylene ($^{13}C_2H_4$) coupling reactions were performed (Scheme 3.1.2. 3). The results showed that all the C_4 products were labeled in contrast to the propene, the major product that contained only two ^{13}C labels. The authors proposed that this was most likely assembled from a molecule of ethylene and an unlabeled C atom originating from **XXI[c]** (either CH_3 or μ-CH_2).[154]

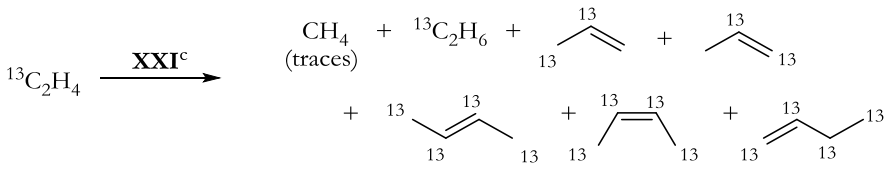

Scheme 3.1.2. 3: Olefins resulting from the reaction of XXI[c] with $^{13}C_2H_4$.[154]

The treatment of the *a*-diimine type ligand (**XXI**) with a base in the presence of a metal salts does not always lead to the formation of compounds of the type **XXI[a]** and **XXI[b]**. With nickel(II) salts, oligonuclear aggregates of $[Ni^{II}_2(\mathbf{XXI})X_3]_x$ (X= Cl, Br) are formed in this complex, here the metal ions are six-coordinate and in a high spin state.[151] The formation of dimers such as $[L_2M_2]^{2+}$ have been observed in some cases and reported.[155,156] Sachse et. al.[157] have reported instances where the *a*-diimine type ligands yields Cu_6 complexes which feature an unusual $\{Cu_6(\mu_4\text{-}O)_2\}$ bitetrahedral core. Also, the structural and magnetic variability of cobalt(II) complexes of the *a*-diimine type complexes have been reported.[158]

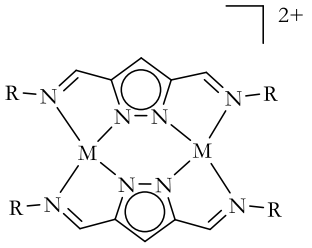

XXVI

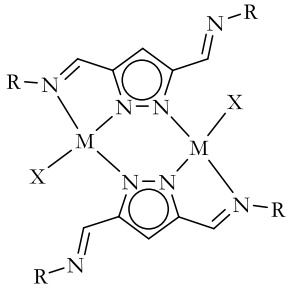

XXVII

L_2M_2

In addition, mononuclear anionic complexes of the *a*-diimine type ligands $K^+[LPt(Ph)_2]^-$ (**XXI[d]**) have been reported by Chen and co-workers.[152] The mononuclear complex $K^+[LPt(Ph)_2]^-$ reacts with CuCl to give a dimeric heterobimetallic $\{LPt(Ph)_2]_2Cu_2\}$(XXI[e]) (Scheme 3.1.2. 4).

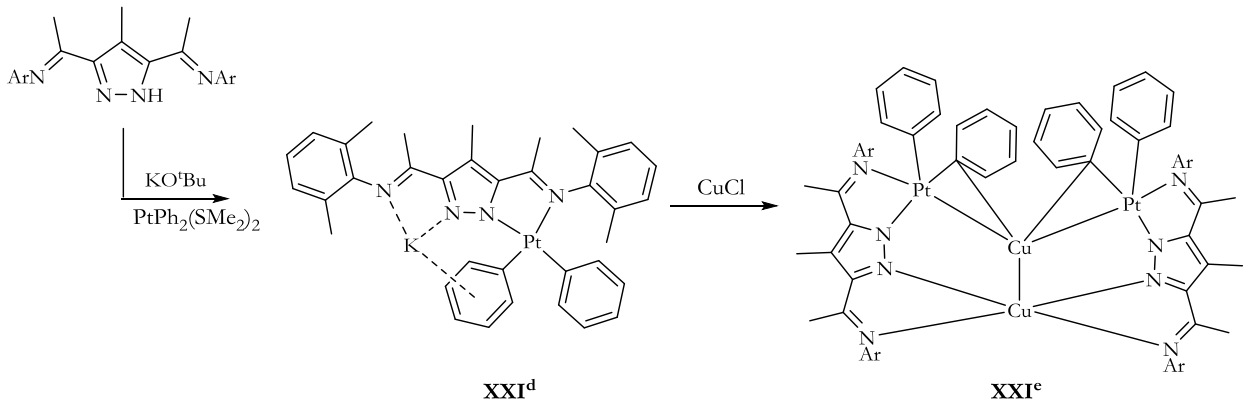

Scheme 3.1.2. 4: Preparation of mononuclear monoanionic Pt and heterobimetallic Cu-Pt complex[152]

The heterobimetallic complex exhibits Pt→Cu dative bonds, Cu-Cu contacts as well as a dynamic behaviour in solution.[152]

4 Renewable and biodegradable natural polymers

The use of biodegradable/bio-based materials is not only a benign way of protecting the environment, but also a possible alternative to depleting petrochemical feedstock.[159,160,161] Biodegradable materials offer new uses in biomedical applications, most especially, the use of surgically implantable devices and use in drug delivery systems.[162,163,164] However, packaging remains one of the most dominant applications of bio-based plastics. Some of the bio-based polymers studied include polyhydroxyalkanoate (PHA), of which the most common member is polyhydroxybutyrate (PHB),[165,166,167] and polylactic acid (PLA).[168] The use of PLA's and their copolymers have been of interest for some time now. Lactide is produced from the dehydration of lactic acid, which is obtained from renewable resources such as corn or sugar beet (Scheme 4. 1).

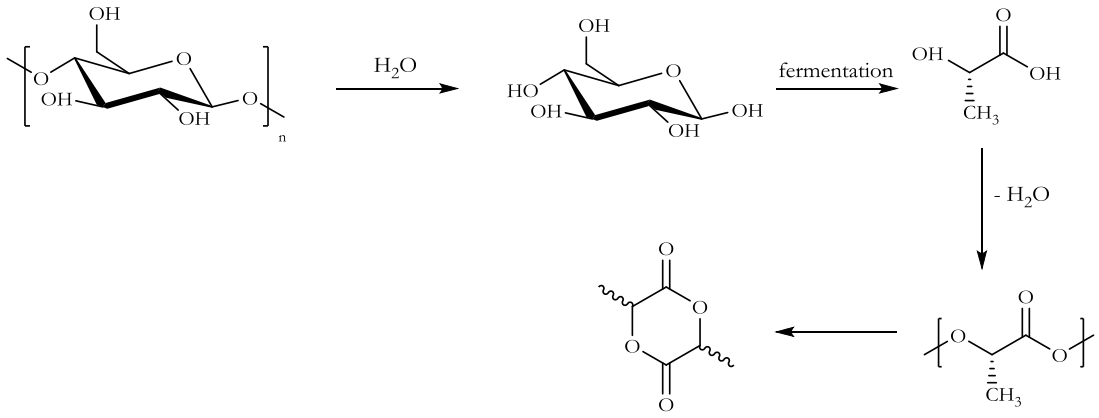

Scheme 4. 1: Synthesis of lactide monomer from natural resources

There are three isomers of lactide, L-lactide, D-lactide and *meso*-lactide. The pure L- and D-lactide form crystalline isotactic polymers. The ring opening polymerization (ROP) of lactide has been one of most efficient routes in the commercial production to PLA.[169,170,171] Commercial production of PLA is still in its infancy with commercial examples of PLA's marketed under trade names such as Ingeo from NatureWorks LLC® (CargillDow)[172] and LACEA® (Mitsui, Japan). Among the ROP processes, which include anionic, cationic, organocatalytic and coordination insertion, the coordination-insertion mechanism is gaining prominence.[173] The mechanism for the ROP of cyclic esters as initially proposed by Dittrich and Schulz,[174] involves a three-step coordination-insertion mechanism as shown in Scheme 4. 2.

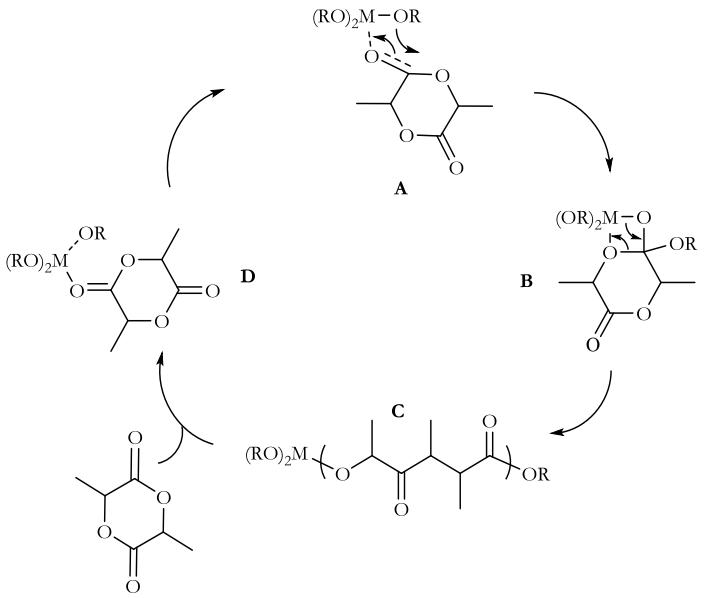

Scheme 4. 2: **Coordination-insertion mechanism of lactide polymerization using metal-alkoxide catalysts**[175]

The initiation of the reaction involves a nucleophilic attack of the alkoxide at the carbonyl (**A**) which leaves the monomer heterocycle intact (**B**). A rearrangement takes place, which orients the acyl oxygen closer to the metal centre (**C**). This eventually results in another metal alkoxide (**D**) which can insert into another monomer unit. A practical demonstration of this mechanism at work can be found in the work of Kricheldorf et. al.[176] and Teyssié et. al.[177] on the polymerization of different lactones using Al(O*i*Pr)$_3$ as initiators.

Two competing reactions are known to influence the stereochemistry of the resulting polymer product. The first mechanism, the chain end control mechanism, occurs when the stereochemistry of the inserted monomer plays a major role in the stereochemistry of the subsequent insertion. This is predominant in complexes that make use of sterically bulky ligands that crowd the active site. The second mechanism, the enantiomorphic site-control mechanism is mostly dependent on the chirality of the ancillary ligand.[178] Some of the more common polymer microstructures include, isotactic L-PLA, produced with the utilization of pure L-lactide, syndiotactic PLA, and heteroatactic PLA.

A number of transition metal complexes have been reported for the ring opening polymerization of *rac* D,L-lactides, some of these include group 3 and lanthanide based complexes,[179,180,181,182] which are good initiators for the ROP of lactide. In addition, metals such as Ca,[183,184,185] Mg,[186,187] Al,[188] Sn[189,190] and other metal initiators have been studied over the past few decades.

Zinc-based initiators are more robust and have the ability to resist the presence of protic impurities in the polymerization medium. A number of zinc-based initiators have been developed for the ROP of lactic acid.[191,192] Since the nature of the ancillary ligand plays a major role in the stereospecific architecture of PLA, the past decades have seen the development of various catalyst systems that have the potential to initiate the stereo controlled ring opening polymerization of lactides (ROP).

Ligand families generally employed with mostly group 2 and group 10 metals can generally be classed as anionic, neutral, and cationic/activated complexes.[193] A number of reviews give extensive details on ligand classes and metals, which have been employed in the synthesis of PLA.[193,194] These ligand classes involve the use of *β*-diiminate (BDI),[195,196] pyrazolate and *tris(*pyrazolyl)borate (TPB) ligands,[197,198] phenolates,[199,200] *bis*(phosphinoimine)methane,[201] N-heterocyclic carbenes,[202,203] and ligands featuring other heterocyclic and amido side arms.[204]

β-diiminate (BDI):

The work of Coates in the use of BDI complexes (**XXVIII**) was a game changer as far as this ligand class was concerned. This class of complexes are remarkably active for the stereocontrolled ROP of *rac*-LA and enabled the formation of heteroatactic-enriched PLA.[205]

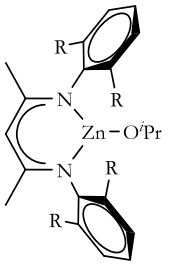

R = ^{i}Pr

XXVIII

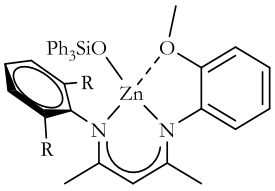

R = ^{i}Pr

XXIX

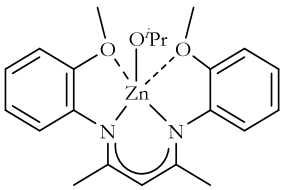

XXX

Attempts to improve the BDI catalysts by modification of the ligand have seen some groups such as Gibson and co-workers[206] installing an ether appendage to generate a new class of ligand. The zinc complex (**XXIX**) is active for the ROP of *rac*-lactide and gives conversions of up 90% but lacks control in polydispersity. Complex (**XXX**), a modification of (**XXIX**), reported by Chisholm et. al.[207] at 1% catalyst loadings is active in lactide polymerization and able to maintain control of polydispersity, but also lacks stereochemical control.

Phenolates:

Another example of ligand class used is phenolates. The work of Hillmyer and Tolman pioneered the use of zinc complexes featuring bulky amino-phenolate based N^N^O-tridentate ancillary ligands (**XXXI**). This family of complexes show remarkable activities for the non-stereocontrolled ROP of *rac*-LA. The poly *rac*-lactide obtained exhibits narrow polydispersities (PDI = 1.34-1.42) even at low catalyst loadings. For example even at 0.15% catalyst loading, 96% conversion is obtained in 5 min.[208]

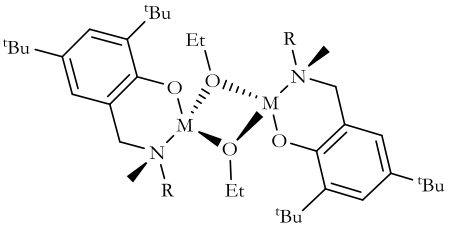

M = Zn
R = $C_2H_4N(Me)_2$
R = Cyclohexyl

XXXI

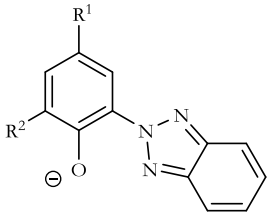

XXXII

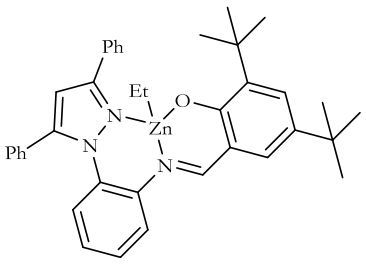

XXXIII

Sobota and co-workers[209] used the same ligand backbone with zinc as in (**XXXI**), but only varied the complex/alcohol combination using benzyl alcohol and butanol in place of ethanol. The catalyst gives up to 98% conversions in 120 min with narrow molecular weight distributions (PDI = 1.09). The zinc complexes incorporating the bis(amine)benzotriazole phenoxide ligand (**XXXII**) reported by Sung et. al.[210] is active in the polymerization of *rac*-lactide to poly-PLA in a well-controlled manner with PDI (<1.13) and affords isotactic polymers. Wang and co-workers[211] have also reported on the zinc complex of a phenoxyimine ligand with a pendant pyrazole unit (**XXXII**). The zinc complex is catalytically active for lactide polymerization at 80°C at high catalyst loadings, but lacks stereochemical control. It also produces low molecular weight polymers (PDI = 1.3). Other similar aminophenolates bearing one or two pyrazolyl donor functionalities have also been reported.[212]

Neutral ligands:

The zinc alkoxide catalyst supported by N-heterocyclic carbene (**XXXIV**) rapidly polymerizes *rac*-lactide to heterotactic enriched PLA in CH_2Cl_2 at 25°C, whiles the free NH-carbene on the

other hand also yields highly isotactic enriched PLA.[213] The chiral complex (**XXXV**), generated *in situ* by the action of diethyl zinc on the chloro analogue, does not yield the desired stereochemical control ,although it is active in the polymerization of *rac*-lactide.[214]

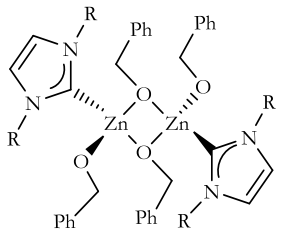

R = 2,4,6-trimethylphenyl

XXXIV

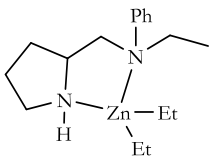

XXXV

Pyrazole based ligand frameworks have also been reported in the ROP of cyclic esters.

Pyrazolates and tris(pyrazolyl) borate (TPB) ligands:

Complexes of pyrazole based ligands with zinc have been used for the ROP of cyclic esters. The work of Chisholm on the use of TPB (**XXXVI**) as useful ligands for lactide polymerization inspired other investigators into its potential.

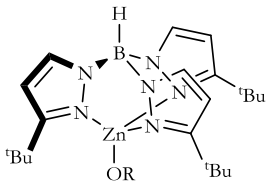

R = $SiMe_3$, Et

XXXVI

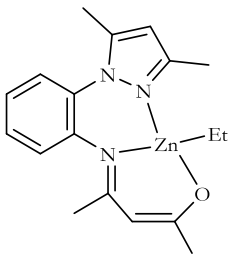

XXXVII

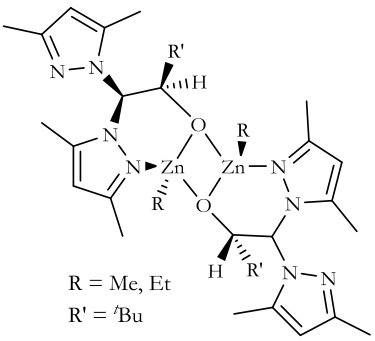

R = Me, Et
R' = ^{t}Bu

XXXVIII

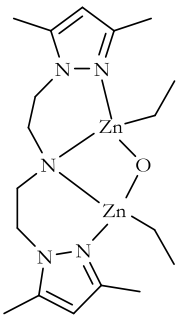

XXXIX

For example, **XXXVII** is highly active in ROP of *rac*-lactide at ambient temperature in the presence of benzyl alcohol with 96% conversion. It also leads to polymerization of 100 mol

equivalent *rac*-lactide in 1-3 min.[215] The chiral alcohol scorpionate (**XXXVIII**) acts a single component catalyst in the polymerization of L-lactide to low molecular weight polymers in 87% conversion in 1 h at 65°C. It also produces heterotactic enriched PLA's with P_r up to 0.77.[216] The work of Carpentier et. al.[217] resulted in the isolation of the N^N^N pyrazolyl zinc complex (**XXXIX**). This complex demonstrates very high activity and low polydispersities (<1.40) at low catalyst loadings and achieves complete conversion in 30 h at room temperature.

5 Aims and scope of this work

The aims and scope of this work include:

(a) To carry out further mechanistic investigations into the formation of the unique tetrapalladium complex **XXI**[c], this would include efforts at isolating and characterizing the proposed intermediates leading to the formation of **XXI**[c].

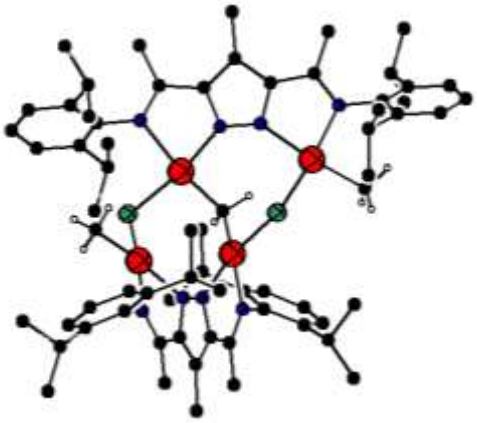

Fig. 5. 1: The unusual tetrapalladium complex XXI[c]

Attempts would also be made at isolating the second but unidentified side product that is formed in excess $SnMe_4$ and longer reaction times. In addition, attempts would be made at establishing the origin of the unlabeled carbon atom in olefin coupled reactions of labeled ethylene with **XXI**[c]. Last but not the least; further investigations would be carried out on the olefin coupling ability of **XXI**[c] with other olefins.

(b) Preparation of heterobimetallic complexes of palladium(II) and rhodium(I) using the symmetrical 3,5-disubstituted *a*-diimine like pyrazolyl ligand and investigation of their catalytic activity in a number of organometallic transformation reactions.

(c) To prepare zinc(II) complexes of the *a*-diimine like pyrazolyl scaffolds as catalyst precursors for the polymerization of *rac*-lactide to polylactide, a bio-renewable polymer.

(d) While the use of symmetrical 3,5-disubstituted pyrazolyl ligands is well known, the use of unsymmetric 3,5-pyrazolyl bridging environments remain scarce. One of the aims of this work is to prepare novel unsymmetric cyclopentadienyl, indenyl, and fluorenyl 3,5-disubstituted pyrazolyl bridging ligands. These ligands would be used for the preparation of heterobimetallic early transition metal complexes. These complexes in turn, would be screened as catalyst precursors for olefin polymerization.

(e) As an extension to work on unsymmetric 3,5-pyrazolyl bridging environments, another aim would be the preparation of a novel class of highly compartmentalized, unsymmetric 3,5-substituted bridging ligands which feature N-heterocyclic carbene and indenyl/fluorenyl side arms as ligands capable of bridging two organometallic fragments and capable of hosting metals in different oxidation states.

6 Results and Discussions

6. 1 Ligand synthesis (*α*-diimine type ligands)

The dialdehyde precursor, **B** was synthesized using established synthetic protocols[218,219,145] as shown below (Scheme 6.1.1).

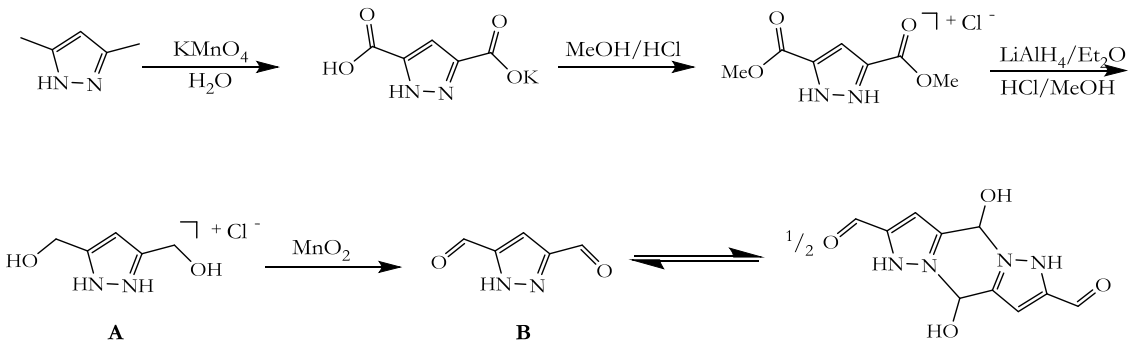

Scheme 6.1.1: Synthetic route to B

The diketone precursor, **C** was synthesized using slightly modified preexisting procedures.[220,151] Toluenesulfonylazide was generated *in situ* under cold conditions by treating toluensulfonylchloride with NaN_3 at 0°C. This mixture added to a previously stirring mixture of 2.0 mol equivalent acetylacetone and K_2CO_3 (1.0 mol equivalent). The reaction was allowed to stir for 48 h, after which a 1.0 M solution of HCl was added and the mixture stirred for a further 24 h. After evaporation of the solvent, the crude product was recrystallized from boiling toluene, and **C** was obtained in *ca* 60% yield.

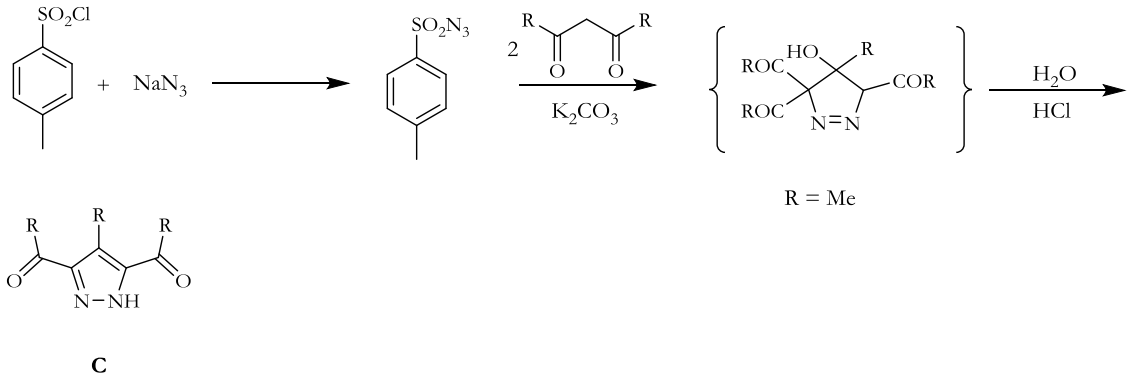

Scheme 6.1.2: Scheme showing a slightly modified synthetic route to C

The Schiff base condensation of **B**/**C** with the appropriate amine (Scheme 6.1.3) affords the imine products in good to excellent yields after refluxing in toluene for 72 h with added weak acid catalyst (p-toluenesulfunic acid).

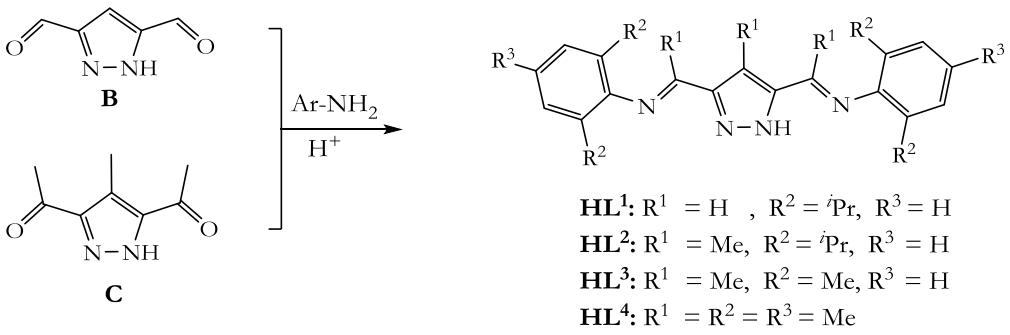

Scheme 6.1.3: Pyrazolyl bridging *α*-diimine type ligands used in this study

6. 2 Further insights into the formation of the unusual tetrapalladium complex

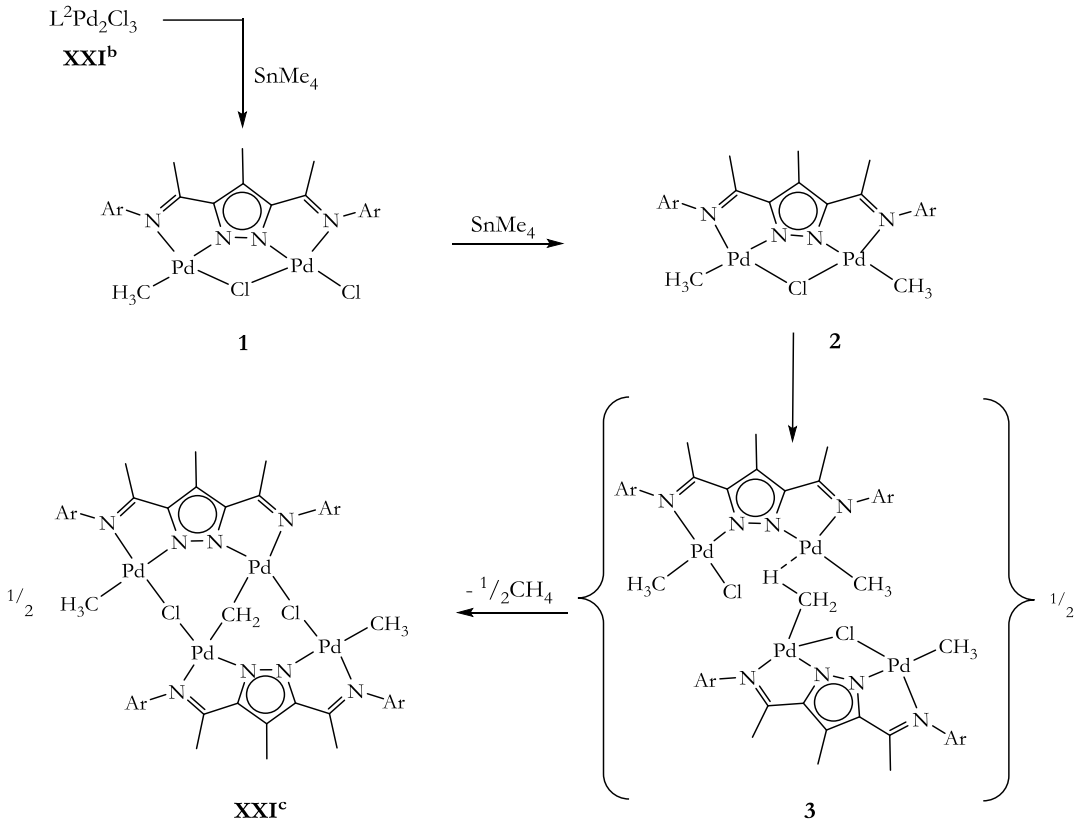

Scheme 6.2. 1: Proposed scheme leading to the formation of the unusual tetrapalladium complex[154]

In the proposed mechanism leading to the formation of unique tetrapalladium complex **XXI**[c], (Scheme 6.2. 1) by treating [$L^2Pd_2Cl_3$] (**XXI**[b]) with 30 mol equivalent $SnMe_4$, the authors detected the sequential formation of two intermediates (C_s (**1**) and a C_{2v} (**2**)) leading to the formation of the tetranuclear palladium complex. NOESY correlations of the isopropyl methyl groups showed the presence of palladium bound methyl groups in both intermediates. Using DOSY experiments, the molecular size of the intermediates were different, although within a narrow range.[154] Although the formation of a C_s and C_{2v} symmetric intermediates leading to the formation of the tetrapalladium core were proposed, not much attempts were made at trapping and isolating these intermediates. Due to the transient nature of these intermediates, they react further to give other reaction products. In addition, the authors did note the formation of a second but unidentified product, which forms in excess $SnMe_4$.[154]

As follow up investigation into the formation of **XXI**[c] formed from the reaction of (**XXI**[b]) with $SnMe_4$, a series of experiments were set up. One of them involved expanding the scope of palladium salts used to cover bromide and iodides (Scheme 6.2. 2), to investigate if the formation of the tetrapalladium complex is reproducible with other halides or exclusive to chlorides.

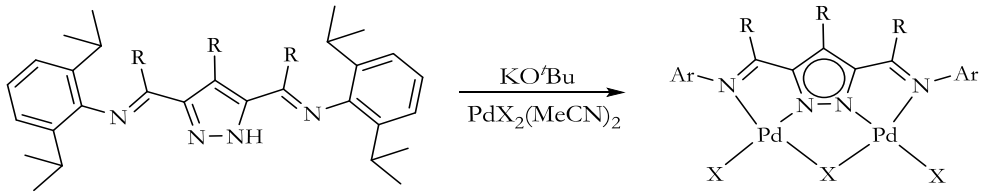

HL[1]: R = H
HL[2]: R = Me

(**1a**)*: R = H, X = Cl
(**1b**): R = H, X = Br
(**1c**): R = H, X = I
(**2a**)*/**XXI[b]**: R = Me, X = Cl
(**2b**): R = Me, X = Br
(**2c**): R = Me, X = I

Scheme 6.2. 2: Synthetic scheme for the preparation of complexes 1a-2c (* previously reported complexes)

By treating a potassium salt solution of the ligand (**L[1]**/**L[2]**) with 2.0 mol equivalent of the appropriate palladium(II) salts, the analogous [$L^xPd_2Br_3$] (**1b**, **2b**) and [$L^xPd_2I_3$] (**1c**, **2c**) were isolated in moderate to good yields (36-71%). The complexes were characterized by ^{1}H and ^{13}C NMR, IR spectroscopy, ESI-MS and elemental analysis.

The ^{1}H NMR spectrum of **1c** is shown in Fig. 6.2. 1. The CH_3^{iPr} group is observed as a pair of doublets at 1.18 and 1.41 ppm ($^3J_{HH}$ = 6.9 Hz), while the CH^{iPr} group is observed as a septet at 3.30 ppm. On the other hand, the CH=N group is observed as a singlet at 7.72 ppm, and the CH^{Pz} is observed at 6.91 ppm.

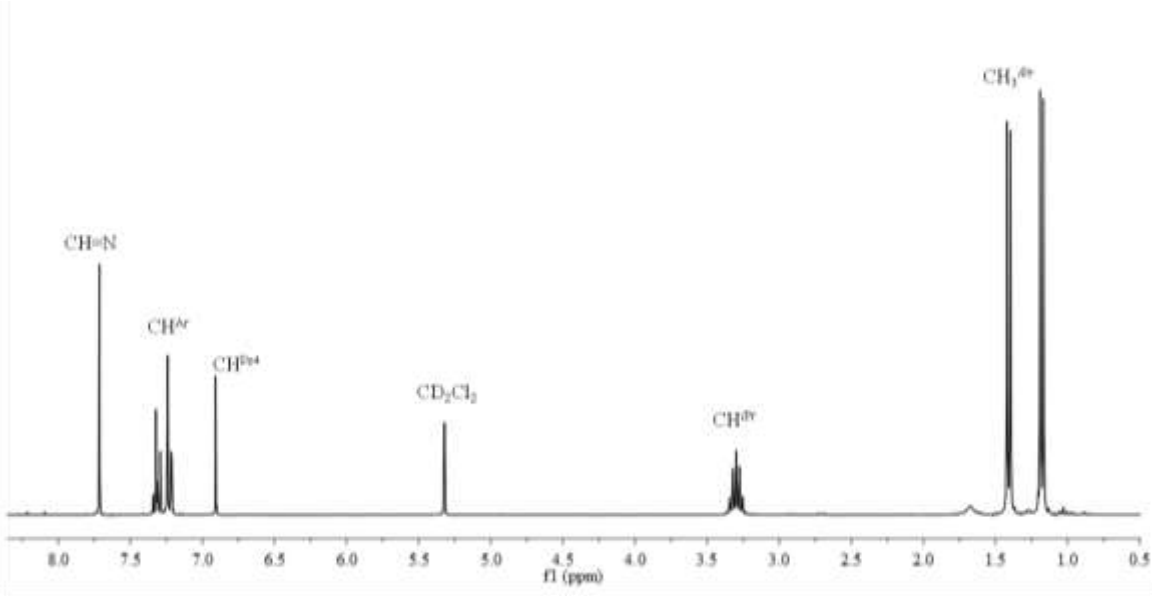

Fig. 6.2. 1: ^{1}H NMR spectrum of 1c measured in CD_2Cl_2 at room temperature

The ^{1}H NMR spectrum chemical shifts of the bromo (**1b**, **2b**) and iodo (**1c**, **2c**) complexes are comparable to the chloro analogues (**1a**, **2a**). For instance, the CH=N peak are observed at δ: 7.73 and 7.71 for **1b** and **1c** respectively, compared to 8.29 ppm in the free ligand, HL[1]. The CH^{Pz4} is also shifted upfield to 7.01 and 6.91 ppm in **1b** and **1c** respectively compared to 7.30 ppm in the free ligand (**HL[1]**), an indication of coordination of the metal ion to the ligand. Table 6.2. 1 compares the chemical shifts observed for the chloro (**2a**), bromo (**2b**), and iodo complexes (**2c**) of **HL[2]**.

Table 6.2. 1: Table comparing the chemical shifts of complexes 2a, 2b and 2c

	[$L^2Pd_2Cl_3$] (2a)*	**[$L^2Pd_2Br_3$ (2b)**	**[$L^2Pd_2I_3$ (2c)**
CH_3^{Pz4}	2.51 (s)	2.50 (s)	2.52 (s)
CH_3C=N	2.19 (s)	2.18 (s)	2.17 (s)
CH_3^{iPr}	1.19 (d, $^3J_{HH}$ = 4.8 Hz)	1.19 (d, $^3J_{HH}$ = 6.9 Hz)	1.15 (d, $^3J_{HH}$ = 6.9 Hz)
CH_3^{iPr}	1.44 (d, $^3J_{HH}$ = 4.8 Hz)	1.44 (d, $^3J_{HH}$ = 6.7 Hz)	1.45 (d, $^3J_{HH}$ = 6.9 Hz)

*NB : The preparation and characterization of **2a** has been reported elsewhere and would not be covered here.

Although very little differences are observed in the chemical shifts in the ^{1}H NMR spectrum, differences in the $CH_3C=N$ stretching vibrations are observed in the IR spectrum. For instance, the $CH_3C=N$ peaks for **2b** and **2c** are observed at 1559 cm^{-1} and 1546 cm^{-1} respectively, due to decreased Pd-X bond strength in moving from bromine to iodine. The ESI mass spectra data for **2a**-**2c** show a common fragmentation pattern of $[M-X]^+$ peaks, although in the case of the iodide complexes, m/z fragments due to high molecular aggregates m/z 2026 (100%) for $[L^2{}_2Pd_4I_5]^+$ are also observed. Having prepared the bromo and iodo complexes in addition to their chloro analogues, methylations of the complexes with $SnMe_4$ were carried out (Scheme 6.2. 3).

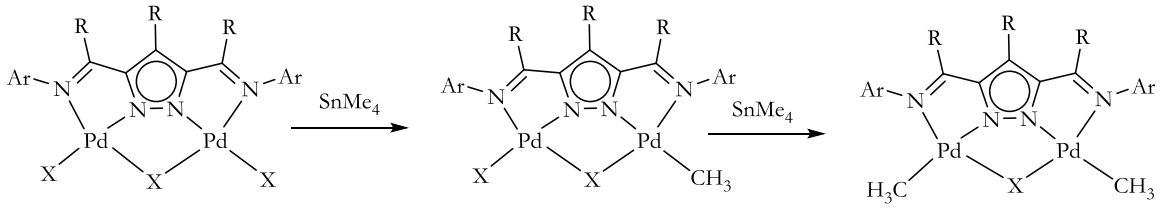

(**1a**): R = H, X = Cl
(**1b**): R = H, X = Br
(**1c**): R = H, X = I
(**2a**): R = Me, X = Cl
(**2b**): R = Me, X = Br
(**2c**): R = Me, X = I

(**2d**): R = Me, X = Cl
(**2e**): R = Me, X = Br

(**2f**): R = Me, X = Cl
(**2g**): R = Me, X = Br

Ar = 2,6-^{i}Pr$_2$-C$_6$H$_3$

Scheme 6.2. 3: Preparation of single and double methylated palladium(II) complexes

Beginning with **2a**, varying **2a**:$SnMe_4$ molar ratios and reaction times were employed in attempts at gaining more insight into the formation of **XXI**[c]. In a typical experiment, very dilute solutions of $SnMe_4$ was added to a stirring CH_2Cl_2 solution of $[L^2Pd_2Cl_3]$ (**2a**) and the reaction monitored by ^{1}H NMR spectroscopy, in attempts at observing and isolating the previously proposed C_s (**2d**) and C_{2v} (**2f**) methyl bound palladium intermediates.

In one such experiment, 1.0 mol equivalent of $SnMe_4$ was added to a CH_2Cl_2 solution of **2a** and the reaction monitored. After 8 h, the ^{1}H NMR spectrum of the reaction mixture (Fig. 6.2. 2), shows two different peaks for a methyl group (CH_3^{Pd}). The two CH_3^{Pd} peaks are observed at -0.03 and 0.04 ppm in a ratio (1:1.4). This is in line with the proposal that the formation of these intermediates reaches their maxima within 6-10 hr respectively.[154] The ^{1}H NMR spectrum of the reaction mixture points to the formation of the C_s and the C_{2v}

symmetry intermediate products **2d** and **2f** respectively. The former (**2d**) showing methyl peaks (CH_3^{Pd}) at 0.04 ppm and two separate signals for $CH_3C{=}N$ group at 2.15 2.18 ppm, whiles the CH_3^{Pz4} peak is observed at 2.50 ppm. The C_{2v} symmetric product **2f**, on the other hand shows CH_3^{Pd} peak at -0.03 ppm and a single peak for $CH_3C{=}N$ at 2.13, whiles the CH_3^{Pz4} peak is observed at 2.47 ppm. The difference in CH_3^{Pd} peaks for the two intermediates is due to stronger donor groups on the C_{2v} product compared to C_s symmetric product.

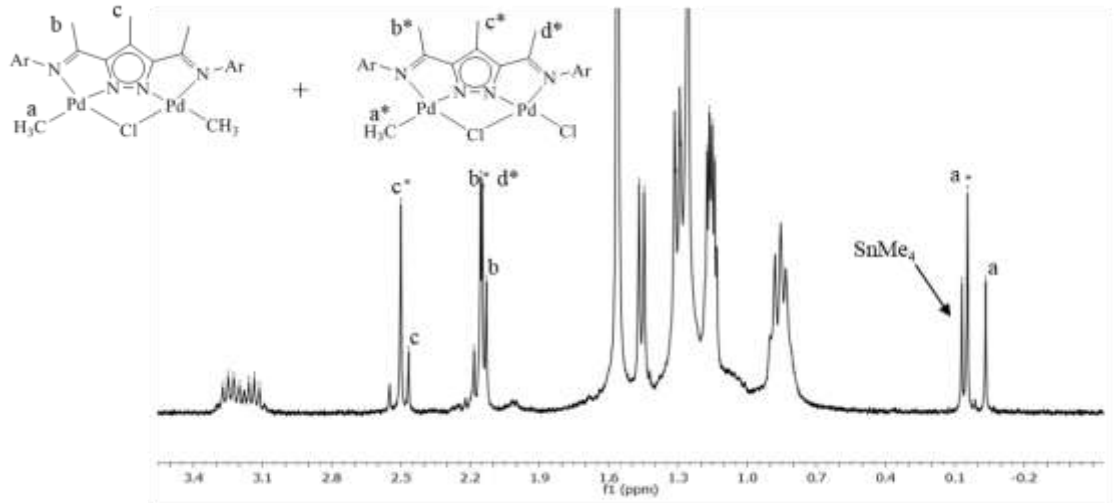

Fig. 6.2. 2: ^{1}H NMR spectrum (selected window) showing the formation of the C_s symmetric (2d)(*)and C_{2v} (symmetric product (2f) after 8 h measured in $CDCl_3$ at room temperature

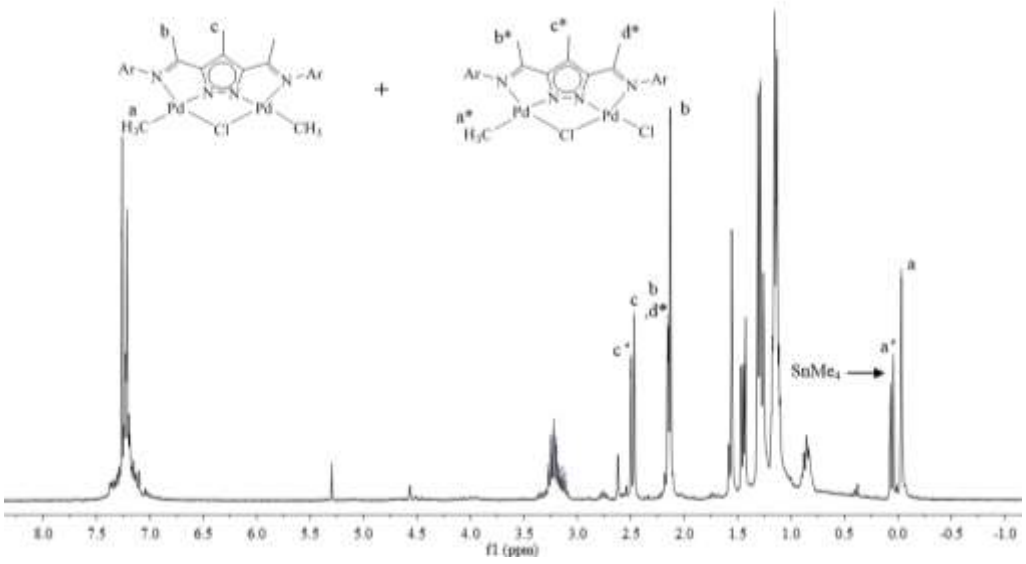

Fig. 6.2. 3: ^{1}H NMR spectrum showing changes in signal intensity of 2d (*) and 2f symmetric products after 16 h measured in $CDCl_3$ at room temperature

With longer reaction times (>12h), the CH_3^{Pd} peak at 0.04 (**2d**) diminishes, whiles the CH_3^{Pd} peak at -0.03 (**2f**) intensifies, thus, showing the further conversion of **2d** to **2f**. The ratio of the two peak intensities changes over a 16 h period (Fig. 6.2. 3). Table 6.2. 2 compares selected ^{1}H chemical shift environments for the educt (**2a**), as well as the C_s (**2d**) and C_{2v} (**2f**) intermediate products.

Table 6.2. 2: Table comparing ^{1}H NMR spectral shifts for educt (2a) and intermediates (2d and 2f)

	$[L^2Pd_2Cl_3]$ (2a)	**$[L^2Pd_2(\mu\text{-}Cl)(CH_3)Cl]$ (2d)**	**$[L^2Pd_2(\mu\text{-}Cl)(CH_3)_2]$ (2f)**
CH_3^{Pz4}	2.51 (s)	2.40 (s)	2.47 (s)
$CH_3C{=}N$	2.19 (s)	2.15 (s), 2.18 (s)	2.13 (s)
CH_3^{iPr}	1.19 (d, $^3J_{HH}$ = 4.8 Hz)	1.14 (d, $^3J_{HH}$ = 6.7 Hz)	1.15 (d, $^3J_{HH}$ = 6.9 Hz)
CH_3^{iPr}	1.44 (d, $^3J_{HH}$ = 4.8 Hz)	1.30 (d, $^3J_{HH}$ = 6.7 Hz)	1.30 (d, $^3J_{HH}$ = 6.9 Hz)
		1.46 (d, $^3J_{HH}$ = 6.7 Hz)	
CH_3^{Pd}	-	0.04 (s)	-0.03 (s)

Differences are observed in the CH_3^{iPr} groups of the educt (**2a**) and intermediate complexes (**2d** and **2f**). In **2a**, the CH_3^{iPr} is observed as two doublets at 1.19 and 1. 44 ppm, compared to **2d**, which has three CH_3^{iPr} groups at 1.14, 1.30 (new) and 1.44 ppm. The C_{2v} symmetric product **2f** on the other hand features two CH_3^{iPr} groups as a pair of doublets at 1.14 and 1.30 ppm. Thus, reflecting the gradual change in symmetry and increasing electron density at the palladium(II) centre on the conversion of **2a** to **2d** and subsequently to **2f**. The chemical shifts observed are identical to experimental data obtained by A. Sachse.[221]

When the experiment was repeated using benzyl chloride in place of CH_2Cl_2 as a solvent, again, a mixture of the singly and doubly methylated products were isolated as well as the formation of $[L_2Pd]$ side product. Other chlorinated solvents such as chlorobenzene also gave similar results. The formation of methylated products is, however, not observed when non-chlorinated solvents such as ether and THF are used.

In another experiment, the amount of $SnMe_4$ used was reduced to 0.75 mol equivalents from the initial 1.0 mol equivalent and the reaction monitored in attempts at forming only the C_s symmetric product **2d** (Scheme 6.2. 4).

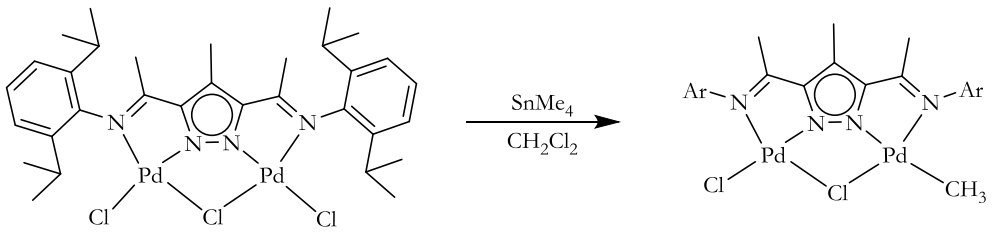

XXI[b]/2a **2d**

Scheme 6.2. 4: *In situ* preparation of the single methylated complex 2d from 2a

After 18 h, the reaction was worked up. Two products were obtained, an orange powder and a dark green filtrate. The dark green filtrate was later identified as the tetrapalladium complex with the characteristic μ-CH_2 and CH_3^{Pd} observed at 3.98 and 0.06 ppm respectively in the ^{1}H NMR spectrum ($CDCl_3$). The orange powder on the other hand, had no bridgingn μ-CH_2 but featured a broad CH_3 peak at 0.10 ppm (CH_3^{Pd}) (Fig. 6.2.4). This peak at 0.10 ppm correlates with a methyl group peak at -1.31 ppm in the ^{13}C NMR spectrum and confirmed by DEPT-90, DEPT-135, and ^{1}H-^{13}C HMBC experiments as a CH_3 group with no multiple bond correlations. In addition, CH_3^{iPr} peaks at δ: 1.14, 1.31, and 1.46 ppm are observed. In **2d**, the CH_3^{Pd} peak is observed as a sharp singlet at δ: 0.04.

Also two different CH_3C=N peaks were observed at 2.14 ppm and 2.17 ppm, pointing to an asymmetric ligand environment. The ESI-MS shows *m/z* values of high molecular aggregates at 1529 (50%) for $[L^2{}_2Pd_4(\mu\text{-}Cl)_3(CH_3)_2]^+$ and 1410 (25%) for $[L^2{}_2Pd_4(CH_3)]^+$ fragments respectively. Based on spectroscopic data the formation of a complex of the nature $[L^2{}_2Pd_4(\mu\text{-}Cl)_3(CH_3)_2]Cl$ (**2d$_2$**), formed from the dimerization of **2d** is proposed.

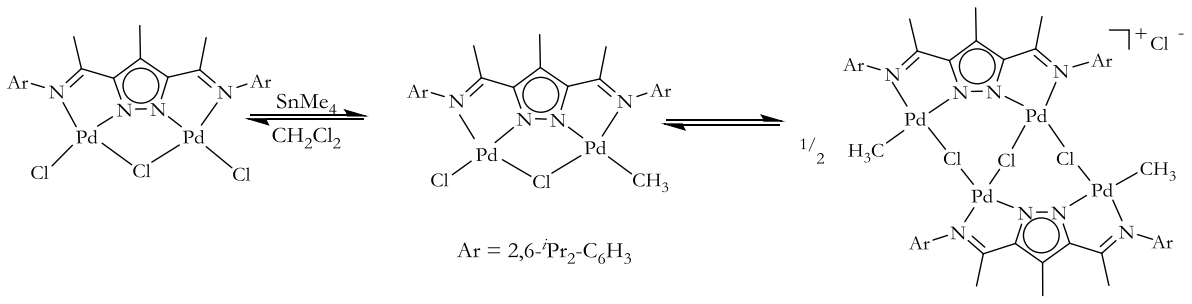

2a **2d** **2d$_2$**

Scheme 6.2. 5: Reversible formation of 2d$_2$ from dimerization of 2d under dilute concentration of SnMe$_4$

All attempts at crystallizing **2d** and **2d$_2$** failed. When left in solution, **2d$_2$** undergoes rearrangement to form the parent compound **2a** in the absence of $SnMe_4$, but reacts further to form **XXI^c** in the presence of $SnMe_4$ (Fig. 6.2.4). It is however stable (**2d$_2$**) in the solid state and can be kept at room temperature for several days.

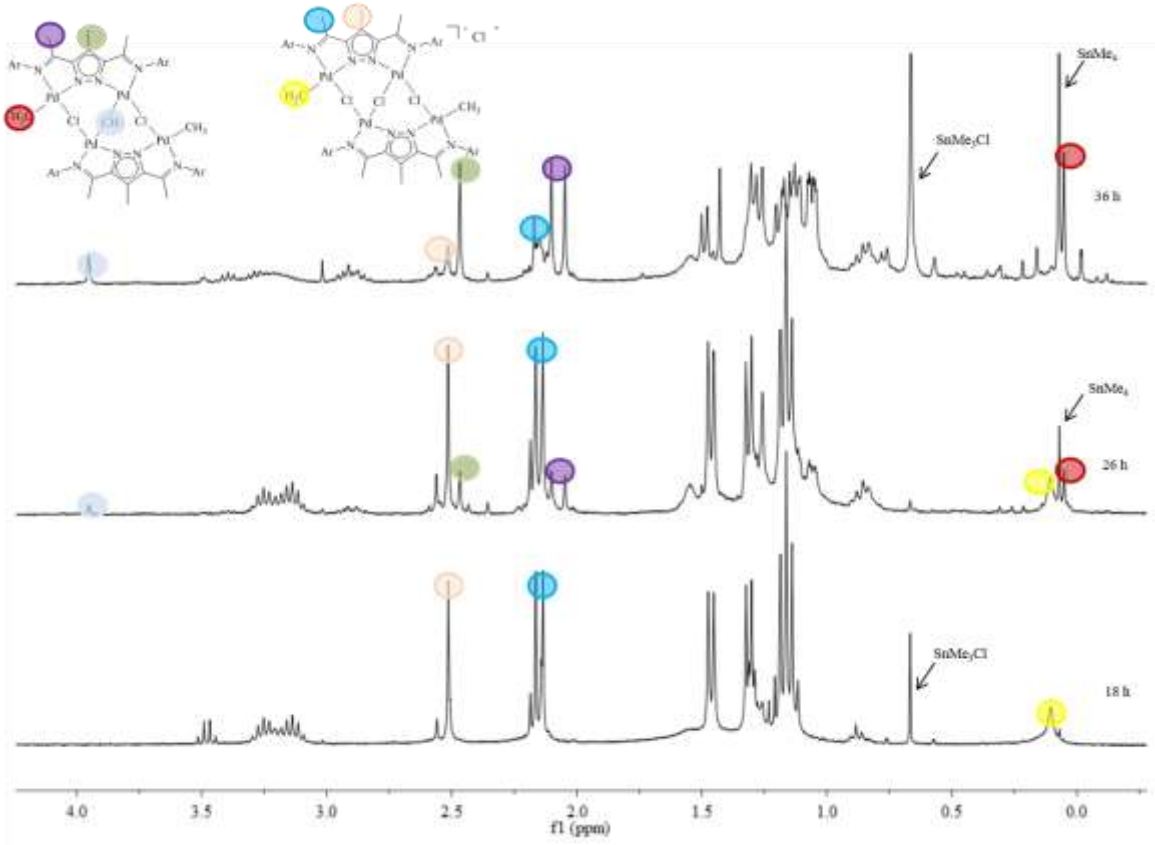

Fig. 6.2.4: ^{1}H NMR spectra (selected window) showing the sequential formation of XXI^c from 2d$_2$ measured in $CDCl_3$ at room temperature

A dilute $CDCl_3$ solution of $SnMe_4$ was added to a $CDCl_3$ solution of **2d$_2$** in a NMR tube and the reaction monitored continuously. The gradual formation of the tetrapalladium complex **XXI^c** is observed after 26 h, until eventually becoming the major product after 36 h (Fig. 6.2.4). In the light of this new observation, similar experiments were set up using the analogous bromo and iodo complexes in attempts at shedding more light on the formation of these intermediates.

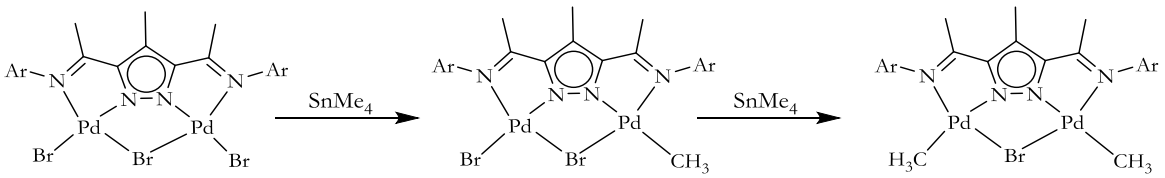

2b **2e** **2g**

Scheme 6.2. 6: Scheme showing the sequential formation of 2g from 2e

Repeated experiments were performed using $[L^2Pd_2Br_3]$ (**2b**) in place of $[L^2Pd_2Cl_3]$ (**2a**). This later gave further credence to the formation of C_s and C_{2v} symmetric intermediates. By treating a CH_2Cl_2 solution of **2b** initially with 1.0 mol equivalent of $SnMe_4$, no change in the ^1H NMR spectrum was observed after several days. However, when the concentration of $SnMe_4$ was increased to 90 equivalents, it was possible to observe the sequential formation of $[L^2Pd_2(\mu\text{-}Br)(CH_3)Br]$ (**2e**) and $[L^2Pd_2(\mu\text{-}Br)(CH_3)_2]$ (**2g**) (Scheme 6.2. 6). The figure below is a representative ^1H NMR spectrum of the reaction mixture after 24 h.

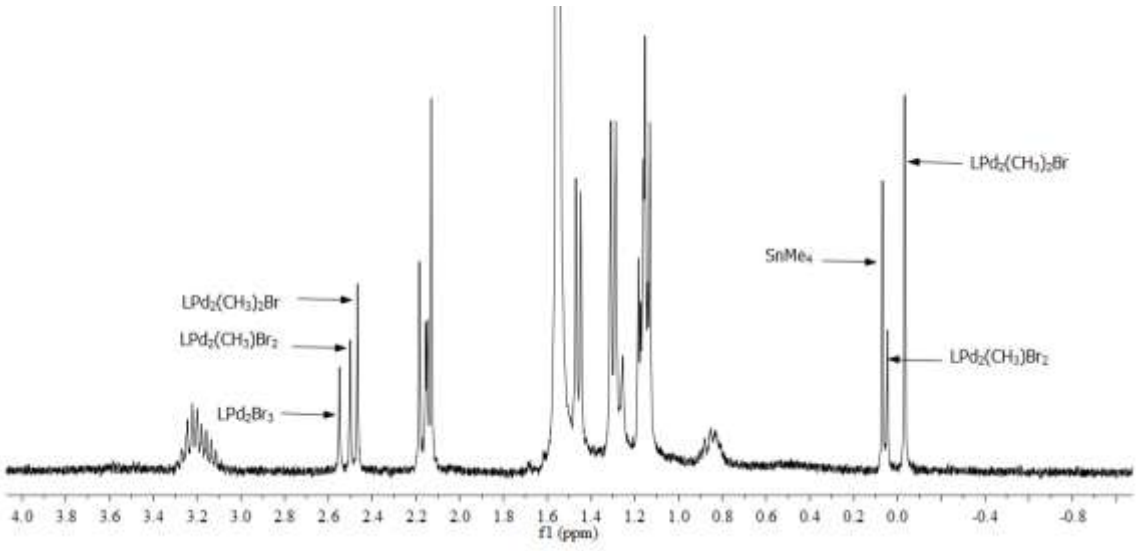

Fig. 6.2. 5: ^1H NMR spectrum (selected region) of reaction mixture showing the educt, C_s, and C_{2v} symmetric products measured in $CDCl_3$ at room temperature

The educt (**2b**), a C_s (**2e**) and a C_{2v} (**2g**) symmetric products are observed (Fig. 6.2. 5). The ^1H NMR spectrum peaks for the three different CH_3^{Pz4} groups at 2.55, 2.50 and 2.47 ppm are assigned for the compounds **2b**, **2e** and **2g** respectively, reflecting the increase in electron density on the pyrazole ring. Like the chloro analogues, two different methyl peaks (CH_3^{Pd}) are observed at 0.04 and -0.03 ppm for **2e** and **2g** respectively. In a similar fashion, the peak intensities for CH_3^{Pd} for **2e** (0.04 ppm) diminish in intensity with time, whiles that for **2g** (-

0.03 ppm) increases until eventually becoming the only CH_3^{Pd} peak. When the reaction is continued for long periods (more than 3 weeks), the reaction still terminates at the C_{2v} symmetric product. Further heating at 40°C for 2 weeks gave no further products, pointing to the kinetic and thermodynamic stability of this complex. The C_{2v} symmetric product **2g** was characterized by 1D and 2D NMR experiments.

The ^{1}H NMR spectrum of **2g** shows the CH_3^{Pd} peak as a singlet at -0.03 ppm and peaks at 2.13 and 2.47 for $CH_3C{=}N$ and CH_3^{Pz4} groups respectively in $CDCl_3$. In addition, the two CH_3^{iPr} groups are observed as two doublets at 1.14 and 1.30 ppm. The ^{1}H NMR spectrum chemical shifts observed for **2g** are identical to that observed for the chloro analogue **2f**.

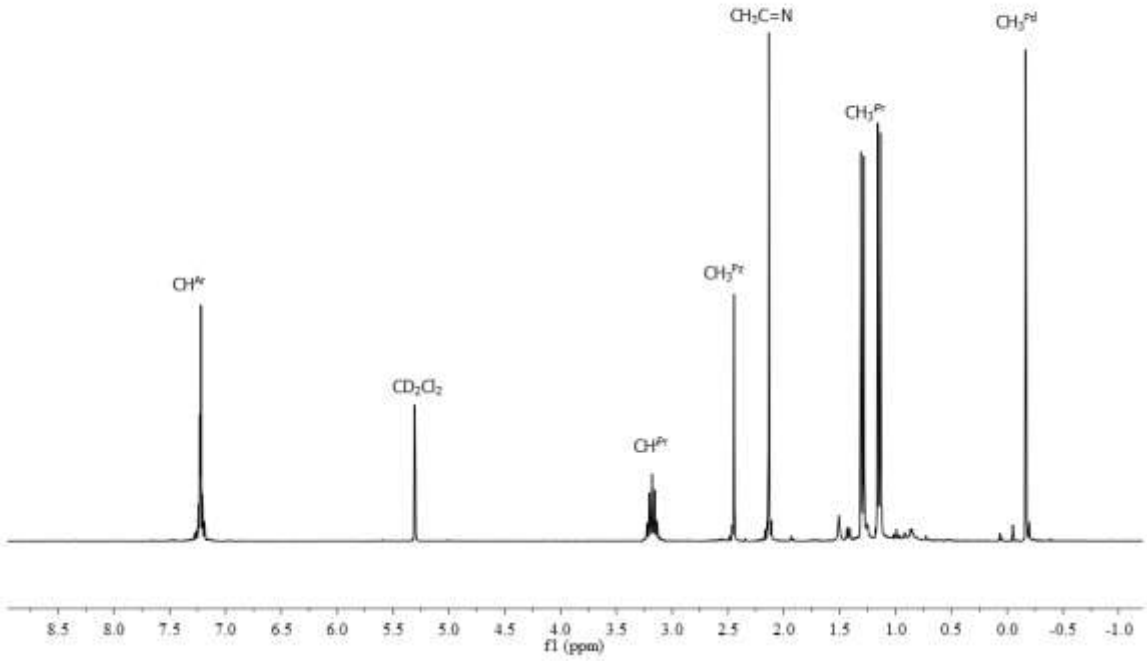

Fig. 6.2. 6: ^{1}H NMR spectrum of the C_{2v} symmetric product 2g measured in CD_2Cl_2 at room temperature

Complete assignment of the ^{1}H and ^{13}C peaks were made with ^{1}H-^{1}H COSY, ^{1}H-^{13}C HSQC (Fig. 6.2. 7), ^{13}C and ^{1}H-^{13}C HMBC NMR experiments. The CH_3^{Pd} peak at (-0.03 ppm) correlates to a CH_3^{Pd} peaks at 1.96 ppm in the ^{13}C NMR spectrum, as well as the $CH_3C{=}N$ peak which is observed in the ^{13}C NMR spectrum at 172 ppm.

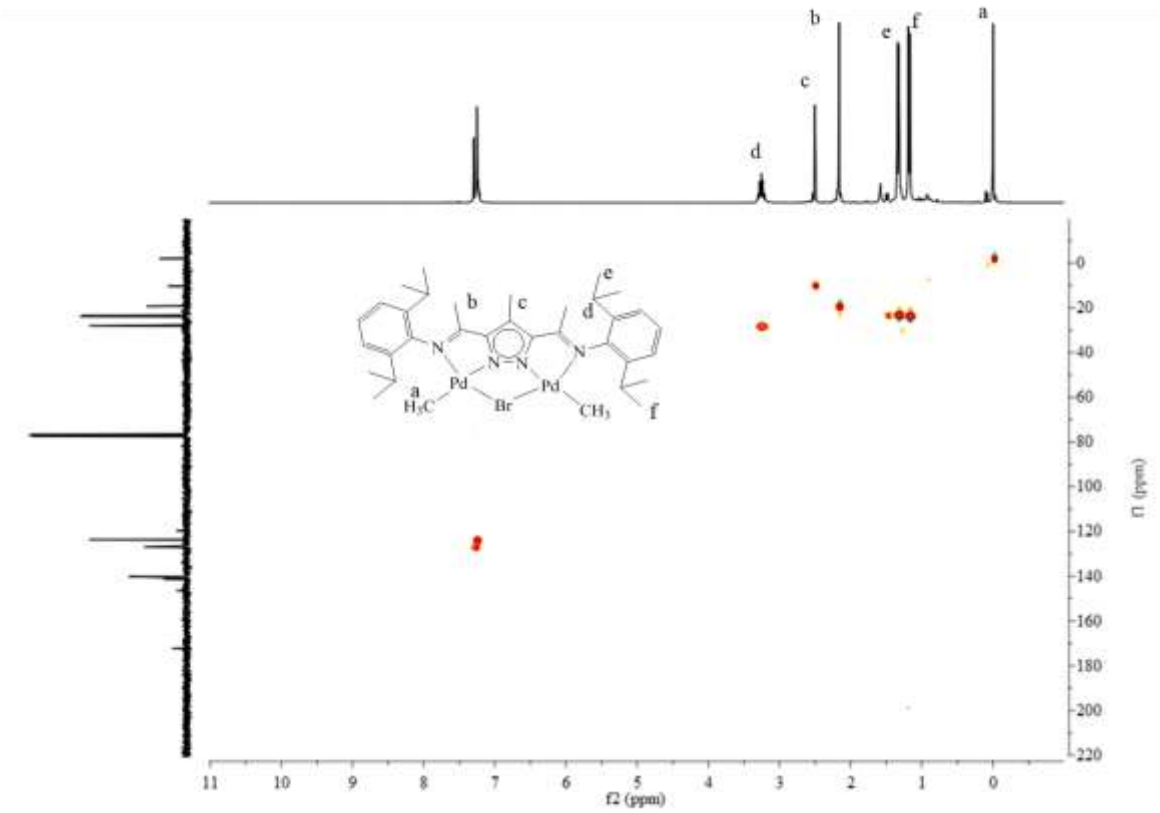

Fig. 6.2. 7: ^{1}H-^{13}C HSQC NMR spectrum for 2g measured in $CDCl_3$ at room temperature

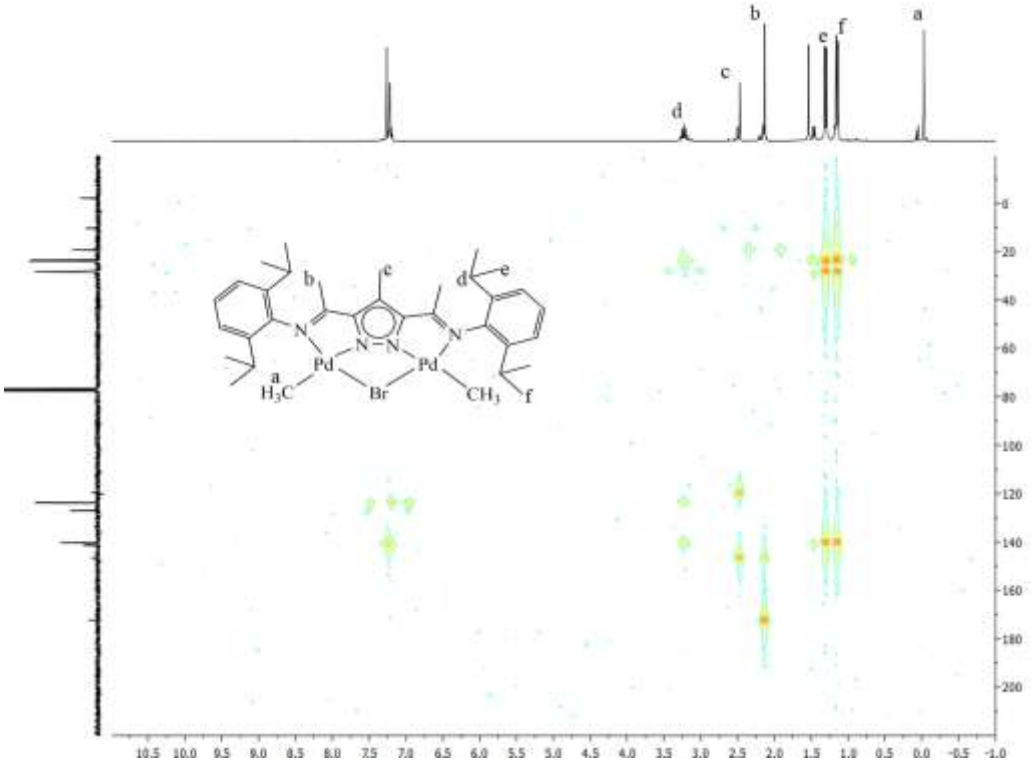

Fig. 6.2. 8: ^{1}H-^{13}C HMBC NMR spectrum for 2g measured in $CDCl_3$ at room temperature

The ESI-MS of **2g** (Fig. 6.2. 9) shows m/z fragment of 725 (22%) for $[M\text{-}Br]^+$. The figure below (Fig. 6.2. 9) shows the observed (left) and simulated (right) isotopic distribution pattern for the $[M\text{-}Br]^+$ fragment.

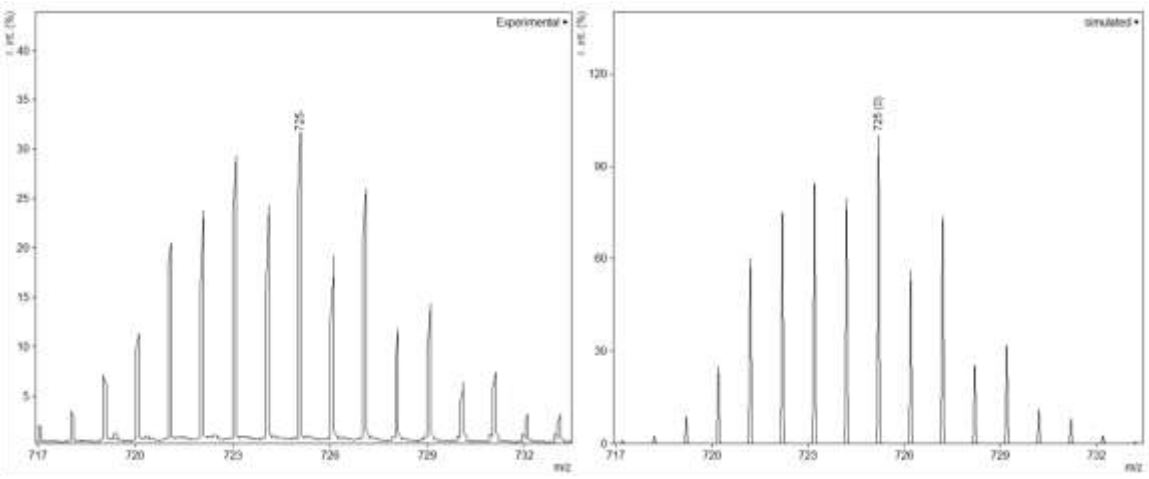

Fig. 6.2. 9: ESI mass spectra of 2g, showing the observed (left), and simulated (right) isotopic distribution pattern

The formation of the C_{2v} symmetry product **2g** is evident, attempts at obtaining single crystals suitable for single crystal X-ray crystallography proved futile.

Considering the fact that methylation of **2b** $[L^2Pd_2Br_3]$ only terminates at the C_{2v} product **2g** $[L^2Pd_2(CH_3)_2Br]$, it does not come as a surprise that **2c** $[L^2Pd_2I_3]$ does not undergo methylation with $SnMe_4$. It is contended that, palladium like platinum, a 'class b' metal (soft acid) has greater bond dissociation energy of the order (M-Cl>M-Br) which results in more stable complexes in bromides than in chlorides in solution and it is a solution phenomena.[222,223]

In this case however, it can be argued that the formation the more strong Sn···Cl bond in $SnMe_3Cl$ acts as a thermodynamic driving force.

As a follow up on the previously made observation that the addition of a large excess of $SnMe_4$ results in the formation of a second but unidentified product, experiments were carried out in attempts at observing and isolating this product. In one such experiment, 40 equivalents $SnMe_4$ were added to a CH_2Cl_2 solution of **2a** with stirring for 48 h (Scheme 6.2. 7).

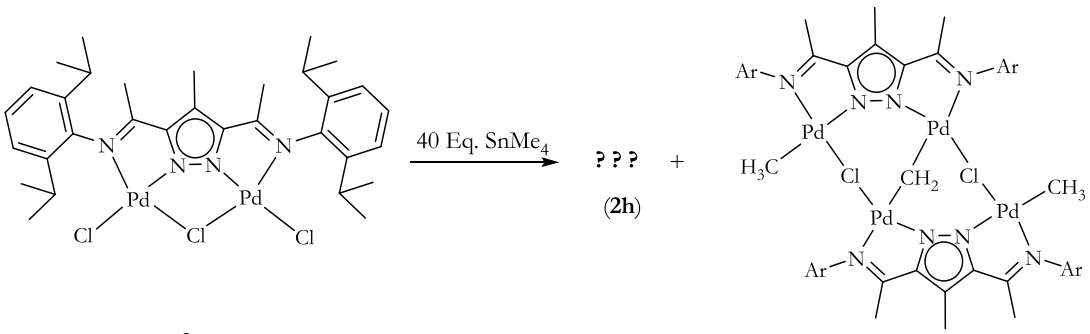

Scheme 6.2. 7: Formation of previously unidentified side product 2h with excess $SnMe_4$ and longer reaction time

After 48 h, the reaction was worked up and all volatiles removed. The ^{1}H NMR spectrum of the reaction mixture showed the formation of the tetrapalladium complex (**XXI**^{c}). Also, the characteristic signal for the bridging μ-CH_2 is observed at 3.89 ppm. However, two new CH_3^{Pz4} peaks were observed downfield at 2.88 and 2.91 ppm, a departure from the ^{1}H NMR spectrum peak of 2.49 ppm that is usually observed for the CH_3^{Pz4} in **XXI**^{c}.

A DOSY NMR experiment performed at 298 K showed a mixture of two distinct compounds, although these two products differed in their diffusion coefficients (7.74 x 10^{-10} m^2s^{-1} for **2h** as against 0.85 x 10^{-9} m^2s^{-1} for **XXI**^{C}.[154] The unidentified product **2h** precipitates as a pale yellow powder with the addition of hexane. Crystals of this new compound were obtained by the slow evaporation of a CH_2Cl_2/hexane solution of the complex at room temperature.

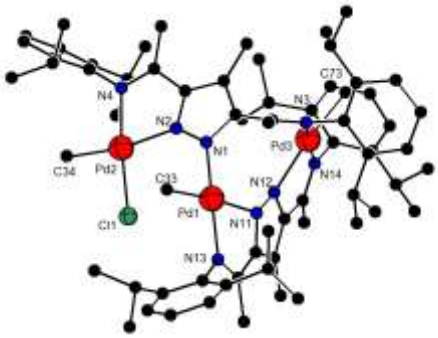

Fig. 6.2. 10: Molecular structure of 2h ($SnMe_3Cl$ omitted), all H atoms omitted for clarity

Single crystal X-ray structure showed it to be a complex of the nature $[L^2_2\{CH_3Pd\}_2\{CH_3PdCl\}(Sn(CH_3)_3Cl)]$ (**2h**) (Fig. 6.2. 10). A molecule of $SnMe_3Cl$ cocrystallizes in the asymmetric unit (not shown). The compound crystallizes in the *P* 21/c

space group. The compound has two ligands bound to three palladium(II) centres in a severely twisted ligand environment.

This new compound **2h** has no μ-CH_2 or μ-Cl environments but features three different CH_3^{Pd} in a bis-chelate ligand environment. One of the CH_3^{Pd} is strongly shielded by two rings of the aryl side arms. There is however no significant difference in the Pd-C bond lengths between the three CH_3^{Pd} environments. The interplanar angle formed by the two pyrazolyl rings is severely twisted at 72.4°. Selected bond lengths [Å] and bond angles [°] are given in Table 6.2. 3.

Table 6.2. 3: Selected bond lengths [Å] and bond angles [°] for 2h

Bond lengths [Å]		Bond angles [°]	
Pd(1)-N(1)	2.017(5)	N(1)-Pd(1)-C(33)	89.32(2)
Pd(1)-C(33)	2.031(5)	N(1)-Pd(1)-N(11)	94.50(17)
Pd(2)-C(34)	2.019(5)	C(33)-Pd(1)-N(11)	175.78(2)
Pd(2)-N(4)	2.067(5)	N(13)-Pd(1)-N(11)	78.34(17)
Pd(3)-C(73)	2.037(6)	C(34)-Pd(2)-N(4)	93.10(2)

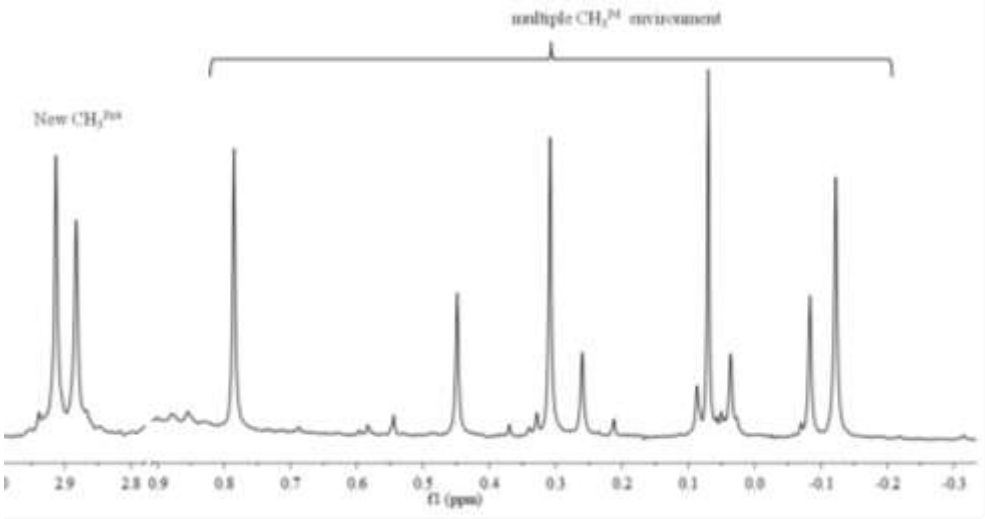

Fig. 6.2. 11: ^{1}H NMR spectrum (selected window) of 3h showing the different CH_3^{Pd} and CH_3^{Pz4} environments measured in $CDCl_3$ at room temperature

The ^{1}H NMR spectrum of **2h** shows multiple CH_3^{Pd} environments at δ: -0.12, -0.08, 0.31, and 0.45 ppm, due to isomers formed from the chloride ligand adopting a *cis* or *trans*

orientation in relation to the imine (Fig. 6.2. 11). In addition, two CH_3^{Pz4} peaks are observed downfield at 2.88 and 2.91 ppm. This is departure from the ^{1}H NMR spectrum peak of 2.49 ppm observed for the CH_3^{Pz4} of the tetrapalladium complex (in $CDCl_3$).

The ESI-MS of **2h** also shows patterns with m/z values of 1329 (55%), 1314 (20%) and 1299 (100%) which can be assigned to $[L^2{}_2Pd_3(CH_3)_3]^+$, $[L^2{}_2Pd_3(CH_3)_2]^+$ and $[L^2{}_2Pd_3(CH_3)]^+$ fragments respectively. Surprisingly by treating the C_{2v} intermediate **2f** with excess $SnMe_4$ for 72 h, **2h** is again formed. This confirms that the formation of **2h** is indeed influenced by excess $SnMe_4$ and longer reaction times.

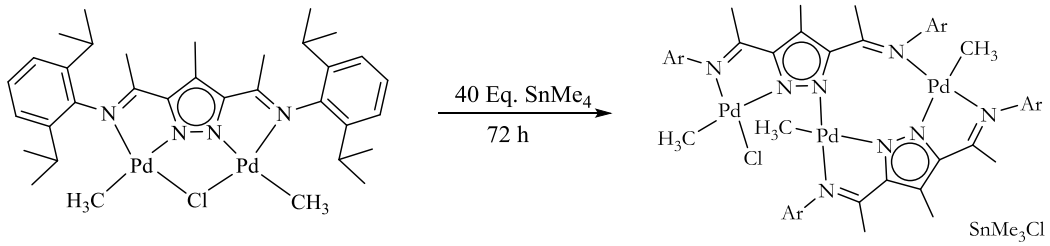

2f **2h**

Scheme 6.2.8: Scheme showing the formation of 2h from treatment of 2f with excess $SnMe_4$

The formation of **2h** is a competing reaction route to the formation of the tetrapalladium complex, **XXI**^{c}, since the addition of excess $SnMe_4$ to **XXI**^{c} does not result in the formation of **2h**, but both are formed concurrently in the same reaction medium. The higher the concentration of $SnMe_4$ and longer reaction time applied, the greater the proportion of **2h** formed in relation to the tetrapalladium complex.

In a separate experiment, single crystals of another side product of the nature $[H_2L^2{}_2Pd][Sn(CH_3)_2Cl_2]_2$ (**2i**) were isolated, however not enough material was available for further characterization. The product **2i** was isolated from a solution containing single crystals of **XXI**^{c} submitted for analysis. In **2i**, the two of the imine nitrogen atoms are protonated in a $[(HL^2)_2Pd]^{2+}$ cationic complex with two $[Sn(CH_3)_2Cl_3]^-$ counterions. This point to the possible release of HCl in the reaction sequence. The molecular structure is shown in Fig. 6.2. 12. As well as selected bond lengths and angles given in Table 6.2. 4.

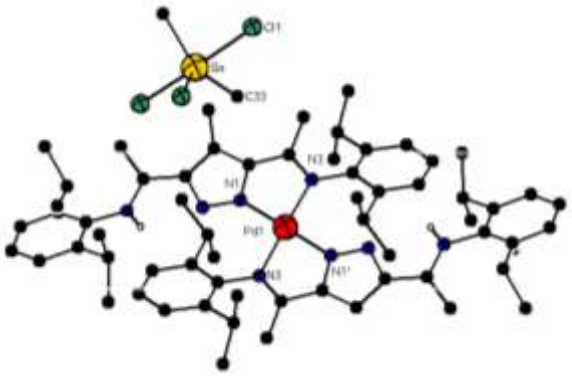

Fig. 6.2. 12: Molecular structure of 2i, most H atoms and one $[Sn(CH_3)_2Cl_3]^-$ molecule, omitted for clarity

The coordination environment around the palladium centre in **2i** is perfectly square planar, the sum of the angles making up the square plane defined by the atoms N(1)/(N(1')/N(2)/N(2) equalling 360°. The interplanar angle defined by the aryl ring and the pyrazole ring with each ligand is nearly perpendicular at 85.7°. The Pd(1)-N(1) and Pd(1)-N(3) bond distance are 1.99 Å and 2.04 Å respectively. Selected bond lengths [Å] and bond angles [°] are given in Table 6.2. 4.

Table 6.2. 4: Selected bond lengths [Å] and bond angles [°] for 2i

Bond lengths [Å]		Bond angles [°]	
Pd(1)-N(1)	1.995(2)	N(1)-Pd(1)-N(1)	180.00(1)
Pd(1)-N(3)	2.041(2)	N(1)-Pd(1)-N(3)	78.79(10)
Sn(1)-C(33)	2.108(5)	C(5)-N(3)-C(7)	121.20(2)
Sn(1)-Cl(1)	2.6560(9)	C(7)-N(3)-Pd(1)	122.10(18)

A third crop of crystals isolated after several days from the same reaction medium showed a completely different ^{1}H NMR spectrum. Crystalline material obtained showed only a single peak for the CH_3^{Pd} group at 0.27 ppm. Attempts to isolate crystals suitable for X-ray crystallography failed. The ESI-MS of this complex shows no large molecular aggregates as seen for **2h**. However, common m/z distributions such as 759 (20%), 725 (100%) and 693 (100%) which can be assigned to $[L^2Pd_2(CH_3)_2Cl]^+$, $[L^2Pd_2(CH_3)_2]^+$, and $[L^2Pd_2]^+$ respectively are observed. DOSY NMR experiments were made on the obtained complexes.

The diffusion coefficients obtained for the observed complexes and intermediates are listed in Table 6.2. 5. An example of a DOSY spectrum is that of **2g** shown in Fig. 6.2. 13, the DOSY spectrum shows only one level diffusion rate and small signals from solvents such as CD_2Cl_2.

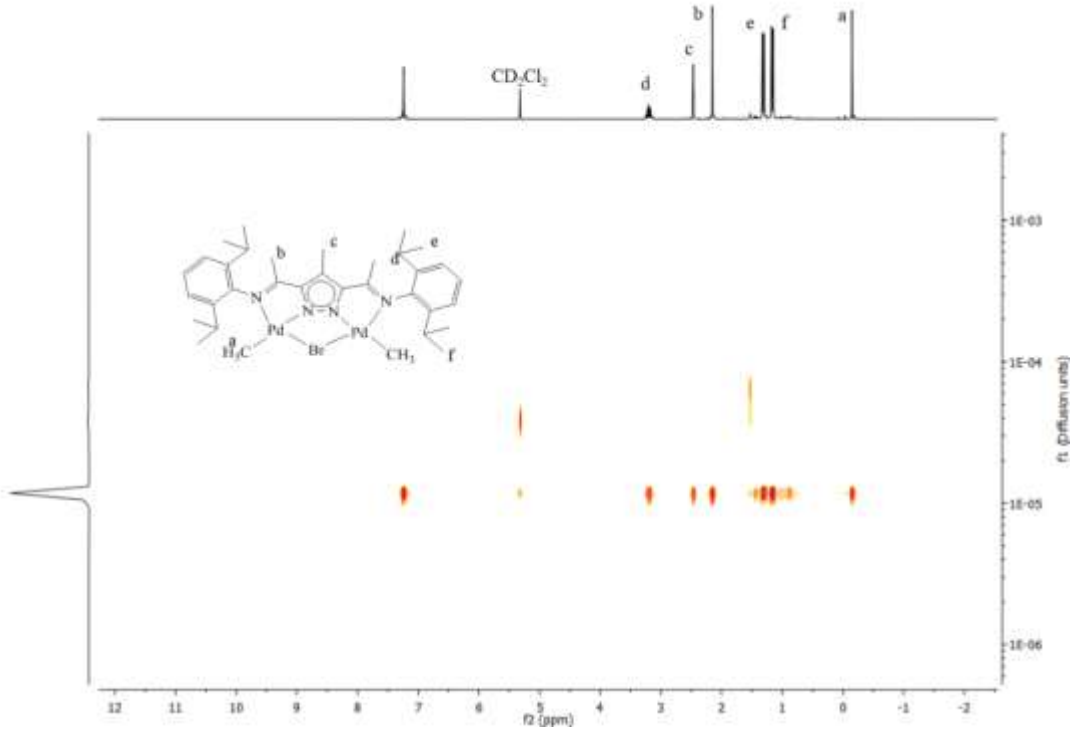

Fig. 6.2. 13: DOSY NMR spectrum of 2g measured in CD_2Cl_2 at room temperature

Table 6.2. 5: Table of diffusion constants for the various palladium complexes

Compound	**(diffusion units)/ cm^2s^{-1}**	**(D)/ m^2s^{-1}**	**log (diffusion units)/ m^2s^{-1}**
$[L^2Pd_2I_3]$ (**2c**)	1.00 x 10^{-5}	1.00 x 10^{-9}	-9.00
$[L^2Pd_2(\mu\text{-}Cl)(CH_3)_2]$ (**2f**)	1.00 x 10^{-5}	1.00 x 10^{-9}	-9.00
$[L^2Pd_2(\mu\text{-}Br)(CH_3)_2]$ (**2g**)	1.29 x 10^{-5}	1.29 x 10^{-9}	-8.89
$[L^2{}_2\{CH_3Pd\}\{CH_3PdCl\}(Sn(CH_3)_3Cl)]$ (**2h**)	7.74 x 10^{-6}	7.74 x 10^{-10}	-9.91

Diffusion coefficient (m^2s^{-1}) values of 1.29 x 10^{-9} were obtained for **2g** compared to 1.00 x $10^{-9}m^2s^{-1}$ for **2f**. The diffusion coefficient of **2f** is smaller compared to that of **2g** due to the larger size of the bromide compared to the chloride. As expected, the diffusion coefficient for **2f** and **2g** is of a magnitude larger compared to **2h** (7.74 x 10^{-10} m^2s^{-1}).

The possibility of the methylene bridge originating from the insertion of methylene chloride into a low valent palladium species can be ruled out as experiments performed in CD_2Cl_2, $CDCl_3$ and chlorobenzene, all yield the tetrapalladium unit **XXI**[c]. It must however be stressed that the formation of **XXI**[c] is dependent on the use of chlorinated solvents. Based on observed results, a modified scheme (Scheme 6.2.9) to explain the formation of the observed products is shown below.

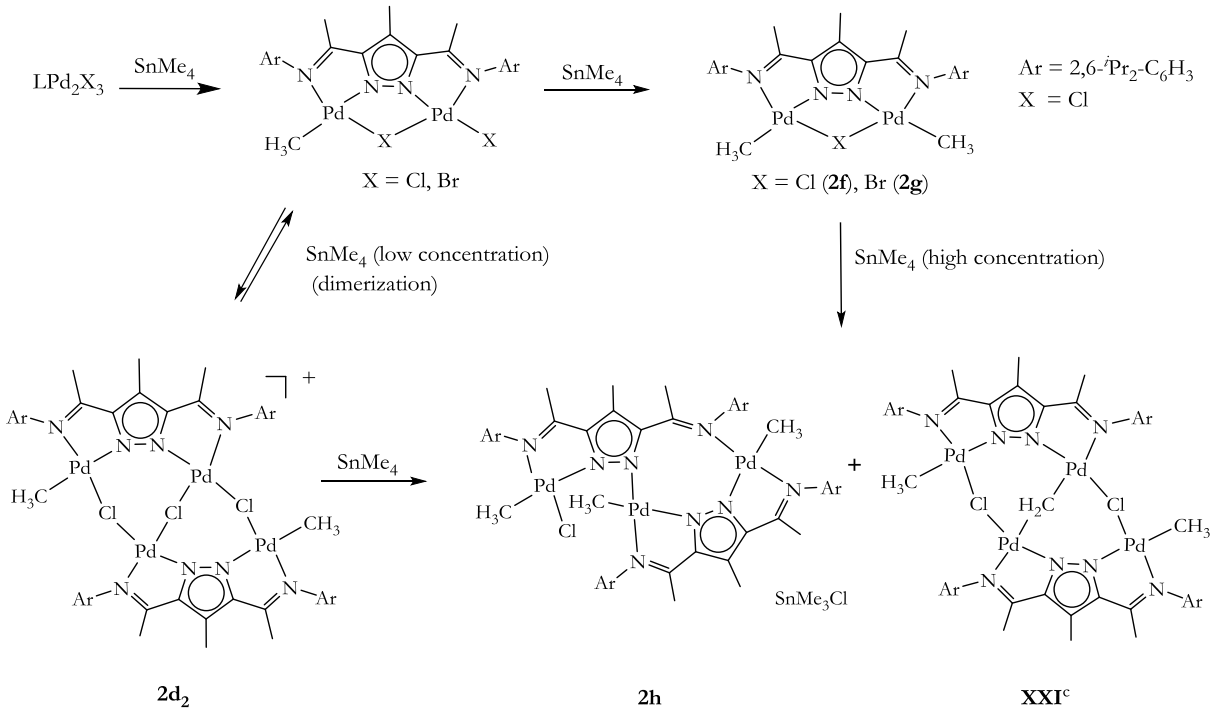

Scheme 6.2.9: Reaction scheme to the formation of XXI[c]

At low $SnMe_4$ concentrations, the C_s symmetric product dimerizes to form **2d$_2$**, which is in a reversible equilibrium with the C_s symmetric product. In the presence of $SnMe_4$, it reacts further to form a mixture of **2h** and **XXI**[c].

Using **1a**, it was possible to isolate the tetrapalladium derivative of L^1 [$L^1_2Pd_4(\mu\text{-}CH_2)(\mu\text{-}Cl)_2(CH_3)_2$] (**2k**) after 18 h in 39% yield. A second yet to be identified side product **2j** is formed in 38% yield.

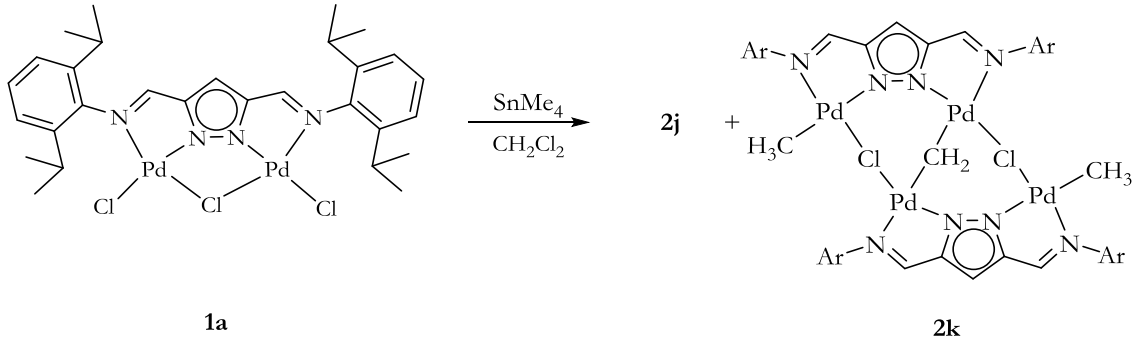

Scheme 6.2. 10: Synthetic scheme for the preparation of 2k

In **2k**, the bridging μ-CH_2 is observed at 4.23 ppm whiles the CH_3^{Pd} is observed at -0.03 ppm, compared to **XXI**[c] where the μ-CH_2 is observed at 3.96 ppm and the CH_3^{Pd} peak at 0.06 ppm (in $CDCl_3$). The CH^{Pz} is observed as a singlet at 6.98 ppm, whiles the CH=N peaks are observed as singlets at 7.91 and 8.04 ppm respectively (Fig. 6.2. 14).

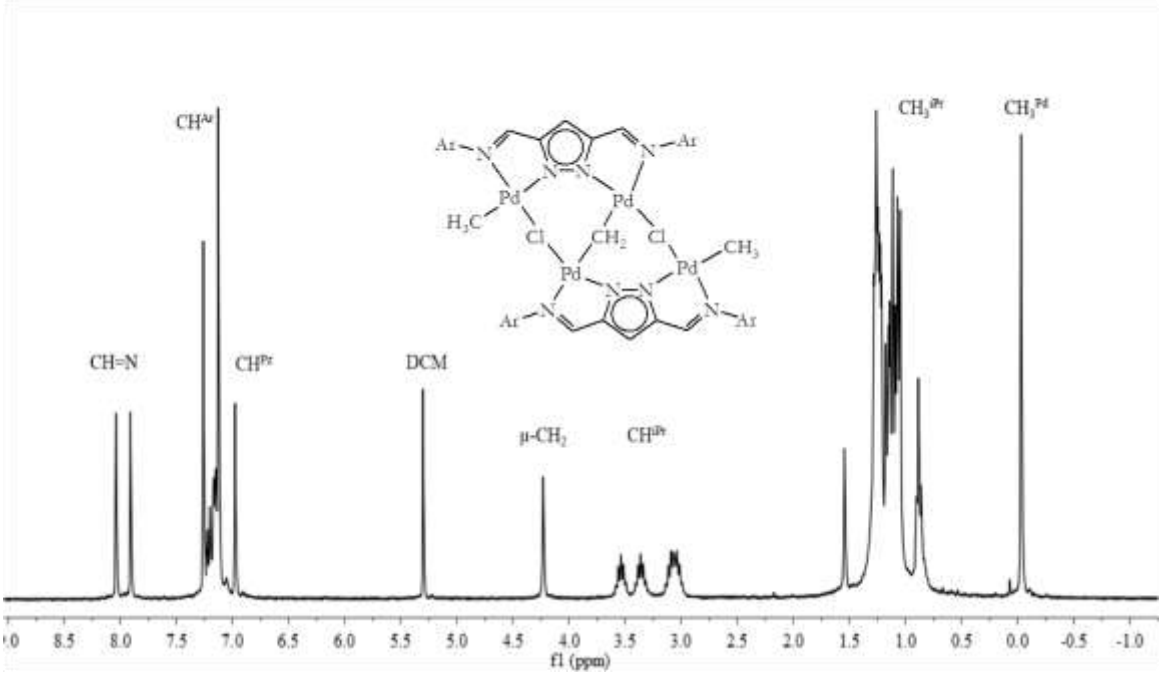

Fig. 6.2. 14: ^{1}H NMR spectrum of 2k measured in $CDCl_3$ at room temperature

Crystals of **2k** were obtained by the slow diffusion of hexane into a CH_2Cl_2 solution of the complex at -10°C. The molecular structure of **2k** is shown in Fig. 6.2. 15. The complex crystallizes in the *P* 21/c space group.

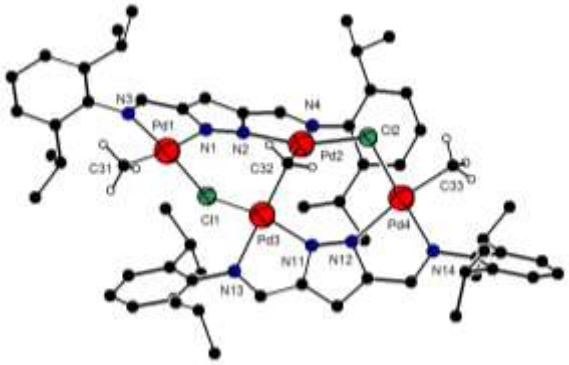

Fig. 6.2. 15: Molecular structure of 2k with most H and solvents omitted for clarity

The coordination around the palladium(II) centres in **2k** is a distorted square planar with two squares connected at one corner by a μ-CH_2. The bridged Pd(2)···Pd(3) bond distance is 3.00 Å in the imine (**2k**), compared to 3.27 Å in **XXI**[c]. Thus, the flexibility of the μ-CH_2 allows for the expansion of the Pd···Pd distance in this complex. The torsional angle formed by the two Pd centres and the two pyrazolyl nitrogen atoms (Pd-N-N-Pd) is less (30.5°) in **2k** compared to **XXI**[c] (50.1°). In addition, the bite angle N-Pd-N in **2k** (78.8°) is slightly greater than that of **XXI**[c] (76.0°). The Pd-C(sp^3) distance, 2.024(4) [Å] is comparable to that found for other Pd-C bonds. [224,225]

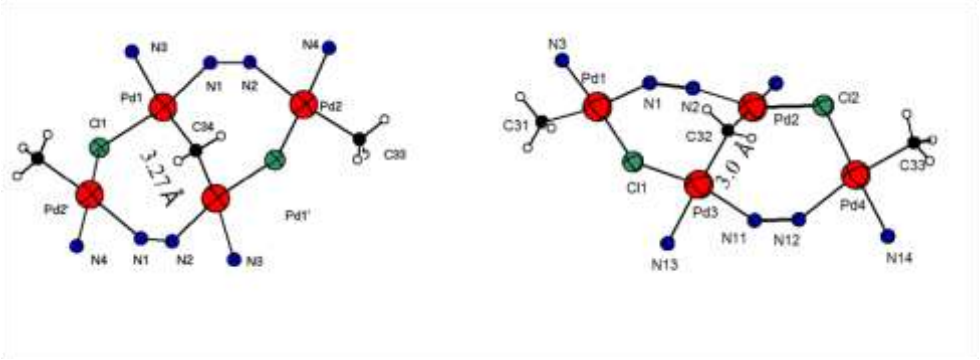

Fig. 6.2. 16: Drawings comparing the bond lengths of the bridged palladium atoms in XXI[c] (left) and 2k (right)

Although the Pd···Pd distance in **2k** is 3.00 Å, there appears to be no basis to speculate the presence of a Pd···Pd metal bond from the formal electron count on the Pd atoms. The Pd···Pd distance is in the range of other reported bridged palladium(II) complexes.[226,227,228] In addition, the Pd(2)-C(32)-Pd(3) angle in **2k** (98.6°) is less acute compared to other complexes with metal-metal bonds (75-78°) with bridging μ-CH_2 group.[229,230]

However it is still in the in the range of μ-CH_2 complexes, which have no metal-metal bonds

(89-123°).[231] Selected bond lengths and bond angles for **2k** are given in Table 6.2. 6.

Table 6.2. 6: Selected bond lengths [Å] and bond angles [°] for 2k

Bond lengths [Å]		Bond angles [°]	
Pd(1)-C(31)	2.023(4)	Pd(2)-C(32)-Pd(3)	98.57(170)
Pd(1)-N(1)	2.185(3)	N(1)-Pd(1)-Cl(1)	103.75(9)
Pd(1)-Cl(1)	2.2983(10)	C(32)-Pd(2)-Cl(2)	88.75(12)
Pd(2)-Pd(3)	3.008(4)	C(32)-Pd(2)-N(2)	98.27(14)

As stated earlier, this complex constitutes only 39% of the reaction product. A second competing reaction product **2j** was isolated (38%). However, the lack of a crystal structure from this complex leaves room for speculation, **2j** lacks a μ-CH_2 bridge and is possibly analogous to the compound $[L^2_2\{CH_3Pd\}_2\{CH_3PdCl\}(Sn(CH_3)_3Cl)]$ (**2h**) formed with excess $SnMe_4$.

Olefin coupling reactions with tetrapalladium complex

Previous work done on this unique complex **XXI**[c] shows it actively dimerizes ethylene to a mixture of propenes and butenes (Scheme 6.2.11). The major product formed with ^{13}C labelled ethylene ($^{13}C_2H_4$) is propene, which contained only two ^{13}C labels, with the origin of the unlabeled C_1 unit purported to have come from either a CH_3 or μ-CH_2 unit of the complex.[154]

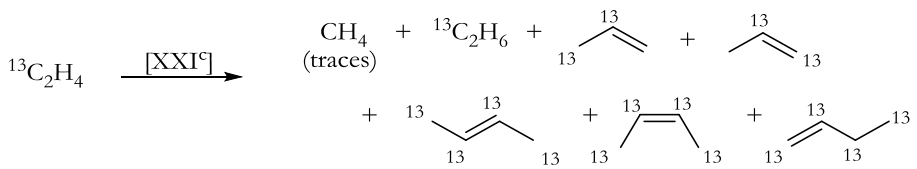

Scheme 6.2.11: Olefins resulting from the reaction of XXI[c] with $^{13}C_2H_4$[154]

This motivated the testing of its reactivity towards a range of other olefins (Scheme 6.2.12).

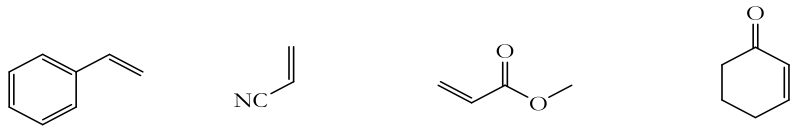

Scheme 6.2.12: Range of olefins tested in coupling reactions with XXI^c

Results obtained showed that solutions of the complex with olefins alone fail to give any observable products when monitored over several days. Activated olefins such as tetracyanoethylene and tetrachloroethylene were also used in an attempt to obtain stable complexes. However, these failed to yield any reliable results as the spectrum of products obtained were difficult to interpret; ESI-MS neither yielded any reliable data.

However, in the presence of chloride abstracting reagents, notable changes in the spectrum are observed. Tests with two different chloride abstracting reagents were performed, mainly $NaBAr^F_4$ and AgOTf. It therefore seems plausible, that with the addition of AgOTf, there is abstraction of the halide to form a highly reactive but unstable cationic $[L^2_2Pd_4(\mu\text{-}CH_2)(\mu\text{-}CH_3)_2]^{2+}$ complex (**2l**) (Scheme 6.2.13).

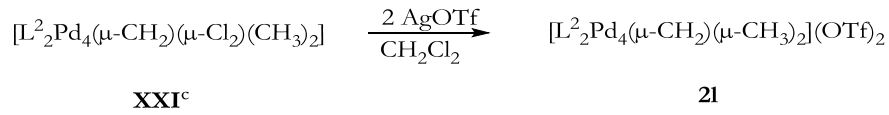

Scheme 6.2.13: Scheme for the reaction of XXI^c with AgOTf to form 2l

Partial characterization of **2l** by ^1H and ^{13}C NMR spectroscopy was made as well as ESI-MS, which showed a dominant m/z peak at 1474 (100%) which can be assigned to $[L^2_2Pd_4(\mu\text{-}CH_2)(\mu\text{-}CH_3)_2(H_2O)_2]^{2+}$.

In **2l**, the CH_3^{Pd} and bridging μ-CH_2 peaks are observed at 0.03 and 4.15 ppm respectively, whiles the $CH_3C{=}N$ groups are observed as a singlet at 2.18 ppm and CH_3^{Pz4} at 2.53 ppm. This point to a symmetric ligand environment, compared to peaks at 0.06 (CH_3^{Pd}), 3.96 (μ-CH_2), 2.05 ($CH_3C{=}N$), 2.10 ($CH_3C{=}N$) and 2.47 (CH_3^{Pz}) ppm in the educt **XXI^c**.

To test if **2l** is a reactive intermediate, two sets of experiments were performed. The first experiment involved treating a 1:0.8 mixture of **XXI^c** and styrene-d_8 with 2 equivalents AgOTf. The reaction sequence was monitored at room temperature over several hours. After 5 hr when all styrene-d_8 is depleted, a new μ-CH_2 is observed at 4.15 ppm. In a control

experiment, treatment of **XXI**^{c} with 1.5 equivalent AgOTf in the absence of styrene sees a gradual build up again of this new μ-CH_2 and a new CH_3^{Pd} peak at 4.15 ppm and 0.03 ppm respectively (Fig. 6.2. 17).

These peaks are the same as those observed for **2l**. The intensity of this new μ-CH_2 diminishes with time, with the concomitant formation of methane, whiles the unreacted μ-CH_2 remains unchanged.

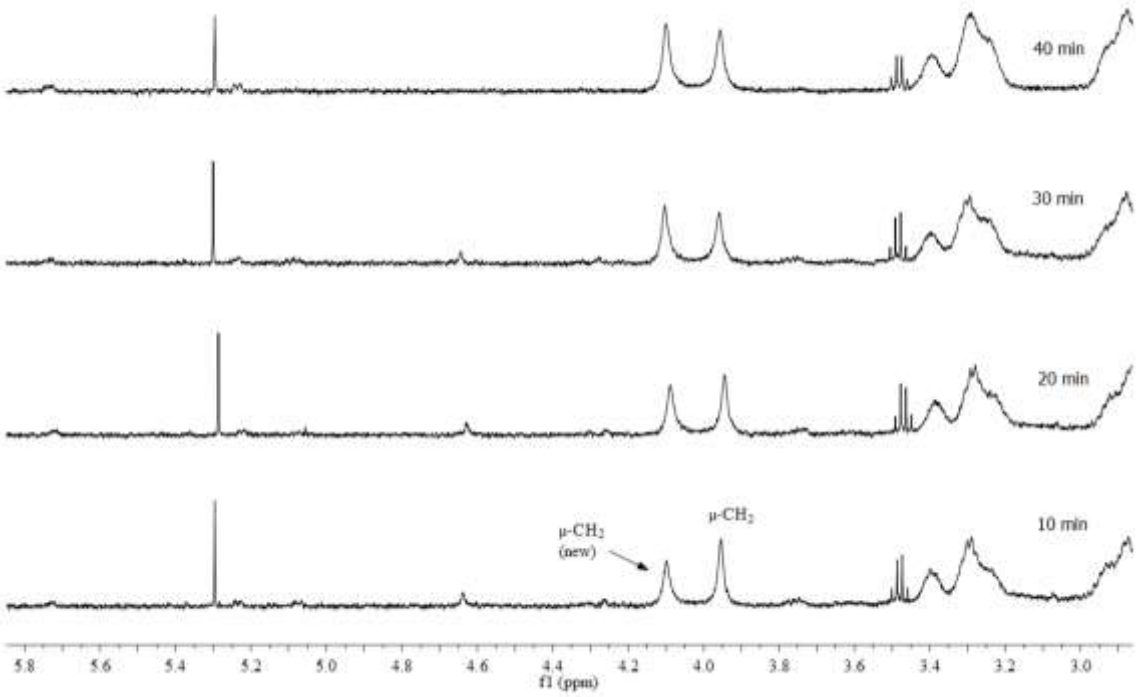

Fig. 6.2. 17: Stacked ^{1}H NMR spectra showing the formation of a new μ-CH_2 (2l) environment from XXI^{c} after addition of AgOTf with time measured in $CDCl_3$ at room temperature

In another experiment, **XXI**^{c} was treated with 2 mol equivalents AgOTf at room temperature in $CDCl_3$ to form again **2l** and the AgCl precipitate quickly filtered over celite.

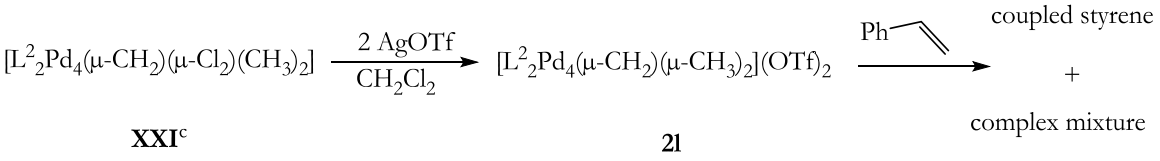

Scheme 6.2. 14: Styrene coupling reaction of XXI^{c} after activation with AgOTf

With the subsequent addition of styrene to **2l**, a new CH_3 environment forms at 1.90 ppm, with the concomitant depletion in the signal intensity of the μ-CH_2 in **2l** (Fig. 6.2. 18).
However, when AgOTf is added as the last step to a mixture of **XXI**[c] and excess styrene, no new μ-CH_2 environment is observed, thus the formation of **2l** is not observed. This suggests the μ-CH_2 group is immediately coupled to the olefin upon chloride abstraction. In addition, with the addition of a chloride-abstracting agent, an increase in signal intensity at 5.30 ppm (same shift as CH_2Cl_2) is observed, possibly pointing to a pathway, which may involve the reductive elimination of CH_2Cl_2.

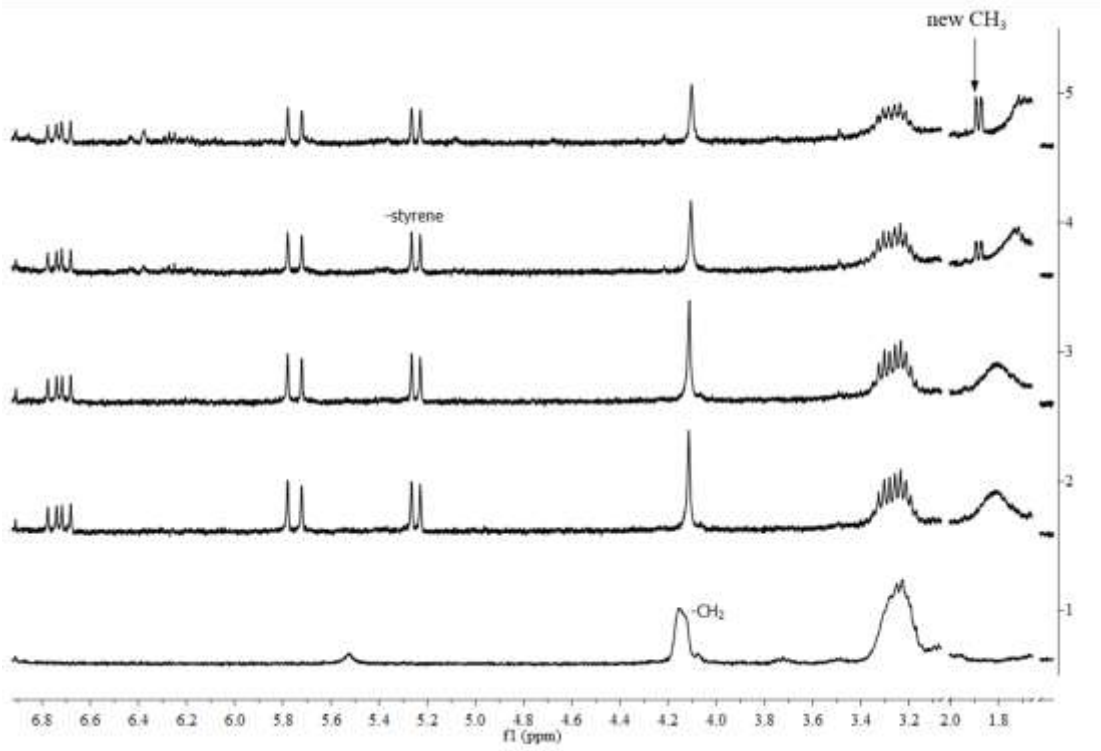

Fig. 6.2. 18: ^{1}H NMR spectra showing the depletion of the new μ-CH_2 environment in 2l and subsequent formation of a new CH_3 environment after addition of styrene measured in $CDCl_3$ at room temperature over a 4 h period

After workup, the crude reaction mixture was obtained as yellow oil. The ^{1}H NMR spectrum of this product (Fig. 6.2. 19) shows two well separated sets of olefin signals which can be assigned to free styrene and a modified styrene molecule. This modified styrene molecule has strong correlations in the olefin region to the new CH_3 environment at 1.90 ppm.

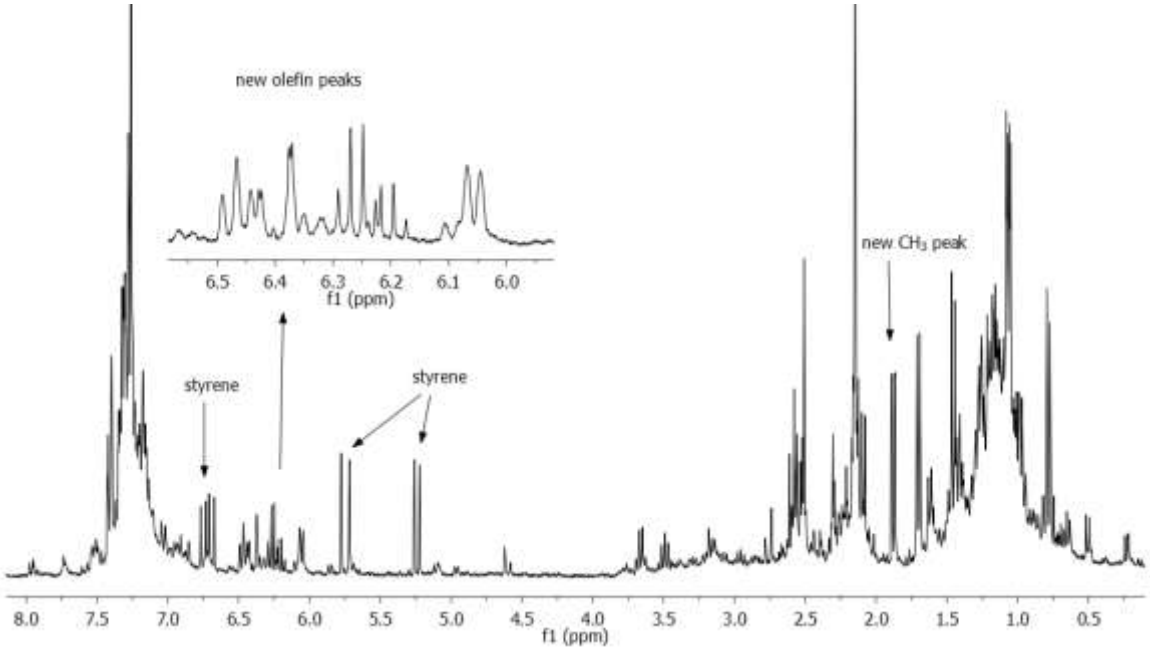

Fig. 6.2. 19: ^{1}H NMR spectrum of crude reaction mixture after treatment of XXI^{c} with AgOTf in the presence of styrene measured in $CDCl_3$ at room temperature

When styrene-d_8 is used in place of normal styrene, there appears to be extensive scrambling of this CH_3 environment at 1.90 ppm. In both cases, the initial bridging μ-CH_2 at 3.96 ppm is also evidently missing from the ^{1}H NMR spectrum.

The product was later identified by NMR analysis to be propenylbenzene. Detailed analysis of the spectrum shows that both *E*- and *Z*-forms of the propenylbenzene are formed in a 50:50 ratio. The ^{1}H assignments for the *cis* and *trans* isomers are shown (red) and their ^{13}C correlations (blue) (Fig. 6.2. 20).

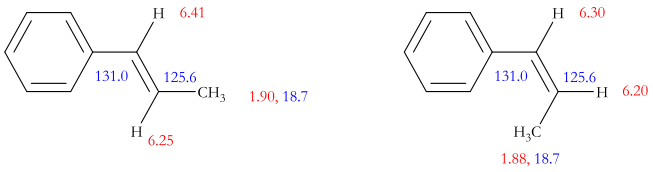

Fig. 6.2. 20: ^{1}H and ^{13}C NMR chemical shifts for *cis* and *trans* propenylbenzene

Based on results obtained and using styrene-d_8 in place of styrene, the origin of the bridging μ-CH_2 unequivocally is from the μ-CH_2 in **XXI^{c}**. The ^{1}H NMR spectrum of the deuterated propenylbenzene shows scrambling/deuterium exchange in the methyl protons as shown in Fig. 6.2. 21 (right).

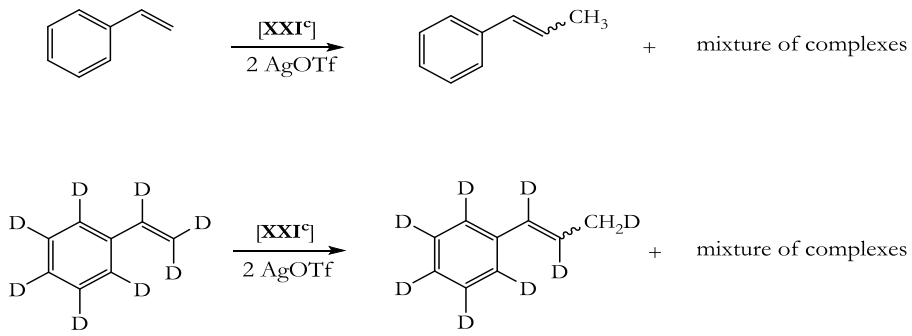

Scheme 6.2.15: Scheme showing the formation of (*E*/*Z*)-prop-1-en-1-ylbenzene

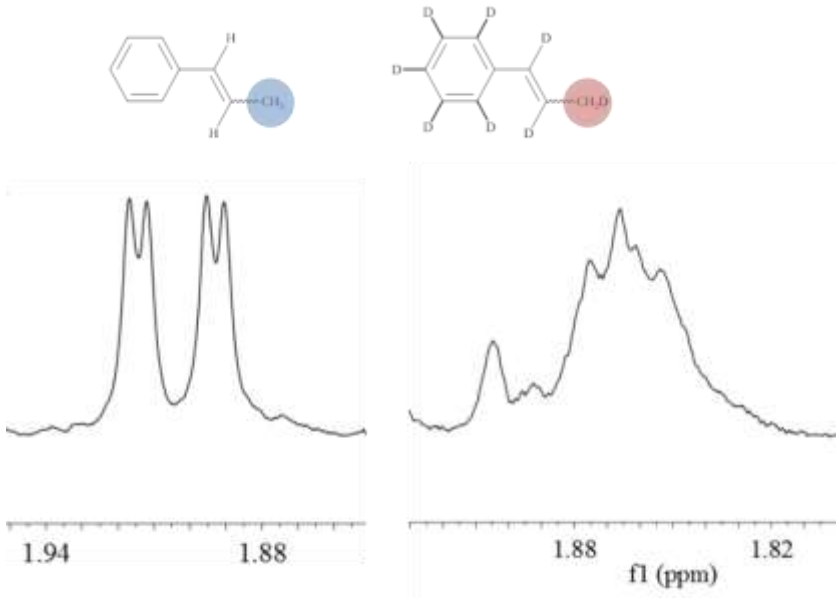

Fig. 6.2. 21: ^{1}H NMR spectra showing the CH_3 region of propenylbenzene formed from deuterated styrene (right) and normal styrene (left) measured in $CDCl_3$ at room temperature

To gain more insights in the mechanism involved in the transfer of the μ-CH_2 to the olefin, further kinetic studies were conducted. In a variable temperature experiment, the transfer of μ-CH_2 is only observed at temperatures exceeding 10°C, at lower temperatures, transfer does not take place, neither is the formation of Pd-H species observed at low temperatures. The sequential formation of propenylbenzene from styrene and **XXI**^{c} was monitored over a 24 h period. The graphical representation of several decays within the complex with the addition of chloride abstracting agents and styrene are shown in (Fig. 6.2. 22 and Fig. 6.2. 23).

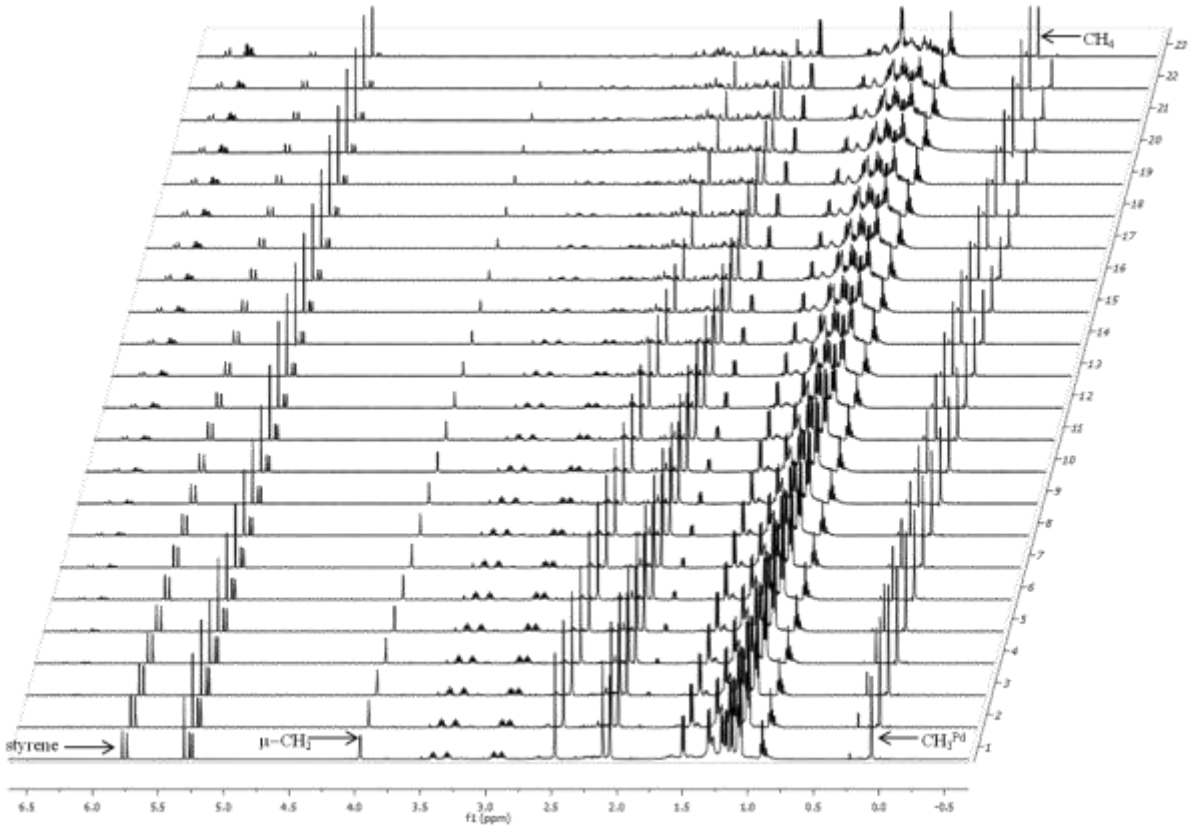

Fig. 6.2. 22: Stacked ^{1}H NMR spectra showing the formation propenylbenzene and depletion of the μ-CH_2 in XXI^c measured in $CDCl_3$ at room temperature over a 24 h period

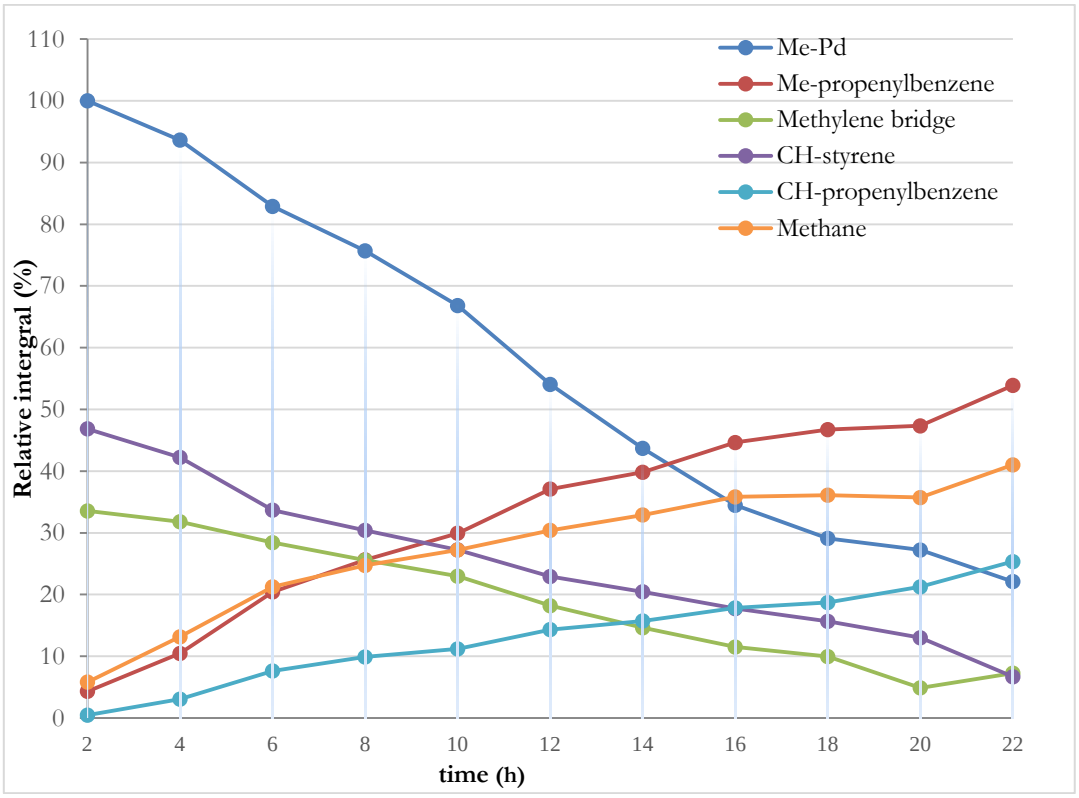

Fig. 6.2. 23: Graphical representation of decays in XXI^c and subsequent propenylbenzene formation from styrene after activation measured in $CDCl_3$ at room temperature

From the graphical representation, it is observed that the formation of propenylbenzene has a direct relation to the release of CH_4 from the reaction. An inverse relation is observed between the rise in propenylbenzene formation with the rate of depletion of the μ-CH_2 and the depletion of styrene. In addition, the rate of depletion of the μ-CH_2 is proportional to the rate of consumption of styrene. Generally, the complete consumption of styrene required *ca* 24 h. Table 6.2. 7 summarize attempts at investigating further, the scope of olefins that are reactive towards **XXI**[c].

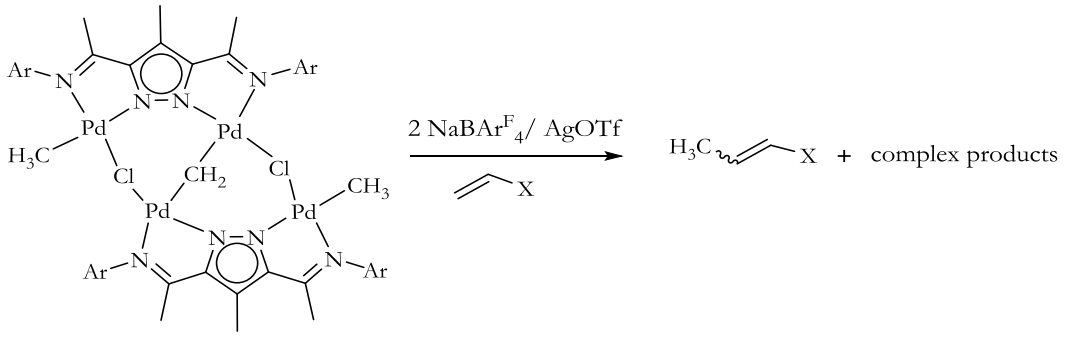

Ar = 2,6-^{i}Pr$_2$-C_6H_3

XXI[c]

Scheme 6.2.16: Olefin coupling reactions of XXI[c] after activation

Table 6.2. 7: Table of results of olefin coupling reactions and conversion (%) obtained with XXI[c]

Substrate	Product	Conversion[a](%)
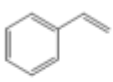	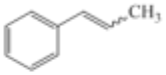	98
		88
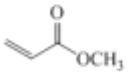	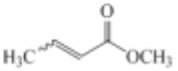	77
	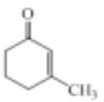	34

[a]conversions obtained by ^{1}H NMR spectroscopy

The general observations are that, **XXI**[c] is active towards different olefins, ranging from aliphatic to cyclic, electron deficient as well as electron rich olefins.

Generally, conversions are better with terminal olefins compared to cyclic olefins, as seen in conversions of 77-98% observed with styrene and acrylonitrile, compared to 34% conversion in the case of cyclohexenone. Electron deficient olefins generally give lower conversion in relation to the use of electron rich olefins. In addition, irrespective of the olefin used, 2,1-insertion product is favoured.

The crude reaction after olefin coupling was workup by drying under high vacuum overnight, followed by gradient elution (ether/methanol) on a micro column, which results in the isolation of a number of fractions/products (Scheme 6.2.17).

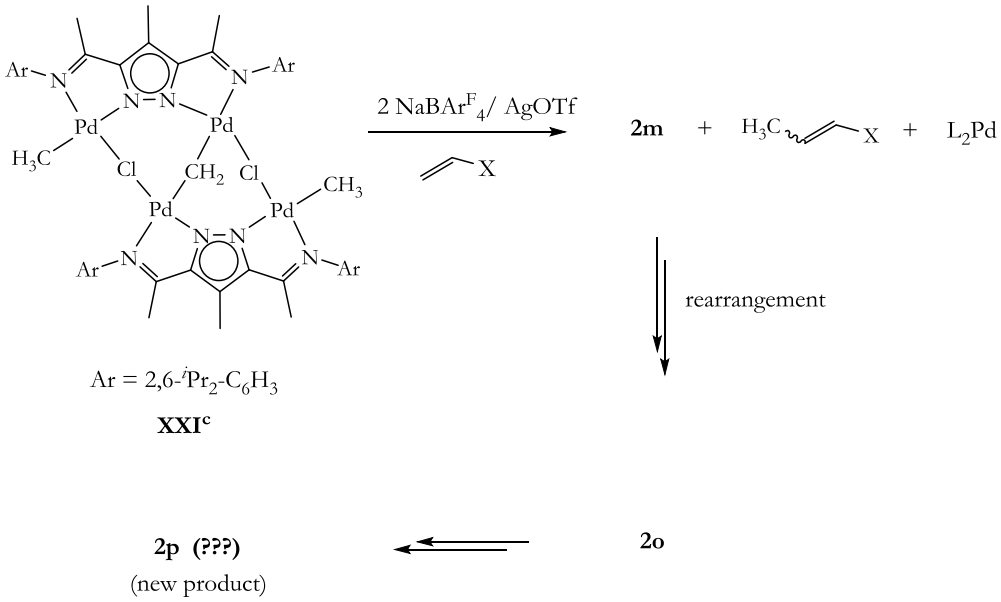

Scheme 6.2.17: Scheme showing the formation of rearrangement products after activation

An L^2_2Pd product is eluted from the column first with ether. This was confirmed by ^{1}H NMR spectroscopy and ESI-MS of the product with m/z values at 1073(100%) which can be assigned to $[L_2Pd]^+$. Another fraction (**2m**) was washed from the column using methanol. The ^{1}H NMR spectrum of **2m** was monitored over a period of 24 h. Although **2m** initially showed only one CH_3^{Pd} peak at 0.73 ppm, further changes takes place.

There is the loss of methane, followed by the appearance of three different CH_3^{Pd} peaks at 0.43, 0.12, and 0.00 ppm respectively. A CH_2Cl_2 solution of **2m** when kept at -20^{o}C for several weeks results in the isolation of bright red crystals (**2o**) that are stable only at low temperature. Effervescence occurs with the addition of $CDCl_3$ to crystals of **2o**.

The ^{1}H NMR spectra of crystals of **2o** obtained shows an upfield proton at -3.78 ppm, which is of low intensity. However, with time, in addition to the peak at -3.78 ppm, a new ^{1}H NMR

peak is observed further downfield at 14.4 ppm. The ^{1}H peak at -3.78 ppm disappears altogether, leaving only the downfield peak at 14.4 ppm as observed in a new product **2p**. There is a loss of one $[BAr^{F}_{4}]^{-}$ counterion in the transition from **2o** to **2p**. That is, in **2p**, the integration of the $[BAr^{F}_{4}]^{-}$ protons is halved (from 24H to 12H) in relation to **2o** (Fig. 6.2. 24). The instability of **2o** therefore hampered its thorough characterization.

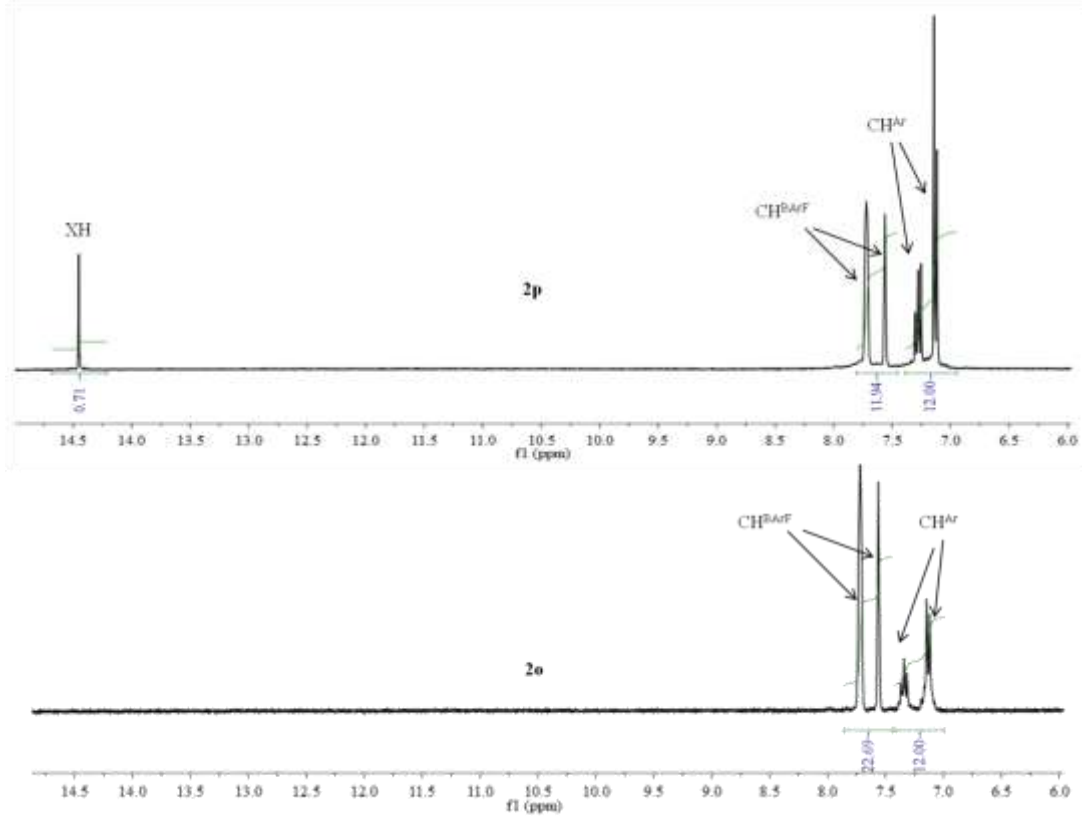

Fig. 6.2. 24: ^{1}H NMR spectra of the aromatic region of complexes 2p and 2o measured in $CDCl_3$ at room temperature

In **2p**, the CH_3^{iPr} groups are observed as two doublets at 1.14 and 1.30 ppm (1.14 and 1.41 in **XXI**[b]). The shift to a higher field in one of the CH_3^{iPr} pointing to the possibility that **2p** has stronger electron donating groups.

The downfield ^{1}H NMR spectrum signal initially suspected to be an NH proton, but a ^{1}H-^{15}N HMBC NMR experiment ruled out this possibility since no correlation between this ^{1}H signal and the nitrogen atoms are observed.

Good crystals of **2p** suitable for single crystal X-ray crystallography were obtained after keeping a CH_2Cl_2 solution of the complex at -20°C for several months. From the crystal structure (Fig. 6.2. 25), the downfield ^{1}H signal at 14.4 ppm without ambiguity is assigned to a hydroxide proton. In **2p**, there are two bridging μ-Cl, a μ-OH, and a μ-O group. The compound crystallizes with a molecule of $[BAr^{F}_{4}]^{-}$ counterion, to balance the +2 oxidation

state on all four palladium atoms. The Pd···Pd bond lengths in this complex is very close at 3.14 Å and the Pd-O bond average bond length of 1.96 Å (Table 6.2. 8) are within the range of other reported palladium hydroxide bridged complexes.[232,233]

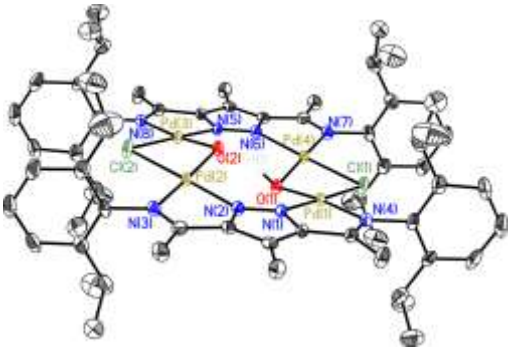

Fig. 6.2. 25: Molecular structure of 2p, most H atoms and one $[BAr^F_4]^-$ counterion, omitted for clarity

Table 6.2. 8: Selected bond lengths [Å] and bond angles [°] for 2p

Bond lengths [Å]		Bond angles [°]	
Pd(1)-Pd(2)	3.145(7)	Pd(1)-O(1)-Pd(2)	106.59(13)
Pd(2)-O(2)	1.962(3)	N(1)-Pd(1)-N(4)	79.83(13)

The ESI-MS data for **2p** further supports the observed structure, *m/z* distribution of 1497 (5%) and 749 (100%) assigned to $[M+1H-BAr^F_4]^{1+}$ and $[M+2H-BAr^F_4]^{2+}$ respectively are observed as shown in (Fig. 6.2. 26).

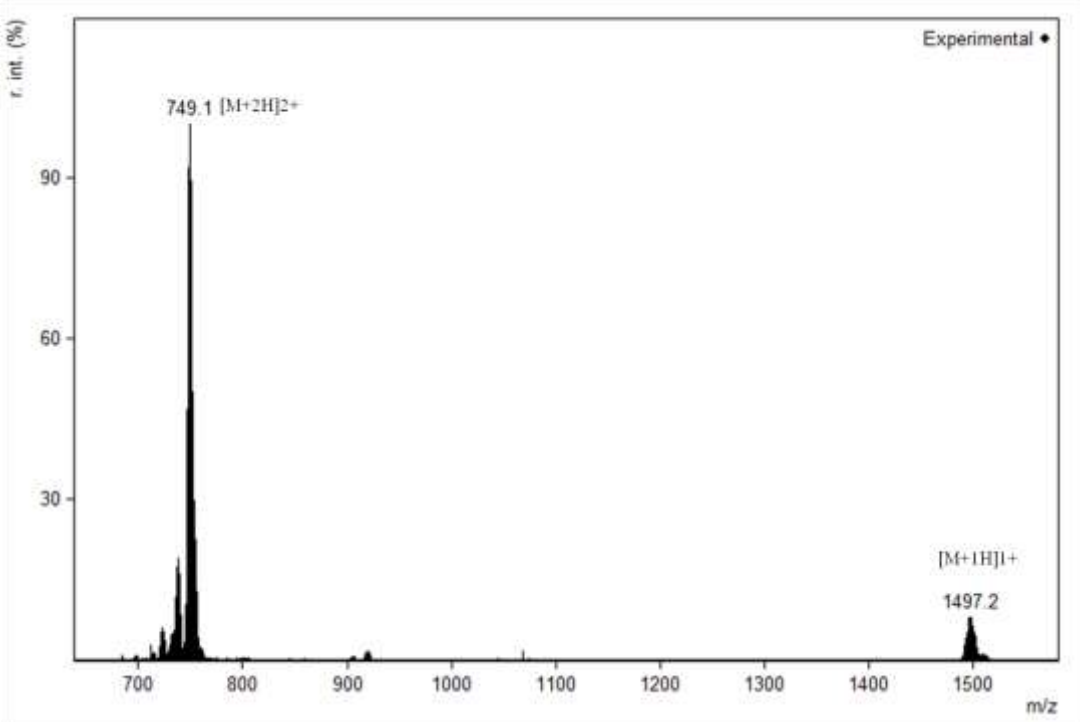

Fig. 6.2. 26: ESI mass spectrum of 2p showing the *m/z* distributions

The observed and simulated isotopic distribution patterns are shown in Fig. 6.2. 27.

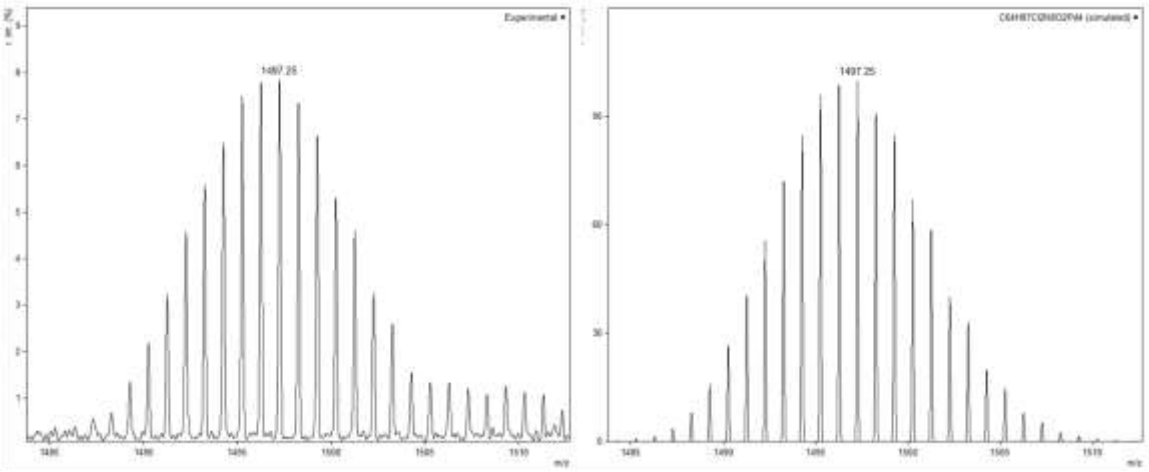

Fig. 6.2. 27: ESI(+) mass spectra of 2p showing observed (left) and simulated (right) isotopic distribution patterns

Irrespective of the nature of the olefin used, the same product **2p** is observed. The complete ^{1}H and ^{13}C NMR assignments of **2p** are shown in Fig. 6.2. 28 and Fig. 6.2. 29 respectively, and are in good agreement with the single crystal X-ray structure.

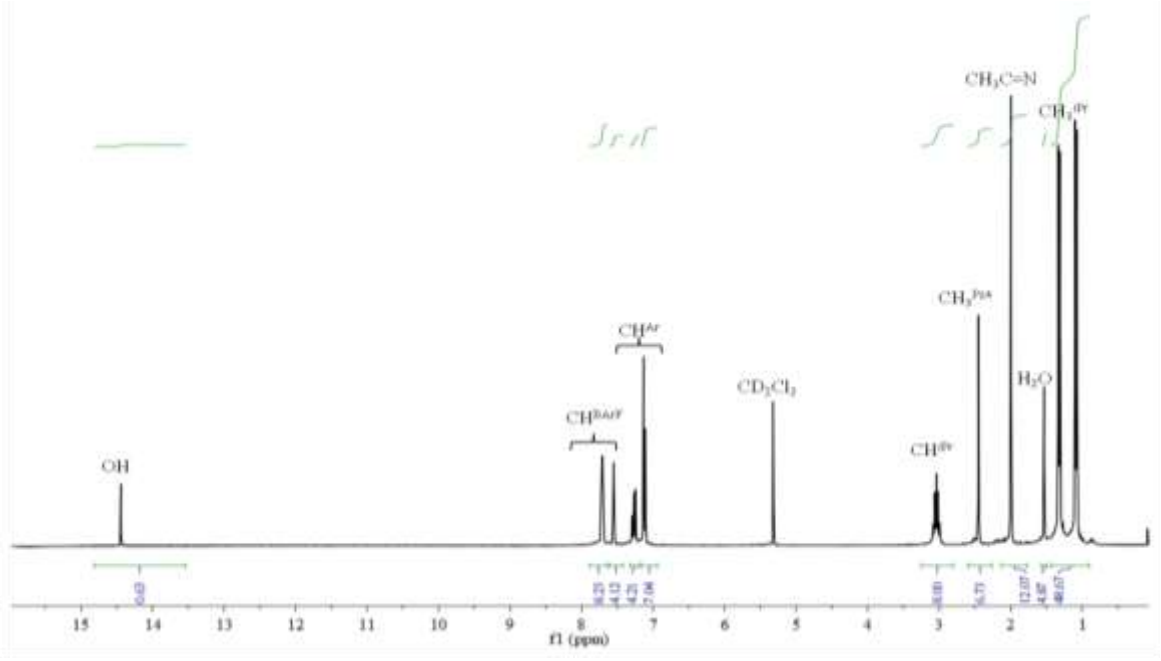

Fig. 6.2. 28: ^{1}H NMR spectrum of 2p measured in CD_2Cl_2 at room temperature

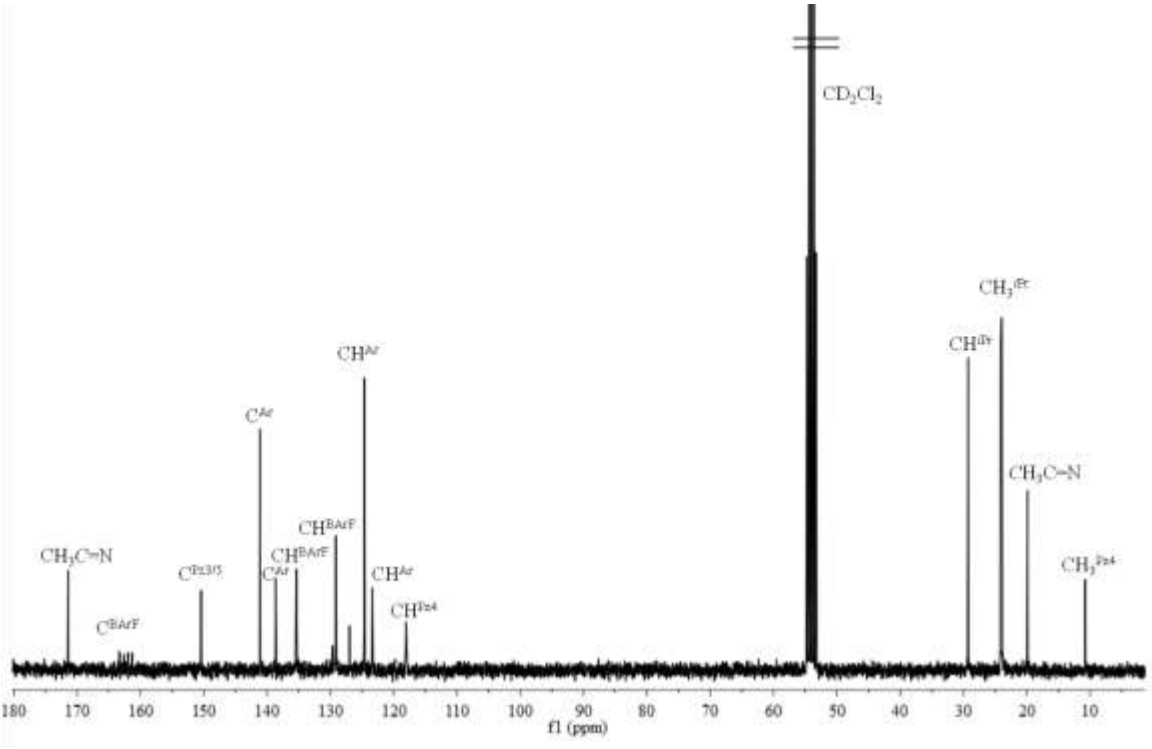

Fig. 6.2. 29: ^{13}C NMR spectrum of 2p measured in CD_2Cl_2 at room temperature

The ^{13}C NMR spectrum of **2p** shows a very simple spectrum with peaks at 10.6, 19.7, 23.7/23.9 and 29.1 ppm which can be assigned to CH_3^{Pz4}, $CH_3C{=}N$, CH_3^{iPr} and CH^{iPr} groups respectively. In addition, only a single peak is observed for the imine carbon at 171.2 ppm (Fig. 6.2. 29). No hydrogen bond interactions were observed in the IR spectrum.

A formulated route to the formation of **2p** is shown in Scheme 6.2.18. A cationic complex is generated when **XXI**^{c} is treated with AgOTf or with an alkali-metal borate salt ($NaBAr^F_4$). This causes the CH_3 groups to move into bridging positions whiles still keeping the μ-CH_2 intact, followed by the coordination of adventitious water. This is corroborated by the ^{1}H NMR spectrum of **2l**, which shows the signal for the μ-CH_3 and μ-CH_2 at 0.03 ppm and 4.15 ppm compared to 0.05 ppm and 3.96 ppm in **XXI**^{c} (in $CDCl_3$). In addition, the formation of such a complex is observed in the ESI-MS with a major m/z peak at 1474 (100%) which can be assigned to $[L^2_2Pd_4(\mu\text{-}CH_2)(\mu\text{-}CH_3)_2(H_2O)_2]^{2+}$. In the presence of an olefin, the μ-CH_2 is coupled to the olefin, as demonstrated previously. After coupling of the μ-CH_2, the highly unstable complex is stabilized by the presences of chloride anions present in the chlorinated solvent due to the loss of the μ-CH_2, thus reforming the bridging μ-Cl.

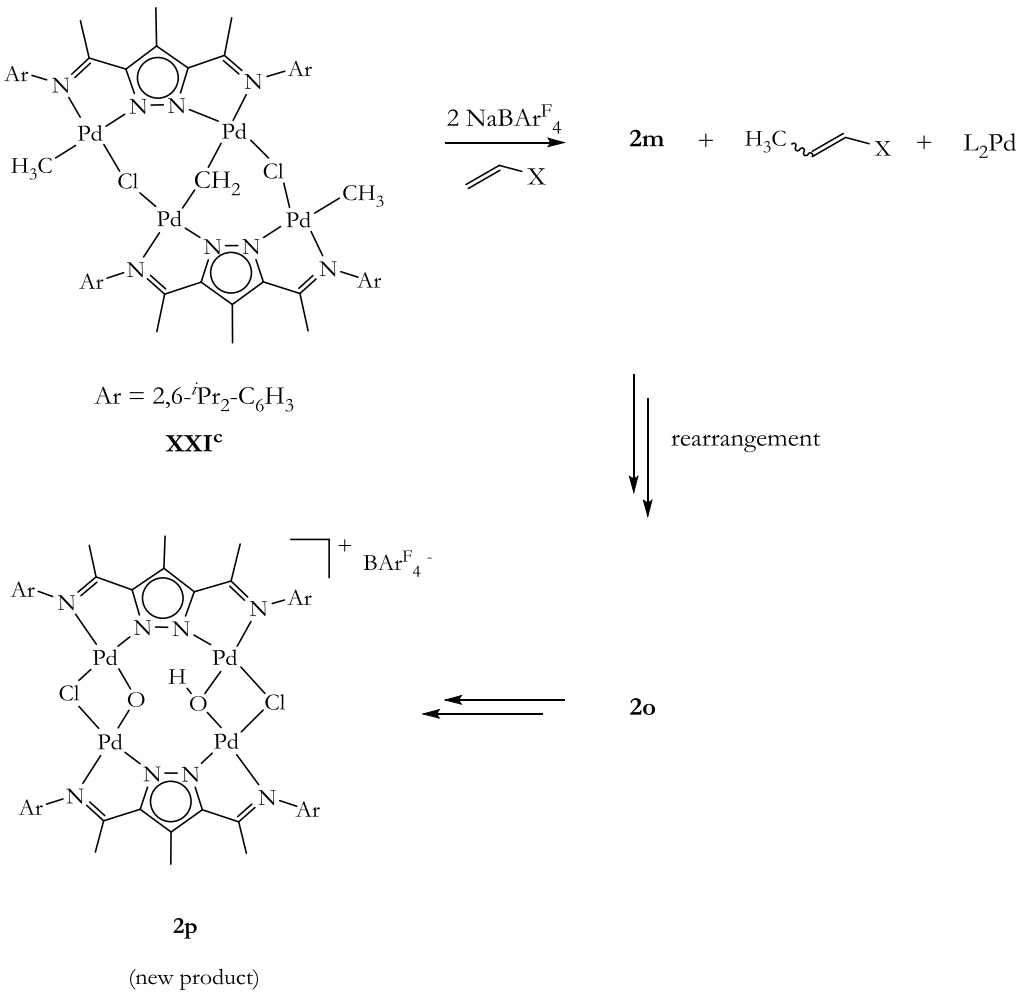

Scheme 6.2.18: Reaction sequence leading to the formation of 2p

Through a series of reactions not yet well understood, there is the eventual formation of **2o** and subsequently to the final product **2p**.

It is worth noting that the observed reaction sequence is reproducible irrespective of the nature of the chloride abstracting agent used (AgOTf/NaBAr$^F_4$), thus possibly ruling out the role of Ag^+ ions as a redox agent.

6. 3 Towards Heterobimetallic complexes

The concept of having two different metals in close proximity in transition metal complexes has been of interest for some time now. A heterobimetallic complex can have each metal centre undergoing reactions observed in their respective mononuclear compounds. In certain instances, the nature of the bridging ligand may allow for new modes of reactivity in the heterobimetallic complex. Also, heterobimetallic complexes have unusual electronic, electrochemical and magnetic properties due to the presence of different metal sites.[234,235,236]

The goal is to prepare heterobimetallic complexes of the *a*-diimine type ligands, in which the two metal centres are held in close proximity to explore potential cooperative effects between the two centres. A number of approaches have been adopted for the preparation of heterobimetallic complexes involving the 3,5-disubstituted pyrazolyl bridging moiety.

Akita and co-workers[136] have described a method for the synthesis heterodinuclear complexes of a pyrazolate based ligand system. The method first involves the preparation of a mononuclear 1:1 adduct (**XLV**) by the addition of the metal reagent to an excess amount of the dinucleating ligand.

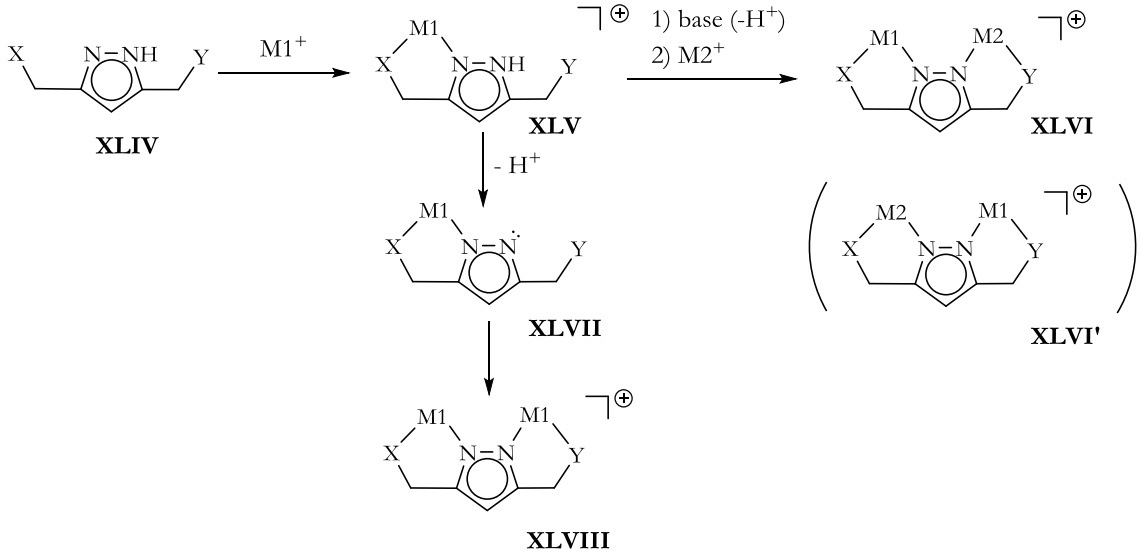

Scheme 6.3. 1: Scheme for the preparation of heterobimetallic complexes.[136]

This is followed by the treatment of the 1:1 educt with a base and a second metal reagent to furnish the heterobimetallic complex (**XLVI**). By changing the addition order, the

regioisomer (**XLVI'**) is also obtained. In addition, side products such as **XLVIII** are also formed from the spontaneous deprotonation of **XLV**.

6.3. 1 Mononuclear palladium(II) complexes as templates to heterobimetallic complexes

The target is to prepare mononuclear complexes of palladium(II) and nickel(II) as templates for the preparation of heterobimetallic complexes (Scheme 6.3.1. 1).

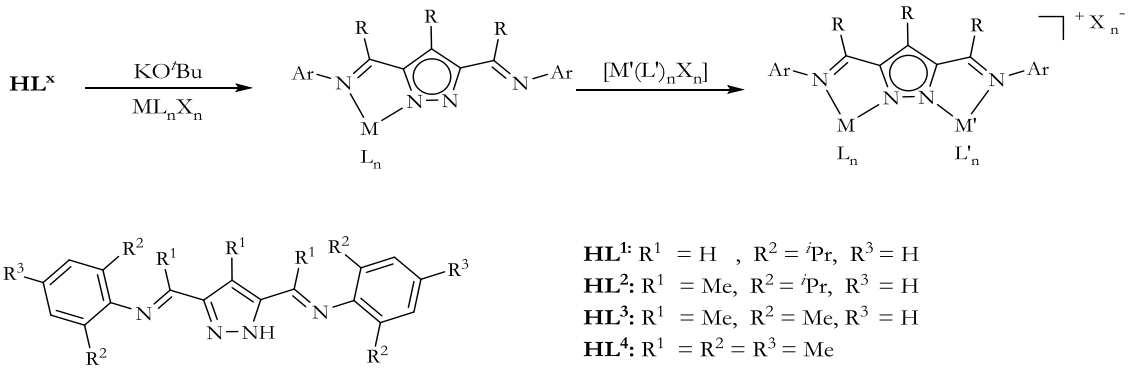

Scheme 6.3.1. 1: Initial adopted scheme for the preparation of heterobimetallic complexes

To begin with, the treatment of the deprotonated ligand L^1/L^2 with 2 mol equivalent $[PdCl(CH_3)(COD)]$ results in the isolation of a homobimetallic complex of the type $[L^x{}_2Pd_2(CH_3)X]$ (X = Cl, CH_3) (Scheme 6.3.1. 2). The formation of this complex is not influenced by the ratio of ligand to metal precursor used. A 1:1 ratio of ligand to metal precursor gives the same type of complex.

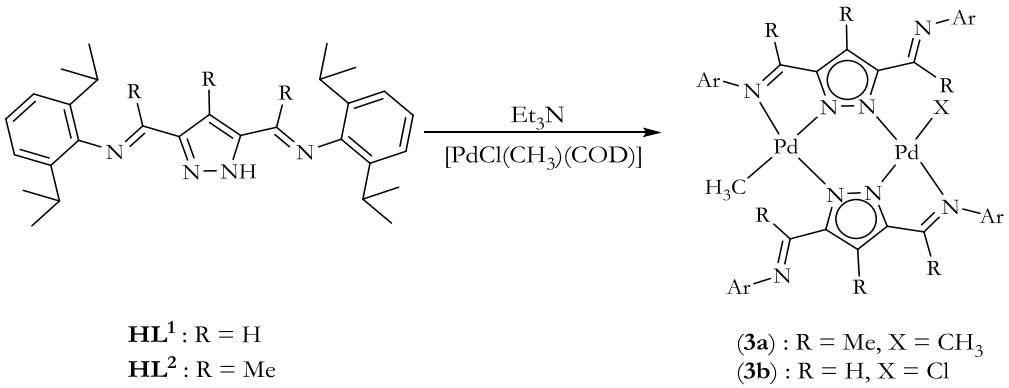

Scheme 6.3.1. 2:Synthetic scheme for the formation of 3a and 3b

The ^{1}H NMR spectrum of **3a** shows a CH_3^{Pd} resonance at 0.15 ppm, and the different $CH_3C{=}N$ groups as singlets at 2.18 and 2.34 ppm respectively, as well as the CH_3^{Pz4} group at 2.57 ppm (Fig. 6.3.1. 1).

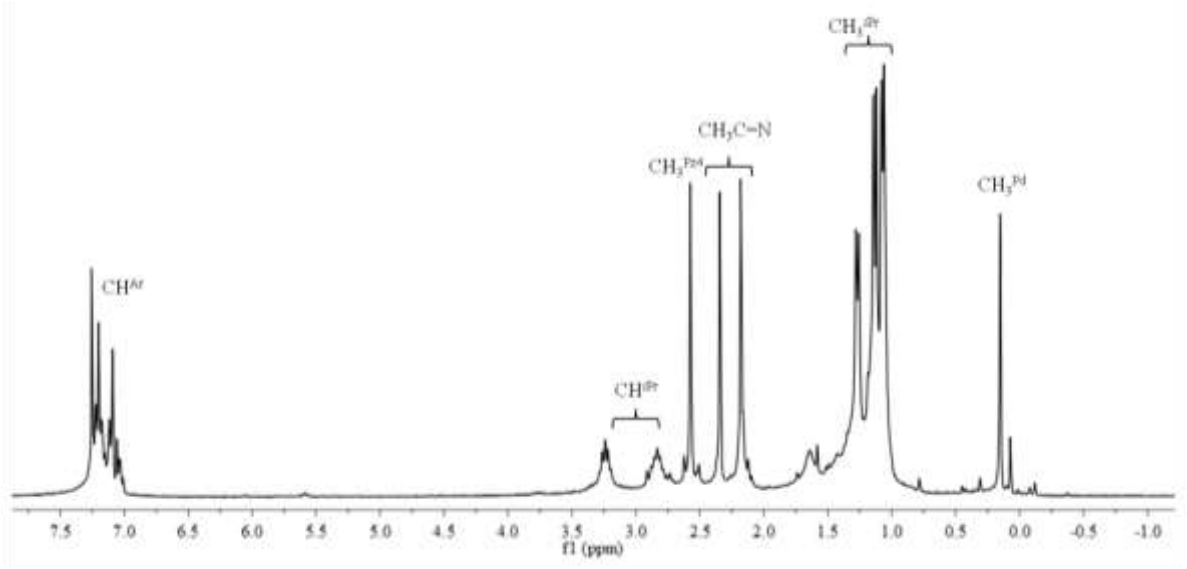

Fig. 6.3.1. 1: ^{1}H NMR spectrum of 3a measured in $CDCl_3$ at room temperature

The CH_3^{iPr} groups are observed as four doublets at 1.06, 1.12, 1.17, and 1.26 ppm respectively. A HSQC NMR spectrum of **3a** shows a ^{13}C correlation for the methyl group (CH_3^{Pd}) at 1.68 ppm, whiles the ^{13}C correlations for the two $CH_3C{=}N$ are observed at 162.3 and 172.0 ppm for the bound and unbound arms respectively. The ESI-MS of **3a** shows a *bis*-chelate complex with m/z peak at 1195 (50%) assigned to $[M\text{-}CH_3]^{+}$.

When the experiment was repeated using a ratio of HL^{1}:$[PdCl(CH_3)(COD)]$ of 1:2, the analogous complex **3b** was isolated. In **3b,** the CH_3^{Pd} peak is observed as a doublet at 0.54 ppm in the ^{1}H NMR spectrum, possibly due to a mixture of isomers. In addition, the CH_3^{Pd} peak is deshielded compared to **3a**. Examples of [N^NPd(CH_3)Cl] (N^N: *a*-diimine) complexes have been reported with the CH_3^{Pd} signal shifted for complexes bearing electron withdrawing ligands and upfield for electron donating ligands.[237]

Crystals of **3a** and **3b** were grown by the slow evaporation of a CH_2Cl_2 of the complexes at room temperature. The molecular structures of the compounds are shown in (Fig. 6.3.1. 2) as well selected bond angles [°] and bond lengths [Å] in Table 6.3.1. 1 and Table 6.3.1. 3.

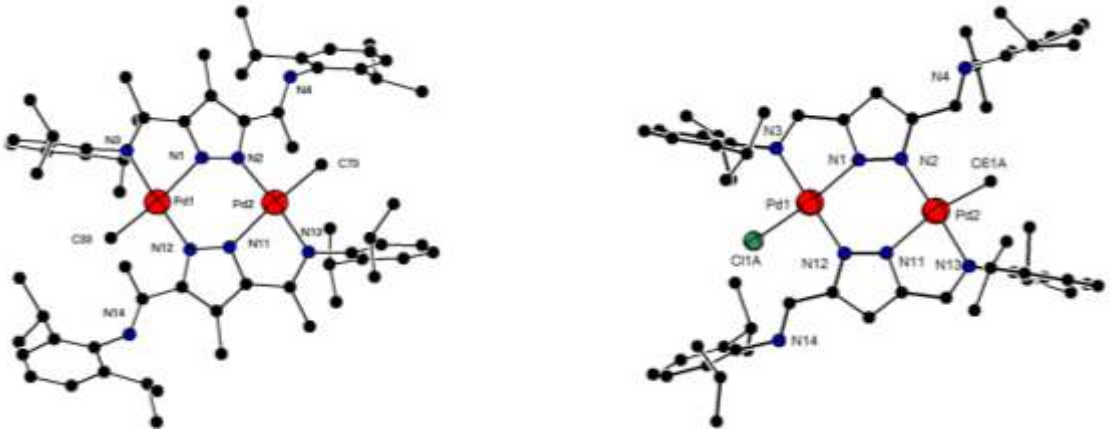

Fig. 6.3.1. 2: Molecular structures of 3a (left) and 3b (right) all H atoms omitted for clarity

The coordination geometry around the palladium centre in both complexes is square planar. The Pd-C bond length in $[L^2{}_2Pd_2(CH_3)_2]$ **3a** (2.03 Å) is significantly shorter than observed in $[L_2{}^1Pd_2(CH_3)Cl]$ **3b** (2.13 Å). The interplanar angle defined by the five atoms, which make up each pyrazole ring is twisted at 48.3° in **3a**, compared to **3b** where the twists is less at 28.9°. The Pd(1)-N(1) bond length is slightly longer (2.12 Å) compared to Pd(1)-N(3) of 2.05 Å in **3a**, thus the palladium imine bond is slightly stronger than the palladium pyrazole bond.

In **3b** there are no significant differences between the Pd-N bond lengths between the two palladium centres bearing the Cl or the CH_3 ligand (Pd(1)-N(1) = 2.06 Å; Pd(1)-N(3) = 2.04 Å; Pd(2)-N(11) = 2.07 Å; Pd(2)-N(13) = 2.05 Å). The Pd-C and the Pd-Cl bond lengths in the two complexes however, fall in the range observed for other palladium(II) complexes.[238,239]

Table 6.3.1. 1: Selected bond lengths [Å] and bond angles [°] for 3a

Bond lengths [Å]		Bond angles [°]	
Pd(1)-C(33)	2.030(9)	C(33)-Pd(1)-N(12)	91.3(4)
Pd(1)-N(12)	2.044(8)	C(33)-Pd(1)-N(3)	94.7(4)
Pd(1)-N(3)	2.057(8)	N(12)-Pd(1)-N(3)	172.3(3)
Pd(1)-N(1)	2.122(8)	C(33)-Pd(1)-N(1)	169.9(4)
Pd(2)-C(73)	2.033(9)	N(12)-Pd(1)-N(1)	97.7(3)

Table 6.3.1. 2: Selected bond lengths [Å] and bond angles [°] for 3b

Bond lengths [Å]		Bond angles [°]	
Pd(1)-N(12)	2.032(3)	N(12)-Pd(1)-N(3)	169.07(16)
Pd(1)-N(3)	2.048(4)	N(12)-Pd(1)-N(1)	97.08(15)
Pd(2)-C(61A)	2.130(2)	N(3)-Pd(1)-N(1)	79.36(14)
Pd(1)-Cl(1A)	2.240(4)	N(3)-Pd(1)-C(61A)	89.81(5)
Pd(2)-N(2)	2.039(4)	N(1)-Pd(1)-C(61A)	160.62(5)
Pd(2)-N(13)	2.059(4)	N(12)-Pd(1)-Cl(1A)	92.47(13)

To avoid the formation of $[L^x{}_2Pd_2(CH_3)X]$ (X = Cl, CH_3) type complexes, the deprotonated ligand was added to $[PdCl(CH_3)(COD)]$ in the presence of coligands such as PPh_3, PMe_3 or pyridine. Indeed, the formation of complexes of $[L^x{}_2Pd_2(CH_3)X]$ (X = Cl, CH_3) complexes were avoided, in place, mononuclear complexes of the type $[L^xPd(L')(CH_3)$ (L'= PMe_3, PPh_3, pyridine) are formed (Scheme 6.3.1. 3).

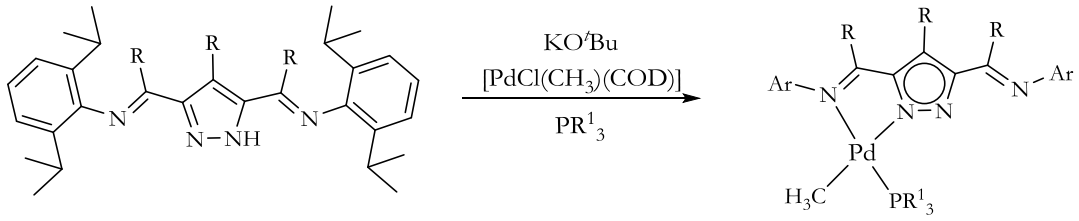

HL^1 : R = H
HL^2 : R = Me

(**3c**): R = Me, R^1 = Me
(**3d**): R = Me, R^1 = Ph

Scheme 6.3.1. 3: Synthesis of $[L^xPd(PR^1{}_3)(CH_3)]$ complexes (3c -3d)

In one such experiment, treating KL^2 with an equivalent $[PdCl(CH_3)(COD)]$ with $PR^1{}_3$ (R^1 = Me, Ph) results in the isolation of the neutral complexes **3c** and **3d**. The ^{1}H NMR spectrum of **3c** shows the $CH_3{}^{Pd}$ resonance as a doublet at -0.32 ppm due to P-H coupling. The $^{13}C\{^1H\}$ NMR spectrum of **3c** shows a doublet at δ 15.9 ppm for PMe_3 ($J_{P\text{-}C}$ = 52.2 Hz), whiles the $CH_3{}^{Pd}$ resonance is observed as a doublet at 0.76 ppm (J_{PC} = 11.5 Hz) due to coupling with the phosphorous nucleus. Only broad and partially resolved signals are observed for the aromatic protons. Crystals of **3c** were obtained by the slow diffusion of Et_2O into a CH_2Cl_2 solution of the complex for several days. Selected bond lengths and bond angles for **3c** are given in Table 6.3.1. 3.

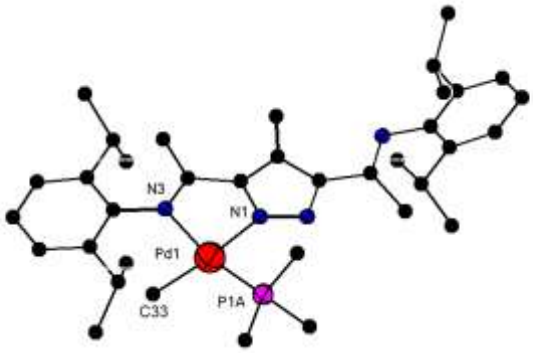

Fig. 6.3.1. 3: Molecular structure of 3c, all H atoms are omitted for clarity

The coordination about palladium(II) atom in **3c** is defined by four ligand atoms N3, N1, C33, and P1A is essentially square planar. The Pd(1)-N(1) bond length (2.06 Å) is smaller than the Pd(1)-N(3) bond length (2.10 Å). This weakening of the Pd(1)-N(3) bond is largely due to the *trans* influence of the PMe_3 group. The palladium centre is part of a largely planar five-membered chelate ring involving N(1)-Pd(1)-N(3) with bond angles near 77°. The P-C bond length of 1.89 is longer than that of free PMe_3 (1.84 Å).[240]

Table 6.3.1. 3: Selected bond lengths [Å] and bond angles [°] for 3c

Bond lengths [Å]		Bond angles [°]	
Pd(1)-N(1)	2.066(3)	N(1)-Pd(1)-C(33)	173.44(12)
Pd(1)-C(33)	2.101(3)	N(1)-Pd(1)-N(3)	77.37(10)
Pd(1)-P(1A)	2.278(2)	N(1)-Pd(1)-P(1A)	95.40(9)
Pd(1)-N(3)	2.133(26)	C(33)-Pd(1)-P(1A)	91.05(104)

On the other hand, neutral complexes of the type [$HL^xPd(CH_3)Cl$] (**3e**, **3f** and **3g**) are formed when the ligands are treated with the metal precursor [$PdCl(CH_3)(COD)$] without the use of a base.

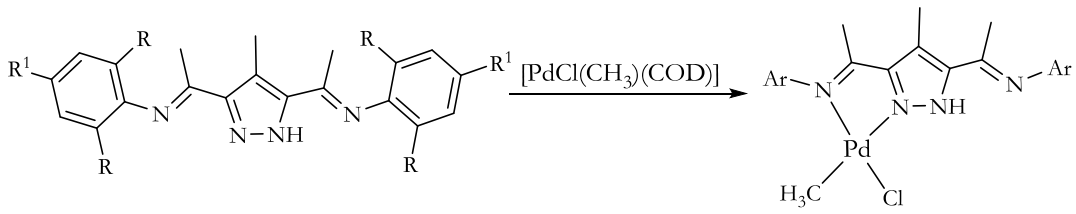

HL^2 : R = ^{i}Pr, R^1 = H (**3e**): HL^2
HL^3 : R = Me, R^1 = H (**3f**): HL^3
HL^4 : R = Me, R^1 = Me (**3g**): HL^4

Scheme 6.3.1. 4: Synthesis of the neutral complexes 3e-3g

In these complexes, the ligands remain protonated. The complexes, **3e**, **3f,** and **3g** were characterized by ^{1}H and ^{13}C NMR, ESI-MS and in some instances elemental analysis, which confirmed the formation of such complexes. In all three complexes, the CH_3^{Pd} peaks in the ^{1}H NMR spectrum are observed at δ: 0.46, 0.27, and 0.32 for **3e**, **3f,** and **3g** respectively. The ligands with the more bulky side arms usually show a lower field signal for the CH_3^{Pd} group. Two ^{1}H NMR spectrum peaks are observed for the CH_3C=N group, reflecting the different CH_3C=N environments. The IR spectra of the complexes as expected also reflect the different CH_3C=N environments.

For instance in **3f**, the coordinated side arm shows a C=N stretch at 1549 cm^{-1}, compared to the free arm which shows a C=N stretch at 1589 cm^{-1}. The complexes **3e**, **3f,** and **3g** are stable in the solid state but undergo reconstitution in solution. For instance, when **3e** is left in solution at room temperature for several weeks, crystals obtained show the formation of [L$^2_2$Pd] type complex (**3h**). Rearrangements reactions involving PdClMe complexes have been reported in literature.[241]

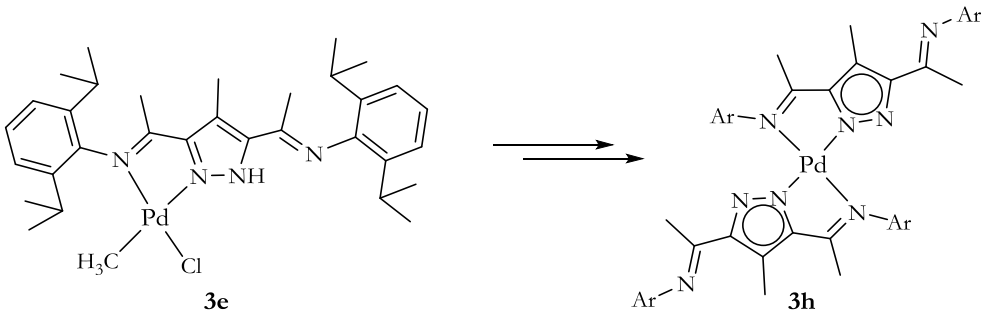

3e **3h**

Scheme 6.3.1. 5: Formation of 3h from rearrangement of 3e in solution at room temperature

The complex **3h** is also isolated as a side product in attempts at preparing a complex of the type [L^2Pd(Pyr)(CH_3)] (Pyr = pyridine). The molecular structure of **3h** is shown below.

Fig. 6.3.1. 4: Molecular structure of 3h, H atoms, and counter ions omitted for clarity

In **3h**, the coordination geometry around palladium centre is square planar, with the square plane defined by four atoms, N(3)/N(1)/N(3')/N(1')/N(3). The palladium-imine bond distance Pd(1)-N(3) is slightly longer 2.03 Å compared to the palladium-pyrazolyl nitrogen bond distance Pd(1)-N(1) of 1.98 Å. The ligand bite angle is ∠N(1)Pd(1)N(3) = 79.8°. In addition, the inter planar angle between the six carbon atoms C(7)/C(8)/C(9)/C(10)/C(11)/C(12) which make up the coordinated aryl side arm and the five atoms which make the pyrazole ring N(1)-N(2)-C(3)-C(1)-C(2) is nearly perpendicular at 88.4°. The orientation of the non-coordinated N^N sidearm is largely *anti* with a dihedral angle of 171.2° (N(2)-C(3)-C(19)-N(4)) compared to -2.40° for the coordinated N^N side arm (N(1)-C(2)-C(5)-N(3)). Selected bond lengths [Å] and bond angles [°] given in Table 6.3.1. 4.

Table 6.3.1. 4: Selected bond lengths [Å] and bond angles [°] for 3h

Bond lengths [Å]		**Bond angles [°]**	
Pd(1)-N(1)	1.989(4)	N(1)-Pd(1)-N(1)	180.00(1)
Pd(1)-N(1)	1.989(4)	N(1)-Pd(1)-N(3)	79.87(18)
Pd(1)-N(3)	2.034(5)	N(1)-Pd(1)-N(3)	100.13(18)
Pd(1)-N(3)	2.034(5)	N(3)-Pd(1)-N(3)	179.98(1)

In a brief attempt of mediating acrylate insertion reactions with **3f**, yellow crystalline blocks (**3i**) were isolated from the reaction medium after several days. However, there was not enough material available for thorough characterization. Single crystal X-ray structure of the crystalline blocks **3i**, showed it to be a $[L^3{}_2Pd_2](BAr^F{}_4)_2$ type complex.

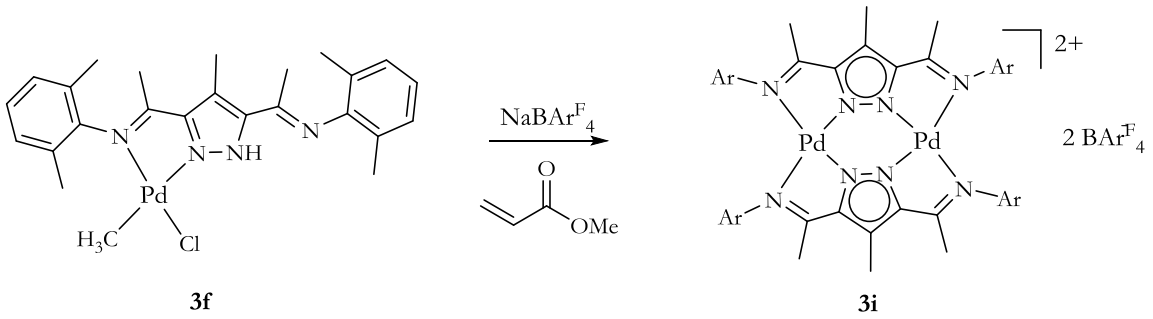

Scheme 6.3.1. 6: Formation of 3i from 3f at acrylate insertion reactions

The molecular structure of **3i** is shown in Fig. 6.3.1. 5. The compound crystallizes in the *P* -1 space group. The two palladium atoms are bound by two pyrazolyl nitrogen atoms and two imine nitrogen atoms. The coordination around the palladium centre consists of four nitrogen donors, two each from the imine side arm and the pyrazolyl nitrogen atoms.

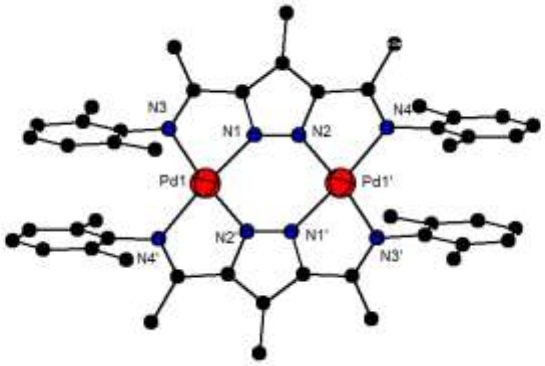

Fig. 6.3.1. 5: Molecular structure of 3i, H atoms, and counterions omitted for clarity

The shortest Pd-N bond is between the pyrazolyl nitrogen and the palladium(II) centre. The inter palladium distance is fixed by the μ-pyrazolate framework at 3.94 Å. The torsional angle defined by Pd(1)-N(1)-N(2)-Pd(1') is 0.68°, and the interplanar angle defined by two aromatic rings on opposite side of the palladium centre is 1.23°, thus the complex is largely planar. Selected bond lengths [Å] and bond angles [°] also given in Table 6.3.1. 5.

Table 6.3.1. 5:·Selected bond lengths [Å] and bond angles [°] for 3i

Bond lengths [Å]		Bond angles [°]	
Pd(1)-N(1)	1.964(3)	N(1)-Pd(1)-N(4)	173.37(12)
Pd(1)-N(3)	2.076(3)	N(3)-Pd(1)-N(4)	108.72(12)
Pd(1)-N(4)	2.080(3)	N(2)-N(1)-Pd(1)	131.7(2)
Pd(1)-Pd(1^{i})	3.943(2)	N(1)-N(2)-C(3)	108.6(3)

The Pd-N bond lengths are in the range of similar reported palladium complexes.[155]

6.3. 2 Mononuclear nickel(II) σ-aryl complexes as templates to heterobimetallic complexes

A general synthetic route for the preparation of the nickel(II) σ-aryl complexes involved treating the deprotonated ligand with one mol equivalent of the precursor [NiBr(Ar)(PPh_3)] in CH_2Cl_2 (Scheme 6.3.2. 1).

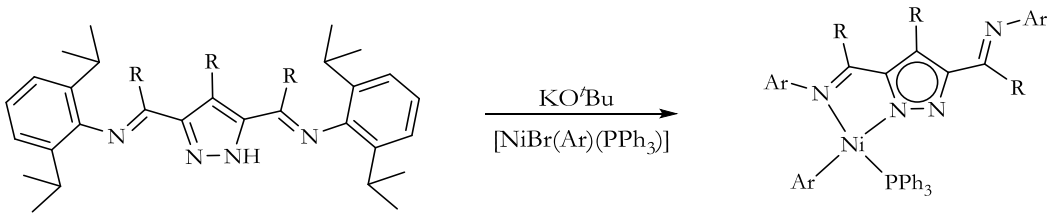

HL^1 : R = H
HL^2 : R = Me

(**3j**) : R = H, Ar = $C_{10}H_7$
(**3k**): R = Me, Ar = $C_{10}H_7$
(**3l**): R = Me, Ar = C_6H_5

Scheme 6.3.2. 1: Preparation of [L^{x}Ni(Ar)(PPh$_3$)] complexes (3j-3l)

The mononuclear nickel(II) complexes (**3j**-**3l**) were generally isolated as orange-yellow powder in moderate yields (44-46%). They are fairly air stable and soluble in toluene, halogenated solvents, hexanes, and ether. The complexes were characterized by ^{1}H and ^{13}C NMR, IR, ESI-MS, elemental analysis and in some instances single crystal X-ray structures.

For example, in a selected complex **3j**, the IR spectrum of **3j** shows two CH=N stretching vibrations at 1637 cm^{-1} and 1583 cm^{-1} for the unbound and metal bound side arms respectively, a shift to lower wavenumber due to coordination to the metal. The ^{1}H NMR spectrum confirms the asymmetric ligand environment, with the CH=N peaks observed at 7.69 and 7.99 ppm for the coordinated and uncoordinated side arms respectively. The complexes also assume a square planar geometry. The ^{1}H NMR spectrum of **3k** (Fig. 6.3.2.1. 1) shows four different CH$^{i\text{Pr}}$ environments (h, r, s, and l) which integrate in 1:1:1:1 ratio, due to the hindered rotation imposed by the presence of the bulky napthyl and triphenylphosphane groups. The ^{1}H NMR spectrum peaks for **3k** were assigned from 1D and 2D experiments. Strong shielding of $CH_3^{i\text{Pr}}$ by the naphthyl ring is observed in the ^{1}H NMR spectrum. The $CH_3^{i\text{Pr}}$ group shielded by the napthyl ring is observed upfield as a doublet at -0.52 ppm due to coupling with the CH proton on the isopropyl group. The

$^{31}P\{^{1}H\}$ signal is observed at 30.3 ppm as a singlet. The ^{1}H NMR spectrum assignments are shown in Fig. 6.3.2. 1. The ^{1}H-^{1}H COSY assignments for **3k** is also shown in Fig. 6.3.2. 2.

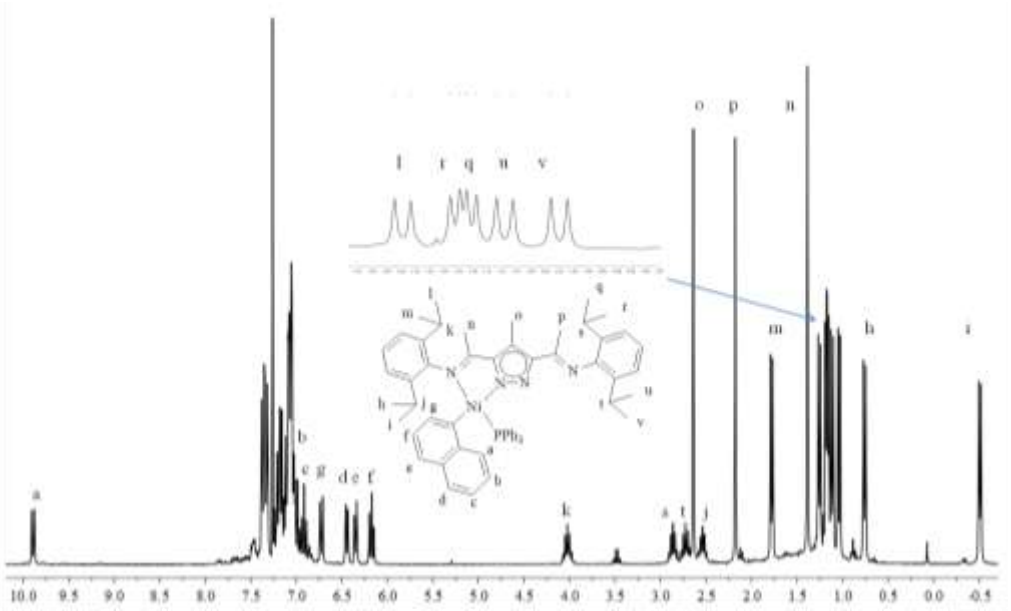

Fig. 6.3.2. 1: ^{1}H NMR spectrum of 3k measured in $CDCl_3$ at room temperature

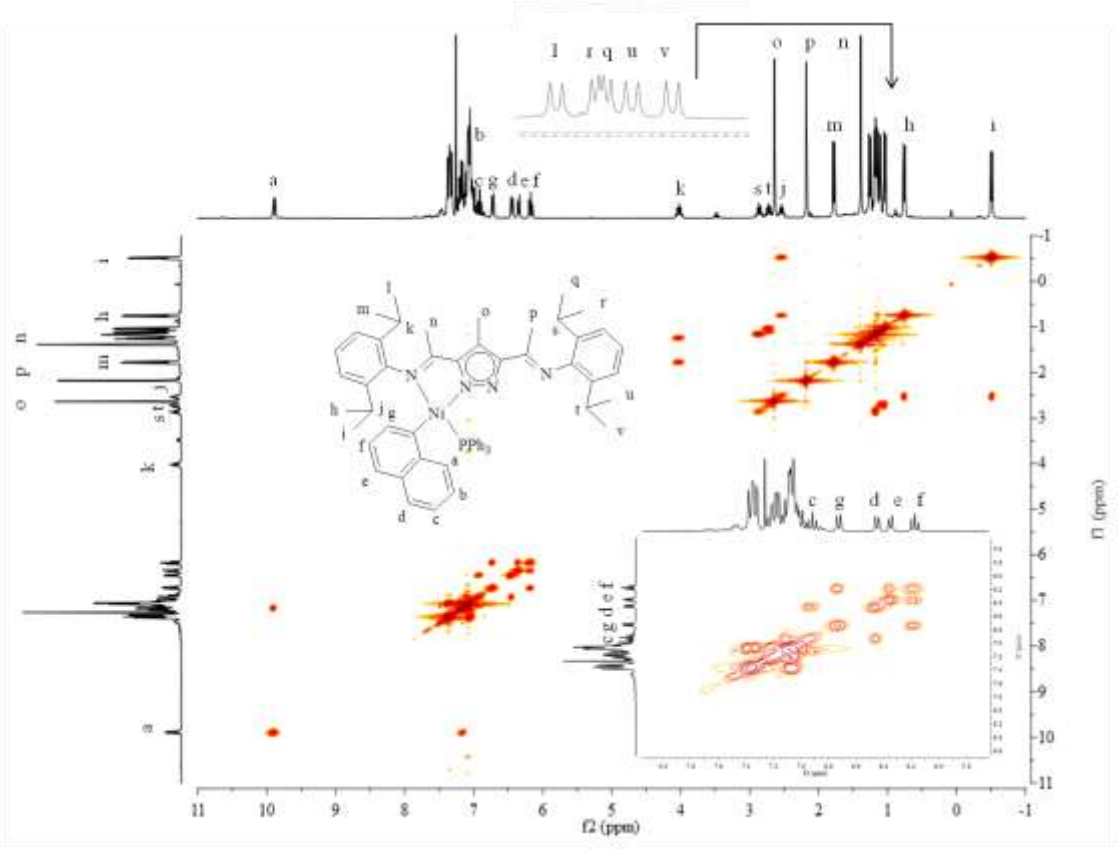

Fig. 6.3.2. 2: ^{1}H-^{1}H COSY NMR spectrum of 3k measured in $CDCl_3$ at room temperature

A notable feature in the ^{1}H NMR spectrum of **3k** is the presence of a downfield aromatic ^{1}H NMR spectrum signal at 9.89 ppm. This is also observed at 9.19 ppm for the analogous compound **3j**, but not observed for **3l**, which has a σ-bonded phenyl ring.

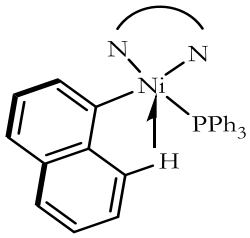

This is possibly, due to the close proximity of an aromatic H on the second ring of the naphthyl group to the metal centre. Single crystals of [L^2Ni($C_{10}H_7$)(PPh_3)] (**3k**) were grown by the slow evaporation of a toluene solution of the complex over several days. The compound crystallizes in the *P* 21/c space group. The structure consists of a mononuclear unit in which the metal binds to one pocket of the ligand whiles the other remains vacant. The geometry about the nickel(II) centre is a largely square planar. The nickel(II) centre is coordinated to the two nitrogen atoms (N1, N3), with the PPh_3 ligand in a *trans* position to the imine nitrogen.

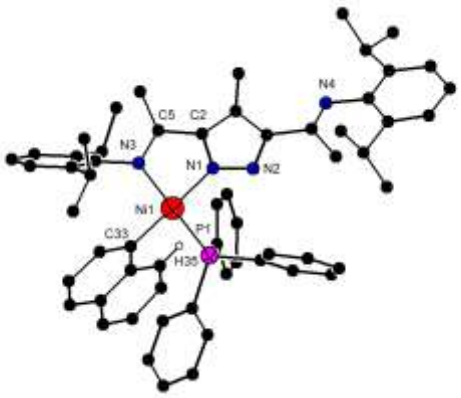

Fig. 6.3.2. 3: Molecular structure of 3k, most H atoms are omitted for clarity

In addition, the aromatic H (H35) is in close proximity to the metal centre (2.66 Á). This distance is substantially shorter than the sum of the van der Waals radii of H and Ni (1.20 and 1.63 Å respectively). The interplanar angle defined by Ni(1), N(3), C(5), C(2), N(1), and the naphthyl ring is 80.36°. The Ni(1)-N(3) bond length is longer, 1.96 Å compared to Ni(1)-

N(1) (1.90 Å) due to the *trans* influence of the PPh_3 group. The interplanar angle between the pyrazole ring and the napthyl ring is nearly perpendicular at 88.3°; this possibly is the only favourable orientation in order to avoid steric clash of the bulky aryl rings of PPh_3, the napthyl ring and the 2,6-diisopropyl aryl ring. Selected bond lengths [Å] and angles [°] are given in Table 6.3.2. 1.

Table 6.3.2. 1: Selected bond lengths [Å] and bond angles [°] for 3k

Bond lengths [Å]		Bond angles [°]	
Ni(1)-C(33)	1.896(7)	C(33)-Ni(1)-N(1)	169.6(3)
Ni(1)-N(1)	1.907(5)	C(33)-Ni(1)-N(3)	93.2(3)
Ni(1)-N(3)	1.964(5)	N(1)-Ni(1)-N(3)	81.5(2)
Ni(1)-P(1)	2.1754(19)	C(33)-Ni(1)-N(3)	93.2(3)

Other compounds, which have the hydrogen of an aromatic group in close proximity with metals reported in literature, are shown below in **XL** and **XLI**.[242,243]

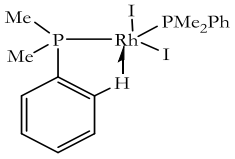

XL

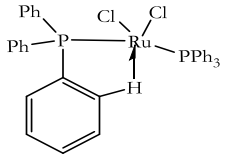

XLI

Studies have been conducted on the close contact between d^8 metal ions such as palladium(II) and platinum(II) metal ions which have N-H or O-H bonds are located above or below the coordination sphere.[244,245] In addition reports have also been made in close contacts which involve sp^2 or sp^3 hybridized C-H bonds.[246,247,248] There are different schools of thought on the nature of these C-H interactions. One school of thought is that these contacts are as a result of three-centre four electron M···H-C bonds which involves the filled d_{z^2} orbital (Scheme 6.3.2. 2).

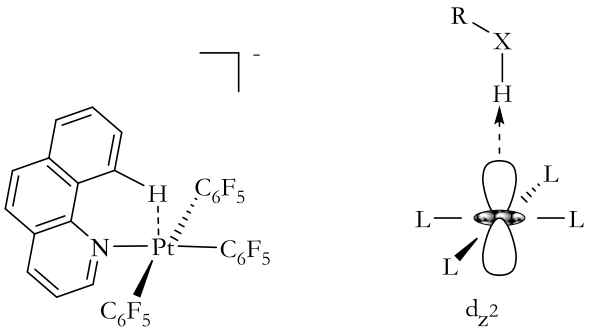

Scheme 6.3.2. 2: Three center four electron M···H-X hydrogen bonds[249]

Some also argue it is as a result of agostic three-center two electron interactions. Whiles another school of thought is that, these close contacts are as a result of mainly repulsive interactions which are mainly due to geometric ligand caused by bulky ligand substituents. [250,155] These forces the H atoms to lie in close to the metal ions. The ESI-MS of **3k** also shows the m/z peak at 931(100%) assigned to the molecular ion $[M]^+$.

The analogous nickel(II) complex with a phenyl substituent $[L^2Ni(Ph)(PPh_3)]$ (**3l**) was prepared in like manner. The IR spectrum of this complex shows two absorption bands at 1626 cm^{-1} and 1566 cm^{-1} that can be attributed to the two different imine environments. The strong absorption band at 1435 ν(P-C) and 696 ν(Ni-P) confirms the binding of PPh_3 to nickel. The ESI-MS shows fragmentation corresponding to the loss of a phenyl and PPh_3 groups. Single crystals of **3l** were grown by the slow evaporation of a CH_2Cl_2 solution of the complex at room temperature. The structure is of poor quality but unequivocally provides the atom connectivity (Fig. 6.3.2. 4).

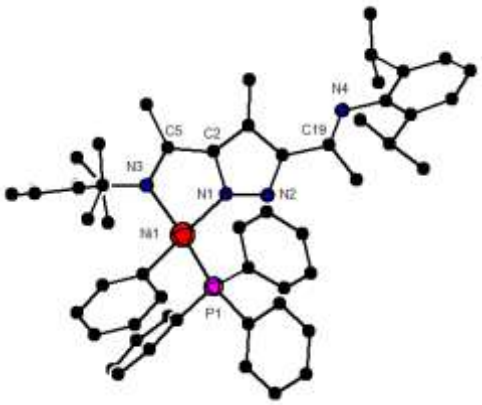

Fig. 6.3.2. 4: Molecular structure of 3l, all H atoms are omitted for clarity

The coordination around the nickel(II) is square planar with the PPh_3 in a *trans* position to the imine nitrogen. Selected bond lengths and bond angles are given in Table 6.3.2. 2. The C(19)-N(4) bond length of the imine group (1.27 Å) is consistent with the double bond character, and shorter than C(5)-N(3) (1.33 Å) as expected. The Ni-P bond length of 2.16 Å is shorter than that reported for the neutral phenoxyimine complex.[40]

Table 6.3.2. 2: Selected bond lengths [Å] and bond angles [°] for 3l

Bond lengths [Å]		**Bond angles [°]**	
Ni(1)-N(1)	1.891(10)	N(1)-Ni(1)-C(34)	161.0(5)
Ni(1)-C(34)	1.892(12)	N(1)-Ni(1)-N(3)	82.4(5)
Ni(1)-N(3)	1.956(12)	C(34)-Ni(1)-N(3)	95.4(6)
Ni(1)-P(1)	2.158(5)	N(1)-Ni(1)-P(1)	99.0(4)
C(5)-N(3)	1.329(189)		
C(19)-N(4)	1.269(185)		

In the course of the experiments, crystal growth attempts yielded two unique systems, one of the crystals having two of the ligands coordinated to the nickel(II) centre (L_2Ni) in a square planar environment. This dimer formed because of PPh_3 dissociation. The formation of L_2Ni types of complexes from PPh_3 dissociation is documented in literature.[251]

Attempts at the use of the nickel σ-aryl complexes (**3j**, **3k** and **3l**) in ethylene polymerization experiments failed. Addition of $[Ni(COD)_2]$ as a PPh_3 scavenger in the presence of ethylene (5 atm) did not yield any polymer nor oligomer product. Rather what was observed is the dimerization of the complex to L^2Ni. Computational work by Ziegler and co-workers indeed shows that the presence of bulky *ortho* substituent is primarily responsible for high catalytic activity by promoting the dissociation of phosphane from the nickel(II) centre.[252] Attention was later focused on testing these nickel(II) σ-aryl complexes in radical polymerization experiments as other nickel aryl complexes have been employed in such reactions.

6.3.2. 1 Nickel(II) σ-aryl catalyzed radical polymerization of styrene to polystyrene

Controlled radical polymerization (CRP) has been one of the most utilized polymerization methods due to its high chemoselectivity, regioselectivity, and ability to obtain polymers with controlled molecular weight and structure. The work of Wang and Matyjaszewski on the living/controlled bulk polymerization of styrene in the presence of the 1-phenylethylchloride/CuCl/2,2'-bipyridyl system[253] has spurred more investigations into CRP. Sawamoto has reported on the use of commercially available $NiBr_2(PPh_3)_2$ (**XLII**) to induce the living radical polymerization of MMA in conjunction with CCl_3Br initiator and a Lewis acid activator.[254] Also, thermally more robust and highly soluble $NiBr_2(PBu_3)_2$ (**XLIII**) has been used for the ATRP polymerization of MMA and MA. Teyssie also reported the use of a homogeneous aryl nickel(II) complex, which with activated alkyl halides gives well-controlled radical polymerization of methacrylate monomers in organic solvents.[255] The complex $[L^2Ni(C_{10}H_7)(PPh_3)]$ **3k** was tested as catalyst for the atom transfer radical polymerization of styrene.

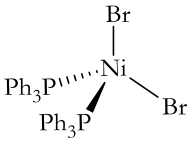

XLII

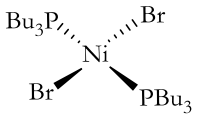

XLIII

It is worth stating that in atom transfer radical polymerization (ATRP), a halogen-capped polymer chain and a transition metal complex are in reversible equilibrium with a polymeric radical and the corresponding higher oxidation state metal halide[256,257] as shown in the simplified scheme below (Scheme 6.3.2.1. 1).

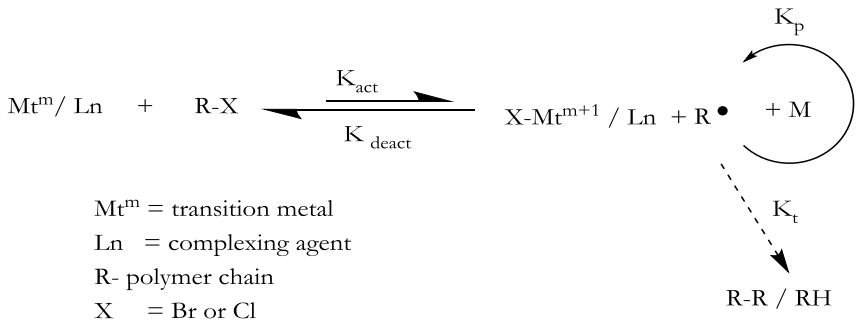

Scheme 6.3.2.1. 1: Mechanism of metal complex-mediated ATRP

Organometallic mediated radical polymerization (OMRP), another controlled radical polymerization technique in contrast to ATRP, involves the reversible formation of a covalent bond between a transition metal and the polymer chain. It is also dependent on the lability of metal–carbon bonds under thermal or photolytic treatment. The complex **3k** was screened for the radical polymerization of styrene to polystyrene. The linear time vs. conversion plot and the ln(1/(1-conv.)) vs. $t^{2/3}$ shows the characteristic plot for a persistent radical effect (Fig. 6.3.2.1. 1).

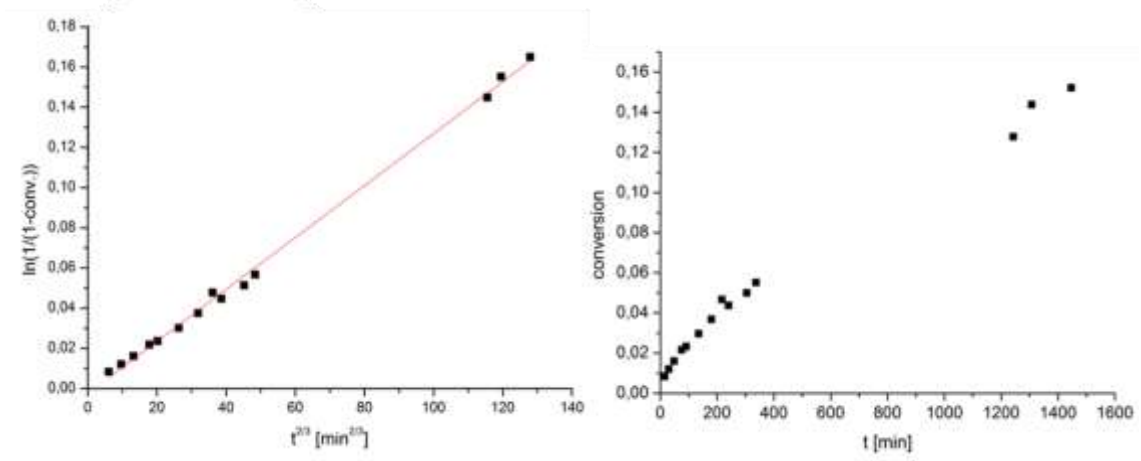

Fig. 6.3.2.1. 1: Kinetic plots for the radical polymerization of styrene using 3k

Usually, the linear first-order kinetic plot accompanied by the linear increase in polymer weight with conversion determines the "livingness "of the polymerization process. It can therefore be inferred that **3k** is active in the living polymerization of polystyrene.

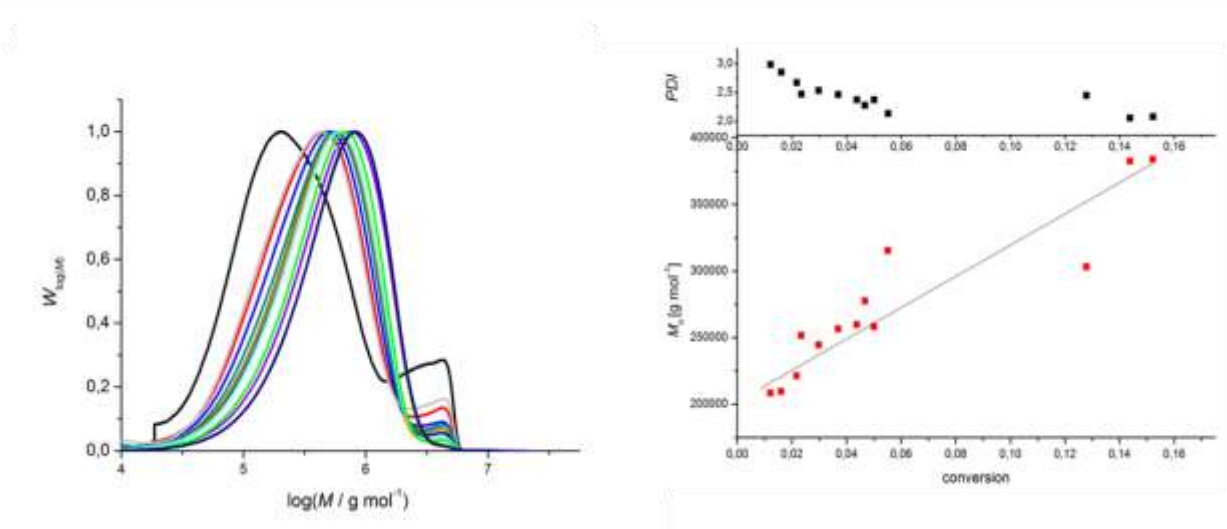

Fig. 6.3.2.1. 2: Molecular weight plots for the ATRP of styrene to polystyrene using 3k

The PDI decreases with conversion but stays well above 2.0. Results also show that the catalyst has higher conversions with increasing reaction times (Fig. 6.3.2.1. 2). Conversions however are generally low, and M_n of the polymers increases with monomer conversion. However, polymerization is uncontrolled with broad polydispersity (>2.0) and molecular weight distributions. The complex **3k** is therefore ineffective at controlling polymerization, and displays very low catalyst efficiency even at high catalyst loadings. Detailed discussions on the results will not be covered here.

6.3. 3 Synthesis towards heterobimetallic palladium(II)-rhodium(I) complexes

Having obtained mononuclear palladium(II) and nickel(II) complexes of the pyrazole-bridged *a*-diimine type ligands (Scheme 6.3.3. 1), attempts were made at preparing heterobimetallic complexes by the addition of coordinatively unsaturated metal species to pre-existing mononuclear complexes (Scheme 6.3.3. 2), similar to the method adopted by Chen and co-workers[152] and the approach adopted by Akita and co-workers.[136]

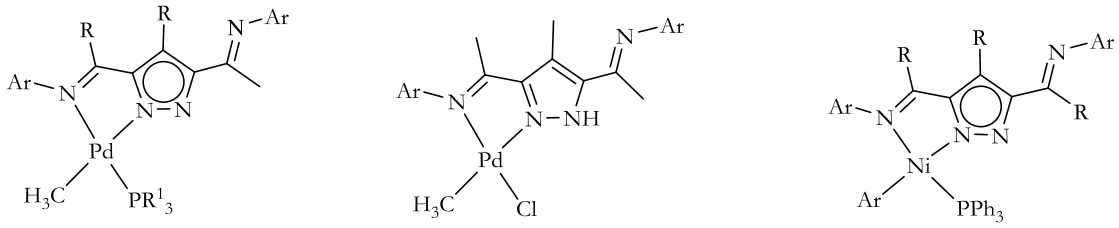

(**3c**): R = Me, R^1 = Me
(**3d**): R = Me, R^1 = Ph

(**3e**): R = Me
Ar = 2,6-^{i}Pr$_2$-C$_6$H$_3$

(**3j**) : R = H, Ar = $C_{10}H_7$
(**3k**): R = Me, Ar = $C_{10}H_7$
(**3l**): R = Me, Ar = C_6H_5

Scheme 6.3.3. 1: Scheme of mononuclear complexes used as templates for the preparation of heterobimetallic complexes

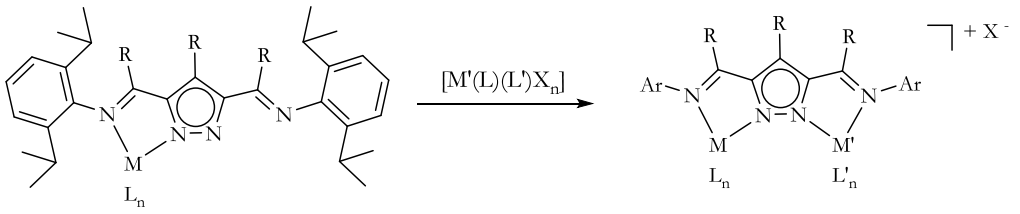

R = H, Me
M = Ni, Pd

M' = Rh, Ni
L_n/L'_n = ligand

Scheme 6.3.3. 2: Attempted route to heterobimetallic complexes

Both approaches were however unsuccessful in this case. As an example, the addition of 1 mol equivalent of $NiBr_2$(dme) to **3e** with and without a base results in the transmetallation of palladium(II) by nickel(II), to form a *bis*-chelate nickel(II) complex [L^2_2Ni]. This was confirmed by ^{1}H and ^{13}C{^{1}H} NMR spectrum of the resulting complex.

Further confirmation was made by ESI-MS with m/z value of 1072 (100%) which can be assigned to $[L^2{}_2Ni]$ as well as single crystal X-ray structure of the resulting complex (already reported).[221]

In another example, 0.5 mol equivalent $[RhCl(COD)]_2$ was added to a $CDCl_3$ solution of **3c** and the reaction mixture monitored for 24 h (Scheme 6.3.3. 3). After 15 min, the ^1H NMR spectrum peak intensity at -0.31 ppm for $CH_3{}^{Pd}$ group decreases, as well as a decrease in $^{31}P\{^1H\}$ at -3.30 ppm (PMe_3). In place of the diminishing $^{31}P\{^1H\}$ peak at -3.30 ppm, a broadened peak at -1.34 ppm and a single $^{31}P\{^1H\}$ resonance at -0.41 ppm are observed with time (Fig. 6.3.3. 1).

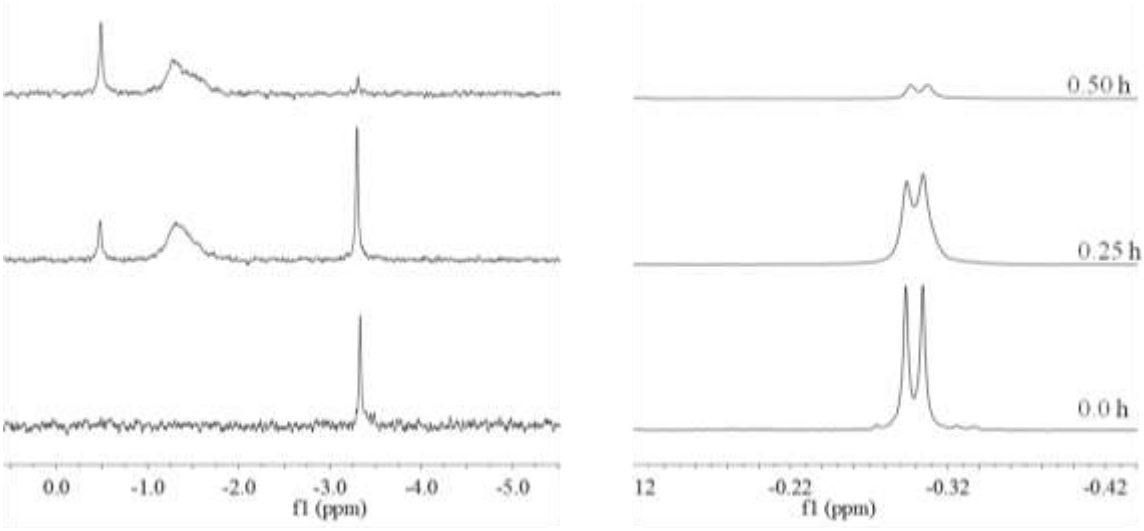

Fig. 6.3.3. 1: Changes in ^1H NMR (right) and $^{31}P\{^1H\}$ NMR spectra (left) of $[L^2Pd(CH_3)(PMe_3)]$ after addition of $[RhCl(COD)]_2$ measured in $CDCl_3$ at room temperature

Two batches of products were obtained after careful separation. The ^1H NMR spectrum of the first product points to the formation of $[PdCl(Me)(PMe_3)]_2$. After recrystallization of the filtrate, the ESI-MS data of the resulting complex shows m/z values of 905 (60%) which can be assigned to $[L^2Rh_2(COD)_2]^+$, and 695 (30%) for $[L^2Rh(COD)]^+$, thus pointing to the formation of a mononuclear $[L^2Rh(COD)]$ and a binuclear $[L^2Rh_2(COD)_2]^+$ complex. The exchange products were isolated and characterized by ^1H and ^{13}C NMR spectroscopy.

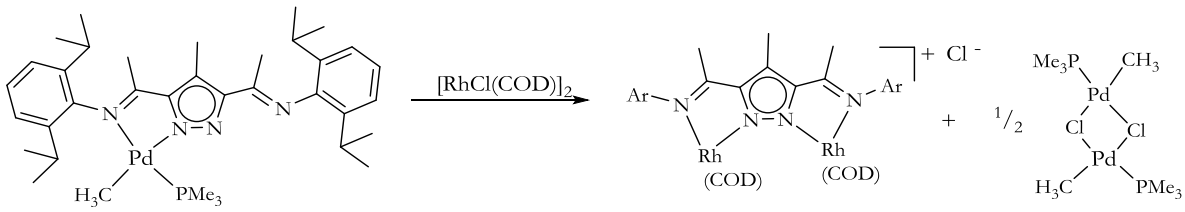

3c **3c$_1$**

Scheme 6.3.3. 3: Transmetallation of 3c to form 3c$_1$ and [Pd(CH$_3$)Cl(PMe$_3$)]$_2$

In view of the limited success achieved with this method, a second synthetic approach was explored having in mind that palladium(II) is easily displaced by rhodium(I) and nickel(II) salts.

6.3. 4 Homobimetallic palladium(II) η^3-allyl complex precursors

The idea was therefore to first prepare homobimetallic complexes of palladium(II) and explore the possibility of a metal exchange in one of the binding pockets. To meet this end, the [L^{x}Pd$_2$(η^3-allyl)$_2$]X (X= BF_4, PF_6) complexes were chosen for this purpose, due to their relative ease of synthesis (Scheme 6.3.4. 1).

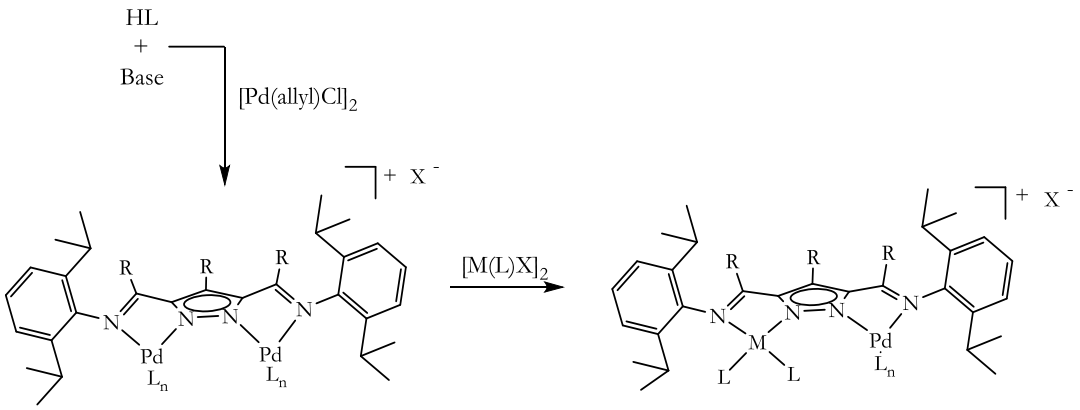

(**3m**): R = H, $L_n = C_4H_7$
(**3n**): R = Me, $L_n = C_4H_7$
(**3o**): R = H, $L_n = C_6H_9$
(**3p**): R = Me, $L_n = C_6H_9$

M = Rh,
R = H, Me
L = COD, CO
X = Cl, BF_4, PF_6, BAr^F_4

Scheme 6.3.4. 1: Metal exchange route to heterobimetallic complexes

In general, the palladium(II)-η^3-allyl complexes (**3m**-**3p**) were prepared in good to moderate yields (58-77%). The $[L^xPd_2(\eta^3\text{-}C_6H_9)_2]X$ (X = PF_6) complexes **3o** and **3p** are generally not very stable in solution at room temperature for long hours. For instance, when **3p** is left in solution at room temperature for 48 h, the formation of Pd "mirror" on the walls of the flask is observed (Scheme 6.3.4. 2). Colourless crystals (**3q**) were later harvested from the bottom of the flask.

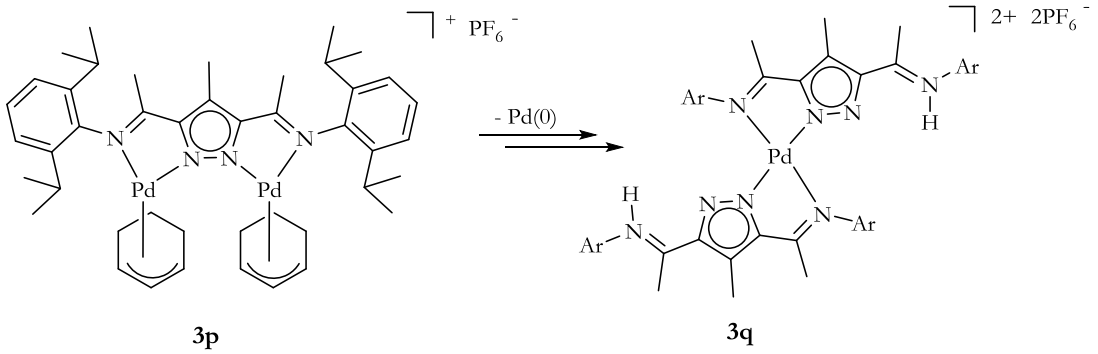

Scheme 6.3.4. 2: Dissociation and redistribution of 3p to form 3q

Single crystal X-ray structure of the colourless crystals points to the formation of a complex of the type $[(HL^2)_2Pd](PF_6)_2$ (Fig. 6.3.4. 1**)**. The compound crystallizes in the *P* -1 space group. The coordination around the palladium atom is square planar, with the plane around the palladium atom formed by N(1), N(3), N(1'), N(3'). The two imine nitrogen atoms, N(4) and N(4') are protonated. The interplanar angle formed between the atoms of the pyrazolyl ring and the atoms that make up the aryl ring is nearly perpendicular at 85.0°.

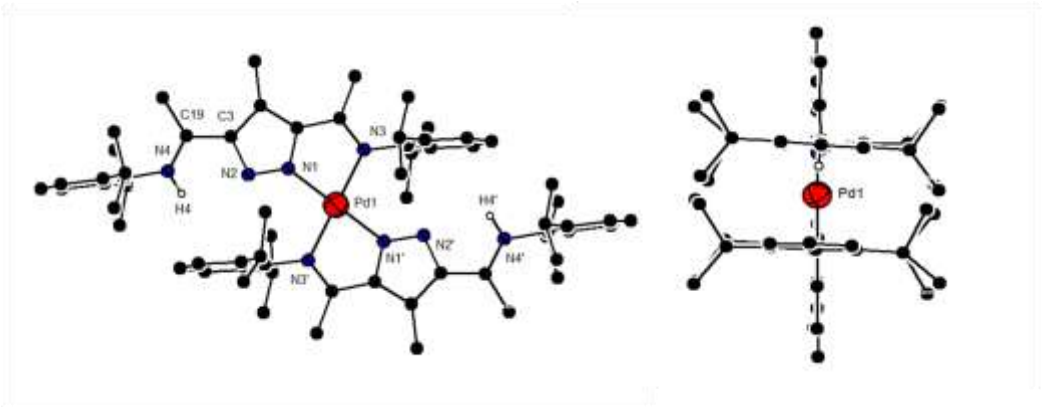

Fig. 6.3.4. 1: Molecular structure of 3q, most H atoms, and counterions omitted for clarity

The interplanar angles between the aryl rings on opposite sides of the palladium centre are nearly planar at 6.27°. In addition, the torsional angle for the non coordinated side arm defined by N(2)-C(3)-C(19)-N(4) is -0.83° compared to 171.2° found in the analogous L^2_2Pd complex (**3h**), thus the presence of the proton causes a change in orientation of the non-coordinating N^N pocket. This may be due to some form of interaction between H4/H4' with the π cloud of the aromatic rings. Selected bond lengths [Å] and bond angles [°] are given in Table 6.3.4. 1.

Table 6.3.4. 1: Selected bond lengths [Å] and bond angles [°] for 3q

Bond lengths [Å]		Bond angles [°]	
Pd(1)-N(1)	1.992(3)	N(3)-Pd(1)-N(3')	179.99(1)
Pd(1)-N(3)	2.053(3)	N(3')-Pd(1)-N(1')	101.29(11)
Pd(1)-N(1)'	1.992(3)	N(1')-Pd(1)-N(3')	78.71(11)
Pd(1)-N(3')	2.053(3)	N(1')-Pd(1)-N(1')	180.00(14)

However, **3p** can be stored for several weeks at cold temperatures in the solid state. The $[L^xPd_2(\eta^3\text{-}C_4H_7)_2]X$ (X= BF_4, BAr^F_4) complexes (**3m** and **3n**) (Scheme 6.3.4. 4) on the other hand are more stable in solution at room temperature. (**NB**: **3n** with a Cl counterion has been reported[221]). In the ESI-MS of the complexes, the most pronounce fragmentation is the loss of the allyl moiety. The complexes were fully characterized by ^1H, ^{13}C NMR, IR, and ESI-MS and in some instances single crystal X-ray structures.

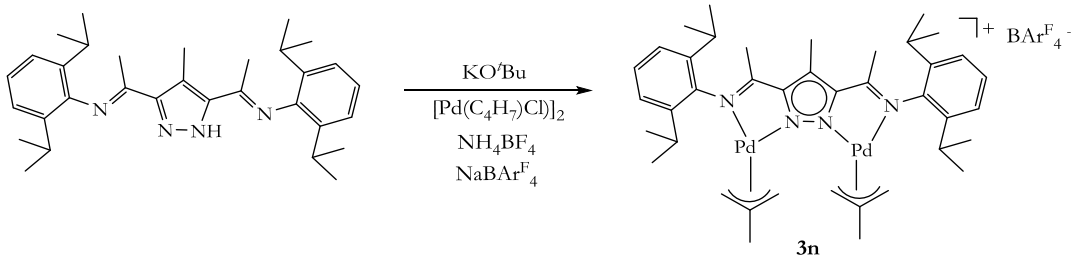

3n

Scheme 6.3.4. 3: Synthetic scheme for the preparation of 3n

For example, the IR spectrum of **3n** shows a η^3-allyl palladium(II) complex; the absence of absorption in the region 1610 cm^{-1} (ATR) suggests the allyl groups are not σ-bonded. The NMR spectrum in $CDCl_3$ is consistent with a η^3-allyl complex, although the spectrum at room temperature indicates a rapid exchange of the *syn* and *anti* protons, a feature common

to palladium(II) allyl complexes.[258] This broadening of the allylic CH_2 is consistent with the η^3-η^1 opening of allylic ligands, usually followed by rotation around the C-C bond and subsequent isomerisation to η^1-η^3 to form the allyl ligand as depicted in Scheme 6.3.4. 4.

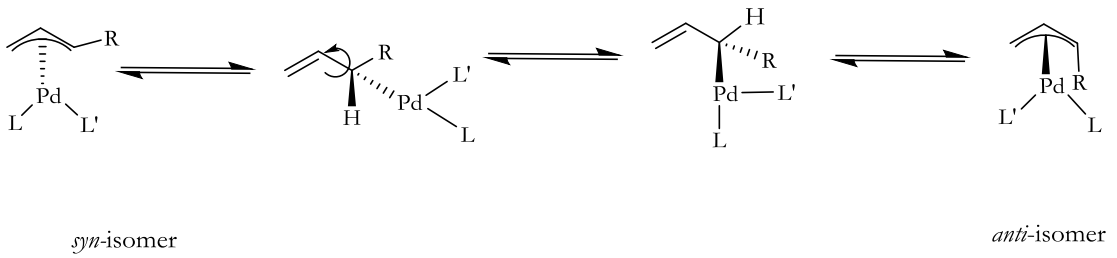

Scheme 6.3.4. 4: η^3- η^1- η^3 isomerization of palladium(II) allyl complexes

Apart from η^3 -η^1-η^3 isomerization that occurs through the change in coordination of the palladium centre from η^3-η^1, and allows free rotation around the C-C bond, with subsequent reformation to η^3 allyl complex; other dynamic processes in η^3-allyl palladium complexes also include: (i) Ligand exchange, which can proceed via either associative or dissociative processes (Scheme 6.3.4. 5).

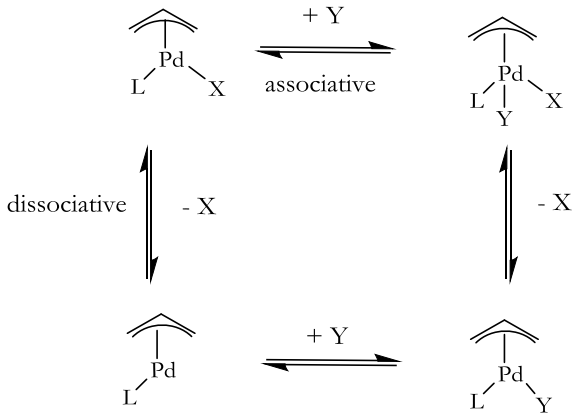

Scheme 6.3.4. 5: Ligand exchange through associative and dissociative pathways

(ii) Apparent rotation (*syn-syn*, *anti-anti* isomerisation); Two different mechanisms have been proposed since the direct rotations in η^3-allyl complexes seem unlikely in square planar complexes. These are the associative pseudo rotation[259] and dissociative mechanism[260,261] (Scheme 6.3.4. 6).

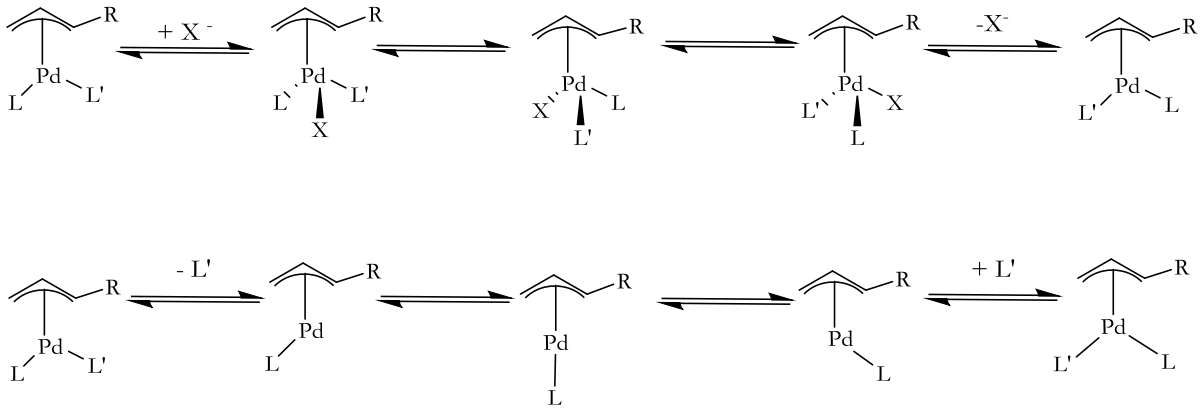

Scheme 6.3.4. 6: Apparent rotation through pseudo rotation (top) and apparent rotation by dissociative mechanism, through a T-shaped intermediate

Crystals of **3n** were obtained by the slow diffusion of hexane into a CH_2Cl_2 solution of the complex at cold temperatures. Molecular structures of **3n** and **3p** complexes are shown in Fig. 6.3.4. 2 and Fig. 6.3.4. 3 respectively, as well as Tables showing selected bond lengths and bonds angles for these complexes.

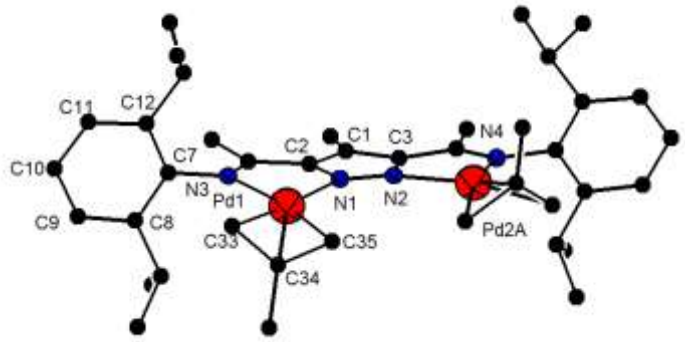

Fig. 6.3.4. 2: Molecular structure of 3n, all H atoms and counterion omitted for clarity

In **3n**, the compound crystallizes in the *P* 21/c space group. The coordination geometry around the palladium(II) centre is square planar. The η^3-allyl bond lengths C(34)-C(35) (1.40 Å) and C(33)-C(34) (1.41 Å) are almost equal. The dihedral angle defined by Pd(1)-N(2)-N(1)-Pd(2A) is 11.9°. The inter palladium distance is 4.57 Å. In addition, the angle between two planes described by six atoms in the aryl side arm (C(7)/C(8)/C(9)/C(10)/C(11)/C(12)) and five atoms of the pyrazole ring (N(2)/N(1)/C(3)/C(1)/C(2)) is nearly perpendicular at 88.2°. This orientation prevents steric interactions between the $CH_3{}^{iPr}$ and the η^3-C_4H_7 group.

The Pd-C bond lengths are in the range of other palladium(II) allyl complexes.[262,263,264] Selected bond lengths [Å] and bond angles [°] are given in Table 6.3.4. 2.

Table 6.3.4. 2: Selected bond lengths [Å] and bond angles [°] for 3n

Bond lengths [Å]		Bond angles [°]	
Pd(1)-N(3)	2.092(4)	N(3)-Pd(1)-N(1)	78.15(14)
Pd(1)-C(35)	2.141(6)	N(3)-Pd(1)-C(35)	168.84(19)
Pd(1)-C(34)	2.171(6)	N(1)-Pd(1)-C(35)	113.01(19)
Pd(1)-Pd(2A)	4.576(21)	N(1)-Pd(1)-C(33)	175.5(2)
C(33)-C(34)	1.415(113)	N(3)-Pd(1)-C(33)	105. 0(209)
C(34)-C(35)	1.406(99)	C(33)-C(34)-C(35)	116.1(658)

Using $[Pd(\eta^3\text{-}C_6H_9)Cl]_2$, it was possible to isolate the analogous $[L^2Pd_2(\eta^3\text{-}C_6H_9)_2]PF_6$ complex **3p** under similar experimental conditions (Scheme 6.3.4. 7).

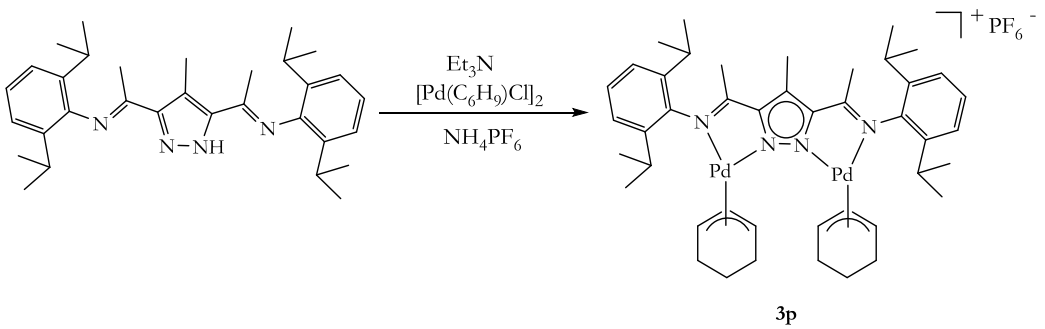

3p

Scheme 6.3.4. 7: Synthetic scheme for the preparation of 3p

In the ^{1}H NMR spectrum of **3p**, the CH_3^{iPr} groups at room temperature appear as overlapping sets of doublets between 1.09-1.29 ppm, possibly due to different orientations of the aryl ring with respect to the pyrazole plane. The methylene groups of the cyclohexenyl ring are also observed as broadened peaks in the ^{1}H NMR spectrum between 1.59-1.86 ppm. The peaks for the $CH_3C{=}N$ and CH_3^{Pz4} groups are observed at 2.29 and 2.62 ppm and integrate for 6H and 3H, respectively. The methine group on the other hand is observed as a triplet at 5.69 ppm (Fig. 6.3.4. 3).

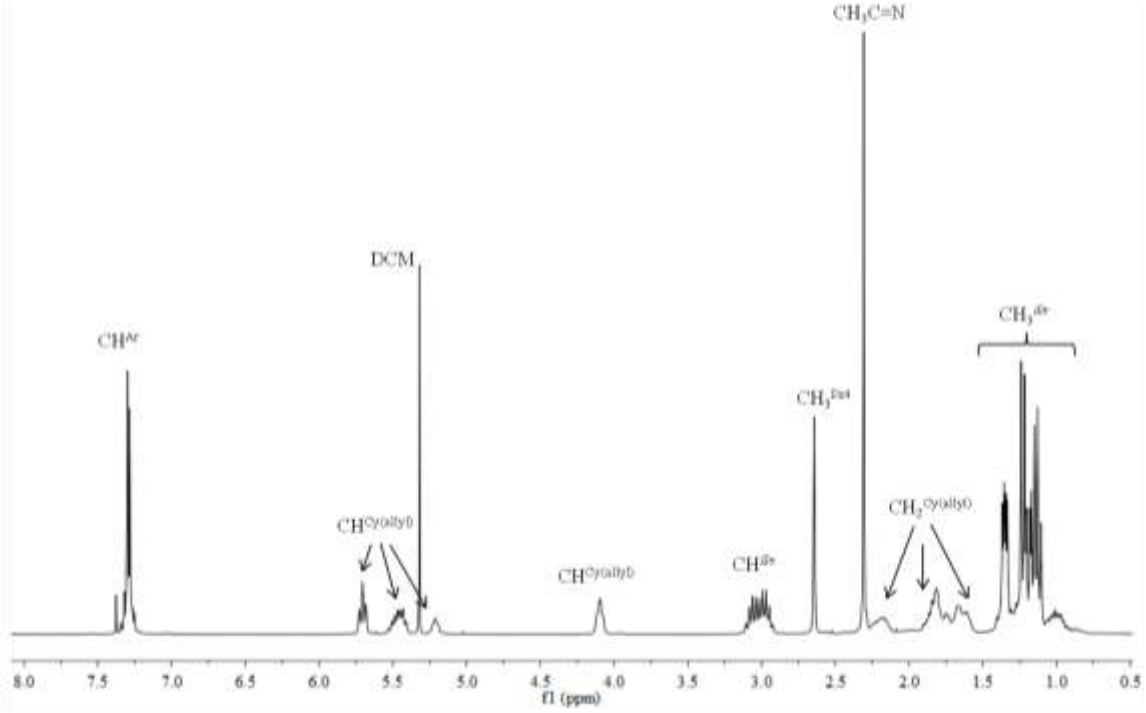

Fig. 6.3.4. 3: ^{1}H NMR spectrum of 3p measured in $CDCl_3$ at room temperature

Single crystals of **3p** were grown by the slow diffusion of Et_2O into a CH_2Cl_2 solution of the complex. The molecular structure of **3p** is shown in Fig. 6.3.4. 4.

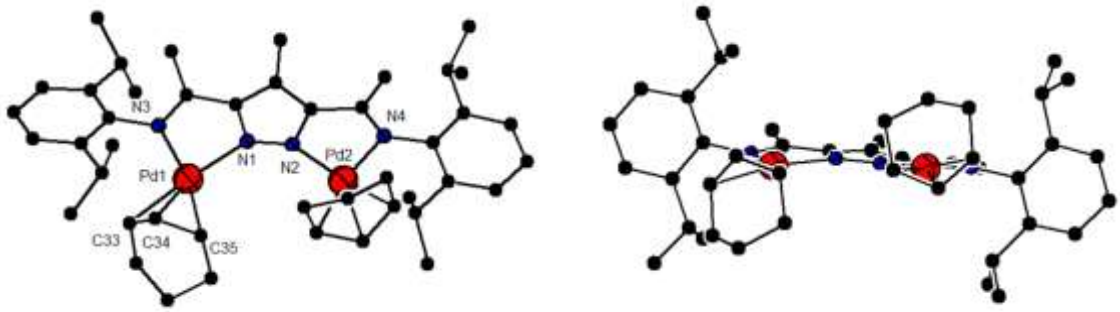

Fig. 6.3.4. 4: Molecular structure of 3p (different orientations) all H atoms and counterion omitted for clarity

The complex crystallizes with a PF_6 counterion and one molecule of CH_2Cl_2. The coordination around the two palladium centres is square planar. The inter palladium distance in **3p** is 4.53 Å compared to 4.57 Å in **3n**. The average Pd-N bond distance is 2.12 Å, and the ligand bite angle (∠N(3)Pd(1)N(1) is equal in both pockets at 77.1°. The dihedral angle defined by Pd(1)-N(1)-N(2)-Pd(2) is -16.0° compared to 11.9° in **3n** due to limitations imposed by the cyclohexenyl ring. The η^3-allyl bond lengths C(34)-C(35) (1.40 Å) and C(33)-

C(34) (1.41 Å) are almost equal and comparable to the η^3-allyl bond lengths observed for **3n**. Selected bond lengths [Å] and bond angles [°] are given in Table 6.3.4. 3.

Table 6.3.4. 3: Selected bond lengths [Å] and bond angles [°] for 3p

Bond lengths [Å]		**Bond Angles [°]**	
Pd(1)-N(1)	2.125(3)	N(1)-Pd(1)-N(3)	76.96(10)
Pd(1)-N(3)	2.113(37)	C(34)-Pd(1)-C(33)	38.74(17)
Pd(1)-Pd(2)	4.529(4)	N(1)-Pd(1)-C(33)	170.08(16)
C(33)-C(34)	1.404(73)	N(3)-Pd(1)-C(33)	101.28(14)
C(34)-C(35)	1.413(83)	N(1)-Pd(1)-C(35)	115.06(17)

With success in obtaining the homobimetallic palladium(II) η^3-allyl complexes (**3m**-**3p**), the next step was to explore metal exchange in one of the palladium(II) pockets with rhodium(I).

6.3. 5 Heterobimetallic palladium(II)-rhodium(I) complexes

Having prepared the homobimetallic palladium(II) complexes, the synthetic route adopted involved treating the homobimetallic complexes with Rh(I) metal salts with the aim of obtaining the corresponding heteronuclear complex *via* a metal exchange process (Scheme 6.3.5. 1).

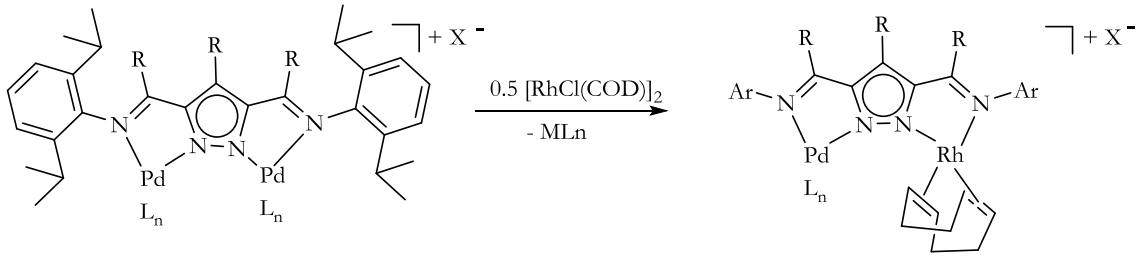

(**3m**): R = H, $L_n = C_4H_7$, X = PF_6
(**3n**): R = Me, $L_n = C_4H_7$, X = $BAr^F{}_4$
(**3o**): R = H, $L_n = C_6H_9$, X = PF_6
(**3p**): R = Me, $L_n = C_6H_9$, X = PF_6

(**3r**): R = H, $L_n = C_4H_7$
(**3s**): R = Me, $L_n = C_4H_7$
(**3t**): R = H, $L_n = C_6H_9$
(**3u**): R = Me, $L_n = C_6H_9$

Scheme 6.3.5. 1:: Metal exchange route to heterobimetallic Pd-Rh complexes

This approach was largely successful, with the corresponding RhPd complexes obtained in moderate to good yields (34-94%). The complexes were characterized by a combination of ^1H and ^{13}C NMR and IR spectroscopy, HRMS and in some instances single crystal X-ray structures. For instance, the treatment of the cationic $[L^2Pd_2(\eta^3\text{-}C_6H_9)_2]PF_6$ complex (**3p**) with 0.5 mol equivalent of $[(Rh(COD)Cl)]_2$ in CH_2Cl_2 gives the corresponding heterobimetallic cationic complex $[L^2Pd(\eta^3\text{-}C_6H_9)Rh(COD)]PF_6$ (**3u**). The HRMS data for **3u** is in good agreement with calculated and observed isotopic mass (881.3232 amu).

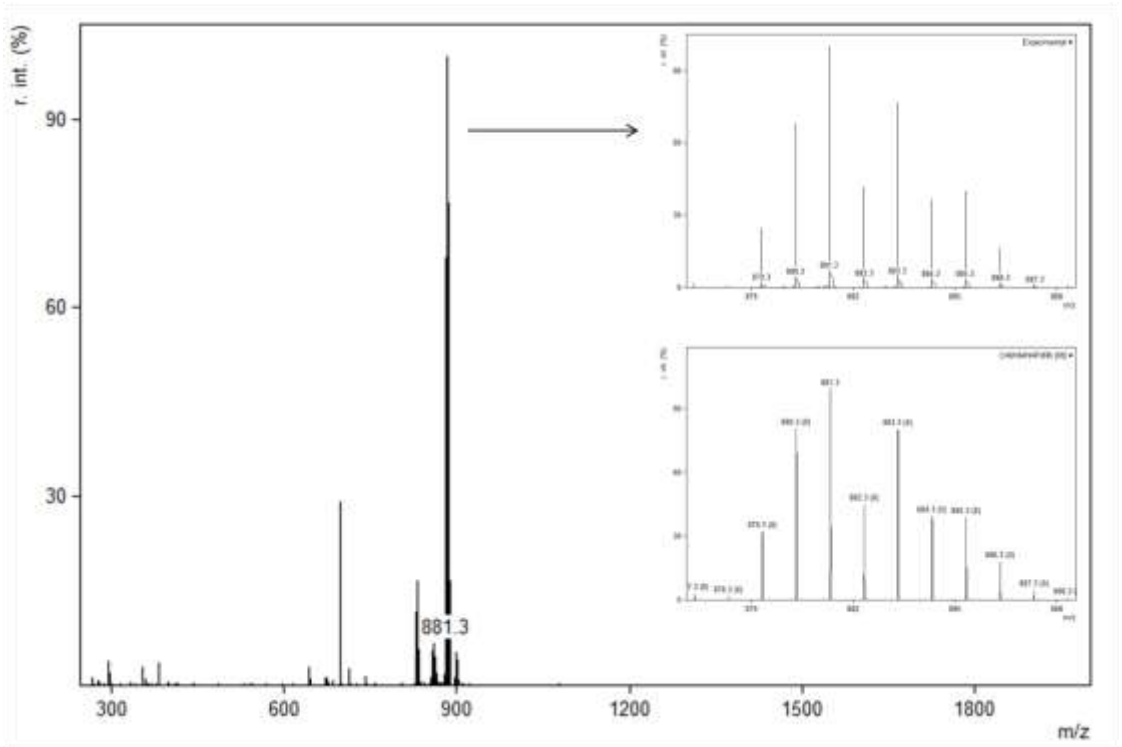

Fig. 6.3.5. 1: ESI mass spectrum of 3u Observed (top) and simulated (bottom) isotopic distribution pattern.

The formation of the heterobimetallic complex **3u** was also observed in ^{1}H and ^{13}C NMR spectra. However, attempts to grow single crystals of **3u** suitable for X-ray crystallography always turn up a homobimetallic rhodium(I) complex $[L^{2}Rh_{2}(COD)_{2}]PF_{6}$ (**3v**) (Scheme 6.3.5. 2). The use of metal exchange processes is known to lead to precipitation of homodinuclear or mononuclear complex species.[265]

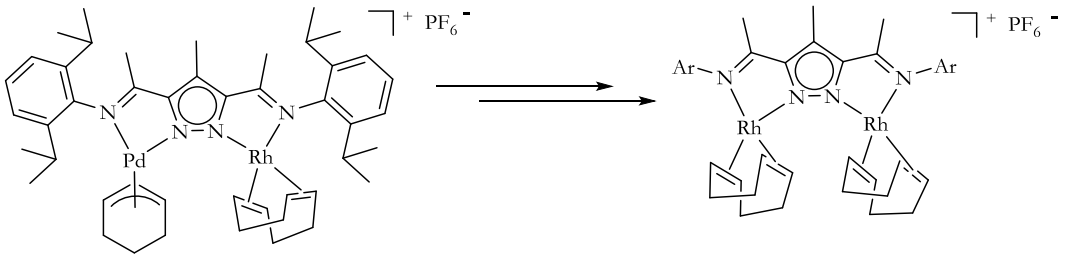

3u **3v**

Scheme 6.3.5. 2: Scheme showing the rearrangement of 3u to form 3v

The mechanism leading to the formation of **3v** is not well understood, but may be largely influenced by the instability of the palladium(II) cyclohexenyl allyl moiety, which easily undergoes homolysis to form Pd(0). The single crystal X-ray structure of **3v** is shown below

in Fig. 6.3.5. 2. Although the X-ray data is not good, the molecular structure invariably shows the atom connectivity.

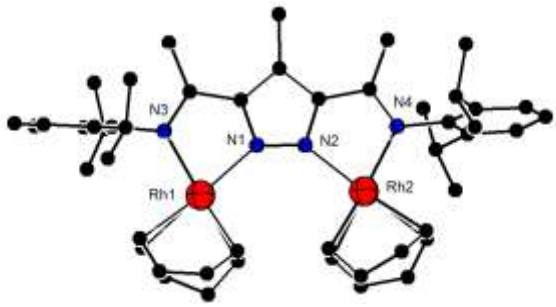

Fig. 6.3.5. 2: Molecular structure of 3v with all H atoms and counterion omitted for clarity

In the crystal structure of **3v**, the coordination around the two rhodium(I) centres is square planar. The Rh···Rh separation is 4.60 Å which is significantly longer than the sum of the covalent radii (2.68 Å). The torsional angle formed by Rh(1)-N(1)-N(2)-Rh(2) is -12.5°. The interplanar angle formed between the phenyl rings of the two peripheral aryl rings is 15.8°. The interplanar angle between the six carbons of the aromatic and the five atoms, which make up the pyrazolyl ring is nearly perpendicular at 84.6°. Selected bond lengths and bond angles are given in Table 6.3.5. 1.

Table 6.3.5. 1: Selected bond lengths [Å] and bond angles [°] for 3v

bond lengths [Å]		bond angles [°]	
Rh(1)-N(1)	2.120(110)	Rh(1)-C(38)-N(3)	160.0
Rh(1)-N(3)	2.079(118)	Rh(2)-C(34)-N(4)	165.2
Rh(2)-N(2)	2.101(110)	Rh(1)-N(3)-N(1)	77.3
Rh(2)-N(4)	2.077(117)	Rh(2)-N(4)-N(2)	78.0
Rh(1)-Rh(2)	4.603(20)	Rh(1)-N(1)-N(2)	138.2

Efforts were made to overcome the formation of the dirhodium complex **3v** in solution by replacing the PF_6^- counter ion with the more bulky $[BAr^F{}_4]^-$ counterion. This technique was largely successful, MS data showed the required molecular ion m/z 882 (100%) which can be assigned to $[M\text{-}BAr^F{}_4]^+$. A single crystal X-ray structure of the resulting heterobimetallic complex **3u** is shown in Fig. 6.3.5. 3. This was obtained by the evaporation of cyclohexane/CH_2Cl_2 solution of the complex at room temperature.

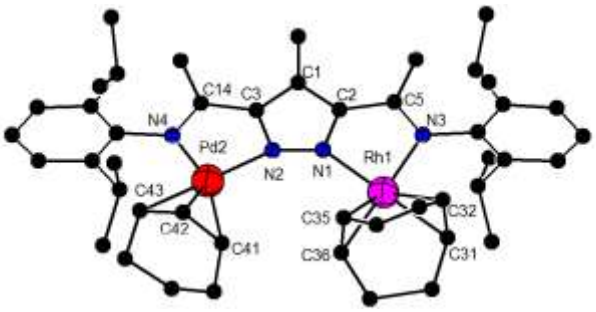

Fig. 6.3.5. 3: Molecular structure of 3u with solvent molecules, H atoms and counterion omitted for clarity

The compound **3u** crystallizes in the *P* -1 space group, with a $[BAr^F_4]^-$ counterion and two molecules of cyclohexane. The intermetallic distance (Pd···Rh) is 4.65 Å. The dihedral angle formed by Pd(2)-N(2)-N(1)-Rh(1) is 23.5°. The Pd(2)-N(4) distance is 2.13 Å compared to Pd(2)-N(2) bond distance of 2.21 Å. Thus, the bond between the imine nitrogen and the palladium atom is stronger compared to the pyrazolyl nitrogen. The Rh-N bond distance is the same (2.08 Å) for both pyrazole N(1) and imine nitrogen N(3).

The interplanar angle defined by six atoms that make the two aromatic rings is nearly planar at 3.83°. On the other hand, the interplanar angles between planes defined by six atoms of the aromatic rings either side of the pyrazolyl ring and the five atoms of the pyrazole ring (N(1)/N(2)/C(3)/C(1)/C(2)) is perpendicular at 90°. This orientation keeps the isopropyl groups away for the coligands. The η^3-allyl bond for C(42)-C(43) (1.43 Å) is longer than C(42)-C(41) (1.35 Å) compared to η^3-allyl bond of 1.40 and 1.41 Å in the homobimetallic complex. Thus, the double bond character lies more between C(42)-C(41). The ligand bite angle is larger in the rhodium pocket (∠N(1)Rh(1)N(3) = 79.0°) compared to the palladium pocket (∠N(4)Pd(2)N(2) = 75.7°) in order to accommodate the larger Rh(I) atom. Selected bond lengths and bond angles are given in Table 6.3.5. 2.

Table 6.3.5. 2: Selected bond lengths [Å] and bond angles [°] for 3u

Bond lengths [Å]		Bond angles [°]	
Pd(2)-N(4)	2.130(4)	C(36)-Rh(1)-N(1)	98.1(2)
Pd(2)-Rh(1)	4.653(8)	C(36)-Rh(1)-N(3)	172.9(3)
Pd(2)-N(2)	2.213(3)	N(1)-Rh(1)-N(3)	79.0(13)
Rh(1)-N(1)	2.081(3)	N(1)-Rh(1)-C(31)	174.7(3)
C(34)-C(35)	1.356(164)	N(3)-Rh(1)-C(31)	98.0(18)
C(41)-C(42)	1.349(141)	N(1)-Rh(1)-C(35)	96.6(2)
C(42)-C(43)	1.431(126)	C(36)-Rh(1)-Pd(1)	39.2(3)

The analogous molecular structure of the heterobimetallic complex [L^1Pd(η^3-C_6H_9)Rh(COD)]PF_6 **3t** is shown in Fig. 6.3.5. 4 .

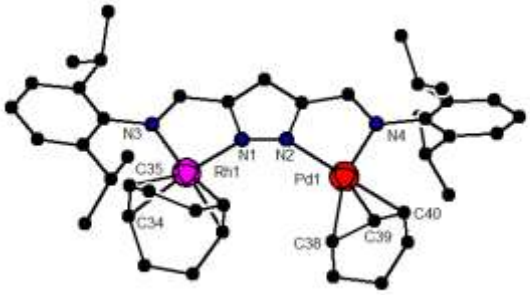

Fig. 6.3.5. 4: Molecular structure of 3t with H atoms and counterion omitted for clarity

Single crystals were obtained by the slow evaporation of a CH_2Cl_2 solution of the complex at room temperature. The compound **3t** crystallizes in the *Cc* space group with a PF_6^- counterion and a molecule of CH_2Cl_2. In **3t**, the intermetallic distance (Pd···Rh) is 4.65 Å, compared to 4.63 Å in **3u**. The dihedral angle formed by Rh(1)-N(1)-N(2)-Pd(1) is 9.81° compared to 23.5° in **3u**. The ligand bite angles in the rhodium and palladium pockets are (∠N(1)Rh(1)N(3) = 79.9°) and (∠N(2)Pd(1)N(4) = 78.19°) respectively. The Pd(1)-N(2) and Pd(1)-N(4) bond lengths are 2.16 and 2.11 Å respectively, whiles the Rh(1)-N(3) (2.10 Å) is slightly longer compared to Rh(1)-N(2) bond lengths of 2.08 Å respectively. The allyl group is again unsymmetrical with C(38)-C(39) and C(39)-C(40) bond lengths of 1.43 Å and 1.37 Å respectively, similar to allyl bond lengths observed in **3u**. The presence of the Rh(I) centre therefore seems to electronically influence the η^3-allyl bond lengths on the palladium(II) centre. Heterobimetallic complexes are known to have unusual electronic, electrochemical and magnetic properties due to the presence of two different metal sites.[266,267] Some selected bond lengths and bond lengths in Table 6.3.5. 3.

Table 6.3.5. 3: Selected bond lengths [Å] and bond angles [°] for 3t

Bond lengths [Å]		Bond angles [°]	
Rh(1)-N(1)	2.088(6)	N(1)-Rh(1)-N(3)	79.9(2)
Rh(1)-N(2)	2.087(54)	N(31)-Rh(1)-C(31)	159.7(3)
Pd(1)-Rh(1)	4.653(8)	N(31)-Rh(1)-C(35)	94.4(3)
Pd(1)-N4(4)	2.110(65)	N(2)-Pd(1)-N(4)	78.2(228)
Pd(1)-N(2)	2.160(54)	C(40)-Pd(1)-N(2)	170.7(4)
C(38)-C(39)	1.432(154)	C(39)-C(40)-Pd(1)	73.0(6)
C(39)-C(40)	1.376(160)	C(41)-C(40)-Pd(1)	102.1(7)

The formation of the heterobimetallic complex was also evident from the ^{1}H and ^{13}C NMR spectra. The figure below (Fig. 6.3.5. 5) shows the ^{1}H NMR spectra of both the homobimetallic (above) and the heterobimetallic complex (below).

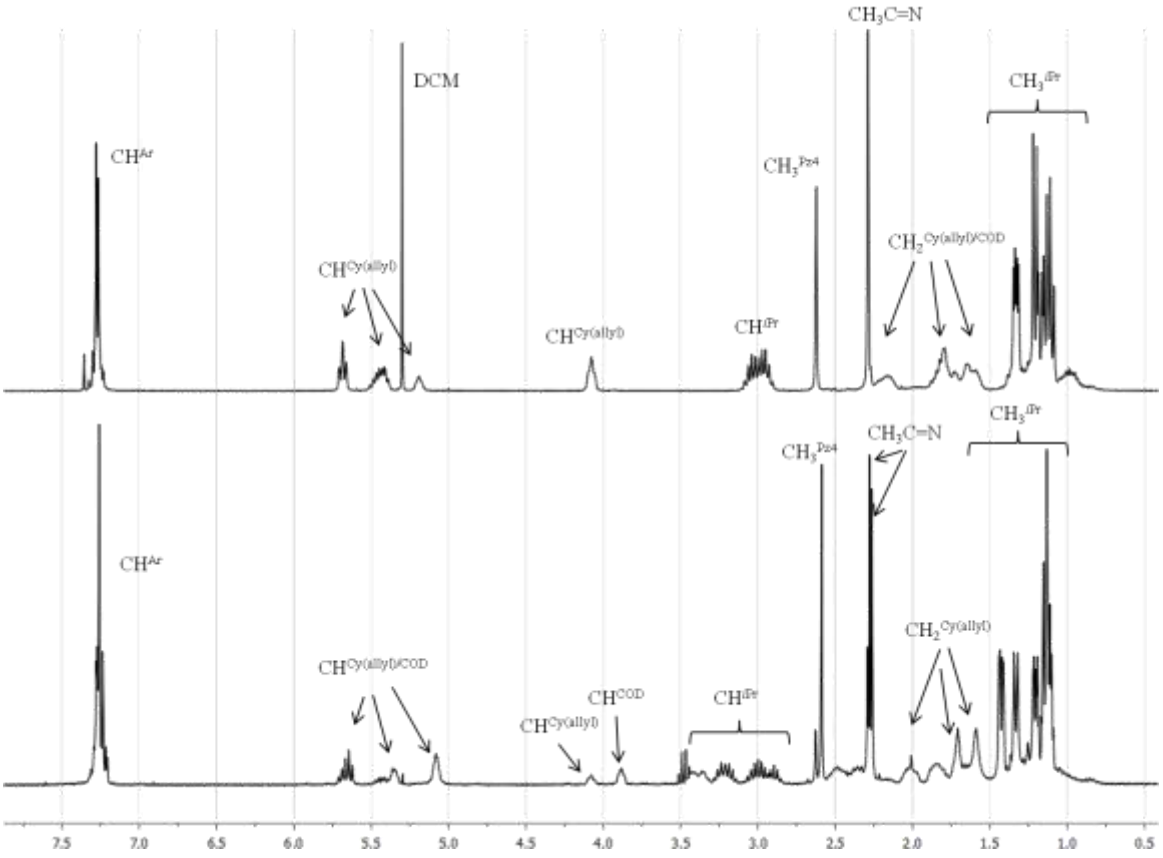

Fig. 6.3.5. 5: ^{1}H NMR spectra of homobimetallic palladium complex 3p (top) and the heterobimetallic palladium-rhodium complex 3u (bottom) measured in $CDCl_3$ at room temperature

As earlier stated, the ^{1}H NMR spectrum of the $[L^{2}Pd_2(\eta^3\text{-}C_6H_9)_2]PF_6$ (**3p**) complex shows $CH_3C{=}N$ and CH_3^{Pz4} resonance peaks at 2.29 and 2.62 ppm which integrate for 6H and 3H respectively, showing the symmetric ligand environment. In the heterobimetallic complex **3u**, the $CH_3C{=}N$ splits into two singlets at 2.26 and 2.28 ppm and integrates for 3H each. These signals have ^{13}C NMR correlation with the $CH_3\mathit{C}{=}N$ at *ca* 170.6 ppm for the imine side arm bearing palladium whiles $CH_3\mathit{C}{=}N$ correlation of *ca* 173.6 ppm for the side arm bearing the rhodium(I) centre. The CH_3^{Pz4} peak however remains unchanged.

^{1}H NMR spectrum peaks at 4.08, 5.08 and 5.62 ppm are assigned to the vinylic protons in COD and allylic protons, while the $CH_2^{COD/Cy}$ protons are observed as multiplets between

1.08-2.47 ppm. Compared to **3n**, the allyl species are locked in *anti-anti* conformation and hence no *syn/anti* isomerisation via π-σ-π exchange is possible.

In the analogous complex $[L^1Pd(\eta^3\text{-}C_6H_9)Rh(COD)]PF_6$ **3t**, the CH=N peaks (H4 and H17) are observed as singlets at 7.97 and 8.22 ppm for the arms bearing the rhodium(I) and palladium(II) atoms respectively.

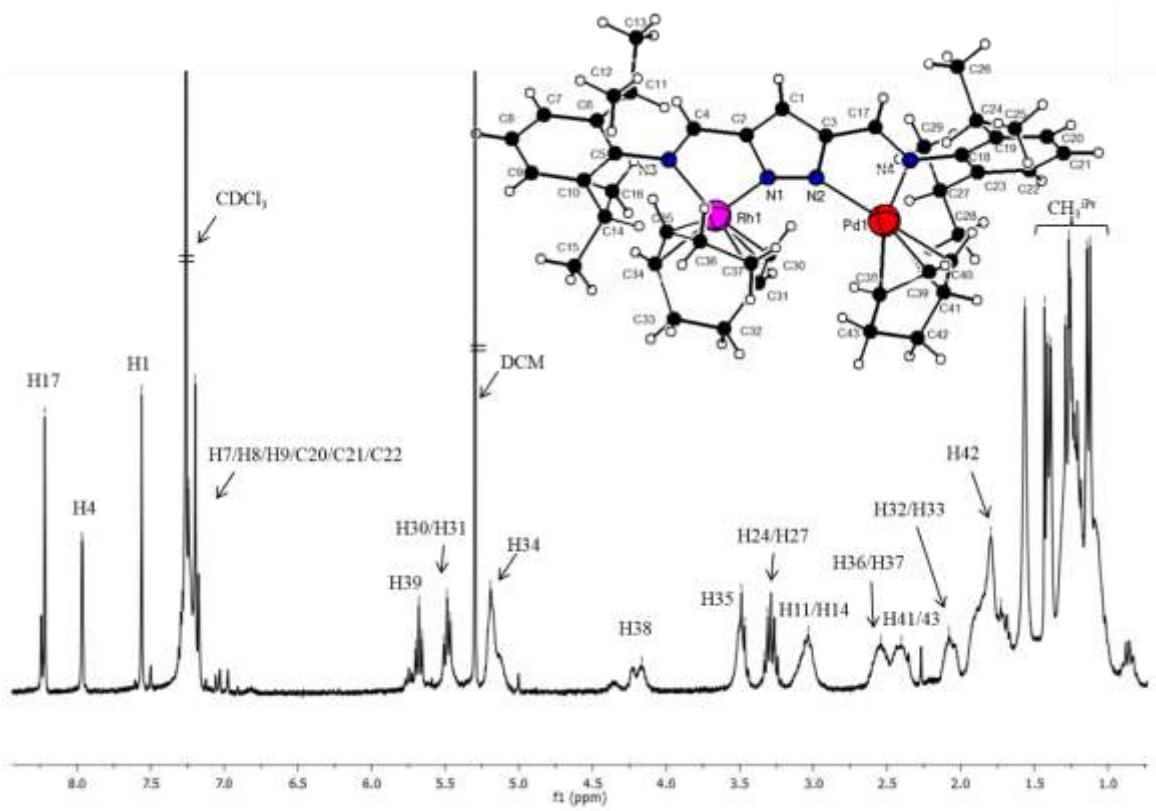

Fig. 6.3.5. 6: ^{1}H NMR spectrum assignments for 3t, NMR measured at room temperature in $CDCl_3$

This is also observed in the IR spectrum where two different CH=N stretching vibrations are observed at 1605 cm^{-1} and 1586 cm^{-1} for the sidearm bearing the palladium(II) and rhodium(I) centres respectively. Compared to the homobimetallic complex $[L^1Pd_2(\eta^3\text{-}C_6H_9)_2]PF_6$ (**3o**) where only one CH=N environment is observed at 1613 cm^{-1}. Thus the presence of the rhodium centre causes the CH=N stretching vibrations to shift to a lower wavenumber likely due to the more effective π-bonding between Rh(I) and COD coligands.

The signals for the allyl ligands are observed at 4.16, 5.49, 5.68 and 5.75 ppm. The methylene groups of the cyclohexenyl ring and COD ligands are observed as slightly broadened signals between 1.08 - 2.54 ppm room temperature. The ^{1}H and ^{13}C NMR spectra assignment of the peaks of **3t** were established by a combination of 1D and 2D (^{1}H-^{1}H COSY, ^{1}H-^{13}C HSQC,

^{1}H-^{13}C HSQC) experiments. ^{1}H NMR spectral peaks were assigned (Fig. 6.3.5. 6) based on ^{1}H-^{1}H COSY and ^{1}H-^{13}C HSQC experiments. COSY correlations between H34 and H33, H38 and H39, H41 and H42 are observed.

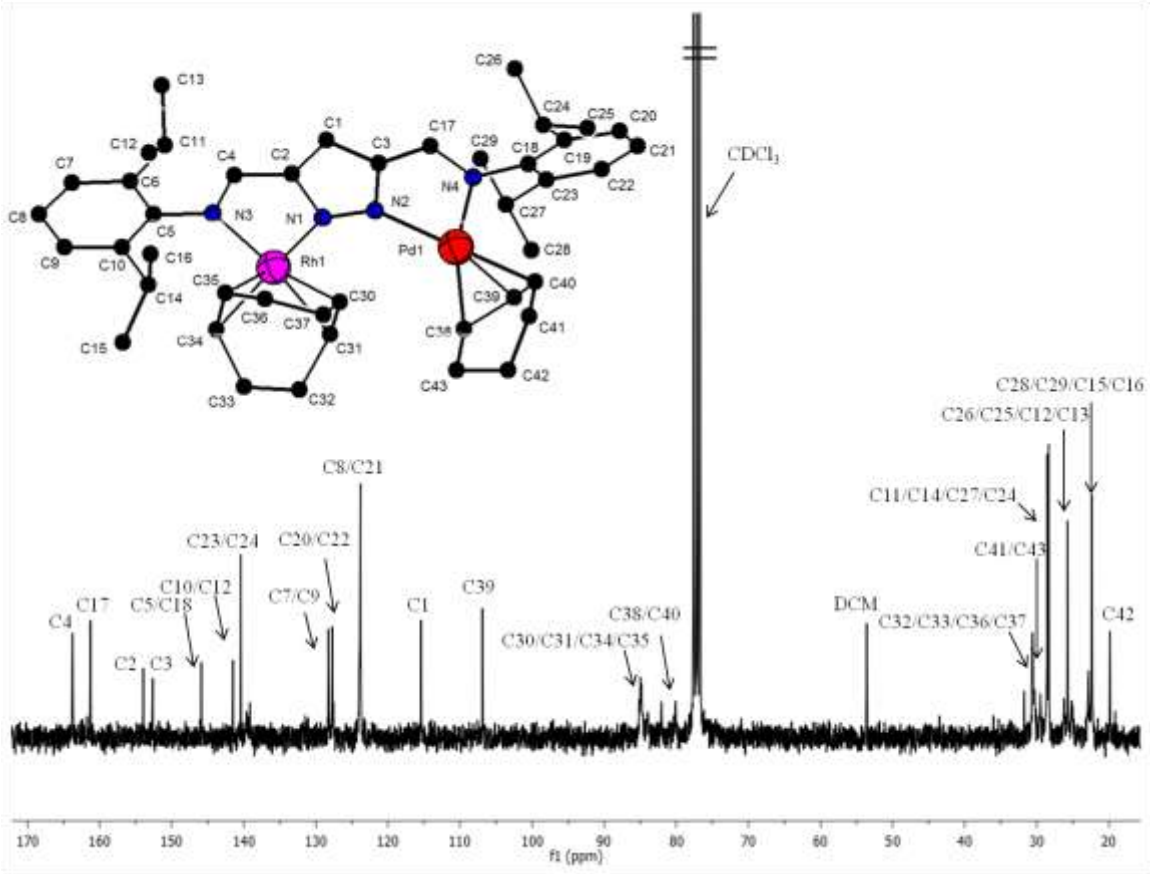

Fig. 6.3.5. 7: ^{13}C NMR spectrum assignments for 3t, NMR measured at room temperature in $CDCl_3$

In the ^{1}H-^{13}C HSQC NMR spectrum, correlations are observed for the CH=N group at 7.97 and 8.22 ppm in ^{1}H NMR spectrum with ^{13}C NMR resonances at 163.7 ppm and 161.2 ppm for the side arms bearing the rhodium(I) (C4) and palladium(II) centres (C17) respectively. In the ^{1}H-^{13}C HMBC spectrum, C1 is identified by its cross peaks with C2 and C3. In addition, C15 is assigned from its cross peaks with C14 and C10. The quaternary carbons C10, C6, C23 and C19 are assigned from their strong peaks with the methyl protons of the isopropyl group. The complete ^{13}C NMR assignments are shown in Fig. 6.3.5. 7. The CH_2 carbons of the COD (C32/C33/C36/C37) and cyclohexenyl (C41/C42/C43) are identified as negative peaks in a DEPT-135 experiment. In addition, a NOESY correlation is observed between the CH^{COD} protons H30 and H35.

The preparation of heterobimetallic complexes of the type $[L^xPd(\eta^3\text{-allyl})Rh(CO)_2]X$ (X = PF_6, BAr^F_4) (**3w**, **3x**, **3z**) was achieved in 41-81% yield. Two synthetic routes were adopted, the first route involved transmetallation of $[L^xPd_2(\eta^3\text{-allyl})_2]X$ complexes with 0.5 mol equivalent $[RhCl(CO)_2]_2$. The second synthetic route involved the carbonylation of the heterobimetallic $[L^xPd(\eta^3\text{-allyl})Rh(COD)]X$ complexes as shown in Scheme 6.3.5. 3.

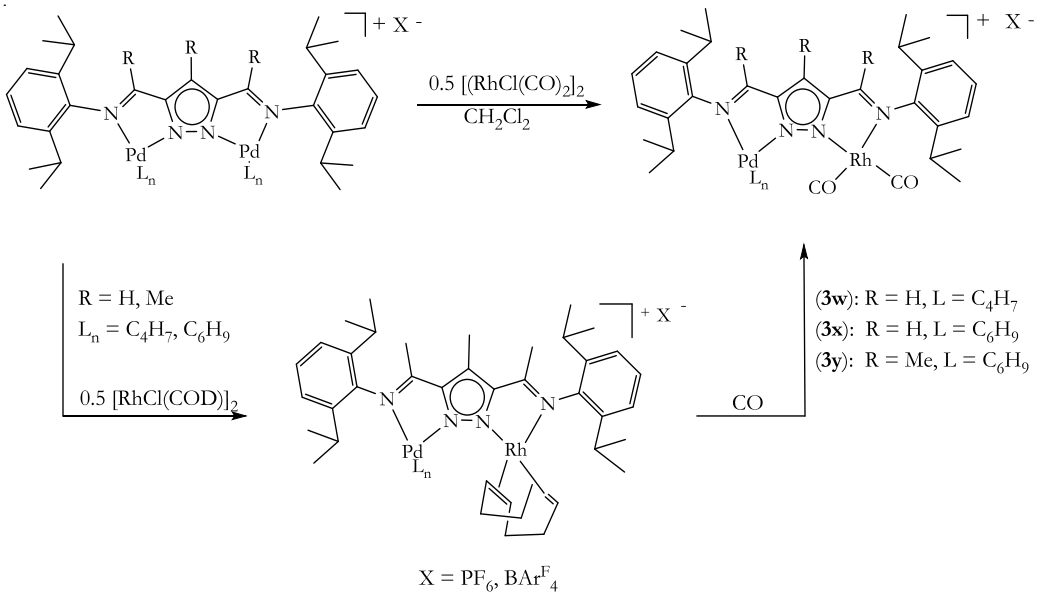

Scheme 6.3.5. 3: Reaction paths to the formation of complexes (3w-3y)

Both synthetic paths lead to the formation of the required product, although the carbonylation path sometimes leads to the formation of homobimetallic $[LRh_2(CO)_2]X$ in some instances. In the second synthetic route, which involves carbonylation of the COD complexes, generally, the CO complexes had to be kept under an atmosphere of CO, to prevent the reversible binding of COD. The complexes were characterized by ^1H and ^{13}C NMR and IR spectroscopy, ESI-MS and HRMS analysis. Attempts at obtaining single crystals were unsuccessful.

Treating a CH_2Cl_2 solution of **3p** with 0.5 mol equivalent $[RhCl(CO)_2]_2$ results in the isolation of the heterobimetallic complex $[L^1Pd(\eta^3\text{-}C_6H_9)Rh(CO)_2]PF_6$ (**3x**) in 41% yield (Scheme 6.3.5. 4).

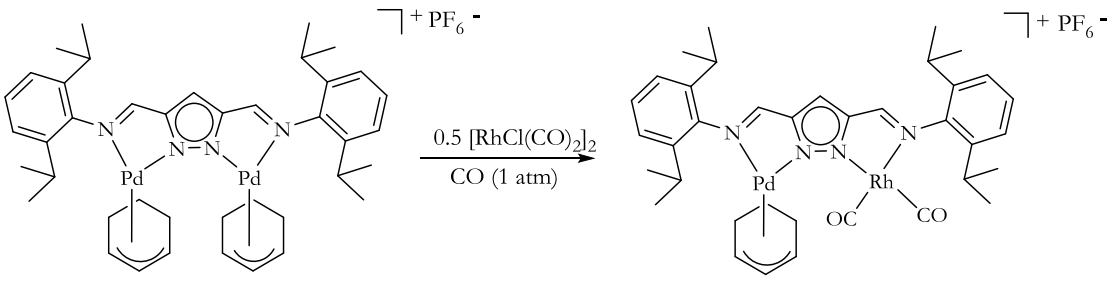

3p **3x**

Scheme 6.3.5. 4: Reaction path to the formation of 3x from rhodium(I) exchange of 3p

The ESI mass spectrum of **3x** shows *m/z* peaks at 817(10%) and 787(100%) assigned to $[M+CO-PF_6]^+$ and $[M-PF_6]^+$ respectively. The IR spectrum of the heterobimetallic complex **3x** shows two different and intense CO stretching vibrations at 2098 and 2039 cm^{-1}, consistent with a terminal CO environment (Fig. 6.3.5. 8). These are lower than the stretching frequency for free CO (2143 cm^{-1}) due to back bonding from the d-orbitals of the metal to the π* antibonding orbitals of CO. In addition, different CH=N imine environments are also observed at 1610 cm^{-1} and 1577 cm^{-1} (Fig. 6.3.5. 8) for the side arms bearing the palladium(II) and rhodium(I) centres, respectively. The lower stretching frequency of the CH_3C=N side bearing the rhodium(I) centre due to lower bond strength compared to the palladium(II) centre.

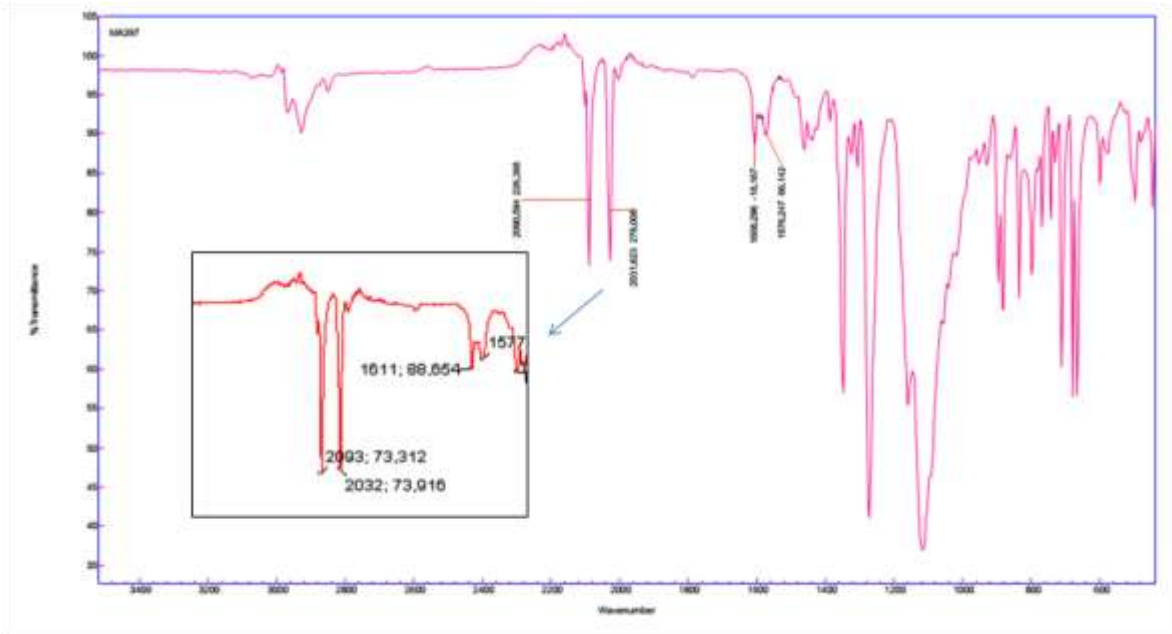

Fig. 6.3.5. 8: IR spectrum of 3x measured at room temperature (ATR)

The ^{1}H NMR spectrum of **3x** also reflects the asymmetric ligand environment. The CH=N groups are observed at 7.93 and 8.31 ppm for side arms bearing the rhodium(I) and palladium(II) centres respectively. Whiles the CH^{Pz} group is observed at 7.80 ppm. The methylene groups of the cyclohexenyl ring are observed at 1.04 ppm (2H) and 1.81 ppm (4H) respectively. The CH allyl groups are also observed at 5.24 (br s), 5.52 (br s) and 5.72 (m), which is consistent with η^3-coordination. The CH_3^{iPr} group on the other hand is observed as three doublets at 1.08, 1.22, 1.36 ppm and integrate for 12:6:6 protons respectively, due to one of the aryl rings adopting a different orientation in relation to the pyrazole plane.

The ^{13}C NMR spectra of the heterobimetallic [L^{x}Pd(η^3-allyl)Rh(CO)$_2$]X complexes on the other hand shows more pronounced downfield shift of the imine carbons in relation to the [L^{x}Pd(η^3-allyl)Rh(COD)$_2$]X complexes. For instance the imine carbon environments for **3x** are observed at 161.7 and 166.3 ppm for the side arms bearing the palladium(II) and rhodium(I) centres compared to [L^{1}Pd(η^3-C$_6$H$_9$)Rh(COD)]PF$_6$ (**3t**) where they are observed at 161.2 and 163.7 ppm respectively in the ^{13}C NMR spectrum. This is due to the CO ligands been a better π-acceptor compared to COD ligand. The differences in ^{1}H, ^{13}C NMR and IR shift frequencies are outlined in Table 6.3.5. 4.

Table 6.3.5. 4: Table showing the ^{1}H, ^{13}C NMR chemical shifts and IR absorptions for complexes 3t, 3x, 3o and HL^1

		[L^{1}Pd(C$_6$H$_9$)Rh(COD)]$^+$ (3t)	**[L^{1}Pd(C$_6$H$_9$)Rh(CO)$_2$]$^+$ (3x)**	**[L^{1}Pd$_2$(C$_6$H$_9$)$_2$]$^+$ (3o)**	**HL^1**
^{1}H NMR (δ)	CH=N^{Pd}	8.22	8.31	8.24	8.29
	CH=N^{Rh}	7.97	7.93	-	-
^{13}C NMR (δ:)	CH=N^{Pd}	161.2	161.7	171.1	N/A
	CH=N^{Rh}	163.7	166.3	-	-
IR /cm^{-1}	CH=N^{Pd}	1605	1611	1613	1625
	CH=N^{Rh}	1586	1577	-	-

Attempts at obtaining single crystals of the carbonylated complexes for X-ray crystallography failed. The synthetic protocols for the formation of the heterobimetallic complexes [L^{x}Pd(η^3-allyl)Rh(COD)]X and [L^{x}Pd(η^3-allyl)Rh(CO)$_2$]X complexes (**3r**-**3u**) are not always without

drawbacks. In some instances, the formation of other metal exchange side products (**3v**, **3z**, **3z1**) was observed (Scheme 6.3.5. 5).

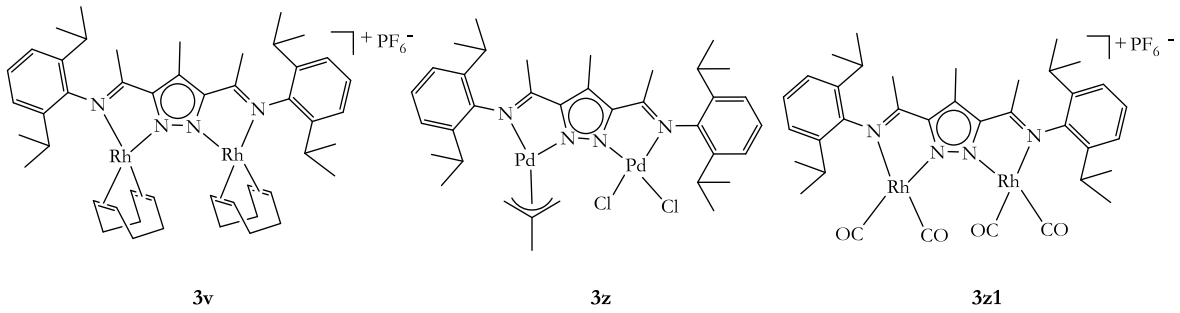

3v **3z** **3z1**

Scheme 6.3.5. 5: Side products obtained through metal exchange reactions

Akita et. al.[268] also observed the formation of a statistical mixture of homo- and heterobimetallic complexes through metal exchange processes in the carbonylation reactions. The additional products such as $[L^2Rh_2(COD)_2]$ (**3v**), $[L^2Pd_2(\eta^3\text{-}C_4H_7)Cl_2]$ (**3z)** and $[L^2Rh_2(CO)_2]^+$ (**3z1**) were characterized by NMR spectroscopy and single crystal X-ray crystallography. The mechanism leading to the formation of the observed side products is not well understood. Nevertheless, it may involve some associative and dissociative processes that occur in solution.

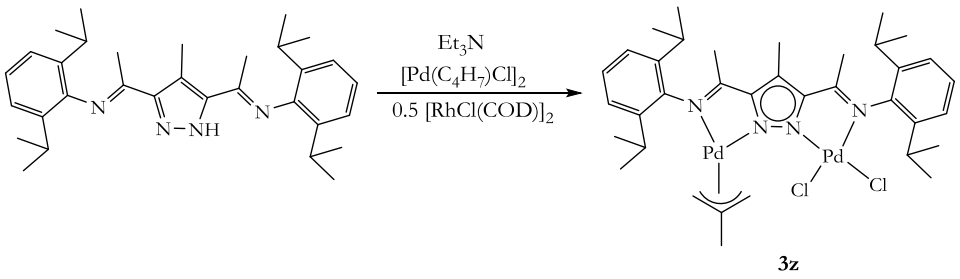

3z

Scheme 6.3.5. 6: Formation of the unexpected side product 3z

The formation of **3z** is possibly from the gradual association of chloride anions, which is followed by the dissociation of the η^3-C_4H_7 ligand. The molecular structure of **3z** is shown (Fig. 6.3.5. 9). Single crystals were grown by the slow evaporation of a CH_2Cl_2/ether solution of the complex at room temperature. The compound crystallizes in the *P* 21/c space group.

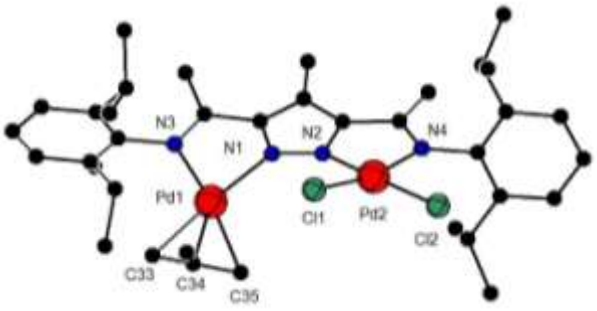

Fig. 6.3.5. 9: Molecular structure of 3z with all H atoms omitted for clarity

The interpalladium distance in **3z** is significantly shorter (4.37 Å) compared to 4.56 Å found in the complex $[L^2Pd_2(\eta^3\text{-}C_4H_7)_2]BAr^F{}_4$. The coordination around both palladium(II) centres are square planar, as usually observed for 16 valence electron four-coordinate d^8 complexes. The torsional angle defined by Pd1-N1-N2-Pd2 is larger (-33.82°) compared to (-11.90°) in $[L^2Pd_2(\eta^3\text{-}C_4H_7)_2]BAr^F{}_4$ (**3n**). Selected bond lengths [Å] and bond angles [°] are given in Table 6.3.5. 5.

Table 6.3.5. 5: Selected bond lengths [Å] and bond angles [°] for 3z

Bond lengths [Å]		Bond angles [°]	
Pd(1)-N(1)	2.091(7)	N(1)-Pd(1)-N(3)	76.6(3)
Pd(1)-N(3)	2.095(7)	N(1)-Pd(1)-C(33)	173.8(4)
Pd(1)-C(33)	2.094(9)	N(3)-Pd(1)-C(33)	105.2(3)
Pd(1)-C(35)	2.132(9)	N(1)-Pd(1)-C(34)	141.0(3)
Pd(2)-N(2)	2.002(7)	N(3)-Pd(1)-C(34)	140.9(3)
Pd(2)-N(4)	2.028(8)	C(33)-Pd(1)-C(34)	39.0(3)
Pd(1)-Pd(2)	4.376(11)	N(1)-Pd(1)-C(35)	109.7(3)

In the ^{1}H NMR spectrum of **3z**, the CH^{iPr} are observed as multiplets between 1.10-1.48 ppm. The $CH_3{}^{Me(allyl)}$ is observed as a singlet at 2.14 ppm, whiles the $CH_3C{=}N$ is observed as two close singlets at 2.18 and 2.20 ppm, reflecting the asymmetric ligand environment. The $CH_3{}^{Pz4}$ is also observed as a singlet at 2.57 ppm (Fig. 6.3.5. 10).

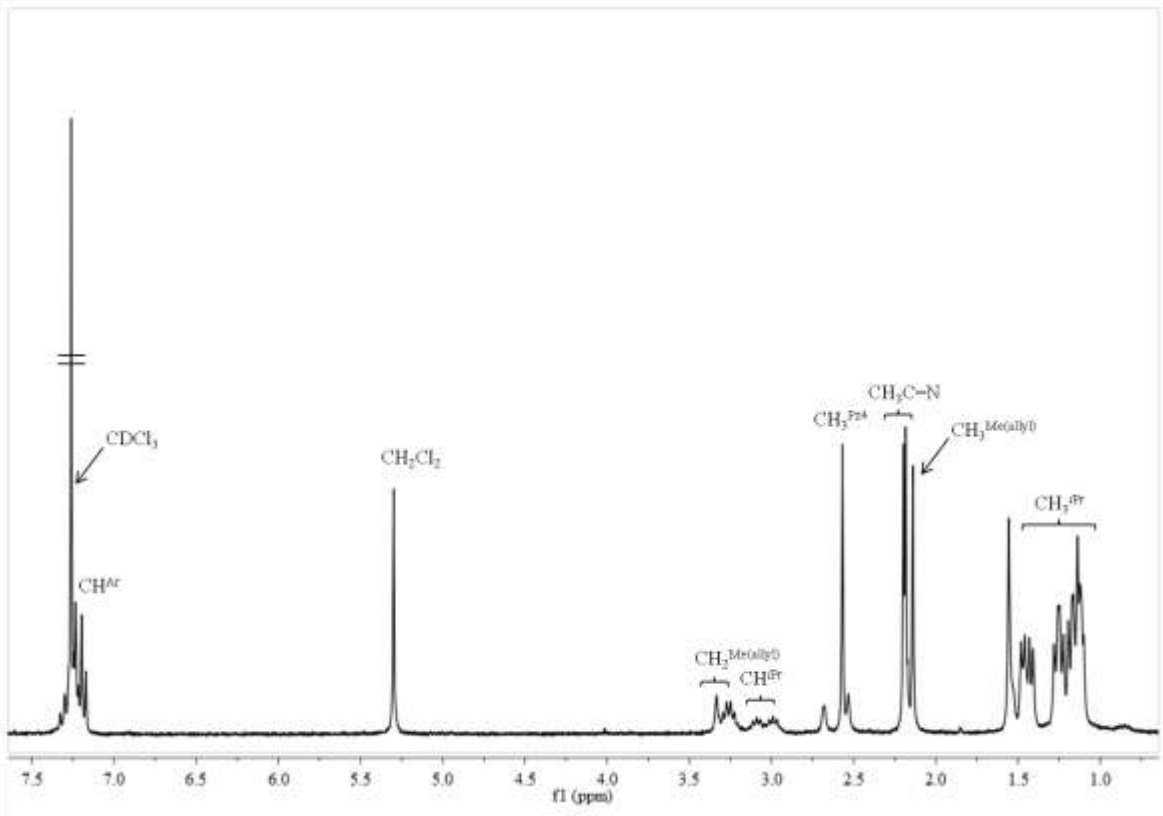

Fig. 6.3.5. 10: ^{1}H NMR spectrum of 3z measured in $CDCl_3$ at room temperature

The ESI mass spectrum of **3z** shows *m/z* fragments at 780 (15%) and 749 (100%) assigned to $[M\text{-}Cl]^+$ and $[M\text{-}2Cl]^+$ respectively, a further confirmation of the formation of this side product.

After successful preparation and the heterobimetallic complexes, some selected complexes were screened towards some basic organometallic addition reactions.

6.3.5. 1 Catalytic screening

The aim was to investigate if the presence of the palladium(II) centre in any way influenced the activity and selectivity of the reaction profile. The complexes $[L^2Pd(\eta^3\text{-}C_6H_9)Rh(COD)]BAr^F{}_4$ (**3u**), $[L^2Rh(COD)]$[221] and $[L^2Pd_2(\eta^3\text{-}C_6H_9)]PF_6$ (**3p**) complexes were screened in the rhodium catalyzed conjugate addition of organoboron reagents to alkenes and alkynes, [269,270,271] as well as the rhodium catalyzed *anti*-Markovnikov intramolecular hydroalkoxylation of terminal acetylenes (Scheme 6.3.5.1. 1).

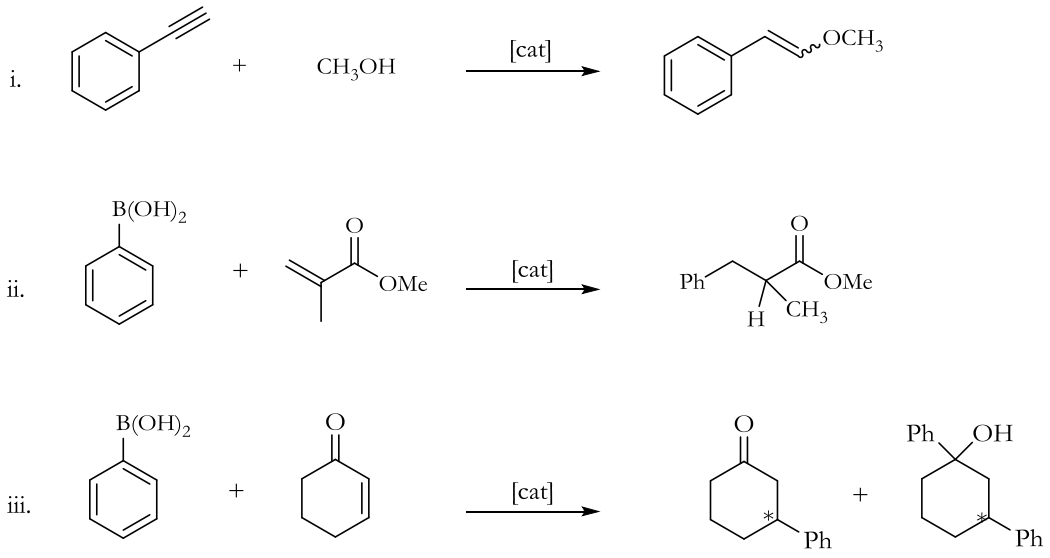

Scheme 6.3.5.1. 1: Some screened organometallic transformation reactions

In the conjugate addition of organoboron reagents to 2-cyclohexenone (Scheme 6.3.5.1. 1-iii) using **3u**, a white volatile crystalline solid with a pleasant aroma was obtained by column chromatography after workup. Analysis of the product by ^{1}H NMR spectroscopy showed the presence of a double bond, which was not consistent with the expected product and different from the ^{1}H NMR spectrum of cyclohexenone. An MS (EI) of the product on the other hand shows molecular peaks that can be assigned to an addition product. A look up in literature shows instances where palladium(II) complexes have been used for the oxidative Heck type addition of phenylboronic acids.

It seems though, that **3u** fails to achieve the conjugative addition product reaction, but rather an oxidative Heck type addition reaction takes place.

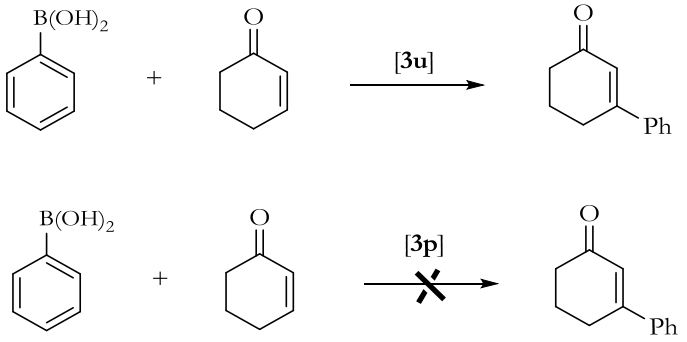

Scheme 6.3.5.1. 2: Oxidative Heck type addition product formed

What is of interest is the fact that the analogous homobimetallic palladium(II) complex **3p** failed to achieve this transformation, the formation of a palladium(0) is always observed. The interesting feature of **3u** is that, the Heck type addition product was obtained up to 98% yield in an hour, compared to other traditional Heck type catalyst, which take up to 24 h to achieve such yields. Jones and James[11] have also investigated the use of Pd/Pt bimetallic complexes for Heck coupling reactions. They reported that the bimetallic catalysts were more active than the monometallic analogues.

Kondo et. al.[272] reported the first transition-metal catalyzed *anti*-Markovnikov intermolecular hydroalkoxylation of terminal acetylenes to enol ethers in high yields (up to 92%) without the use of a base. Using 8-quinolinolato rhodium complexes, arylacetylenes as well as alkenyl- and alkylacetylenes were coupled with aliphatic alcohols, and the products were obtained with high *Z* selectivity in most cases.[272] Attempts were therefore made at investigating the catalytic activity of [L^2Rh(COD)] complex in the rhodium catalyzed *anti*-Markovnikov intramolecular hydroalkoxylation of terminal acetylenes (Scheme 6.3.5.1. 3), inspired by literature work in which rhodium(I) complexes have been used to achieve such transformations.

The reaction using [L^2Rh(COD)] failed to yield the desired hydroxymethylated enol ether. Rather, it catalyzed the polymerization of acetylene to polyphenylacetylene, which under thermal conditions employed, undergoes scission of the polymer product, followed by cyclotrimerization to form 1,3,5-triphenyl benzene (TPB). The formation of 1,3,-5 TPB was observed from the ES-MS of the yellow crystalline solid which shows a peak at m/z 306 (100%).

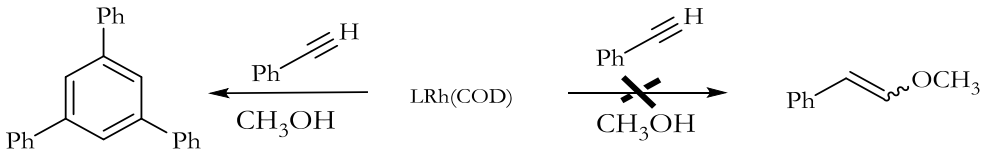

Scheme 6.3.5.1. 3: Thermal isomerisation of *cis* polyphenylacetylene

The thermal *cis-trans* isomerisation of *cis-transoidal* polyphenylacetylene has been studied in literature, and it has been suggested that, the thermal isomerisation of the polymer chain is accompanied by cyclization and scission of the polymer chain.[273] Although cyclization reactions reported in literature are usually performed at temperatures above 120 °C, tricyclization can also occur at lower temperatures (78 °C) as observed with [L^2Rh(COD)] given prolonged reaction times (48 h). No further investigations were carried out.

6. 4 Tetranuclear zinc(II) complexes of *α*-diimine type ligands as catalysts for polymerization of *rac*-D,L-lactide to poly D,L-lactide, a bio-renewable polymer

6.4. 1 Synthesis and characterization of tetranuclear zinc(II) complexes

The complexes $[L^1{}_2Zn_4(\mu\text{-}OAc)_6]$ (**4a**), $[L^2{}_2Zn_4(\mu\text{-}OAc)_6]$ (**4b**), $[L^3{}_2Zn_4(\mu\text{-}OAc)_6]$ (**4c**) and $[L^4{}_2Zn_4(\mu\text{-}OAc)_6]$ (**4d**) were prepared using a general synthetic route which involved the reaction of the appropriate ligand with 2 mol equivalent $Zn(OAc)_2{\cdot}2H_2O$ in methanol with stirring under room temperature for 48 h. The complexes were isolated as white crystalline solids, and purified by recrystallization from dichloromethane/methanol. The complexes were obtained in moderate to good yields (69-81%). The complexes were fully characterized by ^1H and ^{13}C NMR spectroscopy, ESI-MS, IR spectroscopy, elemental analysis and in some instances single crystal diffraction studies.

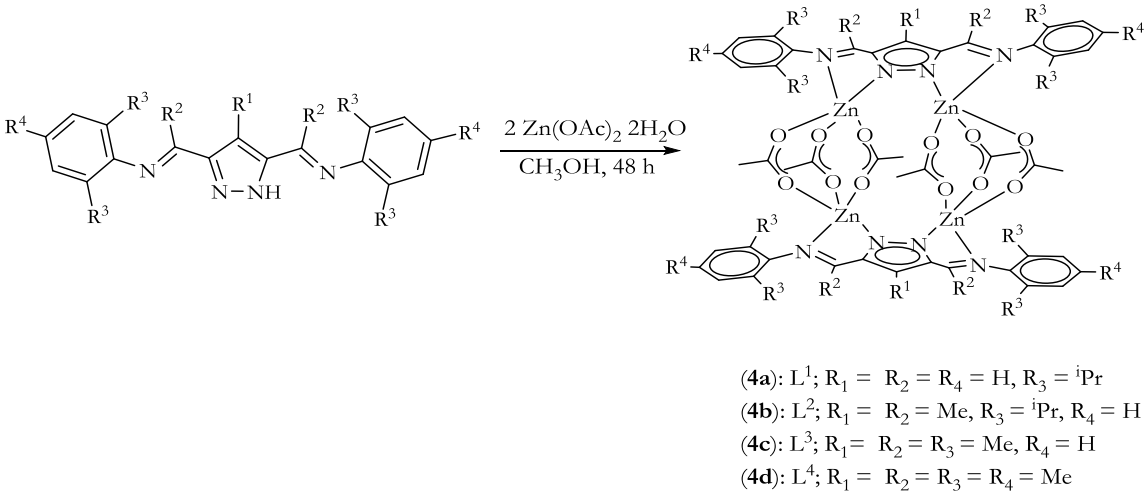

Scheme 6.4.1. 1: Synthetic scheme for the preparation of zinc(II) complexes 4a-4d

The ^1H NMR spectra of the complexes shows only one distinct acetate bridging and pyrazole environment, pointing to only one type of compound in solution, hence a dynamic process takes place at room temperature. The $CH_3{}^{iPr}$ group is broadened and only a single signal is observed for the $CH_3{}^{OAc}$ protons. The ^{13}C NMR resonance for the bridging acetate groups of the complexes are observed between 179-180 ppm, although the imine carbons are not detected. The IR spectrum of the complexes also shows two distinct acetate bridging environments between 1585-1607 cm^{-1} for asymmetric stretching vibrations and 1417-1439 cm^{-1} for symmetric stretching vibrations. The $CH_3C{=}N$ stretching vibrations also swamped

under the broad acetate peak. Table 6.4.1. 1 summarizes the stretching vibrations for the acetate environment as observed in the various zinc(II) complexes. A carboxylate ion, CO_2^-, can coordinate to metals in a number of ways, *viz.* as a unidentate ligand, as a chelating ligand, as a monatomic bridging ligand, or as a bridging bidentate ligand in a *syn-syn, syn-anti or anti-anti* configuration. These carboxylate binding modes are known to give rise to distinct frequencies for the asymmetric $\nu_{as}(CO_2^-)$ and symmetric $\nu_{sy}(CO_2^-)$ vibrations. The difference between the separation of these vibrations $\Delta = \nu_{as}(CO_2^-) - \nu_{sy}(CO_2^-)$ is used as a criterion for distinguishing between the binding modes. The table below shows the Δ for the complexes **4a**-**4d**. In **4a**, Δ = 146 cm^{-1} is smaller than the ionic acetate (164-171 cm^{-1})[274] although the rest are in the range of chelating or bridging acetates.

Table 6.4.1. 1: Table showing the IR stretching frequencies of the acetate environment in complexes 4a-4d

Complex	ν_{as} (cm^{-1})	ν_{sy} (cm^{-1})	Δ (cm^{-1})
$L^1{}_2Zn_4(\mu\text{-}OAc)_6$ (**4a**)	1585	1439	146
$L^2{}_2Zn_4(\mu\text{-}OAc)_6$ (**4b**)	1603	1430	173
$L^3{}_2Zn_4(\mu\text{-}OAc)_6$ (**4c**)	1590	1423	167
$L^4{}_2Zn_4(\mu\text{-}OAc)_6$ (**4d**)	1607	1417	190

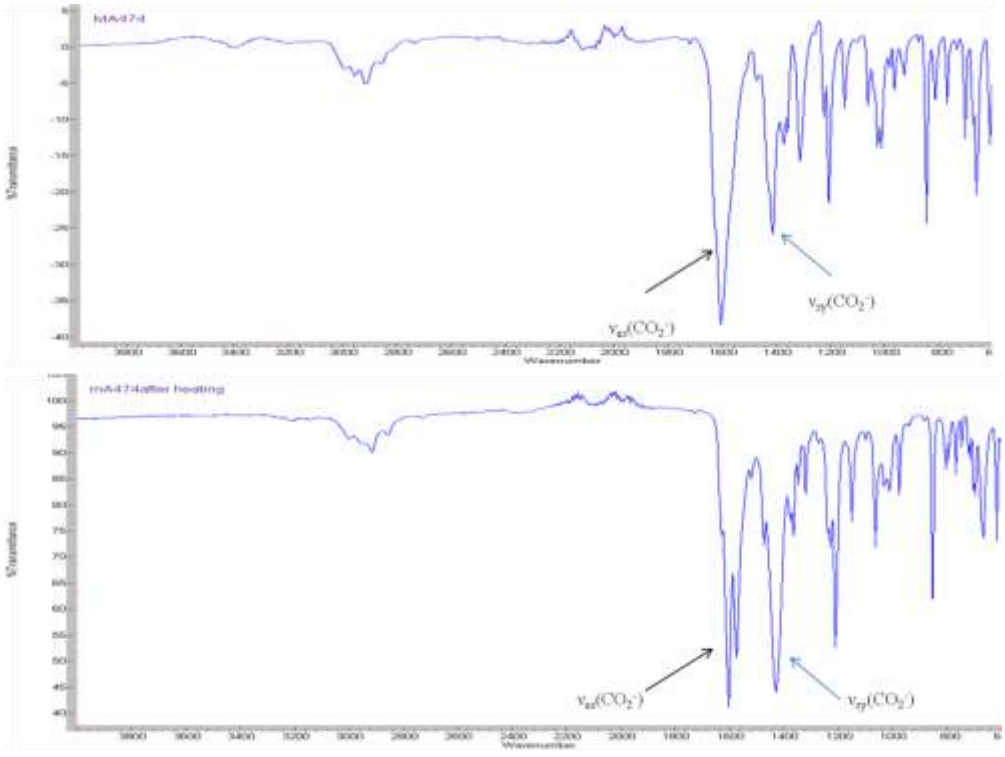

Fig. 6.4.1. 1: IR spectra of 4d showing the acetate bridging environment before (upper) and after heating (lower)

On heating **4d**, the ν_{as} does not change (1607 cm^{-1}), but a change in ν_s (1432 cm^{-1}) is observed. The Δ before heating is (190 cm^{-1}) and Δ after heating is (175 cm^{-1}) (Fig. 6.4.1. 1).

The DSC/TG of **4d** was performed in a dynamic inert atmosphere of nitrogen. The first peak in the curve indicates a melting temperature of 264°C. Two consecutive weight loss points are observed, the first weight loss curve occurred between temperatures of 100°C and 164 °C, representing a weight loss of 3.27%, whiles between 164°C and 300°C only a 1.27% loss in weight is observed (Fig. 6.4.1. 2), the cause for the weight loss, not clear.

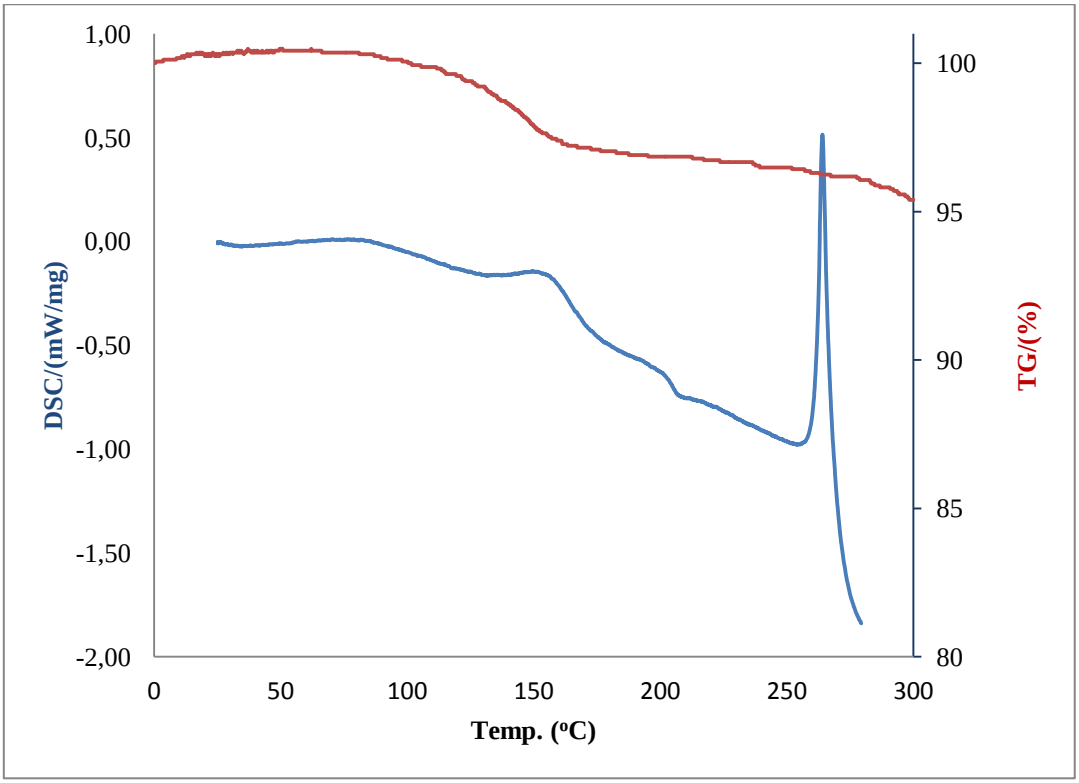

Fig. 6.4.1. 2: A DSC/TG curve for 4d showing the metlting temperature and weight loss over a temperature range

ESI-MS data of the complexes supports a dimeric structure. Generally, the most intense peaks in the ESI-MS of complexes correspond to $[L_2Zn_4(OAc)_x]^+$ peaks. The dimeric nature of the complexes was confirmed by single crystal X-ray structures.

The molecular structure of **4a** is shown in Fig. 6.4.1. 3. Crystals of the complex were obtained by the slow evaporation of a CH_2Cl_2 solution of the complex at room temperature.

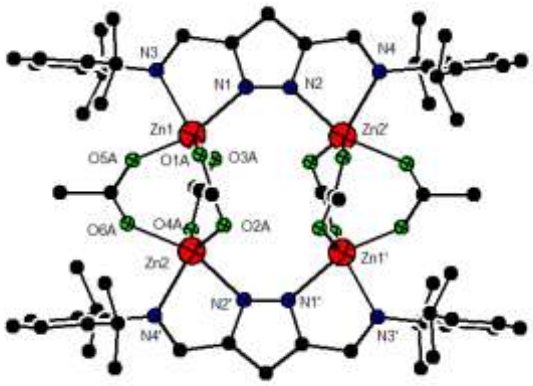

Fig. 6.4.1. 3: Molecular structure of 4a, H atoms, and solvents omitted for clarity

The complex **4a** crystallizes in the *P* 21/n space group and co-crystallizes with five molecules of dichloromethane. The complex has a dimeric structure in the solid state, with two different LZn_2 units bridged together by six acetate units. The geometry about the Zn atom is octahedral. The inter-metallic distance between Zn centres linked by the acetate ligand (Zn···Zn) distance is 3.45 Å. The Zn-O distances are in the range of 1.86 Å and 2.08 Å. The Zn-N^{Pz} bond distance in this complex is 2.10 Å, whiles that of the Zn imine nitrogen is slightly longer at 2.16 Å. The peripheral 2,6-diisopropyl groups are oriented perpendicular to the pyrazolyl plane to avoid steric interactions between isopropyl and acetate groups. Selected bond lengths [Å] and angles [°] are also given (Table 6.4.1. 2).

Table 6.4.1. 2: Selected bond lengths [Å] and bond angles [°] for 4a

Bond lengths [Å]		Bond Angles [°]	
Zn(1)-O(1A)	1.860(3)	O(1A)-Zn(1)-O(3B)	145.1(2)
Zn(1)-O(3A)	2.072(11)	O(1A)-Zn(1)-O(5A)	68.02(18)
Zn(1)-N(1)	2.109(15)	O(3B)-Zn(1)-O(3A)	18.89(11)
Zn(1)-N(3)	2.168(16)	O(3B)-Zn(1)-N(3)	107.62(15)
Zn(2)-O(6A)	2.0648(31)		
Zn(1)-Zn(2)	3.449(3)		
Zn(1)-Zn(2)'	4.493(3)		

The analogous complex **4c** crystallizes in the *P* -1 space group and similar to **4a** in geometry. In **4c**, the intermetallic distance between Zn centres linked by the acetate ligand Zn···Zn distance is significantly shorter 3.30 Å. Whiles the Zn-O distances are in the range of 1.97 to 2.68 Å. The Zn-N bond distance is in the range of 2.03 to 2.23 Å. The Zn-N^{Pz} bond distance

in this complex is short mainly 2.03 Å compared to 2.11 Å in **4a**. Selected bond lengths and angles for **4c** are given in Table 6.4.1. 3.

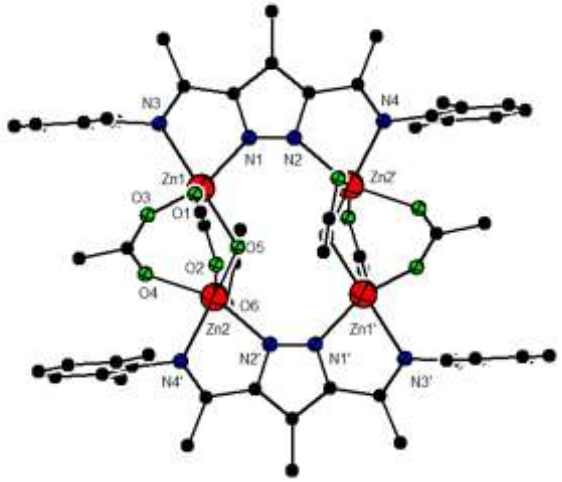

Fig. 6.4.1. 4: Molecular structure of 4c with solvents and H atoms omitted for clarity

Table 6.4.1. 3: Selected bond lengths and bond angles for 4c

Bond lengths [Å]		Bond Angles [°]	
Zn(1)-O(1)	1.978(2)	O(1)-Zn(1)-O(3)	113.99(8)
Zn(1)-O(3)	2.007(2)	O(1)-Zn(1)-N(3)	102.80(9)
Zn(2)-O(2)	1.996(19)	O(3)-Zn(1)-O(5)	101.36(8)
Zn(1)-N(1)	2.037(2)	O(3)-Zn(1)-N(3)	83.59(8)
Zn(1)-N(3)	2.233(2)	N(1)-Zn(1)-N(3)	76.31(9)
Zn(1)-Zn(2)	3.302(5)		
Zn(1)-Zn(2)'	4.3558(5)		

A similar compound with four zinc atoms bridged by 3 acetate-groups has been published by Lewiński et al.[275] Here the Zn···Zn distance is 3.38 Å, the Zn–N bond lengths are in the range of 2.02 Å to 2.09 Å, and the Zn–O bond lengths are in the range of 1.94 Å to 2.08 Å.

Pyrazolyl bearing complexes of the chiral and the enantiopure bis(pyrazol-1-yl)methane-based NNO-donor scorpionate zinc(II) alkyl complexes has been reported by Otero et. al.[276]The zinc(II) complexes were screened towards ability to polymerize *rac*-lactides, the results of which are discussed in the following sections.

6.4. 2 Polymerization of D,L-lactide to heteroatactic polylactide

Heterotactic PLA is obtained from *rac*-lactide when there is the selective insertion of lactide isomer with opposite configuration to the previous inserted monomer. Amorphous polymers on the other hand are formed from *rac*-lactide when there is the lack of stereochemical control. The target usually is to prepare catalysts capable of generating isotactic PLA from *rac*-lactide, since the mixture of isotactic L-PLA and D-PLA have different bulk properties compared to pure PLA.[277] PLA is a rigid transparent thermoplastic with a glass transition temperature (T_g) and melting temperature (T_m) of about 60°C and 170°C respectively. Carothers et. al.[278] as far back as 1952 reported the synthesis of high molecular weight PLA.

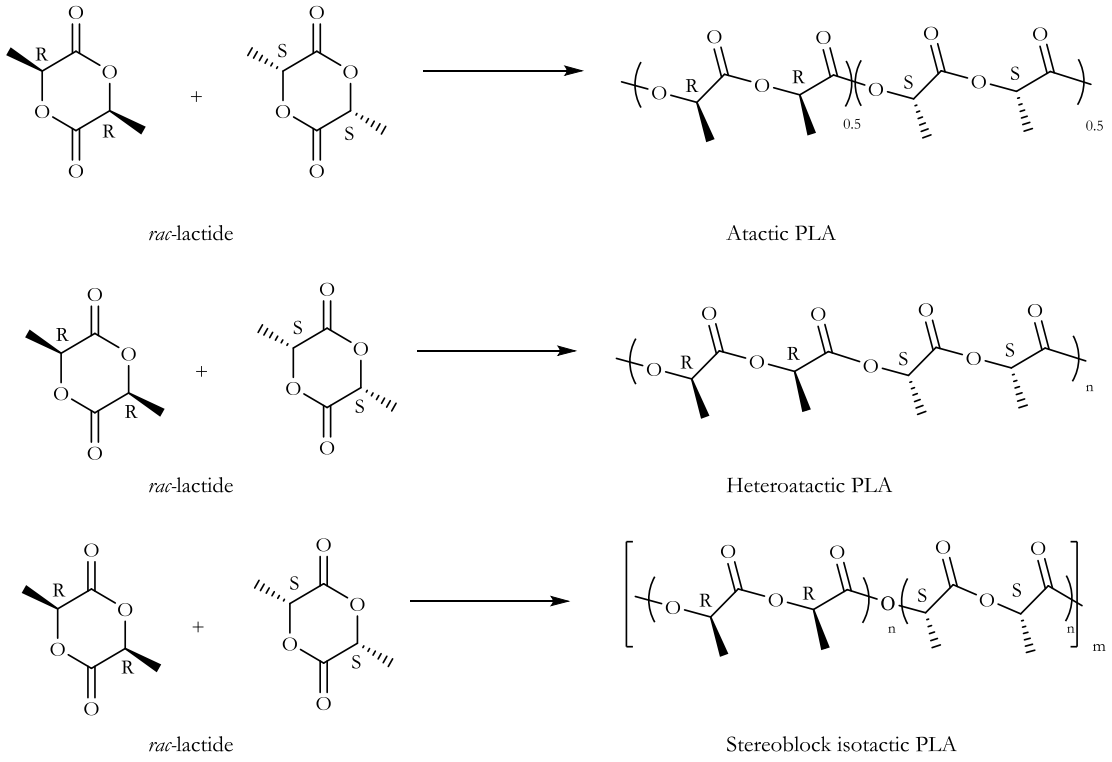

Scheme 6.4.2. 1: Examples of PLA microstructures that can be achieved through polymerization of *rac*-lactide

The catalysts failed to initiate polymerization in solvents such as CH_2Cl_2 and THF at room temperature. Polymerization of lactides is only initiated in the melt at temperatures exceeding 170 °C, about the same temperature range where the second weight loss is observed in the DSC/TG of the complex. Generally, the formation of polymer required ~15 minutes for initiation. The slow initiation of the polymerization process can be attributed to the possible

stable nature of the dimeric complex and *trans* esterification reactions that takes place during initiation.[205]

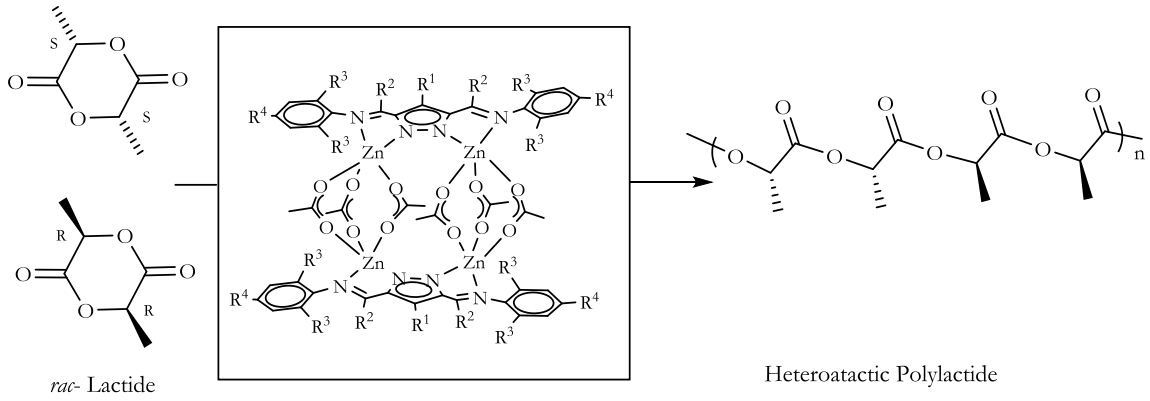

Scheme 6.4.2. 2: Synthetic scheme for the polymerization of *rac* D,L-lactide

Generally, increased polymerization times and monomer to initiator ratio also leads to an increase in the molecular weight of the polymer obtained, but with no further improvement in yields. Oxidation of the polymer is observed at reaction temperatures exceeding 200°C, with the formation of a brown polymer sample. Generally, polymer conversion does not exceed 60%, pointing to the possible inaccessibility of the monomer to the catalyst surface primarily due to the increased viscosity in the reaction media. The results of the polymerization experiment using the various catalysts are summarized in Table 6.4.2. 1.

Table 6.4.2. 1: ROP of *rac*-lactide promoted by zinc(II) complexes 4a-4c

Entry	Catalyst	[M]/[cat]	Time (h)	Yield (g)	Conv. (%)	T_m (°C)	M_w (x10⁴) (g/mol)	M_n (x10³) (g/mol)	PDI	P_r
1	**4a**	500	18	0.46	47	64.0	2.92	1.50	1.9	0.61
2	**4a**	1000	0.5	0.57	59	57.0	5.93	2.65	2.2	0.71
3	**4a**	500	0.5	0.70	58	57.0	3.30	1.92	1.7	0.73
4	**4b**	300	0.5	0.27	45	54.5	2.60	1.28	2.0	0.71
5	**4c**	300	0.5	0.35	58	55.0	2.48	1.23	2.0	0.69
6	**4c**	300	0.5	0.35	50	48.0	2.30	1.29	1.8	0.61

P_r is the probability of racemic linkages between monomer units and is determined from the relative intensity in the tetrads obtained in the decoupled ^{1}H NMR by Pr = 2I1/(I1 + I2), with I1 = δ 5.20−5.25 ppm (mrm, mrr/rrm) and I2 = δ 5.13−5.20 ppm (rrm/mrr, rrr, rmr). Experiments run in the melt at 180°C.

Although polymer conversions generally did not exceed 60% due to the increased viscosity of the reaction medium, the catalysts could achieve as much 85 $kgmol^{-1}$ in 30 min at 0.1% catalyst loadings. The most active catalyst reported to date are mononuclear zinc(II) complexes supported by a phenoxy ligand bearing single ethylenediamine tether reported by Hillmyer and Tolman. These catalysts achieve 96 % conversion at catalyst loadings of 0.15% catalyst loadings and yields 130 kg mol^{-1} of PLA.[200]

The PLA's were characterized by ^{1}H and ^{13}C NMR spectroscopy, IR, GPC, as well as DSC measurements. The IR spectrum of the polymers shows the presence of υ(OH) stretching vibrations between 3650 and 3200 cm^{-1}, which can be attributed to the presence of linear and not cyclic polymers. The ^{1}H NMR spectrum of PLA obtained using [300]: [1] of monomer to **4b** is shown below and is consistent with an acid terminated chain end, which is also observed in the IR spectrum. The ^{1}H NMR spectrum of the precipitated PLA's also shows the isopropoxycarbonyl moiety as multiplets at 1.55 ppm and a multiplet at 5.17 ppm for the methine region as shown in Fig. 6.4.2. 1.

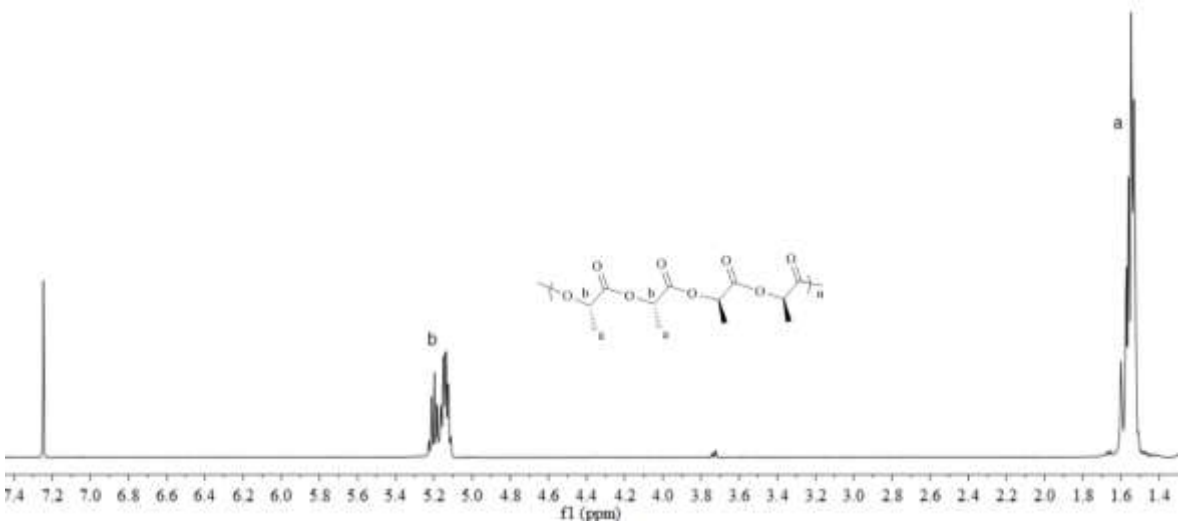

Fig. 6.4.2. 1: ^{1}H NMR spectrum of PLA obtained using 4b measured in $CDCl_3$ at room temperature

The microstructure of the prepared PLAs was determined by analyzing the homonuclear decoupled ^{1}H NMR spectrum of the methine region. The ^{1}H NMR spectrum reveals the formation of mostly heteroatactic microstructures. The homonuclear decoupled ^{1}H NMR spectrum of the methine region of PLA prepared with **4c** is shown in Fig. 6.4.2. 2.

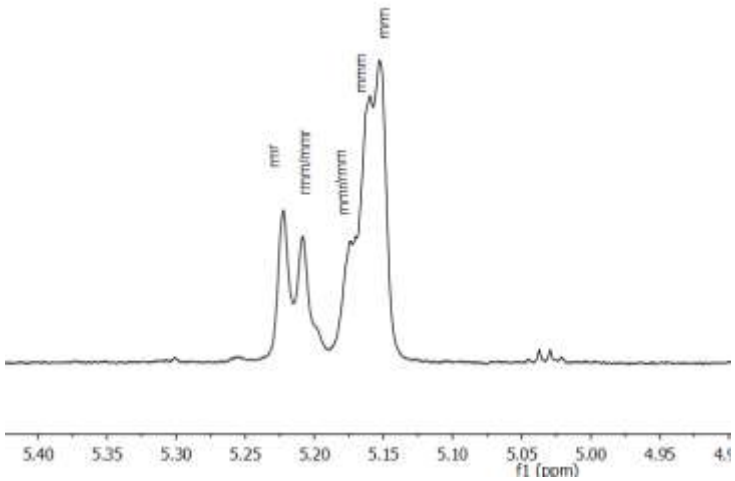

Fig. 6.4.2. 2: Homonuclear decoupled ^{1}H NMR spectrum of the methine region of heteroatactic PLA prepared with 4c measured in $CDCl_3$ at room temperature.

The observed shifts at 5.22 and 5.14 can be assigned to heteroatactic *rmr* and *mrm* tetrads.[279] The nature of ancillary ligand seems not to play any dominant role in the tacticity of the resulting PLA, with P_r (probability of racemic enchainment)[280,281] ranging between 0.61-0.73 for all complexes. That is 61-73% of the linkages are formed between lactides of opposite stereochemistry (heteroatactic junctions). The ^{13}C NMR spectrum shows the two enantiomer units of the lactide, the peak at 19.0 ppm can be assigned to the methyl groups on the polymer chain whiles the peaks at 70.1 and 71.0 ppm can be assigned to the CH protons.

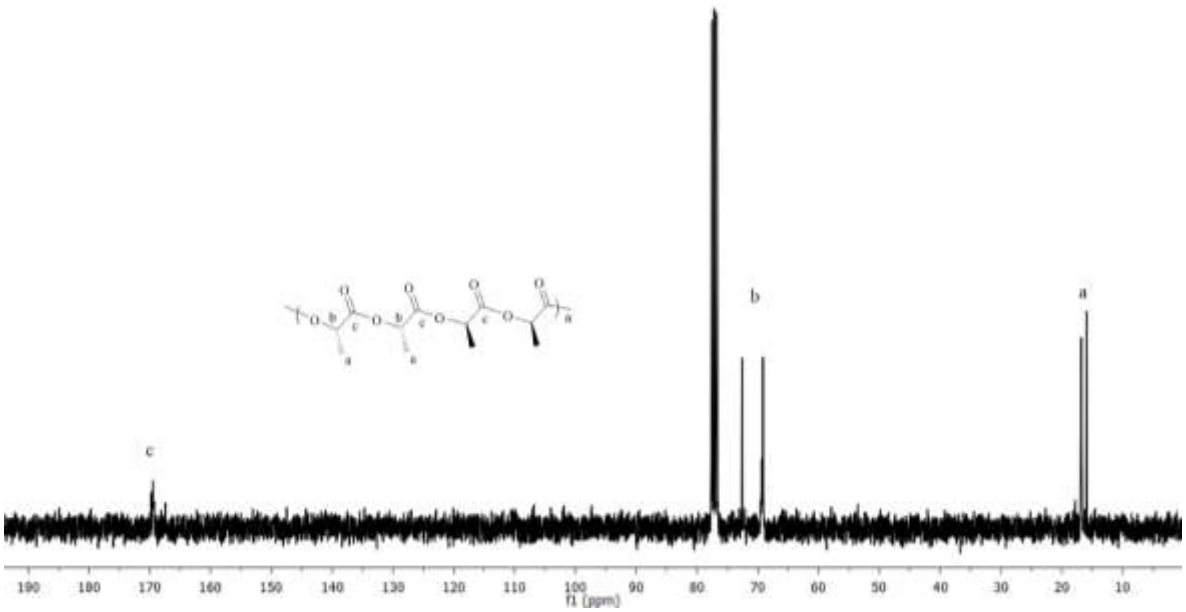

Fig. 6.4.2. 3: $^{13}C\{^{1}H\}$ NMR spectrum of PLA prepared with 4c measured in $CDCl_3$ at room temperature

The ^{13}C NMR spectrum signal for the carbonyl appears as a weak peak at 170 ppm. In addition, methoxy end groups were not observed in the ^{13}C NMR spectrum.

The molecular weight (M_n) distributions of the polymers obtained are between 1200-1500 g/mol. (See Table 6.4.2. 1). The polymers from the zinc(II) complexes are generally of broad molecular weight distribution with polydispersities (M_w/M_n) from 1.8-2.2, pointing to not well controlled reaction process, as observed in the GPC (Fig. 6.4.2. 4). The broadened molecular weights observed can be because of competing reactions such as intermolecular and intramolecular *trans*-esterification, as these competing reactions leads to the cleavage and reformation of the polymer chain. These competing side reactions are known to be significant at higher reaction temperatures. Further confirmation of the uncontrolled nature of this polymerization process comes from the disparities between the calculated and obtained average molecular weights.

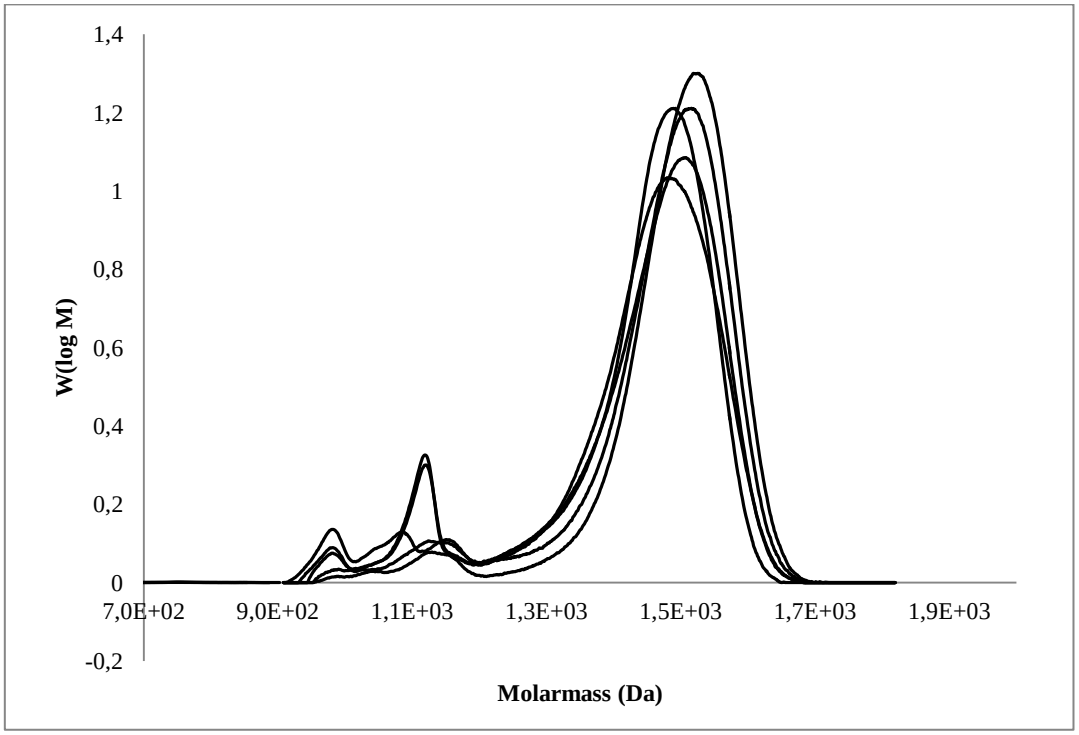

Fig. 6.4.2. 4: A GPC chromatograph of poly *rac*-lactides obtained using the zinc(II) catalysts 4a-4c

The GPC of the polymers shows in most cases bimodal molecular weight distributions with an average molecular weight of about 1530 g/mol. Regardless of the nature of the ligand used, all the molecular weight of the polymers obtained have similar molecular weight distributions.

A careful look at the low-molecular-weight PLAs by MALDI-TOFMS shows the main distributions in the spectrum, indicating the existence of a single polymer chain with consecutive peaks separated by peak differences of 72 Da. In addition, a certain extension of undesirable intermolecular ester-exchange (*trans* esterification) reactions is detected since low intensity distributions are observed. The molecular weight of the polymer determined using MALDI-TOF technique, corroborates with GPC results, although it must be mentioned that this technique provides a direct access to the molecular weight rather than the average values that are compared with standard values (in the case of GPC). The MALDI-TOF spectrum is shown in Fig. 6.4.2. 5.

The nature of the lactide produced can be described as largely amorphous, as the melting temperatures of the lactide are between 48-65°C. In the DSC measurement (Fig. 6.4.2. 6), the samples were first shock cooled in liquid nitrogen after heating for the first time in order to freeze any metastable states and then measured again.

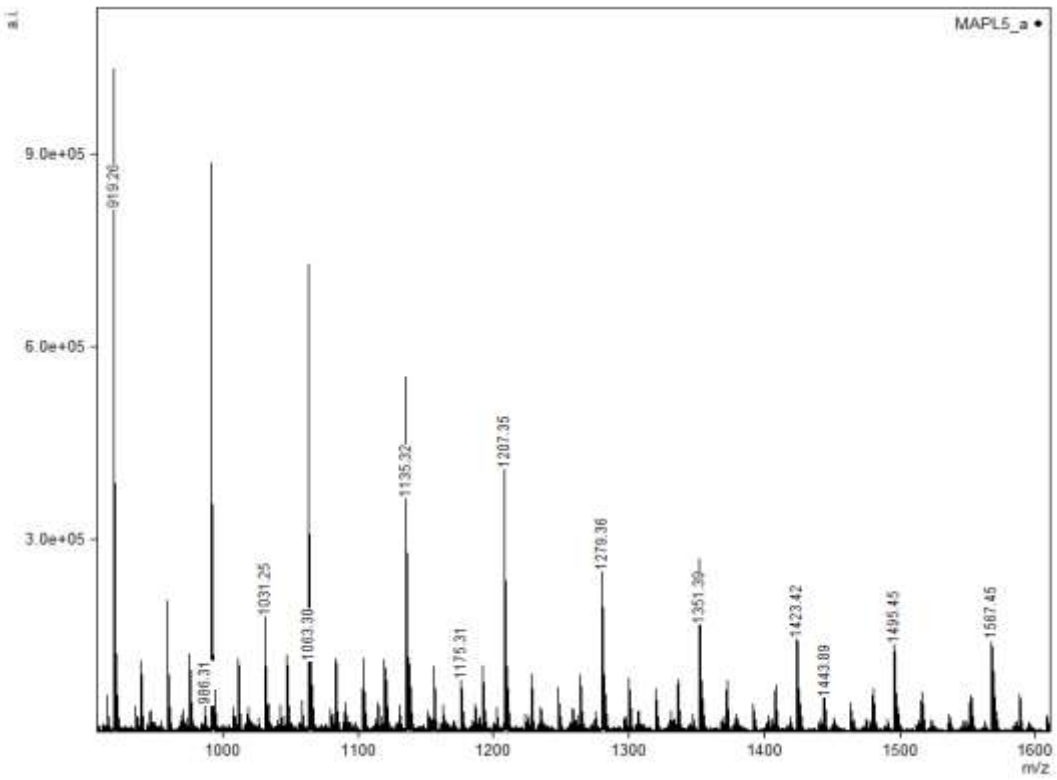

Fig. 6.4.2. 5: MALDI-TOF spectrum of *rac*-PLA prepared with 4c

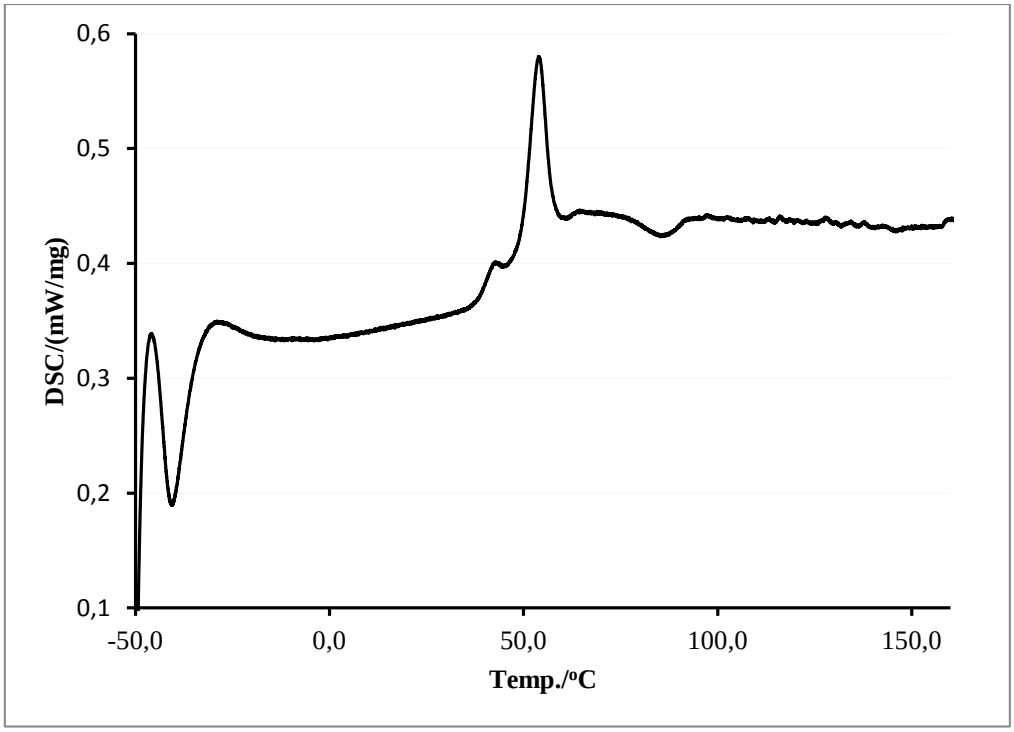

Fig. 6.4.2. 6: A DSC curve of heteroactactic PLA obtained using 4c

Because of the polymeric nature of the products, some of the melting curves, which are concave in shape, were characterized by the temperatures of their peak maxima.

6. 5 Homobimetallic $[Rh_2(O_2CR)_4]$ complexes of α-diimine type ligands

Complexes of the type $[M_2(O_2CR)_4]$ (**XLVIII**) have generally been classified as the metal-metal multiply bonded paddlewheel compounds. They have proven usefulness in a number of catalytic applications and sometimes have very interesting electronic structures.[282]

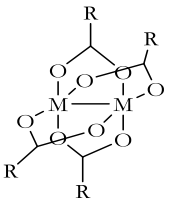

XLVIII

Notable among them is the isolation and characterization of dichromium compounds which sometimes feature quadruple and quintuple bonds in what is called "super short" metal-metal bonds[283]. Metals such as Mo, W, Re, Ru, Os and Rh are known to form paddle wheel complexes. Rh-Rh bonding interactions have been described by the ground state $\sigma^2\pi^4\delta^2\delta^{*2}\pi^{*4}$ for a net Rh-Rh single bond.[284] The first accurate X-ray structure of the Rh paddle wheel complex has a Rh-Rh bond length of 2.39 Å. Rh paddle wheel complexes of the nature Rh_2L_4 have interesting redox chemistry, and have the ability to undergo two redox steps involving reduction (a), oxidation (b) and a possible second one electron oxidation (c) (Scheme 6.5. 1).[285]

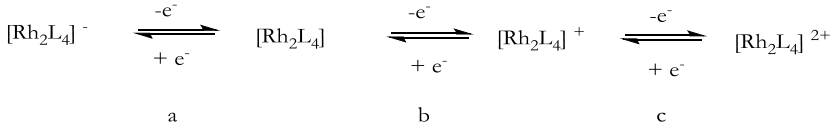

Scheme 6.5. 1: Redox steps of Rh-Rh paddle wheel complexes

The use of rhodiumdiacetate compounds as an important chemical transformation reagent in the generation of carbene diazocompounds has become very prominent.[286,287,288,289] The past decades have seen efforts at changing the ligand environment around the Rh(II) core with the aim of influencing the chemical reactivity and selectivity of the products obtained. The treatment of $Rh_2(OAc)_4 \cdot 2MeOH$ with HL^2 in methanol leads to the formation of a neutral metal-metal bonded paddlewheel complex which was characterized by ^1H and ^{13}C NMR spectroscopy as well as single crystal X-ray crystallography.

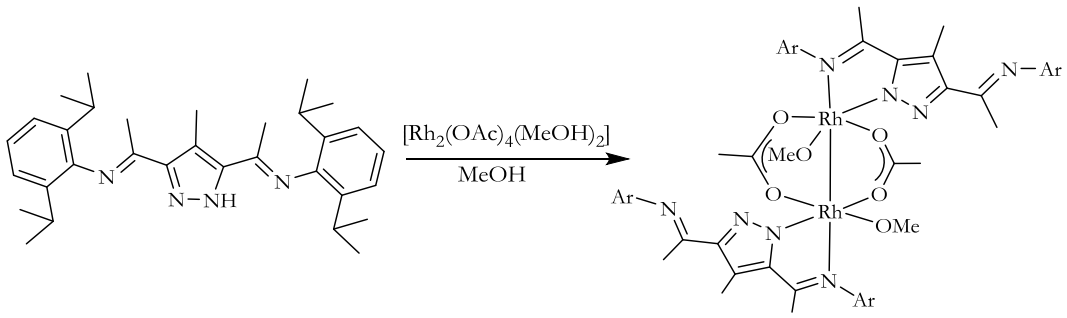

4e

Scheme 6.5. 2: Preparation of rhodium-rhodium metal bridged complex 4e

The ^{1}H NMR spectrum of **4e** shows two different $CH_3C{=}N$ environments, thus pointing to an asymmetric ligand environment, also one group of aromatic protons appear shielded and moved further upfield to 7.0 ppm and integrates for six protons whiles another set of six protons is further downfield at 7.24 ppm. Two different acetate environments are observed at 1.55 and 1.36 ppm respectively, which correlates with ^{13}C NMR peaks at 191.6 and 186.1 ppm respectively. The ^{1}H NMR spectrum of **4e** is shown in Fig. 6.5.1.

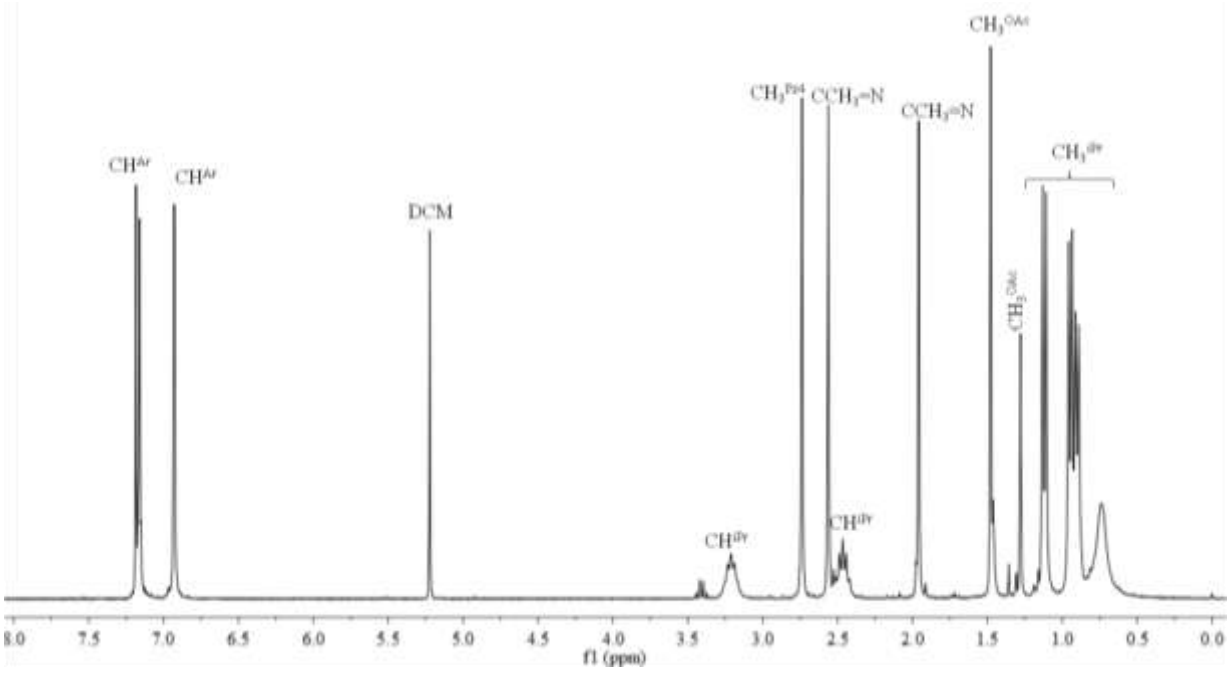

Fig. 6.5. 1: ^{1}H NMR spectrum of 4e measured in $CDCl_3$ at room temperature

Crystals of **4e** were obtained by the slow evaporation of a methanolic solution of the complex. The compound crystallizes in the *P* 21/c space group. In the X-ray structure, one acetate bridge in **4e** is replaced by two methanol molecules.

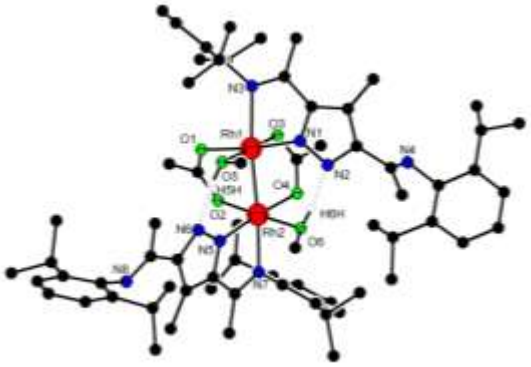

Fig. 6.5. 2: Molecular structure of 4e, most H atoms, and counter ions omitted for clarity

The Rh-Rh distance in this complex is 2.54 Å, a relative increase compared to $Rh_2(OAc)_4$ due to the increased Lewis basicity of the ligand. The Rh-Rh bond distance of 2.54 Ä is longer than that of $[Rh_2(OAc)_2(PPh_3)_2]$ (2.4 Ä).The dirhodium centre is coordinated by two of ligands with the imine nitrogen occupying the axial positions in the complex (Fig. 6.5. 2). The Rh atoms also lie in the middle of six coordinate geometry complex. Two intra-molecular N-H···O hydrogen bonding interactions can be found in the molecule but are very weak due to the suboptimal N-H···O bond angle of 119.5°. Selected lengths [Å] and bond angles [°] are given in Table 6.5. 1.

Table 6.5. 1: Selected bond lengths [Å] and bond angles [°] for 4e

Bond lengths [Å]		Bond angles [°]	
N(1)-Rh(1)	1.978(2)	N(1)-Rh(1)-Rh(2)	173.20(5)
N(3)-Rh(1)	2.344(2)	N(5)-Rh(2)-O(2)	89.75(8)
N(5)-Rh(2)	1.986(2)	N(5)-Rh(2)-O(6)	93.65(8)
N(7)-Rh(2)	2.244(2)	N(7)-Rh(2)-Rh(1)	174.61(6)
N(2)-H(6)···O(6)	2.975(36)	N(2)-H(6)···O(6)	119.52(3)

7 Trimethylsilyl cyclopentadienyl/indenyl/fluorenyl pyrazolyl tethered derivative ligands as precursors for the synthesis of group 4 metal complexes

Different potential roles have been assigned to having side arms tethered to cyclopentadiene (Cp) ligands, roles such as acting as a hemi labile ligand, coordinating to a second metal site or providing improved solubility.[290] Catalysts bearing Cp ligands with pendant amino or amido side chains have been used in olefin polymerization.[291,292,293,294] Meyer et. al.[141,145] have reported on tethered pyrazole derivatives on the 3,5-positions of the pyrazole which bear cyclopentadienyl ($\mathbf{H_3L^A}$- not isolated), indenyl ($\mathbf{H_3L^B}$) and fluorenyl ($\mathbf{H_3L^C}$) side arms in a symmetric ligand environment.

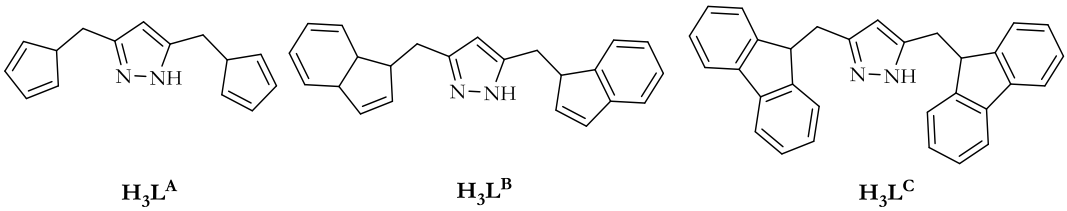

$\mathbf{H_3L^A}$ $\mathbf{H_3L^B}$ $\mathbf{H_3L^C}$

Scheme 7. 1: Previously studied symmetric 3,5-substituted pyrazole bridged proligands

This section is a further study on this ligand system, with the aim of preparing ligands, which combine cyclopentadienyl, indenyl, and fluorenyl pyrazole derivatives in an asymmetric ligand environment ($\mathbf{H_3L^5}$ and $\mathbf{H_3L^6}$).

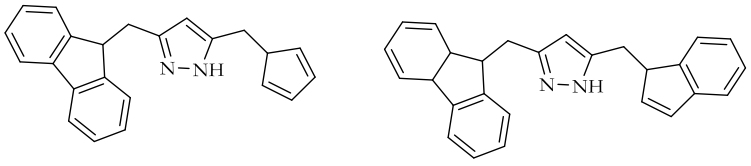

$\mathbf{H_3L^5}$ $\mathbf{H_3L^6}$

Scheme 7. 2: New asymmetric ligands investigated

Attempts would be made at preparing trimethylsilyl (TMS) derivatives of these new classes of ligands, as ligand precursors to the preparation of group 4 metal complexes for olefin polymerization.

7. 1 Ligand synthesis

Following already established synthetic procedures, it was possible to first prepare the single substituted sidearm product (**C**), followed by a second substitution (**D**) from the *bis*(chloromethyl)pyrazole hydrochloride salt (**A**) prepared by Bosnich et. al.[143] using the scheme below.

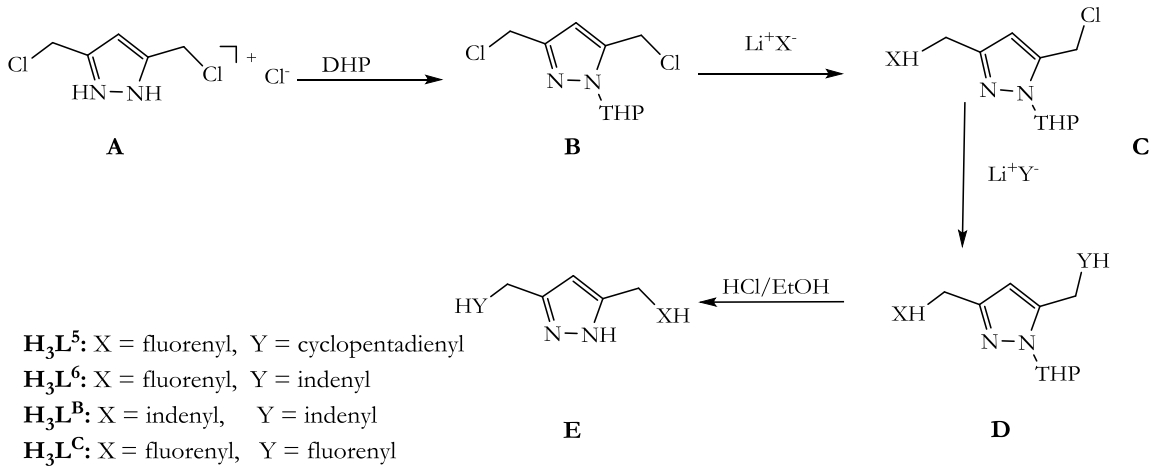

Scheme 7.1. 1: Synthetic scheme for the formation of heteroleptic tethered pyrazole ligands

The ^{1}H NMR spectrum of a singly substituted fluorenyl side arm **C** without THP is shown in Fig. 7.1. 1: The methylene protons H^{a} are observed as a singlet at 4.50 ppm, whiles H^{c} is a doublet at 3.29 ppm due coupling with H^{d}. The methine proton H^{d} is observed as a triplet at 4.22 ppm due to coupling with H^{c}.

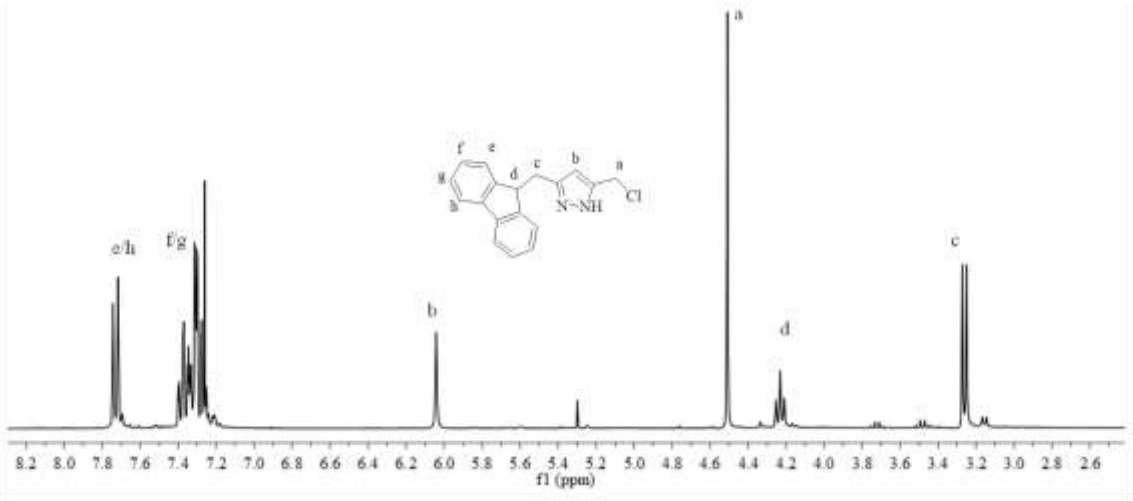

Fig. 7.1. 1: ^{1}H NMR spectrum of a single fluorenyl substituted sidearm (C) with THP removed measured in $CDCl_3$ at room temperature

After the substitution of both 3,5-sidearms, the THP protection was easily removed by treating **D** with an ethanolic HCl solution, to furnish the product **E** in 81-89% yield. The required ligands were obtained in moderate to good yields after recrystallization from a CH_2Cl_2/hexane.

7.1. 1 Synthesis of trimethylsilyl derivatives

The TMS-derivatives were obtained in moderate yields (33-42%) using the reaction Scheme 7.1.1. 1.

H_3L^5: X = fluorenyl, Y = cyclopentadienyl
H_3L^6: X = fluorenyl, Y = indenyl
H_3L^B: X = indenyl, Y = indenyl
H_3L^C: X = fluorenyl, Y = fluorenyl

HL^9: X = fluorenyl, Y = indenyl
HL^{10}: X = fluorenyl, Y = fluorenyl
HL^{11}: X = indenyl, Y = indenyl

Scheme 7.1.1. 1: Synthetic scheme for the formation of TMS derivatives

In a typical reaction procedure, $\mathbf{H_3L^x}$ is treated with 4 mol equivalent *n*-BuLi at -78°C, stirred for 14 h, and warmed up to room temperature. The lithium salt solution is then treated with 3.0 mol equivalent TMSCl. The product was isolated as solids after appropriate workup. The proligands were obtained as air and moisture stable powders.

The ^{1}H NMR spectral analysis of the proligands $\mathbf{HL^9}$-$\mathbf{HL^{11}}$ show the formation of a mixture of double and triple TMS substitutions. For instance, The ^{1}H NMR of $\mathbf{L^9}$ shows three sets of signals for the TMS group at -0.30, -0.16, -0.12 ppm respectively. This corroborates with ESI-MS, which shows *m/z* values at 590 (65%) for $[L^6(SiMe_3)_3]^+$ and 519 (100%) for $[L^6(SiMe_3)_2]^+$ fragments respectively. On the other hand, $\mathbf{HL^{11}}$ shows a singlet for the $SiMe_3$ group at -0.08 ppm in the ^{1}H NMR spectrum and *m/z* value at 468 (100%) which can be assigned to $[L^c(SiMe_3)_2]^+$ in ESI-MS.

The ^{1}H NMR spectrum of the proligands shows the CH_2 linkers as broadened signals at room temperature, pointing to a possible fluxional process involving different orientations

('*E*' and '*Z*') of the aromatic groups with respect to the pyrazole plane. Variable temperature NMR analysis of these compounds shows the folded ("*Z*") conformations does not freeze out at lower temperatures. The ^{13}C NMR assignment of a selected ligand **L^{10}** is shown in Fig. 7.1.1. 1.

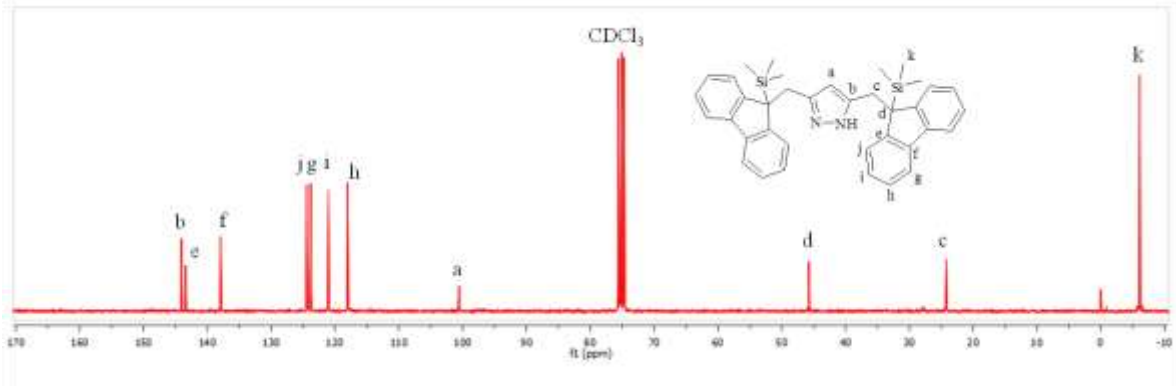

Fig. 7.1.1. 1: ^{13}C NMR spectrum of HL^{10} measured in $CDCl_3$ at room temperature

7.1. 2 Complex synthesis

Treating **HL^{10}** with $CrCl_3$·3THF under inert conditions results in the isolation of air stable colourless crystals, whiles the majority of the product remained green oil. The single crystal X-ray structure of the crystals shows a hydrochloride salt of the nature $[H_2L^{10}]Cl$. The molecular structure (Fig. 7.1.2. 1) and selected bond lengths [Å] and angles [°] are given in Table 7.1.2. 1. The molecule crystallizes in the *P* -1(2) space group and has two molecules linked by hydrogen bonding in the unit cell.

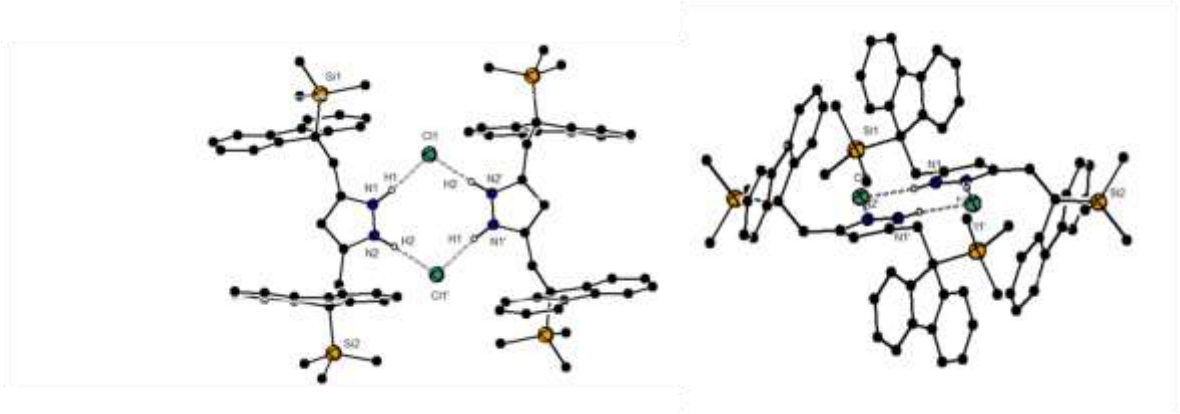

Fig. 7.1.2. 1: Molecular structure of $[H_2L^{10}]Cl$ showing different orientations, most H atoms omitted for clarity

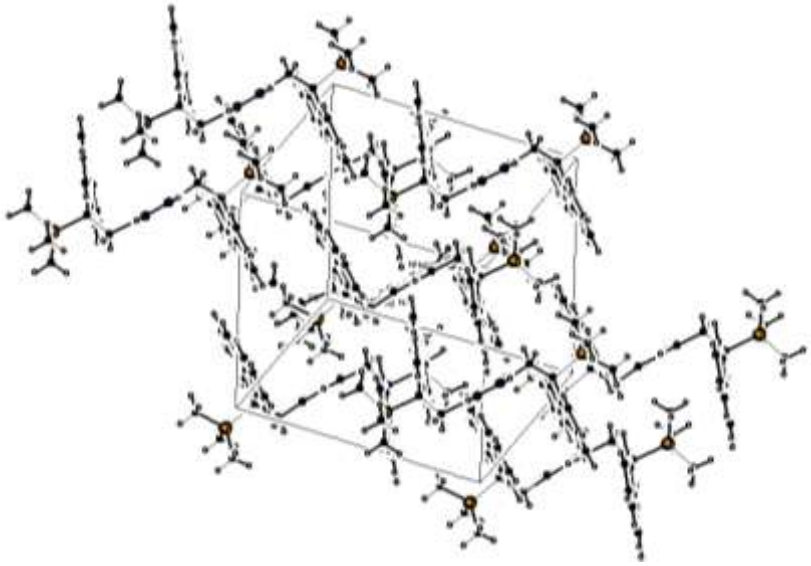

Fig. 7.1.2. 2: Molecular packing structure for HL^{10}

The inter planar angle defined by the five atoms each which make up the two pyrazole rings is 0.00°. Thus, both pyrazole rings lie in the same plane. Two inter molecular N-H··Cl bonding interactions can be found within the molecule. The hydrogen bonds are strong with N-H···Cl angles between 172.5-172.7°. In the crystal structure, some degree of π-stacking is observed, as shown in Fig. 7.1.2. 2.

The molecule adopts an extended "*Z*" conformation as a means of keeping the bulky $SiMe_3$ groups away from each other for steric reasons, as opposed to the folded conformation "*E*".

Table 7.1.2. 1: Selected bond lengths [Å] and bond angles [°] for $[H_2L^{10}]Cl$

Bond lengths [Å]		Bond Angles [°]	
Si(1)-C(20)	1.859(3)	C(20)-Si(1)-C(18)	108.74(14)
N(1)-H(1)···Cl1	3.042(18)	N(1)-H(1)···Cl1	172.56(32)
N(2)-H(2)···Cl1'	3.040(21)	N(2)-H(2)···Cl1'	172.751(36)

Further reactions of the TMS derivatives with group 4 transition metals (Ti, Zr) were not successful after several attempts. The ^1H NMR spectra of the products isolated showed an intact TMS group.

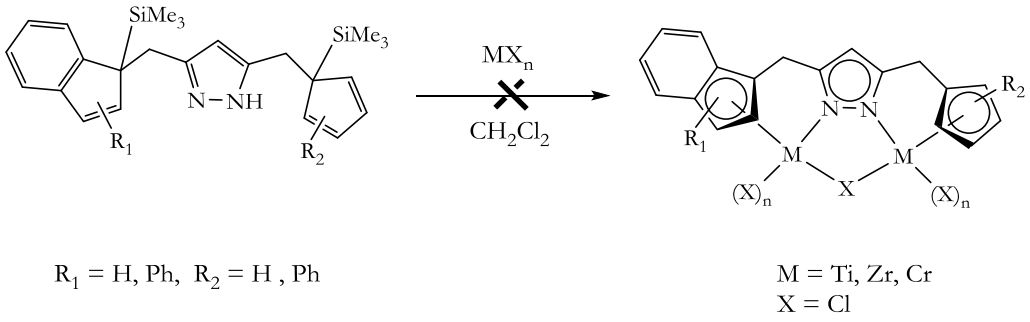

Scheme 7.1.2. 1: Attempted preparation of transition metal complexes with TMS precursors

Attention was therefore focused on the ability of the TMS derivative [$\mathbf{H_2L^{10}}$]Cl to bind to silver cations, inspired by the work done on the conformationally adaptable ligand, 1,4-bis(9-methyl-9H,fluoren-9-yl)methyl]benzene reported by Chebny et. al.[295] The conformationally adaptable receptor undergoes a simple C-C rotation in the presence of silver cations to give a *π*-prismand like receptor with a remarkable efficiency (K *ca* 15000). This ligand readily undergoes C-C bond rotation from the extended ("Z") conformer to an isoenergetic (folded) conformer in the presence of Ag^+, because of a cavity formed by the three aromatic walls in the "Δ" conformation (Scheme 7.1.2. 2).

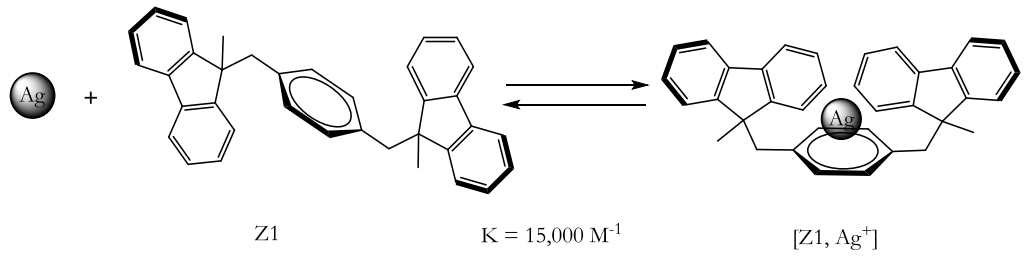

Scheme 7.1.2. 2: Binding of a single Ag^+ by the conformationally adaptable receptor Z1[295]

The reaction was monitored by ^{1}H NMR spectroscopy, by observing changes in the ^{1}H NMR spectrum upon the incremental addition of a solution of Ag(OTf) (14.1 mM) in a 1:1 chloroform-d/methanol-d_4. 66 mM of [H_2L^{10}]Cl.

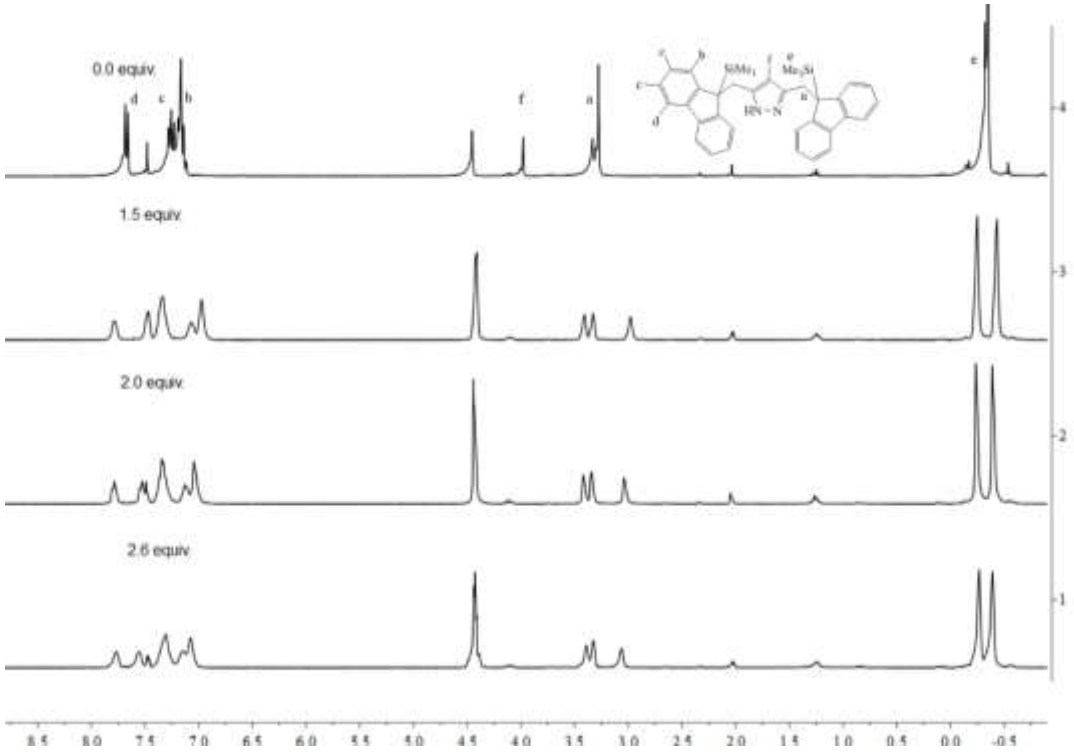

Fig. 7.1.2. 3: ^{1}H NMR spectra showing changes in the aromatic protons, with incremental addition of AgOTf to $[H_2L^{10}]Cl$ measured in $CDCl_3$ at room temperature

Shifts in the ^{1}H NMR spectrum are observed with the addition of AgOTf solution. Notable changes in the spectrum include the upfield shift of the CH^{Pz4} and changes intensity and multiplicity of the aromatic protons (Fig. 7.1.2. 3). After the addition of 10 Eq. of AgOTf, the $SiMe_3$ signal coalesce into a singlet, after which no further changes in the ^{1}H NMR spectrum is observed. From the ^{1}H NMR spectroscopic observations, titration with Ag^+, causes $[H_2L^{10}]Cl$ possibly to undergoes folding into other structures in the presence of Ag^+possibly as shown in **XLIX**. No further analysis were carried out since it was not part of the initially spelt out objectives.

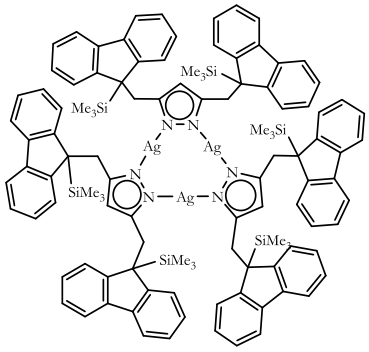

XLIX

8 NHC and cyclopentadienyl/indenyl/fluorenyl pyrazolyl tethered derivative ligands

The first stable isolation of imidazole-2-ylidene by Arduengo et. al.[296,297] has since broadened the chemistry of N-heterocyclic carbenes (NHCs) as very good σ-donors. They have been generally touted as more stable alternatives to tertiary phosphine ligands in relation to their stability and coordination behaviour.[298] They generally form more stable complexes due to their strong σ-donating abilities, and are reported to be less susceptible to reductive elimination and degradative cleavage in catalytic reactions.[299]

N-heterocyclic carbenes as Lewis base 2-electron donors have been applied extensively in coordination chemistry to a range of metals. Apart from their role as good ligands in metal-based catalytic reactions, their coordination chemistry has not only been limited to transition metals but with a range of other metals and periodic elements in the s block and p block (**XLIX-LI**).[300,301302303,304]

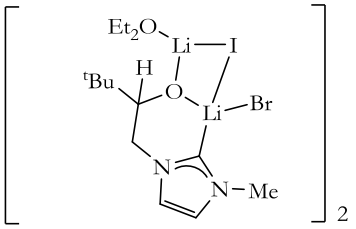

XLIX

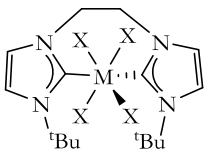

M = In, Tl
X = Cl, Br

L

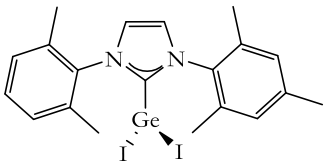

LI

They are also able to form different interactions ranging from ionic to covalent, and in the past few years' research have shown the ability of NHC ligands to react and stabilize elements across the periodic table. Meyer et. al.[150] have reported on Ag_4(I) complexes of pyrazolate-bridged compartmental NHC ligands which provide two binding pockets and gives rise to unique multinuclear Ag(I)-NHC complexes.

Combining polydentate anionic ligands with NHC's gives ligands with improved stability and the ability to stabilize metals in high oxidation states. Although attempts have been made at combining NHC's with other polydentate ligands with anionic functional groups, very few of have been reported to date.[305,306,307,308,309]

Danopoulos and co-workers have combined NHC carbenes with pendant indenyl (**LII**) and fluorenyl groups (**LIII**).[310] In addition, rhodium(I) and iridium(I) complexes of this ligand

system in catalytic studies are weakly active for the hydroformylation of 1-octene with poor selectivity.[311]

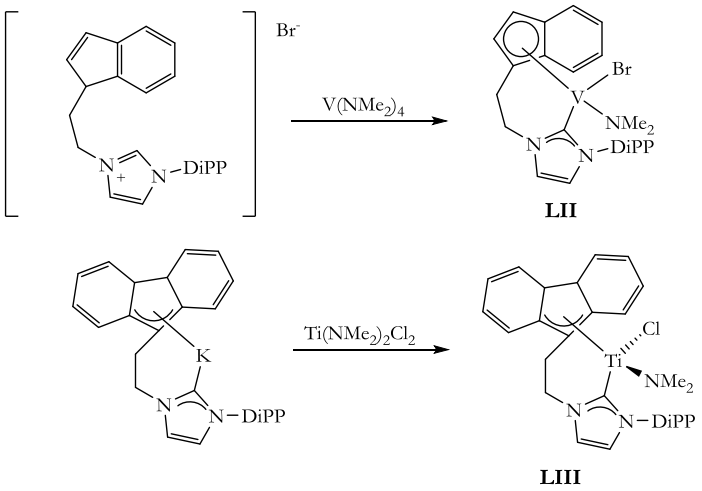

Scheme 8. 1: N-heterocyclic carbenes with pendant indenyl and fluorenyl groups.[310]

Yao et. al.[305] have also reported on fluorenyl-NHC ligated rare earth (Ln) metal precursors which under mild conditions (40°C and normal ethylene pressure) with activation is highly active in the copolymerization of ethylene and 1-hexene (4120 kg mol_{Sc}^{-1} h^{-1} atm^{-1}) with moderate 1-hexene insertion ratio (20.2%).

The aim is to prepare a novel class of asymmetric 3,5-pyrazolyl bridging ligands, which have the potential of hosting two different organometallic fragments (**H_3A**) in a single unit within cooperative distance.

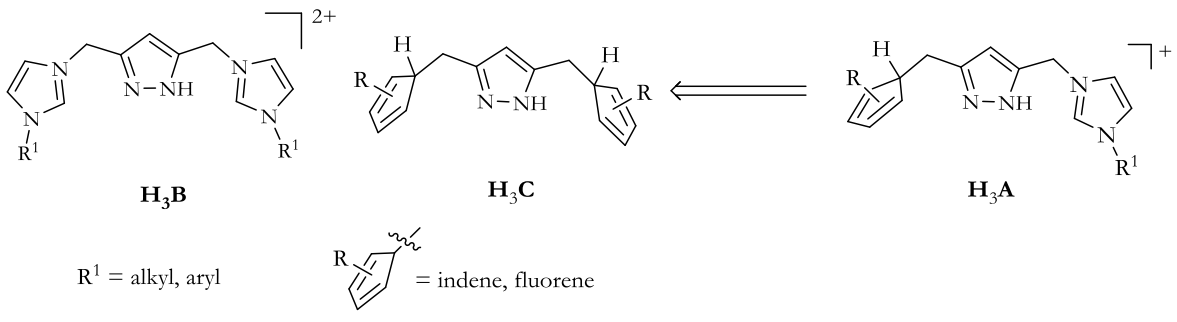

This new class of ligand (**H_3A**) can be described as a combination of a ligand with an NHC side arm (**H_3B**) and a Cp derivative side arm (**H_3C**).

It is envisaged that this new class of ligands can be capable of hosting metals in different oxidation states.

8. 1 Ligand synthesis

The syntheses of the ligands were achieved as outlined in Scheme 8.1. 1. The ligands were obtained in good to moderate yields (60-90%) as moisture sensitive hygroscopic solids. Subsequent treatment of the chloride salts with excess NH_4PF_6 made possible the isolation of the corresponding hexafluorophosphate salts.

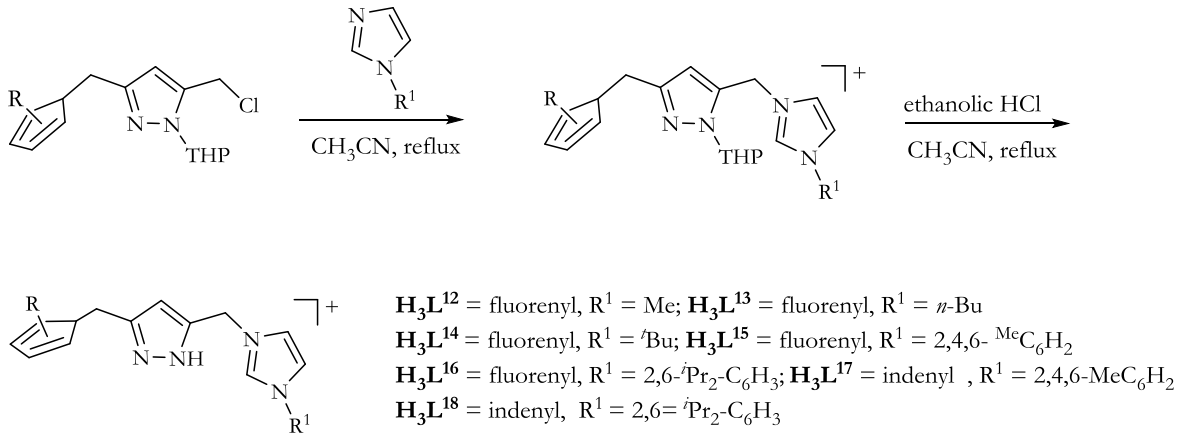

H_3L^{12} = fluorenyl, R^1 = Me; **H_3L^{13}** = fluorenyl, R^1 = *n*-Bu
H_3L^{14} = fluorenyl, R^1 = *t*Bu; **H_3L^{15}** = fluorenyl, R^1 = 2,4,6- $^{Me}C_6H_2$
H_3L^{16} = fluorenyl, R^1 = 2,6-^{i}Pr$_2$-C_6H_3; **H_3L^{17}** = indenyl , R^1 = 2,4,6-MeC_6H_2
H_3L^{18} = indenyl, R^1 = 2,6= ^{i}Pr$_2$-C_6H_3

Scheme 8.1. 1: Synthetic scheme for the preparation of HL^{12}-HL^{18}

All the ligands, **H_3L^{12}-H_3L^{18}** were characterized by ^{1}H and ^{13}C NMR spectroscopy, IR spectroscopy, ESI-MS and elemental analysis. All ligands are soluble in DMSO-d_6. The ^{1}H NMR spectrum of the ligands shows the characteristic imidazolium CH proton between 9.20-9.46 ppm. The CH_2 linker between the imidazolium and pyrazolyl moiety is generally observed as a singlet between 5.35-5.85 ppm, whiles the CH of the fluorenyl moiety is observed as a triplet, due to coupling with the CH_2 linker between 4.31-4.33 ppm. The CH pyrazole proton is observed between 5.94-5.97 ppm. The ^{1}H NMR spectrum of H_3L^{16} with assignments is shown in Fig. 8.1. 1.

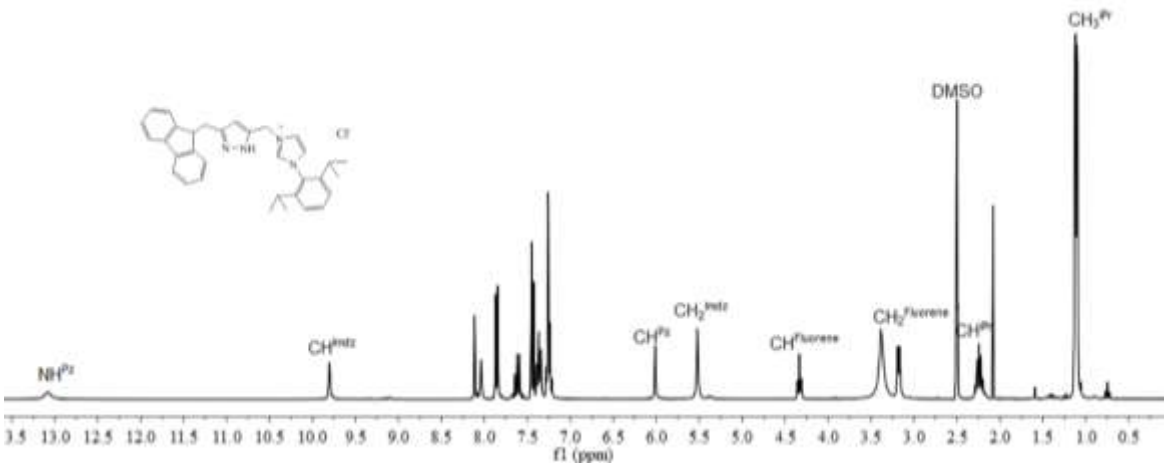

Fig. 8.1. 1: ^{1}H NMR spectrum of H_3L^{16} measured in DMSO-d_6 at room temperature

The ^{13}C NMR spectra assignments were made through a combination of 1D and 2D experiments (HSQC, HMBC, DETP-135, DEPT-90, and ^{13}C NMR). The Fig. 8.1. 2 show a partly assigned spectrum of HL^{13}. Here, the CH_2 group shows negative peaks in the DEPT-135, whiles positive peaks are observed for CH groups in the DEPT-90 NMR spectrum.

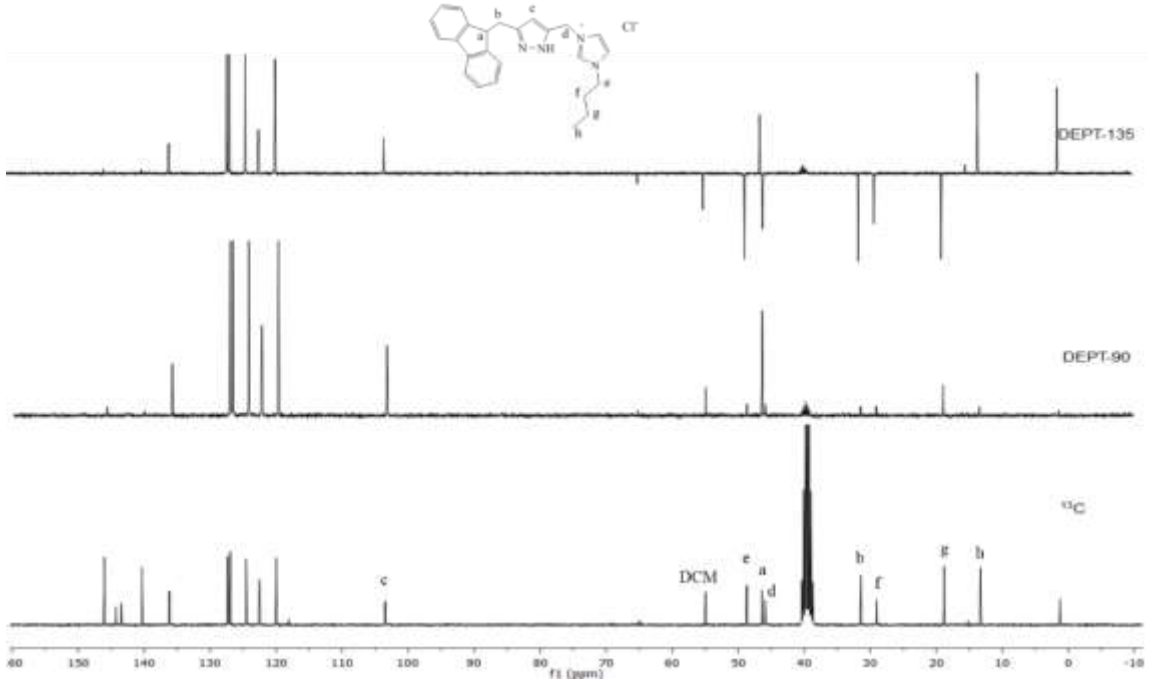

Fig. 8.1. 2: ^{13}C, DEPT-90, and DEPT-135 stacked NMR spectra of H_3L^{13} measured in DMSO-d_6 at room temperature

The molecular structure of of **H_3L^{12}** is shown in Fig. 8.1. 3. Single crystals were obtained by theslow diffusion of Et_2O into a methanolic solution of the ligand. The compound

crystallizes as a salt with two chloride counter ions due to protonation of the second N-atom. Three hydrogen bonding interactions are observed between the protonated nitrogen atoms and the imidazolium protons with the chloride anions.

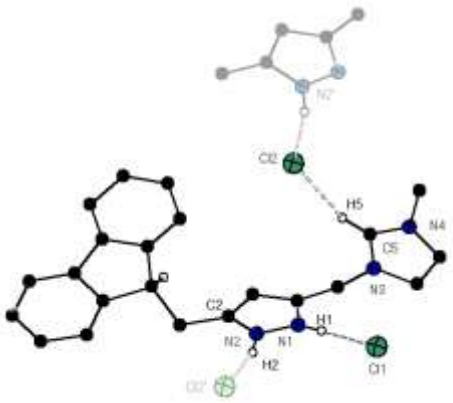

Fig. 8.1. 3: Molecular structure of H_3L^{12} with most H atoms omitted for clarity

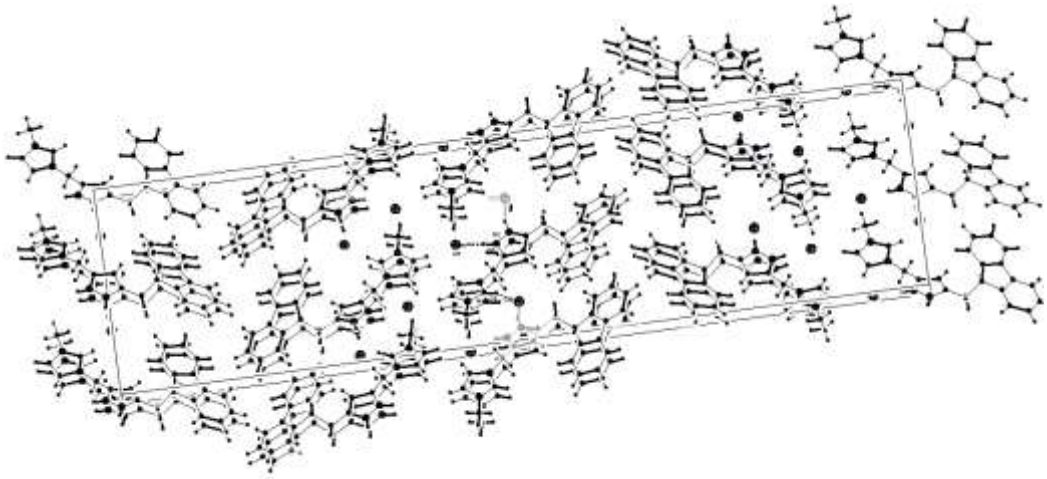

Fig. 8.1. 4: Molecular packing diagram of H_4L^{12}

The C(5)-H(5)···Cl, N(2)-H(2)···Cl2', and N(1)-H(1)···Cl(1) bond angles are 145.3°, 162.3° and 179.4° respectively. The hydrogen bond in N(1)-H(1)···Cl(1) is the strongest because of the optimal hydrogen bond angle of 179.4°. Nevertheless, in the case of C(5)-H(5)···Cl and N(2)-H(2)···Cl2', the hydrogen bonds are considered weaker because of the suboptimal X-H···Cl angles of 145.3° and 162.3° respectively (Table 8.1. 1). It has been shown that Cl atoms may act as moderately strong hydrogen-bond acceptors.[312] The hydrogen bond lengths found in $\mathbf{H_3L^{12}}$ are N(1)-H(1)···Cl(1) (2.99 Å), N(2)-H(2)···Cl(2) (3.00 Å), and C(5)-H(5)···Cl(2) (3.48 Å). The H···Cl bond lengths in $\mathbf{H_3L^{12}}$ are less than the sum of the van der

Waals radii for H and Cl.[313] The C(5)-H(5)···Cl(2) length of 3.48 Å is within the range of other reported C-H···Cl bond lengths.[314,315]

Table 8.1. 1: Selected bond lengths [Å] and bond angles [°] for H_3L^{12}

Bond lengths (Å)		Bond Angles (°)	
N(3)-C(5)	1.318(6)	C(5)-N(3)-C(6)	109.3(3)
N(4)-C(5)	1.321(55)	N(3)-C(5)-N(4)	108.3(4)
N(1)-H(1)···Cl(1)	2.995(35)	N(1)-H(1)···C(1)	162.3(4)
N(2)-H(2)···Cl(2)	3.001(31)	N(10)-H(1)···Cl(1)	179.4(3)
C(5)-H(5)···Cl(2)	3.483(44)	C(5)-H(5)···Cl(2)	145.3(2)

The ligand also shows extensive π-stacking with the molecules layered on top of each other as a means of limiting steric crowding (Fig. 8.1. 4).

8. 2 Synthesis of rhodium(II) complex

Attempts at obtaining Ag(I) complexes of this new ligand system failed, although a wide range of Ag(I) precursors were used. Complexation of $\mathbf{H_3L^{11}}$ with $Rh_2(OAc)_4$·2MeOH leads to the formation of cationic complex $[HL^{14}{}_2Rh_2(OAc)_4](PF_6)_2$ (**4f**).

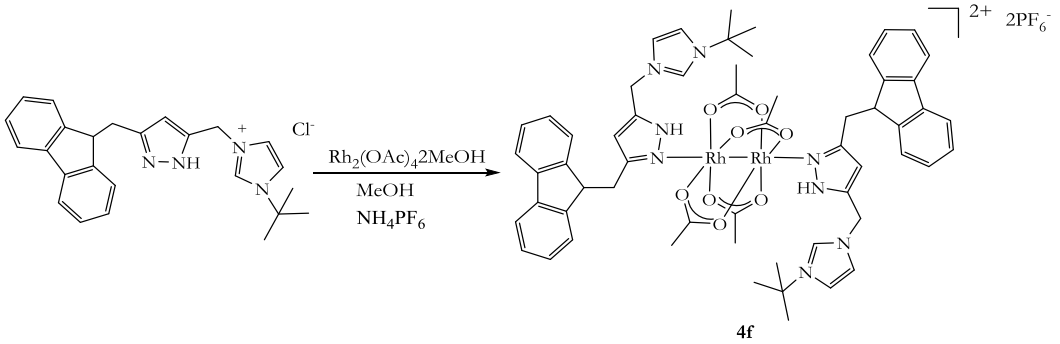

Scheme 8.2. 1: Synthetic scheme for the preparation of 4f

The ^{1}H NMR spectrum of **4f** shows the ^{t}Bu group is unchanged at 1.59 ppm, and the free carbene and NH^{Pz} are observed at 9.34 and 12.78 ppm compared to 9.56 and 15.08 ppm in the free ligand respectively. The IR spectrum of **4f** shows two strong asymmetric acetate bridging environments at 1572 and 1588 cm^{-1} . Dark red single crystals of **4f** were obtained

by the slow evaporation of a 50:50 methanolic/CH_2Cl_2 solution of the complex at room temperature. The complex crystallizes in the *P* 21/c space group. The molecular structure of **4f** is shown in Fig. 8.2. 1.

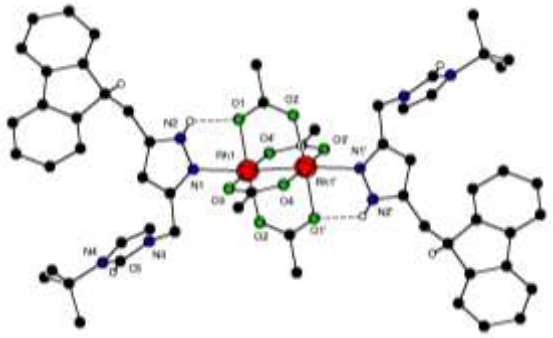

Fig. 8.2. 1: Molecular structure of 4f with counter ions and most H atoms omitted for clarity

The Rh(II) dimer **4f** has two PF_6^- counterions and cocrystalizes with a half molecule of methanol. Each Rh(II) centre is lying in the centre of a six coordinate octahedral geometry. The Rh···Rh bond distance in this complex 2.39 Å, which is significantly shorter than that observed in analogues rhodium-rhodium paddlewheel complexes. Intramolecular hydrogen bonding interactions are observed between an oxygen atom of an acetate molecule O(1) and a proton on the pyrazolyl nitrogen N(2). Selected bond lengths and bond angles for **4f** are given in Table 8.2. 1.

Table 8.2. 1: Selected bond lengths [Å] and bond angles [°] for 4f

Bond lengths (Å)		Bond Angles (°)	
Rh(1)-Rh(1')	2.3961(5)	N(1)-Rh(1)-Rh(1)	175.26(8)
Rh(1)-O(3)	2.045(2)	O(1)-Rh(1)-O(4)	88.91(10)
Rh(1)-N(1)	2.224(3)	O(1)-Rh(1)-N(1)	86.66(10)
Rh(1)-O(4)	2.035(2)	O(1)-Rh(1)-O(2)	175.90(9)

The ESI mass spectrum of **4f** showed the ligand as the prominent m/z peak, 382 (100%) assigned to $[L]^+$. No further reactions were carried out on these new class of ligand system.

9 Conclusion

a). Mechanistic insights into the formation of the unusual tetrapalladium complex

i. Further mechanistic studies have been conducted into the formation of the unusual tetrapalladium complex (**XXI**[c]). The proposed mechanism leading to the formation of **XXI**[c] has been verified with a series of experiments. The proposed C_s (**1**) and C_{2v} (**2**) intermediates have all been identified, and in some instances, characterized using ^{1}H and ^{13}C NMR spectroscopy, ESI-MS and elemental analysis. The analogous tetrapalladium complex of HL[1] **2k** was also isolated, and characterized.

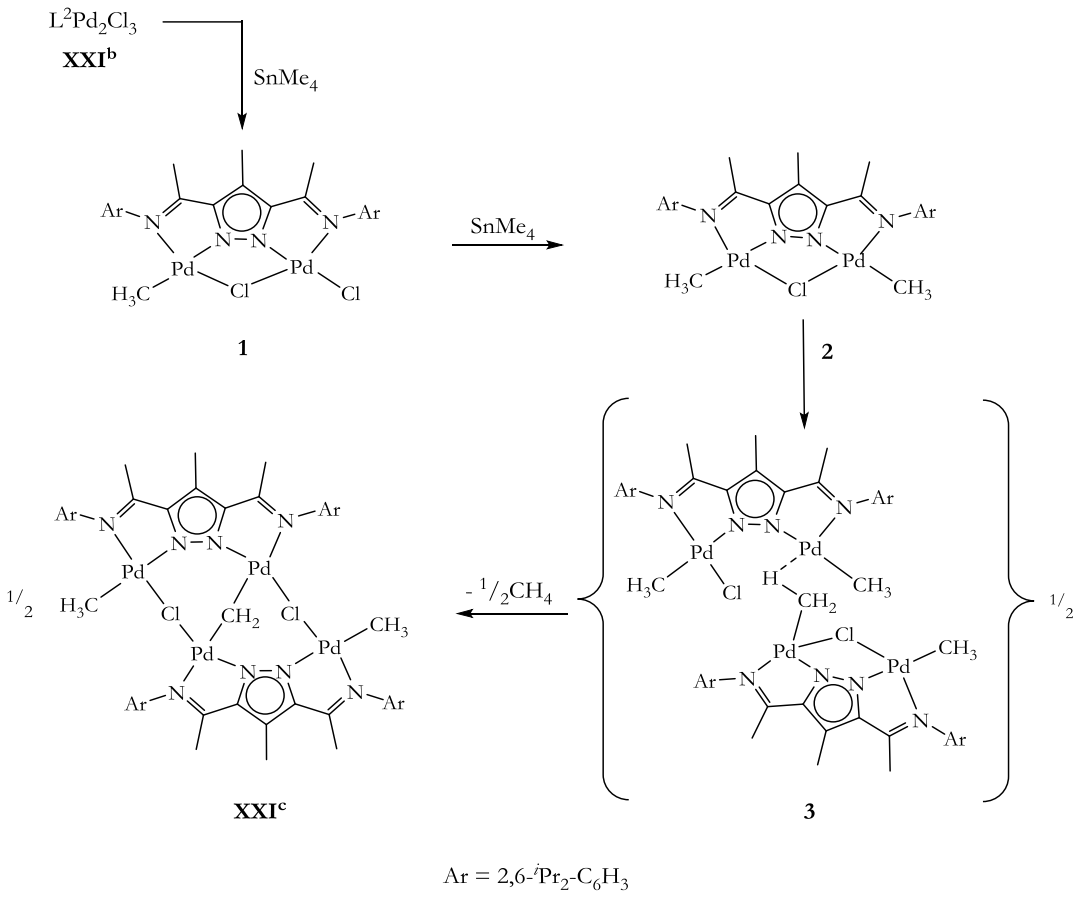

Scheme 9. 1: Proposed scheme to the formation of the unusual tetrapalladium complex XXI[c]

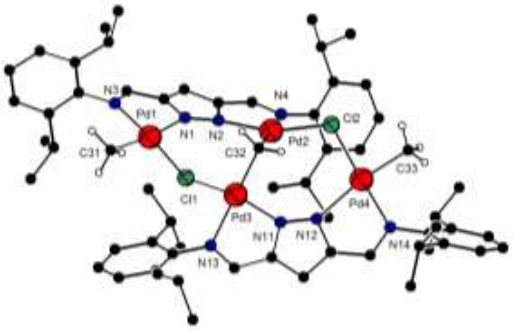

Fig. 9. 1: Molecular structure of the analogous imine complex 2k

ii. The identity of the second observed product, which was formed in the presence of excess $SnMe_4$ and with longer reaction time, has been established as a new tripalladate complex **2h**. This complex is formed as a competing side product to the formation of the tetrapalladium complex. The identity of this complex has been established by ^{1}H, ^{13}C NMR, and elemental analysis and by single crystal X-ray crystallography.

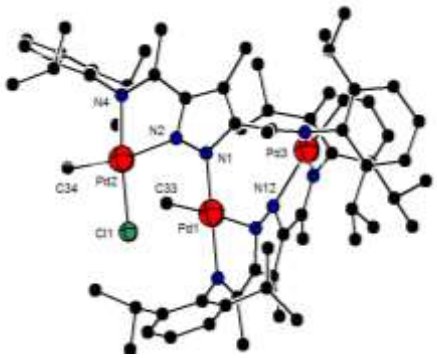

Fig. 9. 2: Molecular diagram of the new tripalladate complex 2h formed as a competing side product

iii. The origin of the unlabeled carbon in olefin coupling reactions with ^{13}C labelled C_2H_4 has been established as emanating from the μ-CH_2 of **XXI**[c]. As proved by the series of reactions of the activated complex with normal styrene and styrene-d_8.

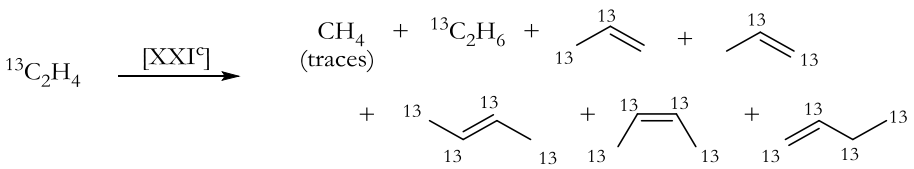

iv. This unusual tetrapalladium complex is also able couple olefins such as styrene, methylacrylate, acrylonitrile, and cyclohexenone in addition to ethylene in moderate to good yields, but only after chloride abstraction.

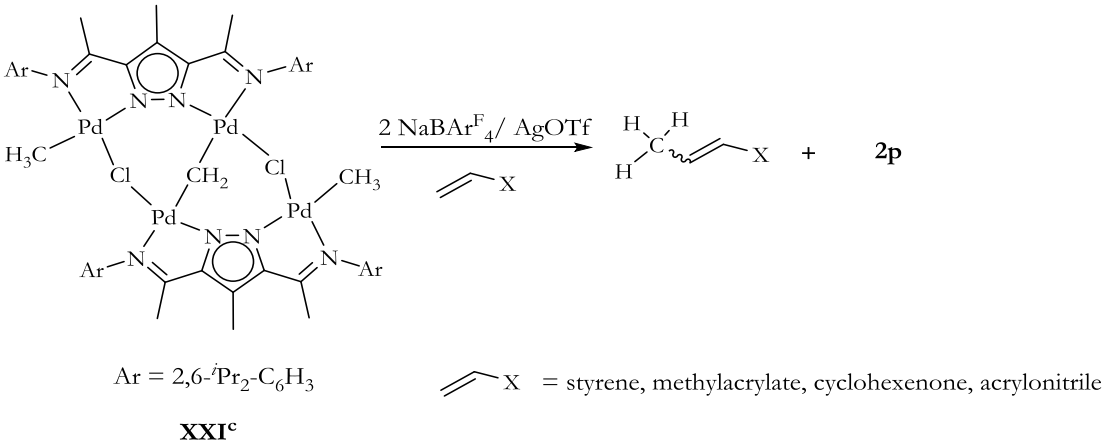

XXI^c

Scheme 9. 2:Olefin coupling ability of XXI^c after activation with NaBAr$^F_4$ or AgOTf

v. A new tetrapalladium compound **2p**, with two μ-Cl, a μ-OH and a μ-O group has been identified and isolated. The complex **2p** has been characterized by ^{1}H, ^{13}C NMR and IR spectroscopy, ESI-MS, elemental analysis, and a single crystal X-ray crystallography. This complex is formed as the final product after activation of the tetrapalladium complex **XXI^c**with a chloride abstracting agent (AgOTf/NaBAr$^F_4$) with or without added olefin. It is formed as the final stable product after a series of complex rearrangements in solution.

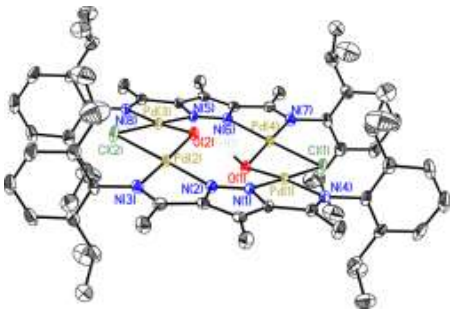

Fig. 9. 3: Molecular structure of final rearrangement product 2p, most H atoms and one [BAr$^F_4$]$^-$ counterion, omitted for clarity

vi. A new class of palladium(II) *a*-diimine complexes with bromides and iodides (**1b**, **1c**, **2c**, **2g**) have been prepared and fully characterized by ^{1}H, ^{13}C NMR, ES-MS,

and elemental analysis. Attempts to obtain single crystals suitable for X-ray crystallography proved futile.

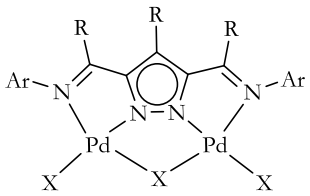

(**1b**): R = H, X = Br
(**1c**): R = H, X = I
(**2b**): R = Me, X = Br
(**2c**): R = Me, X = I

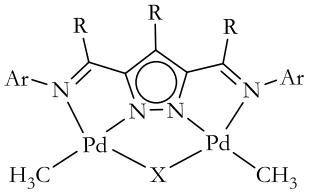

(**2g**): R = Me, X = Br

Ar = 2,6-$^{i}Pr_2$-C_6H_3

Scheme 9. 3: Scheme of new complexes prepared

b). Preparation of heterobimetallic complexes of palladium(II)-rhodium(I) with *α*-diimine type ligands

i) Although the initial route adopted for the preparation of heterobimetallic complexes by addition of a second metal to pre-existing mononuclear complexes failed, a number of monoanionic complexes (**3a**, **3b**, **3c**, **3d**, **3j**, **3k**, **3l**) were isolated and fully characterized. The nickel complex **3k** is active in ATRP reaction, although the polymerization is not well controlled.

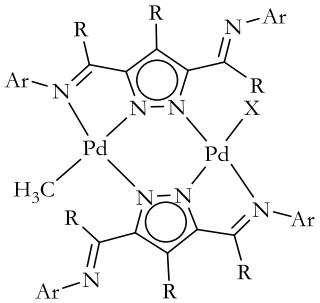

(**3a**): R = Me, X = CH_3
(**3b**): R = H, X = Cl

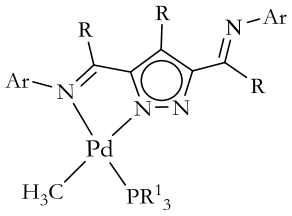

(**3c**): R = Me, R^1 = Me
(**3d**): R = Me, R^1 = Ph

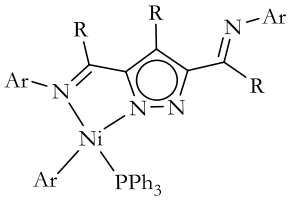

(**3j**) : R = H, Ar = $C_{10}H_7$
(**3k**): R = Me, Ar = $C_{10}H_7$
(**3l**): R = Me, Ar = C_6H_5

Scheme 9. 4: Scheme of new mononuclear and homobimetallic palladium(II) and nickel(II) complexes prepared

ii) The preparation of a new class of heterobimetallic complexes of the *a*-diimine type ligands (**3r**, **3s**, **3t**, **3u**) has been achieved using a more favourable metal

exchange route, which involves the addition of coordinatively unsaturated rhodium(I) complexes to homobimetallic palladium(II) η^3-allyl complexes (**3m**-**3p**).

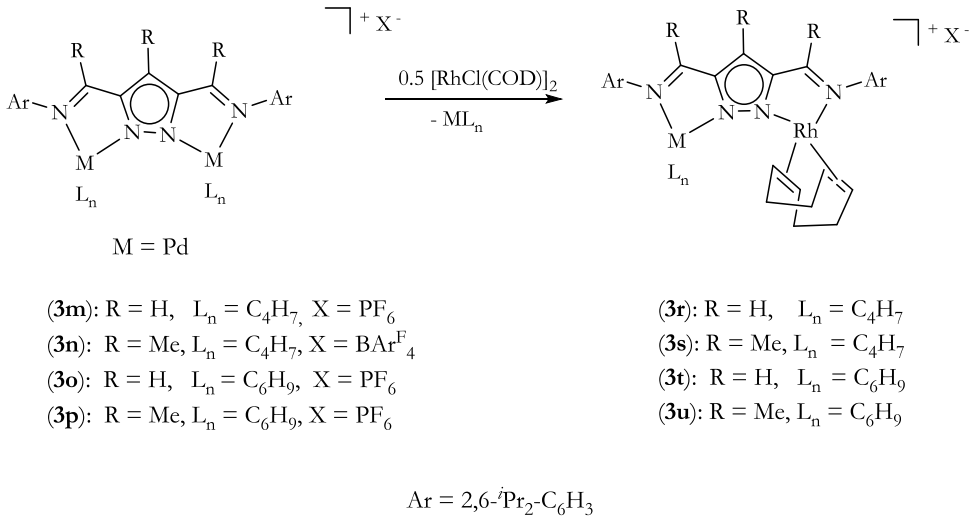

Scheme 9. 5: Scheme of new homobimetallic palladium(II) allyl and heterobimetallic palladium(II)-rhodium(I) complexes prepared

The complexes (**3m**-**3p**) have been fully characterized by ^{1}H, ^{13}C NMR, ES-MS, HRMS and single crystal X-ray crystallography.

iii) Palladium(II) and rhodium(I) complexes (**3v**, **3z**, **3z1**) were also isolated as by-products in the preparation of heterobimetallic complexes.

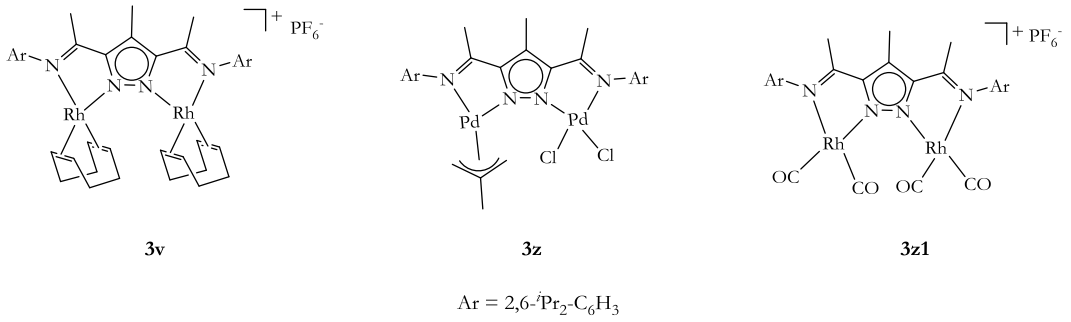

Scheme 9. 6: By-products from synthesis of heterobimetallic complexes

c). Preparation of zinc(II) complexes of the *α*-diimine like pyrazolyl scaffolds as catalyst precursors for the polymerization of *rac*-lactide to polylactide

New tetranuclear zinc(II) complexes) of the *a*-diimine type ligands have been prepared and characterized (**4a**, **4b**, **4c**, **4d**).

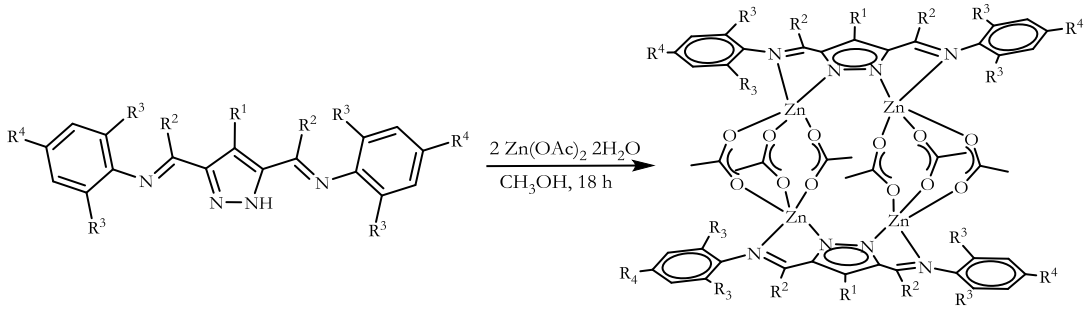

Scheme 9. 7: New zinc(II) complexes (4a-4d) of *α*-diimine type ligands prepared

The ability of these complexes (**4a**-**4d**) to catalyze the ring opening polymerization of *rac*-lactide has been evaluated. These catalysts were found to be moderately active, and catalyzes the conversion of *rac*-lactide to mostly amorphous heteroatactic polylactide with broad polydispersities (>1.7) with up to 60% conversions in the melt. Although polymer conversions do not exceed 60% due to increased viscosity of the reaction media, the catalysts achieves productivities of up to 85 $kgmol^{-1}$ in 30 min at 0.1% catalyst loadings.

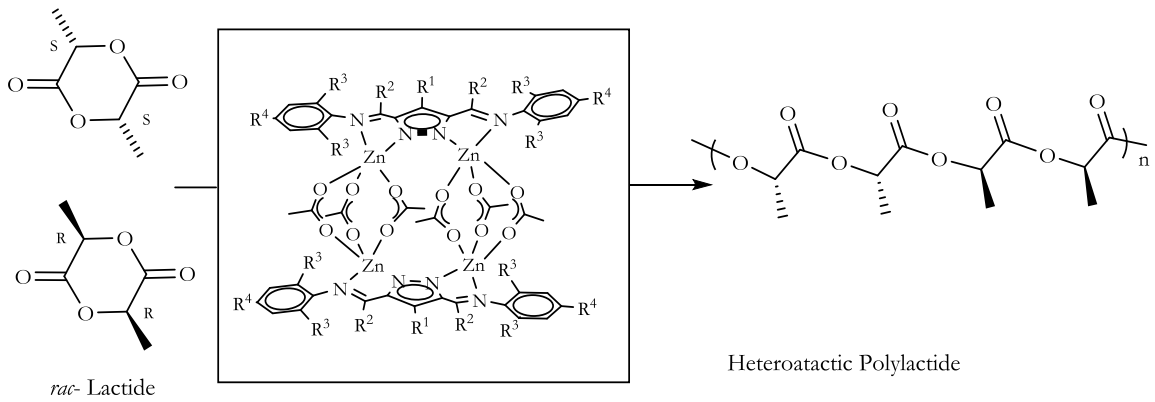

Scheme 9. 8: Lactide polymerization using tetranuclear zinc(II) complexes of *α*-diimine type ligands

d). Preparation of unsymmetric 3,5-indenyl/fluorenyl substituted pyrazole bridging ligand

The synthesis of unsymmetric 3,5-indenyl/fluorenyl substituted pyrazolyl ligands as well as their TMS derivatives has been successfully achieved. The ligands have been characterized, but attempts at preparing bimetallic group 4 metal complexes with this ligand system did not yield the desired results.

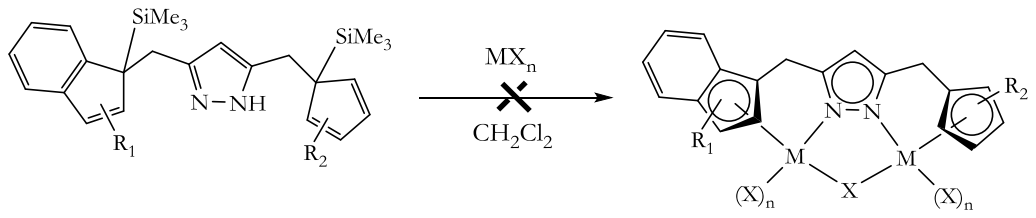

R_1 = H, Ph, R_2 = H , Ph

M = Ti, Zr, Cr
X = Cl

Scheme 9. 9: Unsuccessful attempts at preparation of group 4 metal complexes using a new class of unsymmetrical 3,5 substituted pyrazole ligands

e). Preparation of a novel class of unsymmetric 3,5-NHC and indenyl/fluorenyl substituted bridging ligands

A novel class of unsymmetric 3,5-NHC and indenyl/fluorenyl substituted pyrazolyl ligands (**HL**[12]-**HL**[18]) potentially capable of hosting two different types of organometallic fragments have been prepared and characterized.

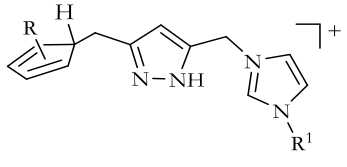

H_3L^{12} = fluorenyl, R^1 = Me; **H_3L^{13}** = fluorenyl, R^1 = *n*-Bu
H_3L^{14} = fluorenyl, R^1 = *t*Bu; **H_3L^{15}** = fluorenyl, R^1 = 2,4,6-^{Me}-C_6H_2
H_3L^{16} = flourenyl, R^1 = 2,6-$^{i}Pr_2$-C_6H_3; **H_3L^{17}** = indenyl , R^1 = 2,4,6-^{Me}-C_6H_2
H_3L^{18} = indenyl, R^1 = 2,6-$^{i}Pr_2$-C_6H_3

This new class of ligand can be likened to a combination of NH carbene ligands (H_3**B**) and the cyclopentadienyl/cyclopentadienyl ligands (H_3**C**) tethered to a pyrazole in the 3,5-positions.

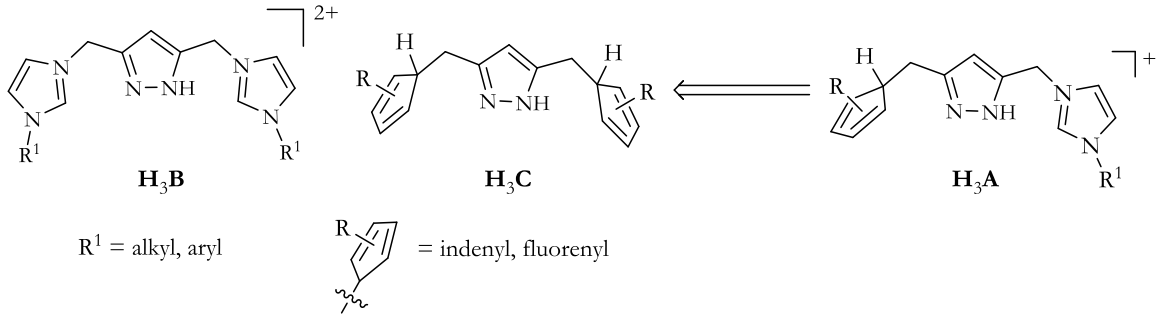

These classes of ligands have been characterized by ^{1}H and ^{13}C NMR, ESI-MS, elemental analysis and in some instances single crystal X-ray crystallography. These ligands in the future can serve as are very good candidates as ligands capable of hosting two different organometallic fragments with metals in different oxidation states in a highly compartmentalized pyrazolyl bridging environment.

10 Perspective

The incorporation of polar monomers such as acrylates into olefins such as ethylene is known to influence important properties such as toughness, surface as well as barrier properties.[316] The challenge now remains in the development of well defined catalysts capable of copolymerizing *a*-olefins with polar monomers under mild conditions. Some catalysts reported to date capable of achieving such feat are the *a*-diimine palladium(II) catalysts reported by Brookhart and co-workers[317318] that copolymerize ethylene and methylmethacrylate to yield highly branched copolymers. Other investigators such as Grubbs[319] and Gibson[320] have also reported metal complexes capable of producing MMA terminated polyethylenes. However, very few reports of bimetallic complexes with enhanced *a*-olefin enchainment have been reported to date.[321,322] The homobimetallic palladium(II) complex $[L^2(CH_3)_2Pd_2Br]$ (**2g**) would be an ideal candidate for exploring the polymerization of ethylene with polar comonomers. Preliminary investigations have shown that this complex after halide abstraction is able to mediate the polymerization of MA to PMMA.

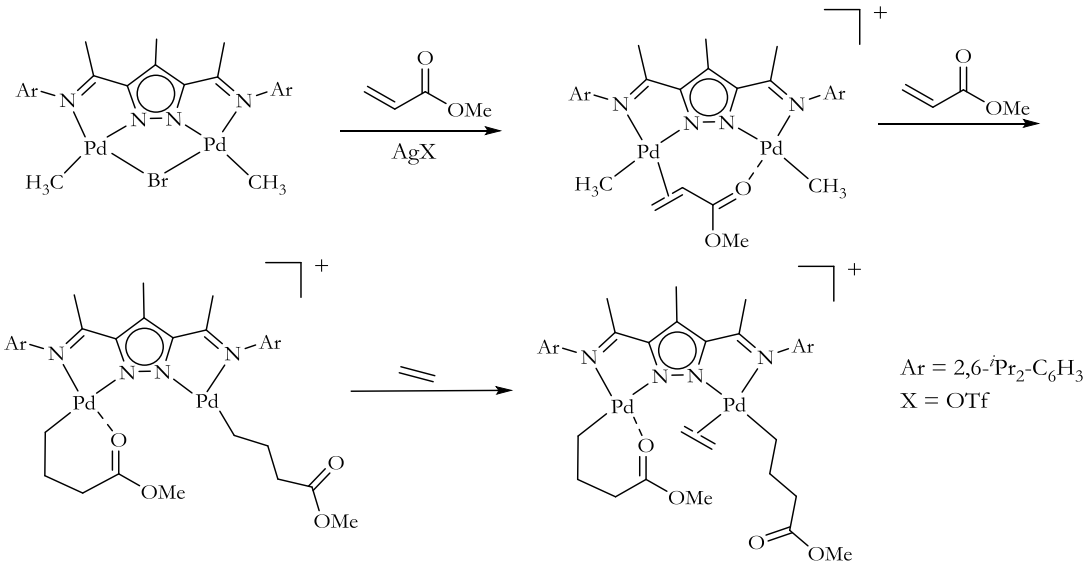

Scheme 10. 1: Proposed catalyst resting stages for ethylene/polar commoner insertion reactions in 2g

This homobimetallic palladium complex would also be a very attractive option for exploring *a*-olefin enchainment with the potential to bind to the two metal centres within a cooperative distance. It would also allow for the study of clear mechanistic insights into potential synergetic effects in multi-centre olefin/polar comonomer copolymerization reactions (Scheme 10. 1).

11 Experimental Section

General methods: All reactions were carried out under dry and oxygen-free nitrogen atmosphere unless otherwise stated. All solvents were dried and distilled prior to use, diethyl ether, THF and toluene were dried and distilled over sodium, whiles CH_2Cl_2 was dried and distilled over calcium hydride.

Reagents:

General reagents were obtained from the chemical store of the Institute of Inorganic Chemistry.

The following reagents and chemicals were obtained from the following sources:

Celite	ABCR
Deuterated solvents	MERCK, SIGMA-ALDRICH
Dichloromethane	FLUKA
2,6-di-isopropylaniline	FLUKA
$NiBr_2$(dme)	ALDRICH
Palladium(II)chloride	UMICORE
Phenylacetylene	MERCK
Rhodium(III)chloride monohydrate	UMICORE
Tetramethyltin	ALDRICH

The following ligands and metal precursors were prepared using established literature procedures:

3,5-Bis-chloromethyl-1-(tetrahydro-pyran-2-yl)-1H-pyrazole[218]

1*H*-pyrazole-3,5-dicarbaldehyde[219]

Toluenesulfonylazide[323]

Diazoacetylacetone[324]

Chloro(1,5-cyclooctadiene)rhodium(I) dimer[325]

(η^3-methylallyl)palladium chloride dimer[326]

(η^3-cyclohexenyl)palladium chloride dimer[327]

XXI[b151]

XXI[c 154]

$[L^2RhCl(COD)]$, $[L^2Pd_2(\eta^3\text{-}C_4H_7)_2]Cl$[221]

NMR:

NMR experiments were performed at 25°C on a Bruker Avance 300 or 500 MHz spectrometer using standard parameters. ^1H and ^{13}C NMR chemical shifts were calibrated with internal solvent signals (δ=5.32 and 53.8 ppm for CD_2Cl_2, δ = 7.26 and 77.16 for $CDCl_3$) and peaks were assigned using 2D experiments: COSY, NOESY (500 ms mixing), CH-COSY/HSQC, and HMBC (optimized for $J_{C\text{-}H}$ = 7 Hz). DOSY spectrum were recorded with 2 ms bipolar z-gradient pulses ramped linearly from 1 to 50 Gcm^{-1} and a diffusion delay of 70 ms. $^1H\{^1H\}$(2.5 kHz decoupling).

Elemental analysis:

Elemental analyses were carried out with a Heraeus CHN-O-RAPID instrument and were performed at the analytical laboratory in the Institute for Inorganic Chemistry, University of Göttingen.

GPC-SEC:

This was performed in THF on a GPC-SEC Analysis Systems 1260 Infinity, at the Institute of Physical Chemistry (IPC), University of Göttingen.

DSC-TG:

Differential scanning calorimetry with thermogravimetry was performed on a Netzsch STA409PC instrument in the analytical laboratory of the Institute of Inorganic Chemistry, University of Göttingen.

IR:

IR was performed on a Cary 630 FTIR spectrometer equipped with a Diamond ATR accessory.

Mass spectrometry:

Mass spectrometry was performed on a Finnigan MAT 8200 (EI, 70 eV), Finnigan MAT 95 (FAB, 3-Nitrobenzyl alcohol), Applied Biosystems API 2000 (ESI), or Finnigan MAT LCQ (HR-ESI) instruments in the Institute of Inorganic Chemistry and the Institute for Organic and

Biomolecular chemistry, University of Göttingen. Isotopic distributions and exact masses were calculated with Mmass data miner.[328,329]

X-ray:

X-ray data were collected on a STOE IPDS II diffractometer (graphite monochromated Mo-Kα radiation, λ= 0.71073 Å, ω scans) at 133 K and corrected for Lorentz and polarization[330] and absorptions[331] the structures were solved by direct methods and refined on F^2 using all reflections with SHELXS-97 and SHELXL-97.[332,333]

ATRP Polymerization:

Conditions: Styrene (20 mL, distilled and stored under argon), a degassed solution of Ethyl-α-bromostyrene in toluene (0.16 mL, 0.23 mmol, dried and stored under argon) and the nickel catalyst (21 mg, 0.23 mmol) were combined under argon and the reactor placed in an oil bath at 70°C. Aliquots were taken via syringe at specified time intervals, cooled to -20°C for at least 10 min, and placed in aluminium bowls. The conversions were determined by gravimetric analysis.

Typical *rac*-polymerization procedure:

Polymerization of *rac*-lactide was performed on a Schlenk line with a flame dried Schlenk flask equipped with a magnetic stirrer. The Schlenk flask was charged with the required amount of lactide and initiator and attached to the vacuum line. After at least three vacuum-nitrogen purge cycles, the flask was immersed in an oil bath heated to the required reaction temperature. Polymerization was stopped by injecting methanol. The polymers were precipitated in hexane, filtered off, reddisolved in CH_2Cl_2 and precipitated again in hexane, and dried in vacuum to a constant weight.

11. 1 Bi- and oligonuclear palladium(II) complexes

11.1. 1 Synthesis of $[L^1Pd_2Br_3]$ (1b)

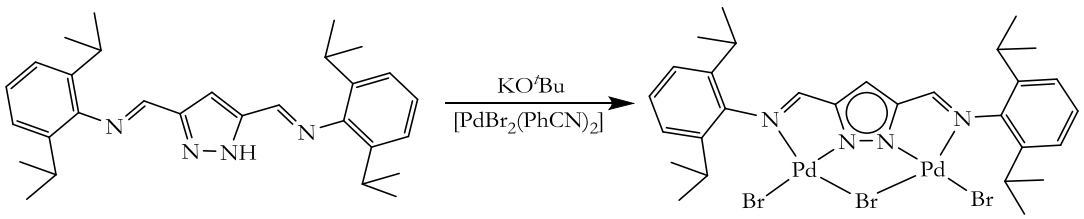

HL^1 **1b**

To a CH_2Cl_2 solution (10 mL) of **HL^1** (45 mg, 0.10 mmol) was added 1.2 equivalent KO^{t}Bu (11.5 mg, 0.12 mmol) with stirring for 30 min. After this, the salt solution of the ligand was added to a stirring suspension of $[PdBr_2(PhCN)_2]$ (96 mg, 0.20 mmol, 2.0 mol Eq.) in CH_2Cl_2 dropwise via a syringe over a 30 min period. A dark red solution was formed which was further stirred under room temperature for 18 h. The suspension was filtered using a filter paper, and the solvent evaporated to obtain a dark red powder. This powder was redissolved in CH_2Cl_2 (20 mL) and 30 ml of Et_2O added, forming a suspension. Filtration of the suspension on a filter paper leaves a dark green hygroscopic solid on the filter paper, whiles a bright orange filtrate was obtained. Evaporation of the filtrate gives the product as a dull brown solid.

Yield:	53 mg, 59%
Molecular formula:	$C_{29}H_{37}Br_3N_4Pd_2$
Molecular weight:	894.2 g/mol.
MS (ESI, CH_2Cl_2) m/z (%):	1708 (50%) $[L_2Pd_4Br_5]^+$; 1072 (60%) $[L_2Pd]^+$; 932 (30%) $[M+K]^+$; 814 (20%) $[M-Br]^+$.
IR (ATR, cm^{-1}):	2057 (m); 2924 (m); 2808 (m); 1547 (vs); 1450 (s); 1305 (vs); 1259 (m); 1138 (vs); 1095 (vs); 1058 (S); 927 (vs); 772 (m); 745 (vs); 668 (m); 579 (m).
^{1}H-NMR ($CDCl_3$) δ:	1.18 (d, $^3J_{HH}$ = 6.9 Hz, 12H, CH_3^{iPr}); 1.41 (d, $^3J_{HH}$ = 6.9 Hz, 12H, CH_3^{iPr}); 3.33 (m, 4H, CH^{iPr}); 7.01 (s, 1H, CH^{Pz}); 7.21-7.36 (m, 6H, CH^{Ar}); 7.73 (s, 2H, CH=N).
$^{13}C\{^1H\}$ ($CDCl_3$) δ:	22.8 (CH_3^{iPr}); 24.5 (CH_3^{iPr}); 29.3 (CH^{iPr}); 110.7 (CH^{Pz}); 123.8 (CH^{Ar}); 129.4 (CH^{Ar}); 141.4 (C^{Ar}); 146.1 (C^{Ar}); 147.8 (C^{Pz}); 165.0 (CH=N).
Elemental analysis:	Calcd. For $C_{29}H_{37}Br_3N_4Pd_2$: (C) 38.95 (H) 4.17 (N) 6.27; Found: (C) 39.02 (H) 4.32 (N) 5.82.

11.1. 2 Synthesis of $[L^1Pd_2I_3]$ (1c)

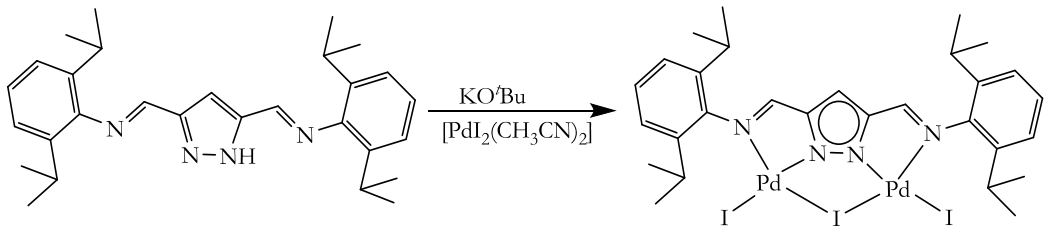

HL^1 **1c**

A similar experimental procedure was followed as done for $[L^1Pd_2Br_3]$. To a CH_2Cl_2 solution (15mL) of the ligand (40 mg, 0.9 μmol) was added 1.1 equivalent KO^{t}Bu (10 mg, 0.92 μmol) with stirring for 30 min. After this, the salt solution of the ligand was added to a stirring suspension of $[PdI_2(CH_3CN)_2]$ (63 mg, 0.18 mmol, 2 mol Eq.) in CH_2Cl_2 dropwise via a syringe over a 30 min period. A red solution was formed which was further stirred at room temperature for 18 h. The suspension was filtered and the solvent evaporated to obtain a dark-red powder. This powder was redissolved in CH_2Cl_2 (20 mL) and 30 ml of Et_2O added, a suspension was formed. Filtration of the suspension on a filter paper leaves a brown solid on the filter paper, whiles a dark red filtrate was obtained. Slow evaporation of the filtrate at room temperature gave the product as fine brown needles.

Yield:	34 mg, 36%
Molecular formula:	$C_{29}H_{37}I_3N_4Pd_2$
Molecular weight:	1035.2 g/mol.
MS (ESI, CH_2Cl_2) m/z (%):	1943 (10%) $[L_2Pd_4I_5]^+$; 908 (5%) $[M\text{-}I]^+$.
IR (ATR, cm^{-1}):	2924 (m); 2955 (m); 2868 (m) ; 1551 (vs); 1468 (vs); 1361 (vs); 1352 (m); 1136 (vs); 1091 (vs); 921 (vs); 802 (vs); 666 (s); 599 (s).
^{1}H-NMR ($CDCl_3$) δ:	1.18 (d, $^3J_{HH}$ = 6.9 Hz, 12H, CH_3^{iPr}); 1.41 (d, $^3J_{HH}$ = 6.9 Hz, 12H, CH_3^{iPr}); 3.30 (m, 4H, CH^{iPr}); 6.91 (s, 1H, CH^{Pz}); 7.19-7.36 (m, 6H, CH^{Ar}); 7.72 (s, 2H, CH=N).
$^{13}C\{^1H\}$ ($CDCl_3$) δ:	22.6 (CH_3^{iPr}); 24.8 (CH_3^{iPr}); 29.3 (CH^{iPr}); 109.8 (CH^{Pz}); 118.5 (CH^{Pz}); 123.7 (CH^{Ar}); 128.9 (CH^{Ar}); 141.0 (C^{Ar}); 146.1 (C^{Ar}); 149.3 (C^{Pz}); 164.9 (CH=N).
Elemental analysis:	Calcd. For $C_{29}H_{37}I_3N_4Pd_2 \cdot 2CH_2Cl_2$: (C) 30.90 (H) 3.43 (N) 4.65; Found: (C) 30.18 (H) 3.17 (N) 4.58.

11.1. 3 Synthesis of $[L^2Pd_2Br_3]$ (2b)

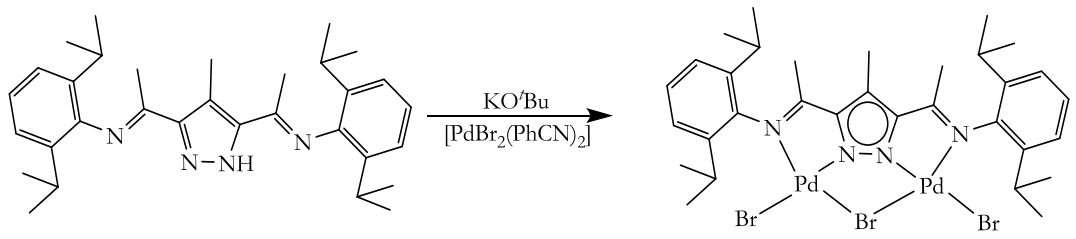

HL^2 **2b**

To a CH_2Cl_2 solution (15 mL) of **HL^2** (125 mg, 0.26 mmol) was added 1.2 mol equivalent KO^{t}Bu (35 mg, 0.31 mmol) with stirring for 30 minutes. The salt solution of the ligand was added dropwise via syringe to a CH_2Cl_2 suspension of $[PdBr_2(PhCN)_2]$ (240 mg, 0.52 mmol) with stirring for 18 h. A dark red suspension formed with time. This was filtered over celite to remove traces of KBr and unreacted $PdBr_2$. The bright red solution was evaporated to obtain a dull yellow powder. Recrystallization from CH_2Cl_2 gives the product as a yellow solid.

Yield:	170 mg, 71%
Molecular formula:	$C_{32}H_{43}Br_3N_4Pd_2$
Molecular weight:	936.3 g/mol.
MS (ESI, CH_2Cl_2) m/z (%):	852 (10%) $[M\text{-}Br]^+$; 696 (40%) $[M\text{-}Br_3]^+$;
IR (ATR, cm^{-1}):	2963 (m); 2924 (m); 2864 (m); 1559 (m); 1477 (s); 1490 (s); 1441 (m); 1385 (s); 1367 (s); 1350 (m); 1264 (m); 1184 (m); 1059 (m); 806 (vs); 782 (vs).
^{1}H-NMR (CD_2Cl_2) δ:	1.19 (d, $^3J_{HH}$ = 6.9 Hz, 12H, CH_3^{iPr}); 1.44 (d, $^3J_{HH}$ = 6.7 Hz, 12H, CH_3^{iPr}); 2.18 (s, 6H, CH_3C=N); 2.50 (s, 3H, CH_3^{Pz4}); 3.19 (p, $^3J_{HH}$ = 6.8 Hz, 4H, CH^{iPr}); 7.22-7.35 (m, 6H, CH^{Ar}).
$^{13}C\{^1H\}$ (CD_2Cl_2) δ:	10.6 (CH_3^{Pz4}); 19.5 (CH_3C=N); 23.2 (CH_3^{iPr}); 23.4 (CH_3^{iPr}); 24.0 (CH^{iPr}); 29.3 (CH^{iPr}); 116.9 (CH^{Ar}); 123.0 (C^{Pz4}); 124.1 (CH^{Ar}); 128.9 (CH^{Ar}); 140.9 (C^{Ar}); 141.1 (C^{Ar}); 146.8 (C^{Pz}); 175.1 (CH_3C=N).
Elemental analysis:	Calcd. For $C_{32}H_{43}Br_3N_8Pd_2{\cdot}CH_2Cl_2$: (C) 38.81 (H) 4.44 (N) 5.49; Found: (C) 39.31 (H) 4.58 (N) 5.36.

11.1. 4 Synthesis of $[L^2Pd_2I_3]$ (2c)

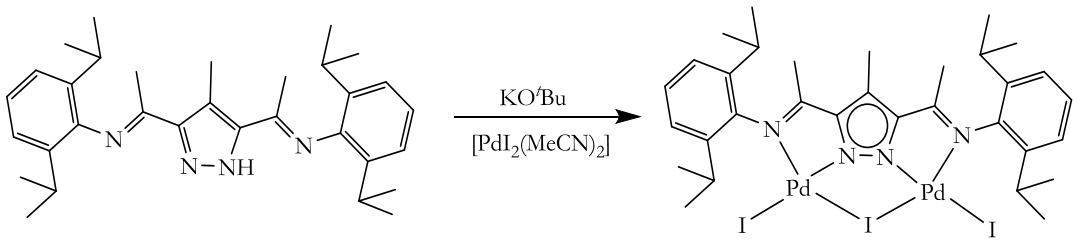

HL^2 **2c**

To a CH_2Cl_2 solution (10 mL) of **HL^2** (150 mg, 0.31 mmol) in CH_2Cl_2 (15 mL) was added 1.8 mol equivalent KO^{t}Bu (70 mg, 0.57 mmol) with stirring for 30 minutes. The CH_2Cl_2 salt solution of the ligand was then added dropwise via a syring to a CH_2Cl_2 suspension of $[PdI_2(CH_3CN)_2]$ (290 mg, 0.61 mmol) with stirring for 18 h. A dark brown suspension formed, the reaction mixture was filtered over celite to remove traces of KI to obtain a dark red solution. The dark red solution was evaporated to obtain a brown powder. The powder was reddisolved in CH_2Cl_2, and allowed to slowly evaporate at room temperature. The product was isolated as brown fluffy solid.

Yield:	110 mg, 33%
Molecular Formula:	$C_{32}H_{43}I_3N_4Pd_2$
Molecular weight:	1077.3 g/mol.
MS (ESI, CH_2Cl_2) m/z (%):	2026 (100%) $[L_2Pd_4I_5]^+$; 950 (20%) $[M\text{-}I]^+$.
IR (ATR, cm^{-1}):	3005 (m); 2961 (s); 2924 (m); 2855 (m); 1546 (vs); 1462 (s); 1441 (m); 1424 (s); 1367 (s); 1385 (s); 1341 (m); 12579 (m); 1059 (s); 1026 (m); 776 (s).
^{1}H-NMR ($CDCl_3$) δ:	1.15 (d, $^3J_{HH}$ = 6.9 Hz, 12H, CH_3^{iPr}); 1.45 (d, $^3J_{HH}$ = 6.9 Hz, 12H, CH_3^{iPr}); 2.17 (s, 6H, CH_3C=N); 2.52 (s, 3H, CH_3^{Pz4}); 3.15 (m, 4H, CH^{iPr}); 6.91-7.24 (m, 6H, CH^{Ar}).
$^{13}C\{^1H\}$ (CD_2Cl_3) δ:	11.2 (CH_3^{Pz4}); 19.4 (CH_3C=N) 23.1 (CH_3^{iPr}); 23.3 (CH_3^{iPr}); 23.8 (CH_3^{iPr}); 23.6 (CH_3^{iPr}); 23.8 (CH_3^{iPr}); 28.4 (CH^{iPr}); 28.9 (CH^{iPr}); 123.0 (CH^{Ar}); 124.0 (CH^{Ar}); 128.1 (CH^{Ar}); 128.5 (CH^{Ar}); 136.5; 140.6 (C^{Ar}); 142.5 (C^{Ar}); 164.9 (CH_3C=N); 175.1 (CH_3C=N)
CHN Analysis:	Calcd. For $C_{32}H_{43}I_3N_4Pd_2$: (C) 35.68 (H) 4.02 (N) 5.20; Found: (C) 39.39 (H) 4.58 (N) 5.36.

11.1. 5 Synthesis of $[L^2Pd_2(\mu\text{-}Cl)(CH_3)_2]$ (2f)

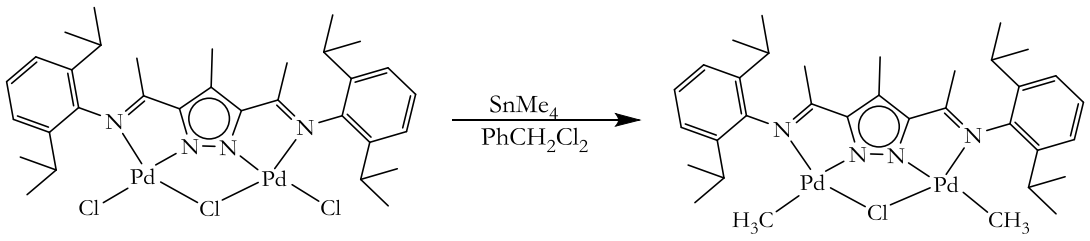

2f

To a benzylchloride solution (10 mL) of $[L^2Pd_2Cl_3]$ (200 mg, 0.25 mmol) was added 4.0 mol equivalent of $SnMe_4$ (0.1 mL, 1.0 mmol) with stirring at room temperature. After 8 h, a dark red solution was formed with traces of Pd(0). The mixture was filtered over celite to obtain an orange solution. The solution was evaporated to obtain a bright orange powder. The powder was re-dissolved in CH_2Cl_2 (5 mL) and slowly layered with Et_2O (15 ml), which results in the precipitation of an orange solid. The suspension was filtered and the solid washed with Et_2O (3x3 mL) and the product dried in air. Slow evaporation of a CH_2Cl_2 solution of the complex gives the complex as a yellow crystalline solid. This solid was contaminated with traces of L_2Pd side product (15%).

Yield:	120 mg, 63%
Molecular formula:	$C_{34}H_{49}ClN_4Pd_2$
Molecular weight:	762.1 g/mol.
MS (ESI, CH_2Cl_2) m/z (%):	1073 (30%) $[L_2Pd]^+$; 801 (50%) $[M+K]^+$; 762 (10%) $[M]^+$; 725 (40%) $[M\text{-}Cl]^+$.
IR (ATR, cm^{-1}):	2963 (m); 2870 (m); 1465 (s); 1439 (s); 1385 (vs); 1367 (vs); 1255 (m); 1147 (vs). 1059 (m); 979 (m); 936 (m); 778 (vs).
^{1}H-NMR ($CDCl_3$) δ:	-0.03 (s, 6H, CH_3^{Pd}); 1.15 (d, $^3J_{HH}$ = 6.7 Hz, 12H, CH_3^{iPr}); 1.30 (d, $^3J_{HH}$ = 6.9 Hz, 12H, CH_3^{iPr}); 2.13 (s, 6H, CH_3C=N); 2.47 (s, 3H, CH_3^{Pz4}); 3.23 (m, 4H, CH^{iPr}); 6.78-7.90 (m, 6H, CH^{Ar}).
^{13}C{^{1}H} ($CDCl_3$) δ:	-1.99 (CH_3^{Pd}); 18.1 (CH_3C=N); 23.4 (CH_3^{iPr}); 23.4 (CH_3^{iPr}); 28.1 (CH^{iPr}); 28.2 (CH^{iPr}); 123.5 (CH^{Ar}); 126.7 (CH^{Ar}); 140.8 (C^{Ar}); 141.0 (C^{Ar}); 145.5 (C^{Ar}); 171.3 (CH_3C=N).

11.1. 6 Synthesis of $[L^2Pd_2(\mu\text{-}Br)(CH_3)_2]$ (2g)

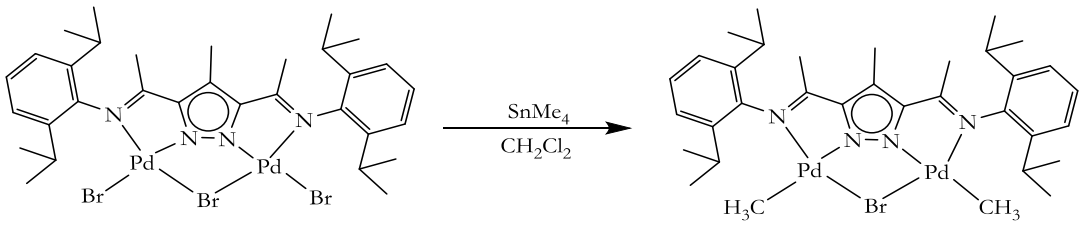

2b **2g**

To a CH_2Cl_2 solution (10 mL) of **2b** (100 mg, 0.11 mmol) was added 90 equivalents of $SnMe_4$ (1 mL, 9.70 mmol) with stirring at room temperature. After 24 h no visible colour change in the bright red solution was observed. Compared to the chloro analogue of the complex where the formation of Pd(0) species can be observed after 18 h. The reaction was stirred for 3 weeks and constantly monitored by ^{1}H NMR spectroscopy. After 3 weeks, the bright red colour was dischared with the formation of a bright yellow solution with trace amounts of Pd(0) species formed. The reaction was filtered over celite to obtain a bright yellow solution. The solution was concentrated to about 5 mL and layered with ether, which results in the precipitation of a bright yellow powder. The solid was filtered and washed with Et_2O (3x3 mL) and the product dried in air.

Yield:	70 mg, 81%
Molecular formula:	$C_{34}H_{49}BrN_4Pd_2$
Molecular weight:	806.5 g/mol.
MS (ESI, CH_2Cl_2) m/z (%):	807 (2%) $[M+H]^+$; 725 (22%) $[M\text{-}Br\text{-}H]^+$.
IR (ATR, cm^{-1}):	2961 (m); 2926 (s); 1532 (vs); 1485 (s); 1439 (vs); 1255 (vs); 1147 (s); 1059 (m); 979 (m); 806 (s); 778 (vs); 594 (m); 547 (m).
^{1}H-NMR ($CDCl_3$) δ:	-0.03 (s, 6H, CH_3^{Pd}); 1.14 (d, 12H, $^3J_{HH}$ = 6.8 Hz, 12H, CH_3^{iPr}); 1.30 (d, $^3J_{HH}$ = 6.8 Hz, 12H, CH_3^{iPr}); 2.13 (s, 6H, CH_3C=N); 2.47 (s, 3H, CH_3^{Pz4}); 3.22 (sept, 4H, $^3J_{HH}$ = 6.8 Hz, CH^{iPr}); 7.21-7.26 (m, 6H, CH^{Ar}).
$^{13}C\{^1H\}$ ($CDCl_3$) δ:	1.96 (CH_3^{Pd}); 10.4 (CH_3^{Pz4}); 19.4 (CH_3C=N); 23.5 (CH_3^{iPr}); 24.0 (CH_3^{iPr}); 28.2 (CH^{iPr}); 119.6 (C^{Pz3}); 123.7 (CH^{Ar}); 123.9 (CH^{Ar}); 127.0 (CH^{Ar}); 140.2 (C^{Ar}); 141.3 (C^{Ar}); 146.5 (C^{Ar}); 172.2 (CH_3C=N).
Elemental analysis:	Calcd. For $C_{34}H_{49}Cl_4N_4Pd_2 \cdot 1.5CH_2Cl_2$: (C) 45.65 (H) 5.61 (N) 6.00; Found: (C) 45.56 (H) 5.88 (N) 6.05.

11.1. 7 Synthesis of $[L^2_2\{CH_3Pd\}_2\{CH_3PdCl\}(Sn(CH_3)_3Cl)]$ (2h)

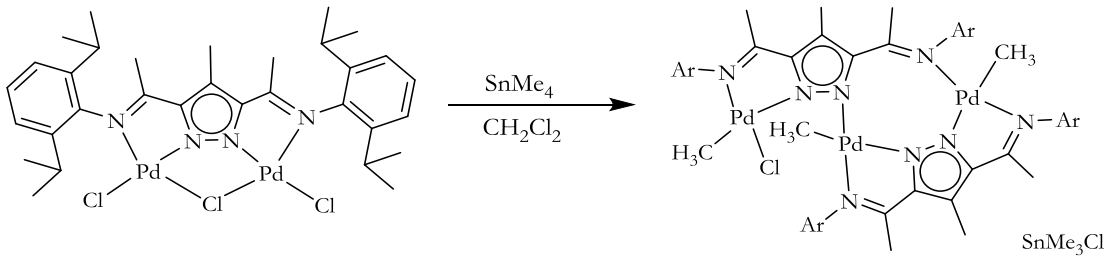

2h

To a CH_2Cl_2 solution (15 mL) of $[L^2Pd_2Cl_3]$ (100 mg, 0.13 mmol) was added 40 equivalents of $SnMe_4$ (0.52 mL, 1.72 mmol) with stirring for 48 h. The reaction mixture was filtered over celite to remove Pd(0). The bright yellow solution obtained was concentrated on a rotary evaporator to about 5 mL and 15 mL of hexane added. Bright yellow crystalline blocks were harvested from the bottom of the beaker after slow evaporation of the CH_2Cl_2/hexane solution of the complex. The NMR of the yellow crystals was different from the rest of the yellow powdery material, which was left at the bottom of the beaker. In a separate but repeated experiment, the same product was obtained by recrystallization of the crude reaction mixture from toluene at a temperature of -30°C.

Yield:	68 mg, 38%
Molecular formula:	$C_{70}H_{104}Cl_2N_8Pd_3Sn$
Molecular weight:	1566.5 g/mol.
MS (ESI, CH_2Cl_2) m/z (%):	1329 (55%) $[L_2Pd_3(Me)_3]^+$; 1314 (20%) $[L_2Pd_3(Me)_2]^+$; 1299 (100%) $[L_2Pd_3(Me)]^+$; 589 (100%)$[LPd]^+$.
IR (ATR, cm^{-1}):	2959 (m); 2926 (m); 2868 (m); 1601 (vs); 1586 (vs); 1462 (s); 1444 (m); 1366 (m); 1346 (m); 1320 (m); 1059 (m); 1044 (m); 1100 (w); 908 (s); 802 (m); 780 (m); 746 (vs).
^{1}H-NMR ($CDCl_3$) δ:	(mixture of isomers); -0.12 (s, 3H, CH_3^{Pd}); -0.08 (s, 3H, CH_3^{Pd}); 0.31 (s, 3H, CH_3^{Pd}); 0.45 (s, 3H, CH_3^{Pd}); 0.79 (s, 9H, CH_3^{SnMe3}); 1.02-1.54 (m, 24H, CH_3^{iPr}); 2.01 (s, 3H, CH_3C=N); 2.12 (s, 3H, CH_3C=N); 2.16 (s, 3H, CH_3C=N); 2.17 (s, 3H, CH_3C=N); 2.19 (s, 3H, CH_3C=N); 2.20 (s, 3H, CH_3C=N); 2.36 (s, 3H, CH_3C=N); 2.51 (s, 3H, CH_3C=N); 2.56 (s, 3H, CH_3C=N); 2.57 (s, 3H, CH_3C=N); 2.58 (s, 3H, CH_3C=N); 2.88 (s, 3H, CH_3^{Pz4}); 2.91 (s,

3H, CH_3^{Pz4}); 3.07 (sept, $^3J_{HH}$ = 6.8 Hz, 2H, CH^{iPr}); 3.22 (sept, $^3J_{HH}$ = 6.8 Hz, 2H, CH^{iPr}); 3.38 (sept, $^3J_{HH}$ = 6.8 Hz, 2H, CH^{iPr}); 3.77 (sept, $^3J_{HH}$ = 6.8 Hz, 2H, CH^{iPr}) 7.01-7.28 (m, 12H, CH^{Ar}).

$^{13}C\{^1H\}$ ($CDCl_3$) δ: -0.25 (CH_3^{SnMe3}); 0.61, 1.85; (CH_3^{Pd}); 1.25; 2.52 (CH_3); 2.52 (CH_3^{Pd}); 4.01 (CH_3^{Pd}); 4.43 (CH_3^{Pd}); 5.0 (CH_3^{Pd}); 11.1 (CH_3^{Pz4}); 12.3 (CH_3^{Pz4}); 12.5 (CH_3^{Pd}); 20.0 (CH_3C=N); 21.0 CH_3C=N); 21.1 (CH_3C=N); 21.2 (CH_3C=N); 22.6; 22.7; 23.3; 23.4; 23.5; 23.7; 23.8; 23.9; 24.1; 24.2; 24.3; 24.4; 24.5; 24.7; 24.8; 25.0; 25.6 (CH_3^{iPr}); 26.3; 26.8; 27.2; 27.4; 27.7; 27.8; 28.0; 28.1; 28.3; 28.4 (CH^{iPr}); 31.7; 116.8 (C^{Pz}); 117.2 (C^{Pz}); 123.9; 123.0; 123.6; 123.8; 123.9; 124.4; 124.5; 124.6; 125.7; 126.4; 126.7; 127.1; 127.2; 127.4 (CH^{Ar}); 139.1; 139.2; 139.7; 139.9; 140.1;140.3; 140.4; 140.5; 140.8; 140.9; 141.0; 141.3; 141.6; 141.7; 141.9; 142.1; 142.6; 144.3; 144.5; 149.5(C^{Ar}); 151.2 (C^{Pz}); 151.5 (C^{Pz}); 152.7 (C^{Pz}); 153.0 (C^{Pz}); 164.3; 168.3; 171.0 (CH_3C=N); 171.3 (CH_3C=N); 172.1 (CH_3C=N); 172.3 (CH_3C=N); 180.5 (CH_3C=N); 181.0 (CH_3C=N).

Elemental analysis: Calcd. For $C_{70}H_{104}Cl_2N_8Pd_{43}Sn$: (C) 53.67 (H) 6.69 (N) 7.15; Found: (C) 53.94 (H) 6.64 (N) 7.38.

11.1. 8 Synthesis of $[L^1{}_2Pd_4(\mu\text{-}CH_2)(\mu\text{-}Cl)_2(CH_3)_2]$ (2k)

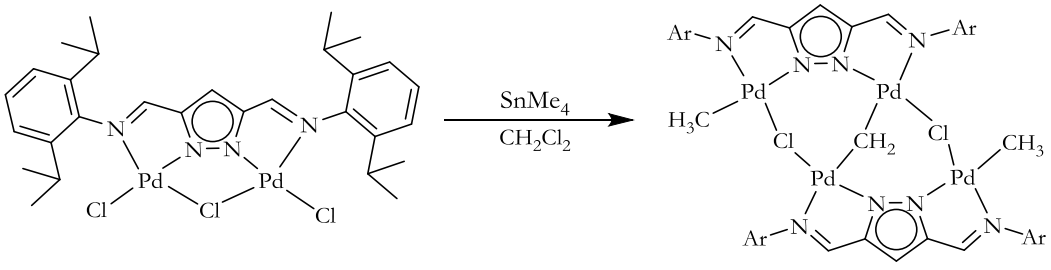

2k

To a CH_2Cl_2 solution (10 mL) of $[L^1Pd_2Cl_3]$ (260 mg, 0.34 mmol) was added 8 mol equivalent $SnMe_4$ (0.27 mL, 2.72 mmol) with stirring under room temperature for 48 h. After this period, a dark green suspension was formed. The reaction was filtered over celite to remove Pd(0), and a CH_2Cl_2 solution of the complex was concentrated and layered with hexane, which results in the precipitation of $SnMe_3Cl$. The yellow filterate was evaporated on a vacuum pump to obtain the

crude product as a yellow solid. The product was redissolved in CH_2Cl_2 and layered with hexane. The required product was isolated as a bright yellow crystalline solids after several days from a CH_2Cl_2 solution at -10°C to give a combined yield of 0.19 g. However, a second crop of yet to be identified side product which is devoid of the μ-CH_2 bridge was quantitatively present in solution (38%).

Yield:	190 mg, 39%
Molecular formula:	$C_{61}H_{82}Cl_2N_8Pd_4$
Molecular weight:	1423.9 g/mol.
MS (ESI, CH_2Cl_2) *m/z* (%):	1463 (100%) $[M+K]^+$.
IR (ATR, cm^{-1}):	2959 (vs); 2868 (s); 1687 (m); 1603 (vs); 1586 (vs); 1441 (s); 1365 (m); 1344 (m); 1275 (m); 1132 (s); 1110 (m); 1024 (S); 907 (s); 800 (vs); 745 (vs).
^{1}H-NMR ($CDCl_3$) δ:	-0.03 (s, 6H, CH_3^{Pd}); 1.05-1.28 (m, 48H, CH_3^{iPr}); 3.01 (sept, $^3J_{HH}$ = 6.8 Hz, 4H, CH^{iPr}); 3.34 (sept, $^3J_{HH}$ = 6.8 Hz, 2H, CH^{iPr}); 3.54 (sept, $^3J_{HH}$ = 6.8 Hz, 2H, CH^{iPr}); 4.23 (s, 2H, μ-CH_2); 6.98 (s, 2H, CH^{Pz4}); 7.13-7.26 (m, 12H, CH^{Ar}); 7.91 (s, 2H, CH=N); 8.04 (s, 2H, CH=N).
^{13}C{^{1}H} ($CDCl_3$) δ:	1.45 (CH_3^{Pd}); 21.6 (CH_3^{iPr}); 22.7 (CH^{iPr}); 22.8 (CH_3^{iPr}); 24.4 (CH_3^{iPr}); 24.6 (CH_3^{iPr}); 25.0 (CH_3^{iPr}); 25.4 (CH_3^{iPr}); 27.9 (CH^{iPr}); 28.0 (CH^{iPr}); 28.2 (CH^{iPr}); 28.7 (CH^{iPr}); 50.2 (CH_2); 111.3 (CH^{Pz}); 122.3 (CH^{Ar}); 123.1 (CH^{Ar}); 123.2 (CH^{Ar}); 123.5 (CH^{Ar}); 125.4 (CH^{Ar}); 125.9 (CH^{Ar}); 127.3 (CH^{Ar});128.3 (CH^{Ar}); 129.1 (CH^{Ar}); 139.7 (C^{Ar}); 140.3 (C^{Ar}); 140.5 (C^{Ar}); 143.9 (C^{Ar}); 145.0 (C^{Ar}); 148.5 (C^{Pz}); 152.4 (C^{Pz}); 156.0 (CH=N); 160.4 (CH=N).
Elemental analysis:	Calcd. For $C_{62}H_{84}Cl_4N_8Pd_4$: (C) 49.35 (H) 5.65 (N) 7.43; Found: (C) 49.97 (H) 5.67 (N) 7.53.

11.1. 9 Synthesis of $[L^2{}_2Pd_4(\mu\text{-}Cl)_3(CH_3)_2]Cl$ ($2d_2$)

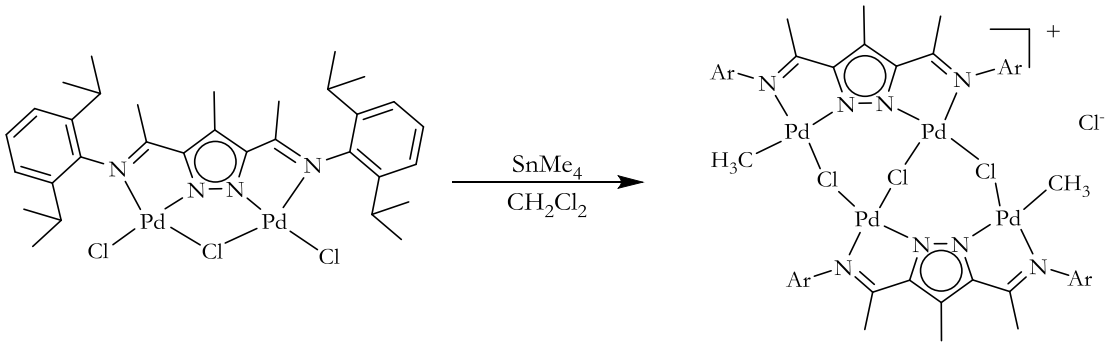

$2d_2$

To a CH_2Cl_2 solution (10 mL) of $[L^2Pd_2Cl_3]$ (100 mg, 0.12 mmol) was added $SnMe_4$ (0.01 mL, 0.09 mmol, 0.75 mol Eq.) with stirring at room temperature conditions. After stirring for 18 h, a dark red solution was obtained. Evaporation of the solution leads to the isolation of an orange solid. The solid was dissolved in 3 mL CH_2Cl_2 and slowly layered with hexane to precipitate an orange powder. The powder is partially soluble in $CHCl_3$, soluble in CH_2Cl_2 and sparingly soluble in methanol, acetonitrile, ether and hexane. This solid was washed several times with Et_2O to obtain the product as an orange powder.

Yield:	74 mg, 39%
Molecular formula:	$C_{66}H_{92}Cl_4N_8Pd_4$
Molecular weight:	1564.9 g/mol.
MS (ESI, CH_2Cl_2) *m/z* (%):	1529 (50%) $[M\text{-}Cl]^+$; 1410 (25%) $[L_2Pd_4(CH_3)]^+$; 1373 (20%) $[M\text{-}Pd(CH_3)Cl]^+$; 589 (20%) $[LPd]^+$.
IR (ATR, cm^{-1}):	2963 (s); 2962 (m); 2866 (m); 1542 (vs); 1524 (s); 1490 (s); 1477 (s); 1184 (m); 1102 (m); 1059 (s); 1035 (m); 998 (s); 806 (vs); 782 (vs); 711 (m).
^{1}H-NMR ($CDCl_3$) δ:	0.10 (br s, 6H, $CH_3{}^{Pd}$); 1.12-1.21 (m, 24H, $CH_3{}^{iPr}$); 1.31 (d, $^3J_{HH}$ = 6.8 Hz, 12H, $CH_3{}^{iPr}$); 1.46 (d, $^3J_{HH}$ = 6.8 Hz, 12H, $CH_3{}^{iPr}$); 2.14 (s, 6H, CH_3C=N); 2.17 (s, 6H, CH_3C=N); 2.52 (s, 6H, $CH_3{}^{Pz}$); 3.20 (m, 8H, CH^{iPr}); 7.18-7.35 (m, 12H, CH^{Ar}).
$^{13}C\{^1H\}$ ($CDCl_3$) δ:	-1.31 ($CH_3{}^{Pd}$); 14.2 ($CH_3{}^{Pz4}$); 23.4 (CH_3C=N); 23.7 (CH_3C=N); 24.0 ($CH_3{}^{iPr}$); 24.1 ($CH_3{}^{iPr}$); 28.3 (CH^{iPr}); 29.0 (CH^{iPr}); 123.8 (CH^{Ar}); 123.9 (CH^{Ar}); 127.5 (CH^{Ar}); 128.7 (C^{Ar}); 139.8 (CH^{Ar}); 140.1 (C^{Ar}); 140.9 (C^{Ar}); 141.1 (C^{Ar}); 174.0 (CH_3C=N).

Elemental analysis: Calcd. For $C_{66}H_{92}Cl_4N_8Pd_4 \cdot CH_2Cl_2$: (C) 48.77 (H) 5.74 (N) 6.79; Found: (C) 48.60 (H) 5.55 (N) 6.85.

11.1. 10 Synthesis of $[L^2{}_2Pd_4(\mu\text{-}CH_2)(\mu\text{-}CH_3)_2](OTf)_2$ (2l)

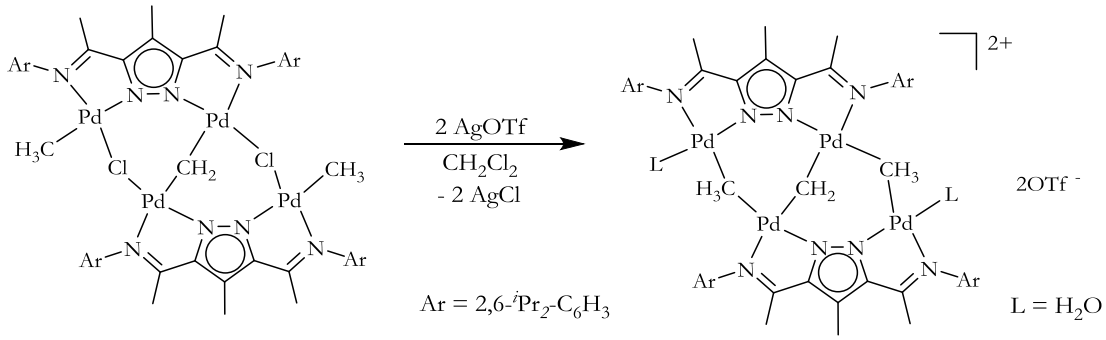

XXI^c **2l**

To a CH_2Cl_2 solution (2 mL) of **XXI^c** (14 mg, 9.3μmol) was added 2 mol equivalent of Ag(OTf) with stirring at 10 °C. After stirring at this temperature for 30 min, the formation of an off-white precipitate was observed. The mixture was filtered over celite to obtain a bright yellow solution. Evaporation of the solution gives the product as a yellow solid which was highly unstable at room temperature. With time there is a gradual darkening of the yellow solid to Pd(0).

Yield: 14.7 mg, 89 %

Molecular formula: $C_{69}H_{98}F_6N_8O_8Pd_4S_2$

Molecular weight: 1768.3 g/mol.

MS (ESI, CH_2Cl_2) m/z (%): 1474 (100%) $[M\text{-}2OTf]^+$.

^{1}H-NMR ($CDCl_3$) δ: 0.03 (s, 6H, μ-CH_3^{Pd}); 1.02-1.54 (m, 48H, CH_3^{iPr}); 2.18 (s, 12H, CH_3C=N); 2.53 (s, 6H, CH_3^{Pz}); 3.19 (m, 8H, CH^{iPr}); 4.15 (s, 2H, μ-CH_2); 7.01-7.32 (m, 12H, CH^{Ar}).

^{13}C{^{1}H} ($CDCl_3$) δ: 7.37 (CH_3^{Pd}); 11.4 (CH_3^{Pz4}); 20.0 (CH_3^{iPr}); 20.4 (CH_3^{iPr}); 23.2 (CH_3^{iPr}); 23.6 (CH_3^{iPr}); 23.7 (CH_3^{iPr}); 24.0 (CH_3C=N); 24.2 (CH_3C=N); 27.9 (CH^{iPr}); 28.5 (CH^{iPr}) 45.4 (μ-CH_2); 120.7 (C^{Pz4}); 123.6 (CH^{Ar}); 123.7 (CH^{Ar}); 123.9 (CH^{Ar}); 125.0; 127.3 (CH^{Ar}); 129.6 (CH^{Ar}); 139.9 (C^{Ar}); 140.3(C^{Ar}); 147.7; (C^{Pz}); 171.4 (CH_3C=N).

11.1. 11 Synthesis of $[L^2{}_2Pd_4(\mu\text{-}Cl)_2(\mu\text{-}O)(\mu\text{-}OH)]BAr^F{}_4$ (2p)

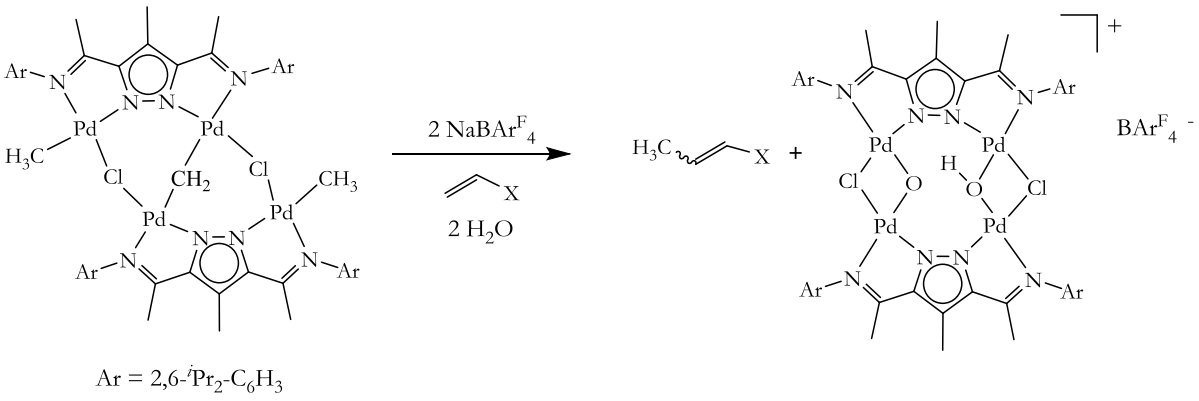

XXI^c **2p**

To a CH_2Cl_2 solution (1 mL) of **XXI^c** (14 mg, 9.3 mmol) cooled to 0°C was added excess styrene (0.05 mL) and 2 mol equivalent of $NaBAr^F{}_4$ (17 mg, 19 mmol), the mixture was stirred over ice for 15 min. The reaction mixture was filtered over celite, after which the gradual formation of Pd(0) was observed when gradually warmed up to room temperature. The bright yellow solution obtained after filteration was dried under vacuum for several hours to obtain a yellow powder. A micro-column of the yellow powder, first with ether, followed by methanol. Analysis of the ether fraction showed the formation of $L^2{}_2Pd$ The methanol fraction was evaporated in vacuo. The yellow powder obtained was again dissolved in CH_2Cl_2. Crystals were grown by slow evaporation of a CH_2Cl_2 of the complex at -30°C for several weeks.

Yield:	7 mg, 50%
Molecular formula:	$C_{96}H_{99}BCl_2F_{24}N_8O_2Pd_4$
Molecular weight:	2356.4 g/mol.
HRMS (TOF-ESI):	Calcd. For : $C_{64}H_{87}Cl_2N_8O_2Pd_4$ (1497.2500); Found: (1497.2490).
MS (ESI, CH_2Cl_2) *m/z* (%):	1497 (100%) $[M+H\text{-}BAr^F{}_4]^+$; 749 (70%) $[M+2H\text{-}BAr^F{}_4]^{2+}$.
IR (ATR, cm^{-1}):	2967 (m); 2931 (m); 2874 (m); 1575 (s); 1467 (s); 1432 (s); 1354 (s); 1275 (vs); 1166 (s); 1121 (vs); 1099 (s); 888 (s); 842 (vs); 735 (s); 715 (s); 684 (m); 674 (m).
^{1}H-NMR ($CDCl_3$) δ:	1.08 (d, $^3J_{HH}$ = 6.8 Hz, 24H, $CH_3{}^{iPr}$); 1.32 (d, $^3J_{HH}$ = 6.8 Hz, 24H, $CH_3{}^{iPr}$); 2.00 (s, 12H, $CH_3C{=}N$); 2.45 (s, 6H, $CH_3{}^{Pz4}$); 3.04 (m, 4H, CH^{iPr}); 7.12 (d, $^3J_{HH}$ = 7.7 Hz, 8H, CH^{Ar}); 7.27 (dd, $^3J_{HH}$ = 8.4, 7.1

Hz, 4H, CH^{Ar}); 7.55 (s, 4H, CH^{BArF4}); 7.71 (dt, J = 5.0 Hz, 2.3 Hz, 8H, CH^{BArF4}). 14.4 (s, 1H, OH)

$^{13}C\{^{1}H\}$ (CD_2Cl_2) δ: 10.6 (CH_3^{Pz4}); 19.7 (CH_3C=N); 23.6 (CH_3^{iPr}); 23.7 (CH_3^{iPr}); 23.9 (CH_3^{iPr}); 29.1 (CH^{iPr}); 117.8 (C^{Pz4}); 123.2 (CH^{Ar}); 124.4 (CH^{Ar}); 126.8 (CH^{Ar}); 128.9 (C^{Ar}); 129.0 (C^{Ar}); 129.4 (C^{Ar}); 135.2 (C^{Ar}); 138.4 (C^{Ar}); 140.9 (C^{Ar}); 150.2 (C^{Pz}); 161.4 (d, $J_{B\text{-}C}$ = 50.4) 171.2 (CH_3C=N).

Elemental analysis: Calcd. For $C_{96}H_{99}BCl_2F_{24}N_8O_2Pd_4$: (C) 48.85 (H) 4.23 (N) 4.75; Found: (C) 48.70 (H) 4.44 (N) 4.52.

11.1. 12 Synthesis of $[L^2{}_2Pd_2(CH_3)_2]$ (3a)

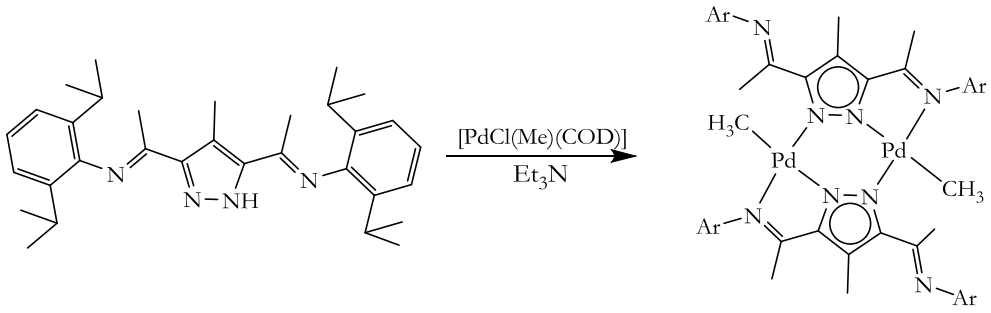

HL^2 **3a**

To a toluene solution (15 mL) of **HL^2** (990 mg, 2.1 mmol) was added an equivalent of [PdCl(Me)(COD)] (450 mg, 2.1 mmol) and an equivalent of Et_3N as base. A pale yellow solution was formed which was stirred for 18 h. The product was filtered over celite to remove traces of Pd(0). The solution was worked up by concentrating the solution to 3 mL and adding hexane dropwise. The product was precipitated as a yellow powder, was filtered and washed with hexane (1x3 mL) and dried in air. Crystals of the complex were grown by the slow evaporation of a CH_2Cl_2 solution of the complex at room temperature.

Yield:	730 mg, 29%
Molecular formula:	$C_{66}H_{92}N_8Pd_2$
Molecular weight:	1210.5 g/mol.
MS (ESI, CH_2Cl_2) m/z (%):	1195 (50%) $[M\text{-}CH_3]^+$
IR (ATR, cm^{-1}):	2959 (m); 1627 (m); 1562 (m); 1436 (s); 1385 (s); 1227 (vs); 780 (vs); 730 (vs); 581 (m).
^{1}H-NMR ($CDCl_3$) δ:	0.15 (s, 6H, CH_3^{Pd}); 1.06 (d, $^3J_{HH}$ = 6.7 Hz, 12H, CH_3^{iPr}); 1.12 (d, $^3J_{HH}$ = 6.7 Hz, 12H, CH_3^{iPr}); 1.17 (d, $^3J_{HH}$ = 6.8 Hz, 12H, CH_3^{iPr}); 1.26 (d, $^3J_{HH}$ = 6 Hz, 12H, CH_3^{iPr}); 2.18 (s, 6H, CH_3C=N); 2.34 (s, 6H, CH_3C=N); 2.57 (s, 6H, CH_3^{Pz4}); 2.56-3.20 (m, 8H, CH^{iPr});7.09-7.26 (m, 12H, CH^{Ar}).
$^{13}C\{^1H\}$ ($CDCl_3$) δ:	1.68 (CH_3^{Pd}); 11.0 (CH_3^{Pz4}); 20.9 (CH_3C=N); 22.3 (CH_3C=N); 23.4 (CH_3^{iPr}); 23.6 (CH_3^{iPr}); 24.5 (CH_3^{iPr}); 27.7 (CH^{iPr}); 28.0 (CH^{iPr}); 119.8; 120.8 (CH^{Ar}); 123.2 (CH^{Ar}); 123.6 (CH^{Ar}); 126.9 (CH^{Ar}); 140.6 (C^{Ar}); 141.2 (C^{Ar}); 146.0 (C^{Ar}); 149.3 (C^{Pz}); 153.5 (C^{Pz}); 162.3 (CH_3C=N); 172.0 (CH_3C=N).
Elemental analysis:	Calcd. For $C_{66}H_{92}N_8Pd_2$: (C) 65.50 (H) 7.66 (N) 9.26; Found: (C) 65.53 (H) 7.65 (N) 9.12.

11.1. 13 Synthesis of $[L^1_2Pd_2(CH_3)Cl]$ (3b)

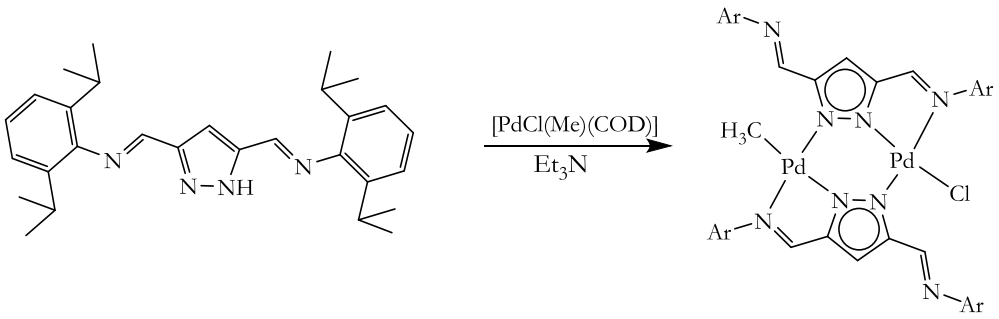

HL[1] **3b**

To a toluene solution (10 mL) of **HL[1]** (150 mg, 0.34 mmol) was added 2 mol equivalent [PdCl(Me)(COD) (180 mg, 0.68 mmol) with stirring at room temperature. This was followed with the addition of a mol equivalent of Et_3N. A bright yellow solution was formed which was allowed to stir for 18 h. A white crystalline salt of $Et_3N{\cdot}HCl$ was filtered and the yellow solution evaporated. Attempts at recrystallization, by the slow evaporation of CH_2Cl_2 solution in a test tube yield the product as a yellow crystal on the walls of the tube, which was not the bulk of the reaction product.

Yield:	27 mg, 7%
Molecular formula:	$C_{59}H_{77}ClN_8Pd_2$
Molecular weight:	1146.6 g/mol.
MS (ESI, CH_2Cl_2) m/z (%):	1145 (30%) $[M\text{-}2H]^+$; 1111 (100%) $[M\text{-}Cl]^+$.
IR (ATR, cm^{-1}):	2959 (m); 2926 (m); 1575 (m); 1430 (m); 1367 (m); 938 (m); 808 (vs); 778 (vs); 753 (m).
^{1}H-NMR ($CDCl_3$) δ:	0.54 (d, J = Hz, 3H, CH_3^{Pd}); 1.28-1.44 (m, 48H, CH_3^{iPr}); 3.10 (sept, $^3J_{HH}$ = 6.8 Hz, 4H, CH^{iPr}); 3.56 (sept, $^3J_{HH}$ = 6.8 Hz, 4H, CH^{iPr}); 7.24-7.36 (m, 12H, CH^{Ar}); 7.58 (s, 2H, CH^{Pz}); 8.15 (s, 2H, CH=N); 8.27 (s, 2H, CH=N).
$^{13}C\{^1H\}$ ($CDCl_3$) δ:	1.61 (CH_3^{Pd}); 22.6 (CH_3^{iPr}); 23.7 (CH_3^{iPr}); 25.1 (CH_3^{iPr}); 25.2 (CH_3^{iPr}); 27.8 (CH^{iPr}); 28.0 (CH^{iPr}); 109.8 (CH^{Pz}); 123.0 (CH^{Ar}); 123.5 (CH^{Ar}); 127.8 (CH^{Ar}); 137.7 (C^{Ar}); 141.4 (C^{Ar}); 143.4 (C^{Ar}); 148.4 (C^{Ar}); 154.4 (C^{pz}); 155.2 (C^{Pz}); 162.8 (CH=N).

11. 2 Mononuclear palladium(II) complexes

11.2. 1 Synthesis of $[L^2Pd(CH_3)(PMe_3)]$ (3c)

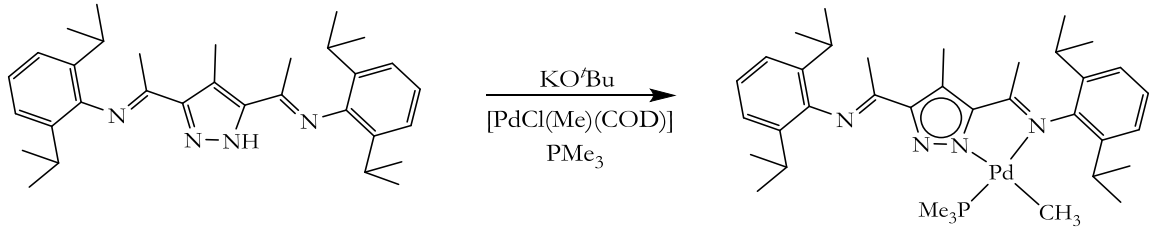

HL^2 **3c**

A THF solution (10 mL) of the deprotonated ligand **L^2** (300 mg, 0.62 mmol) was added dropwise to a mol equivalent [PdCl(Me)(COD)] (160 mg, 0.62 mmol) in the presence of PMe_3 (0.6 mL, 1 mol Eq.) with stirring. The reaction was stirred overnight at room temperature. The solvent was evaporated to obtain an off-white solid. The solid was washed with Et_2O (3x3 mL) and the product dried in vacuum to give a pure off-white solid. Colourless crystals of **3c** were obtained by the slow diffusion of Et_2O into a CH_2Cl_2 solution of the complex at room temperature.

Yield:	250 mg, 59%
Molecular formula:	$C_{36}H_{55}N_4Pd$
Molecular weight:	681.2 g/mol.
MS (ESI, CH_2Cl_2) *m/z* (%):	681 (100%) $[M]^+$.
IR (ATR, cm^{-1}):	2959 (vs); 2924 (vs); 2868 (vs); 1631 (vs); 1570 (vs); 1436 (vs); 1328 (s); 1229 (vs); 1097 (s); 1057 (s); 961 (vs); 863 (m); 810 (m); 780 (vs); 724 (m); 419 (m).
^{1}H-NMR ($CDCl_3$) δ:	-0.32 (d, J = 3.2 Hz, 3H, CH_3^{Pd}); 1.12–1.22 (m, 21H, CH_3^{iPr}); 1.62 (d, $^3J_{P\text{-}H}$ = 10.8 Hz, 9H, CH_3^{PMe3}); 1.65 (s, 3H, CH_3^{iPr}); 2.24 (s, 6H , CH_3C=N); 2.77 (s, 3H, CH_3^{Pz4}); 2.95 (sept, $^3J_{HH}$ = 6.8 Hz, 2H, CH^{iPr}); 3.09 (sept, $^3J_{HH}$ = 6.8 Hz, 2H, CH^{iPr}); 7.02–7.26 (m, 6H, CH^{Ar}).
$^{13}C\{^1H\}$ ($CDCl_3$) δ:	0.76 (d, $J_{P\text{-}C}$ = 11.5 Hz, CH_3^{Pd}); 11.8 (CH_3^{Pz4}); 15.1 (CH_3^{PMe3}); 15.9 (CH_3^{PMe3}); 19.0 (CH_3C=N); 19.6 (CH_3C=N); 22.9 (CH_3^{iPr}); 23.3 (CH_3^{iPr}); 23.5 (CH_3^{iPr}); 24.0 (CH_3^{iPr}); 28.1 (CH^{iPr}); 28.2 (CH^{iPr}); 120.3 (C^{Pz4}); 122.4 (CH^{Ar}); 122.8 (CH^{Ar}); 123.5 (CH^{Ar}); 126.3;

136.2; 140.7; 141.3 (CH^{Ar}); 147.6 (CH^{Ar}); 150.6 ($C^{Pz3/5}$); 150.8 ($C^{Pz3/5}$); 164.0 (CH_3C=N); 170.9 (CH_3C=N).

$^{31}P\{1H\}$ δ: -3.3

11.2. 2 Synthesis of [$L^2Pd(CH_3)(PPh_3)$] (3d)

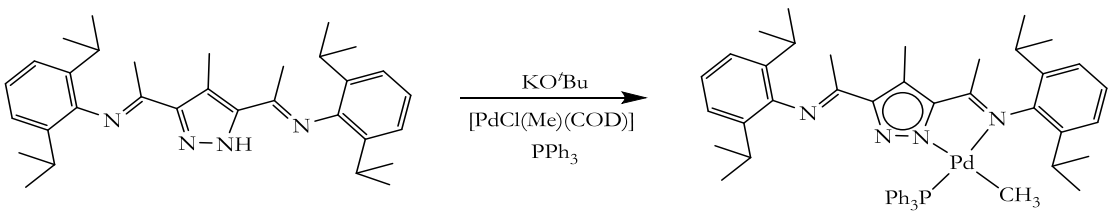

HL^2 **3d**

A CH_2Cl_2 solution (5 mL) of the deprotonated ligand **L^2** (30 mg, 0.062 mmol) was added to a mol equivalent of [PdCl(Me)(COD)] (16.4 mg, 0.62 mmol) in the presence of PPh_3 (16.0 mg, 1 mol Eq.) with stirring. The reaction was stirred overnight at room temperature. The solution was concentrated to 3 mL on a rotary evaporator and Et_2O (10 mL) added. There was the gradual precipitation of a white crystalline solid, the solid was filtered and washed with cold Et_2O (3x3 mL) and the product dried in air.

Yield: 12 mg, 23%

Molecular formula: $C_{51}H_{61}N_4PPd$

Molecular weight: 868.5 g/mol.

MS (ESI, CH_2Cl_2) *m/z* (%): 867 (100%) $[M]^+$.

IR (ATR, cm^{-1}): 2959 (s); 1564 (vs); 1437 (s); 1383 (vs); 1329 (s); 775 (vs).

^1H-NMR ($CDCl_3$) δ: -0.31 (d, $^3J_{Pd\text{-}P}$ = 3.1 Hz, 3H, CH_3^{Pd}); 1.08 (d, $^3J_{HH}$ = 4.5 Hz, 6H, CH_3^{iPr}); 1.10 (d, $^3J_{HH}$ = 4.4 Hz, 6H, CH_3^{iPr}); 1.16 (d, $^3J_{HH}$ = 6.9 Hz, 6H, CH_3^{iPr}); 1.26 (m, 6H, CH_3^{iPr}); 1.64 (s, 3H, CH_3C=N); 2.26 (s, 3H, CH_3C=N); 2.70 (s, 3H, CH_3^{Pz4}); 2.82 (sept, $^3J_{HH}$ = 6.8 Hz, 2H, CH^{iPr}); 3.28 (sept, $^3J_{HH}$ = 6.8 Hz, 2H, CH^{iPr}); 6.96-7.24 (m, 21H, CH^{Ar}).

$^{13}C\{^1H\}$ ($CDCl_3$) δ: 6.37 (CH_3^{Pd}); 11.8 (CH_3^{Pz4}); 14.2; 19.3 (CH_3C=N); 19.4 (CH_3C=N); 19.8 (CH_3C=N); 22.8 (CH_3^{iPr}); 23.0 (CH_3^{iPr}); 23.4

(CH_3^{iPr}); 23.6 (CH_3^{iPr}); 24.3 (CH_3^{iPr}); 28.0 (CH^{iPr}); 28.2 (CH^{iPr}); 28.3 (CH^{iPr}); 28.4 (CH^{iPr}); 117.6; 119.9; 122.3; 122.7; 123.0(CH^{Ar}); 123.2 (CH^{Ar}); 123.5 (CH^{Ar}); 124.2; 126.4; 127.9 (CH^{Ar}); 128.1; 130.2 (CH^{Ar}); 131.4; 132.1; 134.8 (CH^{Ar}); 135.0; 135.8; 136.3(C^{Ar}); 136.6(C^{Ar}); 140.9 (C^{Ar}); 141.2 (C^{Ar}); 147.7 (C^{Pz}); 150.6 (C^{Pz}); 150.7; 164.6 (CH_3C=N); 171.2 (CH_3C=N).

$^{31}P\{1H\}$ δ: 40.8.

11.2. 3 Synthesis of [$HL^2Pd(CH_3)Cl$] (3e)

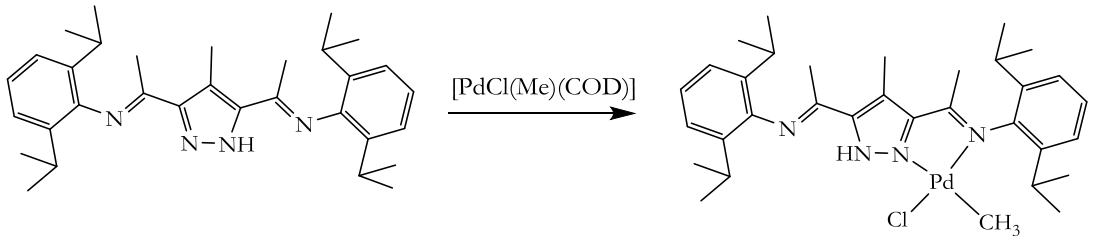

HL^2 **3e**

To a toluene solution (10 mL) of **HL^2** (220 mg, 0.45 mmol) was added a mol equivalent of [PdCl(Me)(COD)] (120 mg, 0.46 mmol) with stirring. A bright yellow solution was formed instantly. The reaction was stirred further at room temperature for 8 h. The solution was concentrated on a rotary evaporator to *ca.* 3 mL and the solution allowed to stand for some time, after which an off-white precipitate began to form. The precipitate was filtered, and the solid washed several times with cold ether (3x3 mL) and dried in air. The product was obtained as an off-white solid. Recrystallization from CH_2Cl_2 gives the product as an off-white crystalline solid.

Yield: 100 mg, 34%

Molecular formula: $C_{33}H_{47}ClN_4Pd$

Molecular weight: 641.6 g/mol.

MS (ESI, CH_2Cl_2) *m/z* (%): 646 (80%) $[M+4H]^+$; 628 (25%) $[M-Cl+Na]^+$.

IR (ATR, cm^{-1}): 2959 (m); 2926 (m); 2868 (m); 1564 (s); 1462 (s); 1437 (vs); 1229 (s); 775 (vs); 730 (s).

^{1}H-NMR ($CDCl_3$) δ:	0.46 (s, 3H, CH_3^{Pd}); 1.16 (d, $^{3}J_{HH}$ = 6.8 Hz, 12H, CH_3^{iPr}); 1.31 (d, $^{3}J_{HH}$ = 6.8 Hz, 12H, CH_3^{iPr}); 2.13 (s, 3H, CH_3C=N); 2.24 (s, 3H, CH_3C=N); 2.66 (sept, $^{3}J_{HH}$ = 6.8 Hz, 2H, CH^{iPr}); 2.70 (s, CH_3, 3H, CH_3^{Pz4}); 3.12 (sept, $^{3}J_{HH}$ = 6.8 Hz, 2H, CH^{iPr}); 7.15-7.27 (m, 6H, CH^{Ar}).
^{13}C{^{1}H} ($CDCl_3$) δ:	2.8 (CH_3^{Pd}); 11.0 (CH_3^{Pz4}); 19.3 (CH_3^{iPr}); 21.0 (CH_3^{iPr}); 22.9 (CH_3^{iPr}); 23.3 (CH_3^{iPr}); 23.4 (CH_3^{iPr}); 24.0 (CH^{iPr}); 28.1 (CH^{iPr}); 28.3 (CH^{iPr}); 123.1 (C^{Pz4}); 123.8 (CH^{Ar}); 124.4 (CH^{Ar}); 129.0 (C^{Ar}); 135.9 (C^{Ar}); 136.0 (C^{Ar}); 139.6 (C^{Ar}); 140.3 (C^{Ar}); (CH_3C=N)-not observed.
CHN Analysis:	Calcd. For $C_{33}H_{46}ClN_4Pd{\cdot}CH_2Cl_2$ (C) 56.28 (H) 6.67 (N) 7.72; Found: (C) 55.00 (H) 6.63 (N) 7.36.

11.2. 4 Synthesis of [HL^{3}Pd(CH$_3$)Cl] (3f)

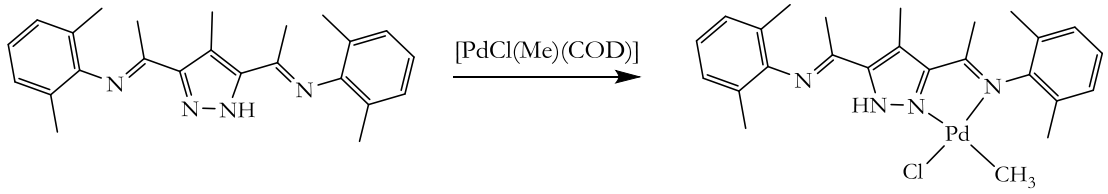

HL^3 **3f**

To a toluene solution (10 mL) of **HL^3** (300 mg, 0.8 mmol) was added a mol equivalent [PdCl(Me)(COD)] (210 mg, 0.8 mmol). The solution was stirred overnight, forming a bright yellow suspension. The suspension was filtered to obtain an offwhite powder which was washed with cold Et_2O (3x3 mL) and the product dried in air. Recrystalization from a 50:50 mixture of CH_2Cl_2 and hexane gave an offwhite powder.

Yield:	280 mg, 66%
Molecular formula:	$C_{25}H_{30}ClN_4Pd$
Molecular weight:	528.4 g/mol.
MS (ESI, CH_2Cl_2) *m/z* (%):	534 (35%) $[M^+$-Me+Na$]^+$; 477 (100%) $[LPd]^+$.
IR (ATR, cm^{-1}):	2998 (vs); 2901 (s); 1631 (vs); 1589 (m); 1549 (m); 1465 (m); 1370 (w); 1270 (s); 1233 (s); 1199 (m); 764 (s).

^{1}H-NMR ($CDCl_3$) δ:	0.27 (s, 3H, CH_3^{Pd}); 1.98 (s, 6H, CH_3^{Mes}); 2.13 (s, 6H, CH_3^{Mes}); 2.16 (s, 3H, CH_3C=N); 2.53 (s, 3H, CH_3C=N); 2.66 (s, 3H, CH_3^{Pz4}); 6.90-7.26 (m, 6H, CH^{Ar}); NH-not observed.
$^{13}C\{^{1}H\}$ ($CDCl_3$) δ:	-0.31 (CH_3^{Pd}); 10.0 (CH_3^{Pz4}); 10.2 (CH_3^{Pz4}); 17.0 (CH_3^{Mes}); 17.1 (CH_3^{Mes}); 17.3 (CH_3^{Mes}); 17.7 (CH_3^{Mes}); 17.9 (CH_3^{Mes}); 18.0 (CH_3C=N); 18.2 (CH_3C=N); 18.3 (CH_3C=N); 117.8 (C^{Pz4}); 122.5; (CH^{Ar}) 124.2 (CH^{Ar}); 124.3 (CH^{Ar}); 125.4 (CH^{Ar}); 127.0 (CH^{Ar}); 127.2 (CH^{Mes}); 128.1 (C^{Ar}); 128.2 (C^{Ar}); 128.8 (C^{Ar}); (CH_3C=N)-not observed.

11.2. 5 Synthesis of [$HL^4Pd(CH_3)Cl$] (3g)

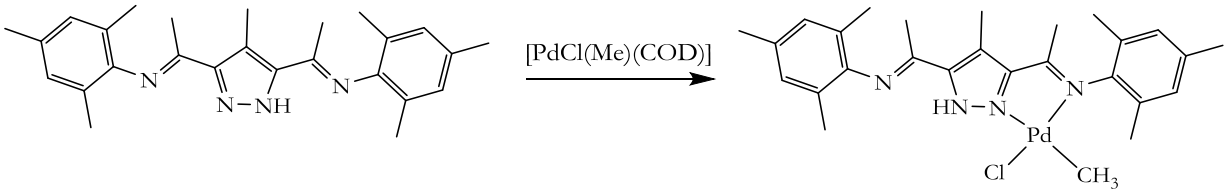

HL^4 **3g**

To a toluene solution (15 mL) of **HL^4** (300 mg, 0.57 mmol) was added a mol equivalent [PdCl(Me)(COD)] (190 mg, 0.57 mmol). The reaction was stirred for 18 h. The suspension was filtered and the product washed with Et_2O (3x3 mL) and dried in air. Product was obtained as an off-white powder.

Yield:	200 mg, 32 %
Molecular formula:	$C_{27}H_{34}ClN_4Pd$
Molecular weight:	556.5 g/mol.
MS (ESI, CH_2Cl_2) *m/z* (%):	562 (85%) $[M\text{-}Cl+K]^+$; 505 (100%) $[M\text{-}Cl(Me)]^+$.
IR (ATR, cm^{-1}):	2916 (br); 1633 (vs); 1583 (s); 1462 (w); 1373 (m); 1268 (s); 1222 (m); 1153 (s); 1002 (m); 964 (m); 852 (s); 766 (m).
^{1}H-NMR ($CDCl_3$) δ:	0.32 (s, 3H, CH_3^{Pd}); 1.96 (s, 6H, CH_3^{Mes}); 2.11 (s, 3H, CH_3^{Mes}); 2.13 (s, 6H, CH_3^{Mes}); 2.16 (s, 3H, CH_3C=N); 2.28 (s, 3H, CH_3C=N); 2.30 (s, 3H, CH_3^{Mes}); 2.66 (s, 3H, CH_3^{Pz4}) 6.98-7.22 (m, 6H, CH^{Mes}).

$^{13}C\{^{1}H\}$ ($CDCl_3$) δ:	1.1 (CH_3^{Pd}); 11.1 (CH_3^{Pz4}); 18.0 (CH_3^{Mes}) 18.1 (CH_3^{Mes}); 18.3 (CH_3^{Mes}); 18.7 (CH_3^{Mes}); 18.8 (CH_3^{Mes}); 18.9 (CH_3^{Mes}); 19.3 (CH_3^{iPr}); 20.7 (CH_3^{iPr}); 20.9 (CH_3^{iPr}); 21.2 (CH_3^{iPr}); 118.7 (C^{Pz4}); 125.2; 126.7; 129.2; 129.5; 129.7; 132.8 (C^{Ar}); 135.9 (C^{Ar}); 137.0 (C^{Ar}); 140.9 (C^{Ar}); 148.6 (C^{Ar}); 150.0 (C^{Pz}); 157.7 (C^{Pz}); 169.4 (CH_3C=N); 177.9 (CH_3C=N).

11.2. 6 Synthesis of $[L^2_2Pd]$ (3h)

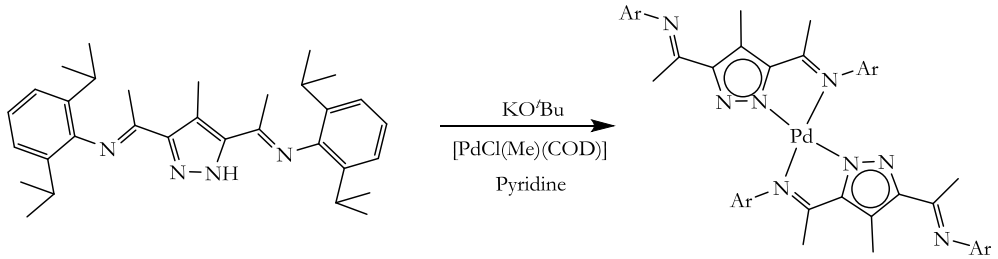

HL^2 **3h**

To a CH_2Cl_2 solution (15 mL) of **HL^2** (50 mg, 0.13 mmol) was added a mol equivalent of KO^{t}Bu (11.6 mg, 0.13 mmol). To the stirring solution were added [PdCl(Me)(COD)] (34 mg, 0.13 mmol) and an equivalent pyridine. A bright yellow solution was formed, which was allowed to stir at room temperature for 18 h. The reaction was filtered and filtrate evaporated to obtain a bright yellow solid. The solid was redissolved in CH_2Cl_2 (5 mL) and layered with hexane, which again results in the precipitation of a bright yellow solid. The solid was filtered, washed with cold Et_2O (3x3 mL) and dried in air. Yellow crystals of the complex were grown by the slow evaporation of a CH_2Cl_2 solution of the complex at room temperature.

Yield:	13 mg, 10 %
Molecular formula:	$C_{64}H_{86}N_8Pd$
Molecular weight:	1072.6 g/mol.
MS (ESI, CH_2Cl_2) m/z (%):	1073 (100%) $[M+H]^+$.
IR (ATR, cm^{-1}):	2926 (m); 2808 (m); 1631 (s); 1564 (s); 1437 (s); 1326 (m); 1227 (vs); 1097 (s); 1059 (s).

^{1}H-NMR ($CDCl_3$) δ: 1.11-1.19 (m, 48 H, CH_3^{iPr}); 1.59 (s, 6H, CH_3C=N); 2.16 (s, 6H, CH_3C=N); 2.63 (s, 6H, CH_3^{Pz4}); 2.74 (sept, $^{3}J_{HH}$ = 6.8 Hz, 4H, CH^{iPr}); 3.35 (sept, $^{3}J_{HH}$ = 6.8 Hz, 4H, CH^{iPr}); 7.00-7.26 (m, 12H, CH^{Ar}).

$^{13}C\{^{1}H\}$ ($CDCl_3$) δ: 11.2 (CH_3^{Pz4}); 18.1 (CH_3C=N); 19.5 (CH_3C=N); 22.9 (CH_3^{iPr}); 23.1 (CH_3^{iPr}); 23.4 (CH_3^{iPr}); 23.7 (CH_3^{iPr}); 28.0 (CH_3^{iPr}); 28.5; 120.4 (C^{Pz4}); 122.5 (CH^{Ar}); 122.6 (CH^{Ar}); 123.4 (CH^{Ar}); 127.6 (CH^{Ar}); 136.1(C^{Ar1}); 140.7 ($C^{Ar2/6}$); 147.3($C^{Pz3/5}$); 148.8 ($C^{Pz3/5}$); 164.3 (CH_3C=N); 172.1 (CH_3C=N).

CHN Analysis: Calcd. For $C_{64}H_{86}ClN_8Pd\cdot0.5CH_2Cl_2$: (C) 69.23, (H) 7.90, (N) 10.09; Found: (C) 70.16 (H) 7.77 (N) 10.03.

11. 3 Mononuclear nickel(II) complexes

11.3. 1 Synthesis of $[L^1Ni(C_{10}H_7)(PPh_3)]$ (3j)

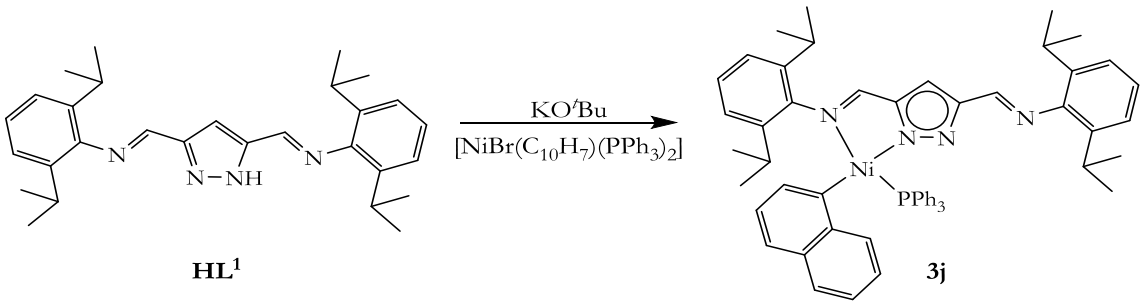

A CH_2Cl_2 solution (15 mL) of the deprotonated ligand **L^1**(150 mg, 0.34 mmol) was added dropwise to a CH_2Cl_2 solution of $[NiBr(C_{10}H_7)(PPh_3)_2]$ (270 mg, 0.34 mmol) with stirring for 18 h, forming a bright yellow solution. The bright yellow solution was filtered over celite to remove traces of KBr. Slow evaporation of the CH_2Cl_2 solution of the complex precipates the product as a bright orange powder.

Yield:	130 mg, 44%
Molecular formula:	$C_{57}H_{59}N_4NiP$
Molecular weight:	889.8 g/mol.
MS (ESI, CH_2Cl_2) *m/z* (%):	889 (100%) $[M]^+$.
IR (ATR, cm^{-1}):	3052 (m); 2959 (m); 2926 (m); 1637 (vs); 1583 (vs); 1375 (s); 1365 (s); 1436 (vs); 1383 (s); 1184 (s); 1097 (vs); 692 (vs); 510 (s); 497 (vs).
^{1}H-NMR ($CDCl_3$) δ:	0.14 (d, $^3J_{HH}$ = 6.7 Hz, 3H, CH_3^{iPr}); 0.87 (d, $^3J_{HH}$ = 6.8 Hz, 3H, CH_3^{iPr}); 1.02-1.44 (m, 15H, CH_3^{iPr}); 1.65 (d, $^3J_{HH}$ = 6.8 Hz, 3H, CH_3^{iPr}); 2.74 (m, $^3J_{HH}$ = 6.8 Hz, 1H, CH^{iPr}); 3.00 (sept, $^3J_{HH}$ = 6.8 Hz, 2H; CH^{iPr}); 4.20 (sept, $^3J_{HH}$ = 6.8 Hz, 1H; CH^{iPr}); 6.29 (t, *J* = 7.5 Hz, 1H, CH^{Ar}); 6.42-6.51 (m, 2H, CH^{Ar}); 6.68 (d, *J* = 7.0 Hz, 1H, CH^{Ar}); 6.74 (d, *J* = 8.7 Hz, 2H, CH^{Ar}) 6.87 (t, *J* = 7.7 Hz, 1H, CH^{Ar}); 7.18 (s, 1H, CH^{Pz}); 7.69 (s, 1H, CH=N); 6.98-7.55 (m, 21H, $CH^{Ar,\ PPh3}$); 7.99 (d, *J* = 5.8 Hz, 1H, CH=N); 9.19 (d, $^3J_{HH}$ = 5.9 Hz, 1H, CH^{Napth}).

$^{13}C\{^{1}H\}$ ($CDCl_3$) δ:	20.3 (CH_3^{iPr}); 22.5 (CH_3^{iPr}); 22.7 (CH_3^{iPr}); 23.4 (CH_3^{iPr}); 23.7 (CH_3^{iPr}); 23.8 (CH_3^{iPr}); 26.1 (CH_3^{iPr}); 27.8 (CH^{iPr}); 27.9 (CH^{iPr}); 28.9 (CH^{iPr}); 29.1 (CH^{iPr}); 31.0 (CH_3^{iPr}); 105.0 (CH^{Pz}); 123.0 (CH^{Ar});123.8 (CH^{Ar}); 127. 1 (CH^{Ar}); 128.4 (CH^{Ar}); 131.5 (CH^{Ar}); 131.7 (CH^{Ar}); 137. 2 (C^{Ar}); 138.7 (C^{Ar}); 141.1 (CAr); 140.8 (C^{Ar}); 150.2 (C^{Pz});154.4 (C^{Pz});158.4 (CH=N); 162.3 (CH=N).
$^{31}P\{^{1}H\}$:	30.75.

11.3. 2 Synthesis of $[L^2Ni(C_{10}H_7)(PPh_3)]$ (3k)

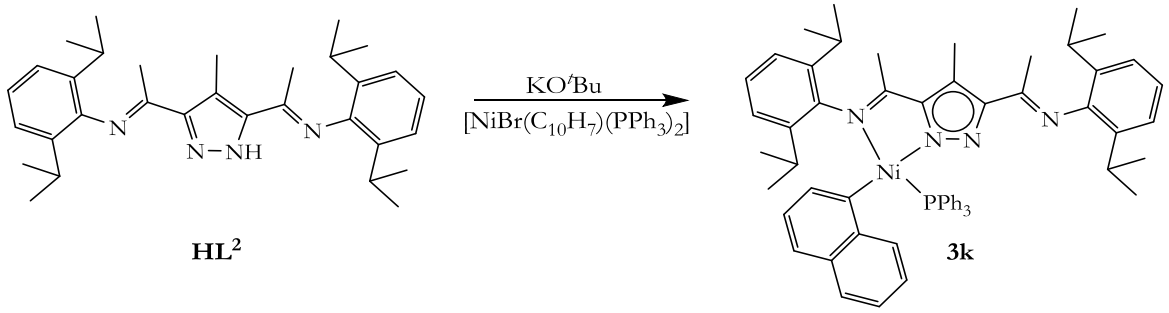

A CH_2Cl_2 solution (10 mL) of the deprotonated ligand, **L^2** (110 mg, 0.23 mmol) was added dropwise to a CH_2Cl_2 solution of $[NiBr(C_{10}H_7)(PPh_3)_2]$ (180 mg, 0.22 mmol) with stirring for 18 h, forming a yellow solution. The bright yellow solution was filtered over celite to remove traces of KBr. Slow evaporation of the CH_2Cl_2 solution of the complex precipates the product as a bright orange powder. Crystals were grown by the slow evaporation of a toluene solution of the complex at room temperature.

Yield:	97 mg, 46%
Molecular formula:	$C_{60}H_{65}N_4NiP$
Molecular weight:	931.9 g/mol.
MS (ESI, CH_2Cl_2) m/z (%):	931 (100%) $[M]^+$.
IR (ATR, cm^{-1}):	2969 (m); 2928 (m); 1620 (vs); 1578 (vs); 1385 (vs); 1311 (m); 1222 (vs); 1059 (m); 756 (vs).
^{1}H-NMR ($CDCl_3$) δ:	-0.52 (d, $^3J_{HH}$ = 6.6 Hz, 3H, CH_3^{iPr}); 0.75 (d, $^3J_{HH}$ = 6.8 Hz, 3H, CH_3^{iPr}); 1.04 (d, $^3J_{HH}$ = 6.9 Hz, 3H, CH_3^{iPr}); 1.12 (d, $^3J_{HH}$ = 6.9 Hz,

3H, CH_3^{iPr}); 1.16 (d, $^3J_{HH}$ = 4.1 Hz, 3H, CH_3^{iPr}); 1.18 (d, $^3J_{HH}$ = 4.0 Hz, 3H, CH_3^{iPr}); 1.26 (d, $^3J_{HH}$ = 6.8 Hz, 3H, CH_3^{iPr}); 1.39 (s, 3H, CCH_3=N); 1.77 (d, $^3J_{HH}$ = 6.8 Hz, 3H, CH_3^{iPr}); 2.18 (s, 3H, CCH_3=N); 2.54 (sept, $^3J_{HH}$ = 6.8 Hz, 1H, CH^{iPr}); 2.64 (s, 3H, CH_3^{Pz4}); 2.73 (sept, $^3J_{HH}$ = 6.8 Hz, 1H, CH^{iPr}); 2.86 (sept, $^3J_{HH}$ = 6.8 Hz, 1H, CH^{iPr}); 4.02 (sept, $^3J_{HH}$ = 6.8 Hz, 1H, CH^{iPr}); 6.17 (t, $^3J_{HH}$ = 7.5 Hz, 2H, CH^{Ar}); 6.35 (d, $^3J_{HH}$ = 7.0 Hz, 1H, CH^{Ar}); 6.45 (d, $^3J_{HH}$ = 7.3 Hz, 1H, CH^{Ar}); 6.72 (d, $^3J_{HH}$ = 8.0 Hz, 2H, CH^{Ar}); 6.86-7.50 (m, 21H, CH^{Ar}); 9.89 (d, $^3J_{HH}$ = 8.1 Hz, 1H, CH^{Ar}).

$^{13}C\{^1H\}$ ($CDCl_3$) δ: 11.4 (CH_3^{Pz4}); 18.7 (CH_3C=N); 20.4 (CH_3C=N); 21.1 (CH_3^{iPr}); 23.0; 23.2; 23.7; 24.5 (CH_3^{iPr}); 25.0; 28.1 (CH^{iPr}); 28.5 (CH^{iPr}); 28.6 (CH^{iPr}); 121.2 (CH^{Ar}); 123.0; 123.6; 125.8; 127.1; 127.3; 129.3; 132.0; 132.6 (CH^{Ar}); 134.2 (CH^{Ar}); 134.3; 134.8; 136.3; 140.5 (C^{Ar}); 142.0 (C^{Ar}); 164.7 (CH_3C=N); 172.0 (CH_3C=N).

$^{31}P\{1H\}$ δ: 30.3.

Elemental analysis: Calcd. For $C_{60}H_{65}N_4NiP$: (C) 77.33 (H) 7.03 N (6.01); Found: C (76.46) H (6.85) (N) (5.90).

11.3. 3 Synthesis of $[L^2Ni(C_6H_5)(PPh_3)]$ (3l)

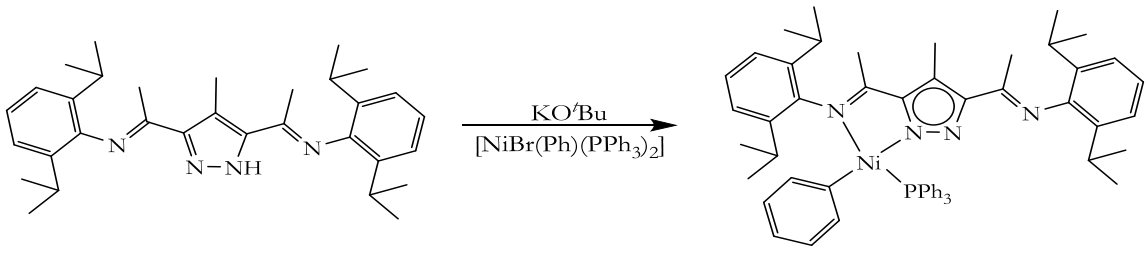

HL² **3l**

Following a similar procedure as done for **3k**, using **L²** (120 mg, 0.25 mmol) and $[NiBr(Ph)(PPh_3)_2]$ (120 mg, 0.25 mmol). The product was obtained as an orange powder. Single crystals were obtained by the slow evaporation of a CH_2Cl_2 solution of the complex at room temperature.

Yield: 98 mg, 45%

Molecular formula: $C_{56}H_{63}N_4NiP$

Molecular weight:	881.8 g/mol.
MS (ESI, CH_2Cl_2) m/z (%):	539 (100%) $[M\text{-}Ph\text{-}PPh_3]^+$.
IR (ATR, cm^{-1}):	2959 (m); 2918 (m); 1626 (vs); 1566 (vs); 1385 (vs); 1324 (m); 1229 (vs); 1059 (m); 730 (vs); 696 (vs).
^{1}H-NMR ($CDCl_3$) δ:	1.08-1.15 (m, 24H, CH_3^{iPr}); 1.49 (s, 3H, $CH_3C{=}N$); 2.20 (s, 3H, $CH_3C{=}N$); 2.53 (s, 3H, CH_3^{Pz4}); 2.78 (sept, $^3J_{HH}$ = 6.6 Hz, 2H, CH^{iPr}); 3.33 (sept, $^3J_{HH}$ = 6.6 Hz, 2H, CH^{iPr}); 4.01 (sept, $^3J_{HH}$ = 6.6 Hz, 1H, CH^{iPr}); 6.17 (t, $^2J_{HH}$ = 6.0 Hz, 2H, CH^{Ar}); 6.32 (t, $^3J_{HH}$ = 6.0 Hz, 1H, CH^{Ar}); 6.56 (d, $^2J_{HH}$ = 7 Hz, 1H, CH^{Ar}); 7.07–7.67 (m, 21H, CH^{Ar}).
$^{13}C\{^1H\}$ ($CDCl_3$) δ:	11.1 (CH_3^{Pz4}); 18.2 ($CH_3C{=}N$); 19.2 ($CH_3C{=}N$); 21.5 (CH_3^{iPr}); 22.9 (CH_3^{iPr}); 23.0 (CH_3^{iPr}); 23.1 (CH_3^{iPr}); 23.3 (CH_3^{iPr}); 23.5 (CH_3^{iPr}); 24.0 (CH_3^{iPr}); 24.5 (CH_3^{iPr}); 28.0 (CH^{iPr}); 28.1 (CH^{iPr}); 28.6 (CH^{iPr}); 29.2 (CH^{iPr}); 120.2 (C^{Pz4}); 122.6 (CH^{Ar}); 122.9 (CH^{Ar}); 123.3 (CH^{Ar}); 125.1 (CH^{Ar}); 125.3 (CH^{Ar}); 127.2 (CH^{Ar}); 127.4 (CH^{Ar}); 127.5 (CH^{Ar}); 128.2 (CH^{Ar}); 128.4 (CH^{Ar}); 128.5 (CH^{Ar}); 128.6 (CH^{Ar}); 128.7 (CH^{Ar}); 129.1 (CH^{Ar}); 129.4 (CH^{Ar}); 132.0 (CH^{Ar}); 132.1 (CH^{Ar}); 132.3 (CH^{Ar}); 132.4 (CH^{Ar}); 134.3 (CH^{Ar}); 134.4 (CH^{Ar}); 135.2 (CH^{Ar}); 135.3 (CH^{Ar}); 136.9 (CH^{Ar}); 136.5 (CH^{Ar}); 137.1 (CH^{Ar}); 141.1 (CH^{Ar}); 141.2 (CH^{Ar}); 142.4 ($C^{Pz3/5}$); 147.3 ($C^{Pz3/5}$); 149.2 (C^{Ar}); 150.4 (C^{Ar}); 164.1 ($CH_3C{=}N$); 172.6 ($CH_3C{=}N$).

11. 4 Homobimetallic palladium(II) η^3-allyl complexes

11.4. 1 Synthesis of $[L^1Pd_2(\eta^3\text{-}C_4H_7)_2]PF_6$ (3m)

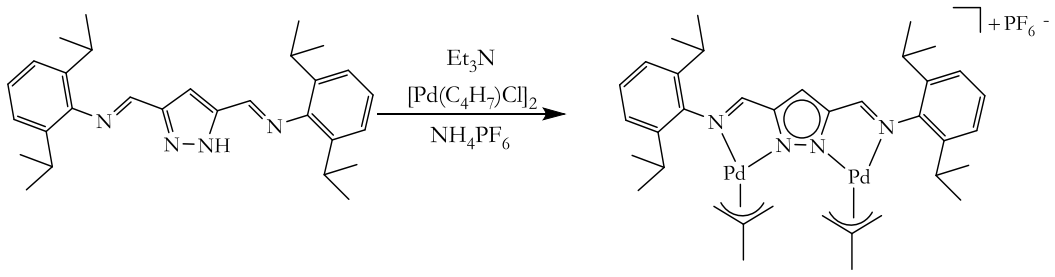

HL[1] **3m**

To a CH_2Cl_2 solution (10 mL) of **HL[1]** (91.7 mg, 0.21mmol) was added an equivalent Et_3N as base with stirring for 10 min. To this solution was added $[Pd(C_4H_7)Cl]_2$ (81 mg, 0.21 mmol) and NH_4PF_6 (20 mg, 0.12 mmol), and the reaction mixture stirred further for 18 h. The reaction was filtered and the mixture washed with water (3x5 mL). The organic phase was combined and dried over $MgSO_4$. The solution was evaporated to remove all volatiles, giving an off-white crystalline solid. The product was recrystallized from a CH_2Cl_2/hexane mixture at room temperature. The product was obtained as a light yellow solid.

Yield:	110 mg, 58%
Molecular formula:	$C_{37}H_{51}BF_4N_4Pd_2$
Molecular weight:	909.7 g/mol.
HRMS (TOF-ESI):	Calcd. For: $C_{37}H_{51}N_4Pd_2$ (765.2199); Found: 765.2187.
MS (ESI, CH_2Cl_2) m/z (%):	764 (100%) $[M\text{-}PF_6]^+$.
IR (ATR, cm^{-1}):	2959 (m); 2924 (m); 2868 (m); 1605 (vs); 1588 (vs); 1489 (m); 1462 (m); 1389 (m); 1365 (m); 1343 (m); 1300 (m); 1070 (vs); 1043 (vs); 1028 (vs); 927 (m); 802 (m); 756 (m); 745 (m).
^{1}H-NMR ($CDCl_3$) δ:	1.22-1.29 (m, 24H, CH_3^{iPr}); 2.13 (s, 6H, $CH_3^{Me(allyl)}$); 3.07 (br s, 12H, CH^{iPr}, $CH_2^{Me(allyl)}$); 7.19-7.30 (m, 6H, CH^{Ar}); 7.70 (s, 1H, CH^{Pz4}); 8.32 (s, 2H, CH=N).
$^{13}C\{^1H\}$ ($CDCl_3$):	23.3 ($CH_3^{Me(allyl)}$); 28.2 (CH^{iPr}); 46.3 ($CH_2^{Me(allyl)}$); 114.5 (CH^{Pz}); 123.7 ($CH^{Ar3/5}$); 127.5 (CH^{Ar4}); 134.4 ($C^{Me(allyl)}$); 139.2 ($C^{Ar2/6}$); 146.7 (C^{Ar1}); 153.0 ($C^{Pz3/5}$); 162.6 (CH=N).

11.4. 2 Synthesis of $[L^1Pd_2(\eta^3\text{-}C_6H_9)_2]PF_6$ (3o)

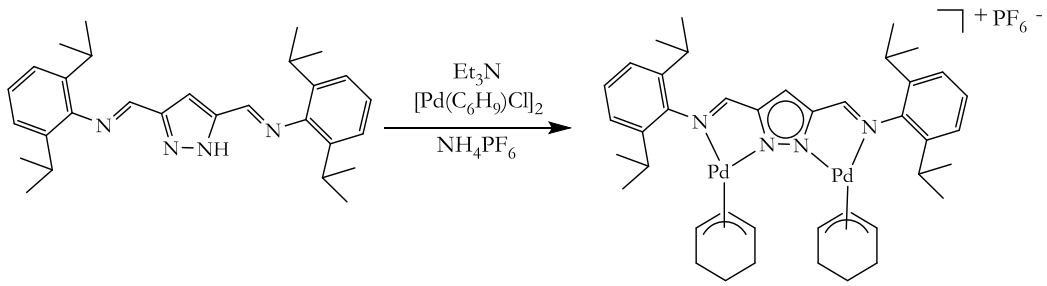

HL[1] **3o**

To a CH_2Cl_2 solution (15 mL) of **HL[1]** (55.0 mg, 0.12 mmol) was added an equivalent of Et_3N and stirred for 10 min. To this solution was added $[Pd(\eta^3\text{-}C_6H_9)Cl]_2$ (56 mg, 0.12 mmol). The initial bright yellow colour was discharged to a colourless solution with time after addition of NH_4PF_6 (65 mg, 0.40 mmol). After 2 h, the formation of Pd(0) species was observed. The reaction mixture was filtered over celite and the solution washed with water (3x5 mL). The organic phase was combined and dried over $MgSO_4$. Evaporation of all the volatiles gives an off-white crystalline solid.

Yield:	92 mg, 77 %
Molecular formula:	$C_{41}H_{55}F_6N_4PPd_2$
Molecular weight:	961.7 g/mol.
HRMS (TOF-ESI):	Calcd. For: $C_{41}H_{55}N_4Pd_2$+H (816.7345); Found: 816.2510.
MS (ESI, CH_2Cl_2) m/z (%):	817 (100%) $[M\text{-}PF_6]^+$.
IR (ATR, cm^{-1}):	2957 (m); 2870 (m); 1613 (vs); 1465 (m); 1450 (s); 1441 (vs); 1346 (m); 1301 (s); 1141 (m); 1072 (m); 1057 (m); 840 (vs); 804 (vs); 748 (m); 558 (vs).
^{1}H-NMR ($CDCl_3$) δ:	1.09-1.33 (m, 16H, CH_3^{iPr}, $CH_2^{Cy(allyl)}$); 1.25 (d, $^3J_{HH}$ = 6.9 Hz, 12H, CH_3^{iPr}); 1.78-1.84 (br m, 4H, $CH_2^{Cy(allyl)}$); 2.22 (br s, 4H, $CH_2^{Cy(allyl)}$); 3.11 (m, 4H, CH^{iPr}); 4.36 (br t, 1H, $CH^{Cy(allyl)}$); 5.22 (br t, 2H, $CH^{Cy(allyl)}$); 5.53-5.62 (m, 2H, $CH^{Cy(allyl)}$); 5.77 (t, $^3J_{HH}$ = 6.4 Hz, 1H, $CH^{Cy(allyl)}$); 7.24-7.36 (m, 6H, CH^{Ar}); 7.56 (s, 1H, CH^{Pz}) 8.24 (s, 2H, CH=N).

$^{13}C\{^{1}H\}$ ($CDCl_3$) δ: 19.0 (CH_2); 22.5 (CH_3^{iPr}); 22.7 (CH_3^{iPr}); 22.9 (CH_3^{iPr}); 23.6 (CH_3^{iPr}); 24.9 (CH_3^{iPr}); 25.2 (CH_3^{iPr}); 24.9 (CH_3^{iPr}); 25. 9 (CH_3^{iPr}); 26.0 (CH_3^{iPr}); 28.3 (CH^{iPr}); 29.0 ($CH_2^{Cy(allyl)}$); 29.9 ($CH_2^{Cy(allyl)}$); 30.1 ($CH_2^{Cy(allyl)}$); 74.1 ($CH^{Cy(allyl)}$); 75.4 ($CH^{Cy(allyl)}$); 81.0 ($CH^{Cy(allyl)}$); 81.9 ($CH^{Cy(allyl)}$); 114.3 ($CH^{Cy(allyl)}$); 123.8 (CH^{Ar}); 123.9 ($CH^{Ar3/5}$); 127.5 (CH^{Ar}); 128.4 (C^{Ar}); 139.1 (C^{Ar}); 139.5 ($C^{Ar2/6}$); 139.6 (C^{Ar}); 146.0 (C^{Ar}); 152.8 ($C^{Pz3/5}$); 161.6 (CH=N).

Following similar reaction procedures, other homobimetallic palladium(II) η^3-allyl complexes were prepared.

11.4. 3 Synthesis of $[L^2Pd_2(\eta^3\text{-}C_6H_9)_2]PF_6$ (3p)

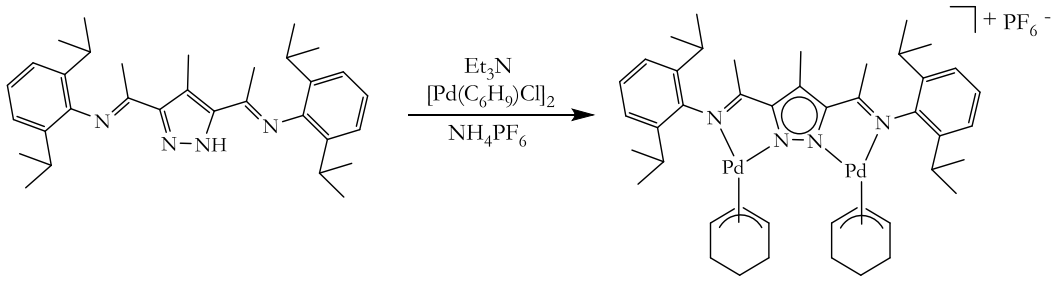

HL² **3p**

Using **HL²** (270 mg, 0.56 mmol), $[Pd(\eta^3\text{-}C_6H_9)Cl]_2$ (250 mg, 0.55 mmol, 1.0 Eq), NH_4PF_6 (500 mg, 3.1 mmol, 5.5 Eq) and an equivalent Et_3N. The product was obtained as an offwhite solid, after all volatiles were removed. This solid is unstable at room temperature, but can be kept for several weeks at cold temperatures. Single crystals were grown by the slow diffusion of Et_2O inot a CH_2Cl_2 solution of the complex at low temperature.

Yield:	270 mg, 48 %
Molecular formula:	$C_{44}H_{61}F_6N_4PPd_2$
Molecular weight:	1003.8 g/mol.
HRMS (TOF-ESI):	Calcd. For $C_{44}H_{61}N_4Pd_2$ (859.2991); Found: 859.2976
MS (ESI, CH_2Cl_2) m/z (%):	859 (100%) $[M\text{-}PF_6]^+$.

IR (ATR, cm^{-1}): 2933 (m); 2959 (m); 2874 (m); 1598 (s); 1585 (s); 1452 (s); 1432 (m); 1326 (m); 1309 (m); 838 (vs); 780 (m) 558 (s).

^{1}H-NMR ($CDCl_3$) δ: 0.95-1.02 (m, 4H, $CH_2^{Cy(allyl)}$); 1.09-1.22 (m, 18H, CH_3^{iPr}); 1.22 (dd, $^{3}J_{HH}$ = 6.8 Hz, 3.4 Hz, 6H, CH_3^{iPr}); 1.59-1.86 (br m, 8H $CH_2^{Cy(allyl)}$); 2.29 (s, 6H, CH_3C=N); 2.62 (s, 3H, CH_3^{Pz4}); 2.91-3.09 (m, 4H, CH^{iPr}); 4.08 (br t, 1H, $CH^{Cy(allyl)}$); 5.19 (br t, 2H, $CH^{Cy(allyl)}$); 5.39-5.51 (m, 2H, $CH^{Cy(allyl)}$); 5.69 (t, $^{3}J_{HH}$ = 6.4 Hz, 1H, $CH^{Cy(allyl)}$); 7.23-7.32 (m, 6H, CH^{Ar}).

^{13}C{^{1}H} ($CDCl_3$) δ: 11.6 (CH_3^{Pz4}); 19.2 (CH_2); 20.8 (CH_3C=N); 23.4 (CH_3^{iPr}); 23.8 (CH_3^{iPr}); 24.4 (CH_3^{iPr}); 24.7 (CH_3^{iPr}); 28.3 (CH^{iPr}); 28.9 (CH^{iPr}); 30.1 ($CH_2^{Cy(allyl)}$); 81.5 ($CH^{Cy(allyl)}$); 107.4 (C^{Pz4}) 120.1 (CH^{Ar}); 124.3 (CH^{Ar}); 127.2 (CH^{Ar}); 128.4 (CH^{Ar4}); 138.9 ($C^{Ar2/6}$); 143.6 (C^{Ar}); 152.7 ($C^{Pz3/5}$); 171.1 (CH_3C=N).

11.4. 4 Synthesis of $[L^2Pd_2(\eta^3\text{-}C_4H_7)Cl_2]$ (3z)

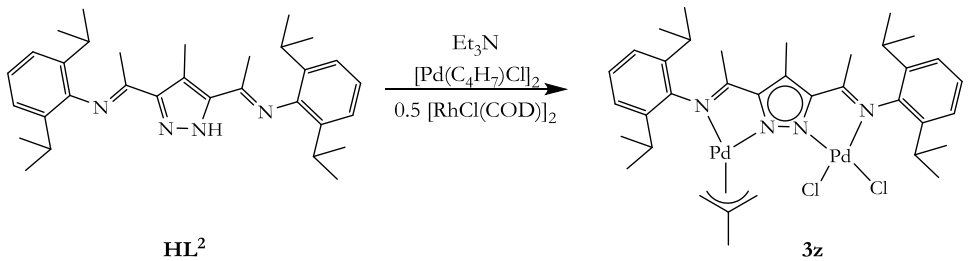

HL² **3z**

To a CH_2Cl_2 solution (10 mL) of **HL²** (100 mg, 0.21 mmol) was added with stirring an equivalent Et_3N. After 30 minutes $[(Pd(\eta^3\text{-}C_4H_7)Cl]_2$ (90 mg, 0.23 mmol) and NH_4PF_6 (300 mg, 1.8 mmol) were added and the mixture stirred for 6 h. A bright yellow solution was formed. After 6 h, 0.5 mol equivalent of $[RhCl(COD)]_2$ (50 mg, 0.11 mmol) was added to the reaction mixture and stirred overnight. The reaction was filtered to remove excess NH_4PF_6. The filtrate was washed with water (3x3 mL) and the organic phase was combined and dried over $MgSO_4$. A CH_2Cl_2 solution of the complex was layered with ether and allowed to slowly evaporate at room temperature. 23 mg of yellow crystalline solid was havested from the sides of the test tube, and colourless solid (14 mg), was later harvested from the buttom of the test tube. The colourless solid was later identified by ESI-MS as $[(Pd(\eta^3\text{-}C_4H_7)Cl]_2$.

Experimetal

Yield:	23 mg, 34%
Molecular formula:	$C_{36}H_{50}Cl_2N_4Pd_2$
Molecular weight:	822.6 g/mol.
MS (ESI, CH_2Cl_2) *m/z* (%):	786 (15%) $[M\text{-}Cl]^+$; 749 (100%) $[M\text{-}2Cl]^+$.
IR (ATR, cm^{-1}):	2983 (vs); 2967 (vs); 2872 (vs); 2857 (vs); 1575 (m); 1385 (m); 1326 (m); 1244 (m); 1087 (vs); 923 (m); 806 (m); 778 (m); 733 (m).
^{1}H-NMR ($CDCl_3$) δ:	1.10-1.48 (m, 24H, CH_3^{iPr}); 2.14 (s, 3H, $CH_3^{Me(allyl)}$); 2.18 (s, 3H, CH_3C=N); 2.20 (s, 3H, CH_3C=N); 2.57 (s, 3H, CH_3^{Pz4}); 2.97-3.12 (m, 2H, $CH_2^{Me(allyl)}$); 3.27-3.30 (m, 4H, CH^{iPr}); 3.30 (br s, 2H, $CH_2^{Me(allyl)}$); 7.17-7.34 (m, 6H, CH^{Ar}).
$^{13}C\{^1H\}$ ($CDCl_3$) δ:	10.6 (CH_3^{Pz4}); 19.7 (CH_3C=N); 22.3 (CH_3^{iPr}); 23.7 ($CH_3^{Me(allyl)}$); 24.1 (CH_3^{iPr}); 28.3 (CH^{iPr}); 28.5 (CH^{iPr}); 121.0 (C^{Pz4}); 123.6 ($CH^{Ar3/5}$); 124.0 ($CH^{Ar3/5}$); 127.1 (C^{Ar4}); 128.0 (C^{Ar4}); 140.6 ($C^{Ar2/6}$); 141.2 ($C^{Ar2/6}$); 144.2 (C^{Ar}); 150.8 ($C^{Pz3/5}$); 169.4 (CH_3C=N).

11. 5 Heterobimetallic palladium(II)-rhodium(I) complexes

11.5. 1 Synthesis of $[L^1Pd(\eta^3\text{-}C_4H_7)Rh(COD)]BAr^F{}_4$ (3r)

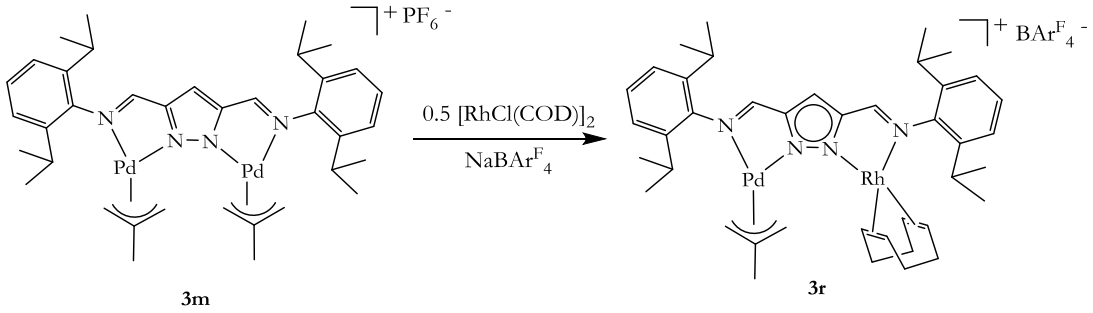

To a CH_2Cl_2 solution (15 mL) of **3m** (30.0 mg, 0.033 mmol) was added 0.5 mol equivalent $[RhCl(COD)]_2$ (8.6 mg, 0.017 mmol) with stirring for 30 min. A red/orange solution was formed. The formation of Pd(0) species was not observed in this instance. The reaction mixture was filtered over celite to obtain a bright orange solution. Hexane was added drop wise to the CH_2Cl_2 solution of the complex, resulting in the precipitation of a bright orange powder. This was filtered and dried in vacuum for several minutes. Yield: 17 mg, 63% (PF_6). The PF_6 counter ion was exchanged to $[BAr^F{}_4]^-$ by stirring the complex over a mol $NaBAr^F{}_4$ for 2 hours.

Yield:	17 mg, 63%
Molecular formula:	$C_{73}H_{68}BF_{24}N_4PdRh$
Molecular weight:	814.3 g/mol.
HRMS (TOF-ESI):	Calcd. For: $C_{41}H_{56}N_4PdRh$ (813.2605); Found: 813.2604.
MS (ESI, CH_2Cl_2) m/z (%):	813 (100%) $[M\text{-}BAr^F{}_4\text{-}H]^+$; 764 (45%) $[LPd_2(C_4H_7)_2]^+$.
IR (ATR, cm^{-1}):	2928 (m); 2959 (m); 2872 (m); 1609 (vs); 1588 (s); 1463 (s); 1414 (m); 1365 (m); 1387 (m); 1352 (m); 1303 (m); 1139 (s); 1056 (vs); 1031 (vs); 804 (m); 746 (m); 679 (m).
^{1}H-NMR ($CDCl_3$) δ:	(Isomer 1); 1.17 (d, $^3J_{HH}$ = 6.8 Hz, 8H, $CH_3{}^{iPr}$); 1.26 (d, $^3J_{HH}$ = 6.8 Hz, 8H, $CH_3{}^{iPr}$); 1.39 (d, $^3J_{HH}$ = 6.9 Hz, 8H, $CH_3{}^{iPr}$); 1.86-2.09 (m, 5H, $CH_2{}^{COD}$, $CH_3{}^{Me(allyl)}$); 2.39-2.52 (br m, 2H, $CH_2{}^{COD}$); 2.92-3.29 (m, 12H, $CH_2{}^{COD}$, $CH_2{}^{Me(allyl)}$, CH^{iPr}); 3.55 (br s, 1H, CH^{COD}); 4.00-4.15 (m, 1H, CH^{COD}); 4.24 (br s, 1H, CH^{COD}); 5.07 (br s, 1H, CH^{COD}); 7.21-7.27 (m, 6H, CH^{Ar}); 7.50 (s, 4H, CH^{BArF4}); 7.69 (s,

8H, CH^{BArF4}); 7.81 (s, 1H, CH^{Pz}); 8.09 (s, 1H, $CH{=}N^{Rh}$); 8.32 (s, 1H, $CH{=}N^{Pd}$).

$^{13}C\{^{1}H\}$ ($CDCl_3$) δ: 22.2 (CH_3^{iPr}); 22.4 (CH_3^{iPr}); 22.6 (CH_3^{iPr}); 22.8 ($CH_3^{Me(allyl)}$); 23.2 (CH_3^{iPr}); 24.5 (CH_3^{iPr}); 24.8 (CH_3^{iPr}); 24.9 (CH_3^{iPr}); 25.6 (CH_3^{iPr}); 27.0 (C^{BArF4}); 28.3 (CH^{iPr}); 28.6 (CH^{iPr}); 30.4 (CH_2^{COD}); 30.5 (CH_2^{COD}); 62.6 ($CH_2^{Me(allyl)}$); 64.8 ($CH_2^{Me(allyl)}$); 65.7 ($CH_2^{Me(allyl)}$); 85.4 (CH^{COD}); 113.1 (CH^{Pz4}); 117.5; 122.8; (C^{Ar}); 124.0 (CH^{Ar}); 126.5 (CH^{Ar}); 128.3 (CH^{Ar}); 128.7 (CH^{Ar}); 129.2 (CH^{Ar}); 134.6 ($C^{Me(allyl)}$); 134.9 (C^{BArF4}); 138.7 ($C^{2/6}$); 139.1 ($C^{2/6}$); 140.1 (C^{Ar}); 146.2 (C^{Ar}); 152.6 ($C^{Pz3/5}$); 153.4 ($C^{Pz3/5}$); 160.4 ($CH{=}N^{Pd}$); 160.8 ($CH{=}N^{Rh}$); 162.8 ($CH{=}N^{Rh}$).

11.5. 2 Synthesis of $[L^2Pd(\eta^3\text{-}C_4H_7)Rh(COD)]PF_6$ (3s)

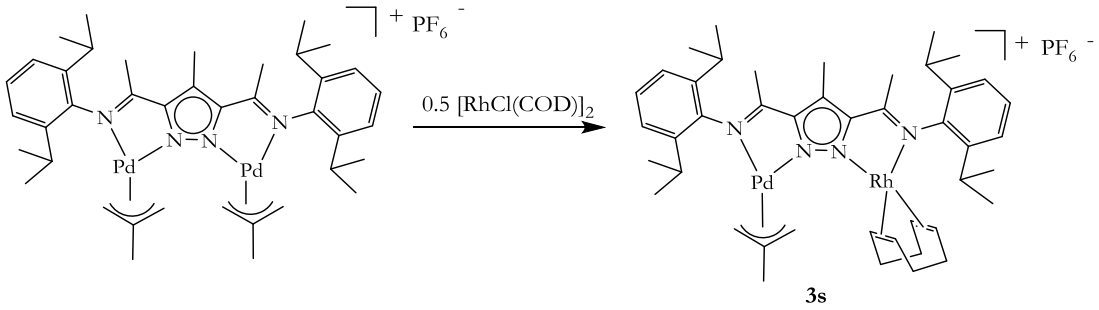

To a CH_2Cl_2 solution (10 mL) of $[L^2Pd_2(\eta^3\text{-}C_4H_7)_2]PF_6$ (20.0 mg, 21.0 μmol) was added 0.5 mol equivalent $[RhCl(COD)]_2$ (5.10 mg, 10.5 μmol) with stirring. The formation of a yellow suspension was observed. After 18 h, the reaction mixture was filtered over celite to obtain a bright yellow-orange solution. A CH_2Cl_2 solution (5 mL) of the complex was layered with ether and kept in the fridge at -20 °C. A yellow powdery material was harvested from the solution after several days.

Yield:	9 mg, 43%
Molecular formula:	$C_{44}H_{62}F_6N_4PPdRh$
Molecular weight:	1001.3 g/mol.
HRMS (TOF-ESI):	Calcd. For: $C_{44}H_{62}N_4PdRh$+H (855.3074); Found: 855.3076.

MS (ESI, CH_2Cl_2) m/z (%): 855 (100%) $[M\text{-}H\text{-}PF_6]^+$; 804 (35%) $[LPd_2(C_4H_7)_2]^+$.

IR (ATR, cm^{-1}): 2959 (m); 2928 (m); 2870 (m); 1626 (s); 1564 (s);1462 (m); 1434 (m); 1413 (s) 1385 (s); 1326 (m); 1313 (m); 1059 (m); 838 (vs); 778 (vs); 558 (s).

^{1}H-NMR ($CDCl_3$) δ: 1.13 (d, $^3J_{HH}$ = 6.8 Hz, 6H, CH_3^{iPr}); 1.18 (d, $^3J_{HH}$ = 6.8 Hz, 6H, CH_3^{iPr}); 1.27 (d, $^3J_{HH}$ = 6.8 Hz, 6H, CH_3^{iPr}); 1.42 (d, $^3J_{HH}$ = 6.8 Hz, 3H, CH_3^{iPr}); 1.44 (d, $^3J_{HH}$ = 6.8 Hz, 3H, CH_3^{iPr}); 1.79-1.89 (m, 2H, CH_2^{COD}); 2.03 (s, 3H, $CH_3^{Me(allyl)}$); 2.26 (s, 3H, CH_3C=N); 2.27 (s, 3H, CH_3C=N); 2.33-2.52 (m, 4H, CH_2^{COD}); 2.60 (s, 3H, CH_3^{Pz4}); 2.63-3.12 (m, 2H, CH_2^{COD}); 3.07 (sept, $^3J_{HH}$ = 6.8 Hz, 2H, CH^{iPr}); 3.19 (sept, $^3J_{HH}$ = 6.8 Hz, 2H, CH^{iPr}); 3.40 (br s, 2H, $CH_2^{Me(allyl)}$); 4.15 (br s, 2H, $CH_2^{Me(allyl)}$); 4.91-5.03 (m, 4H, CH^{COD}); 7.22-7.32 (m, 6H, CH^{Ar}).

$^{13}C\{^1H\}$ ($CDCl_3$) δ: 11.6 (CH_3^{Pz4}); 19.9 (CH_3C=N); 20.6 (CH_3C=N); 21.6; 22.6 ($CH_3^{Me(allyl)}$); 23.2 (CH_3^{iPr}); 23.4 (CH_3^{iPr}); 23.6 (CH_3^{iPr}); 23.6 (CH_3^{iPr}); 24.0 (CH_3^{iPr}); 24.3 (CH_3^{iPr}); 25.0 (CH_3^{iPr}); 28.4 (CH^{iPr}); 28.5 (CH^{iPr}); 28.6 (CH^{iPr}); 30.2 (CH_2^{COD}); 30.4 (CH_2^{COD}); 30.5 (CH_2^{COD}); 53.5 ($CH_2^{Me(allyl)}$); 63.8 ($CH_2^{Me(allyl)}$); 64.5 ($CH_2^{Me(allyl)}$); 65.4 ($CH_2^{Me(allyl)}$); 77.3; 83.3 (CH^{COD}); 83.5 (CH^{COD}); 83.7; 85.0; 85.1 (CH^{COD}); 123.9 (C^{Pz4}); 124.0 (CH^{Ar}); 124.1 (CH^{Ar}); 124.3 (CH^{Ar}); 124.4 (CH^{Ar}); 127.4 (CH^{Ar}); 127.5 (CH^{Ar}); 128.0 (CH^{Ar}); 133.8 ($C^{Me(allyl)}$); 134.7 ($C^{Me(allyl)}$); 138.6; 138.7; 138.9($C^{Ar2/6}$); 139.0 ($CAr^{2/6}$); 140.2 ($C^{Ar\text{-}Rh}$); 144.5 ($C^{Ar\text{-}Pd}$); 152.9 ($C^{Pz3/5}$); 154.5 ($C^{Pz3/5}$); 170.9 (CH_3C=N^{Pd}); 173.6 (CH_3C=N^{Rh}).

11.5. 3 Synthesis of $[L^1Pd(\eta^3\text{-}C_6H_9)Rh(COD)]PF_6$ (3t)

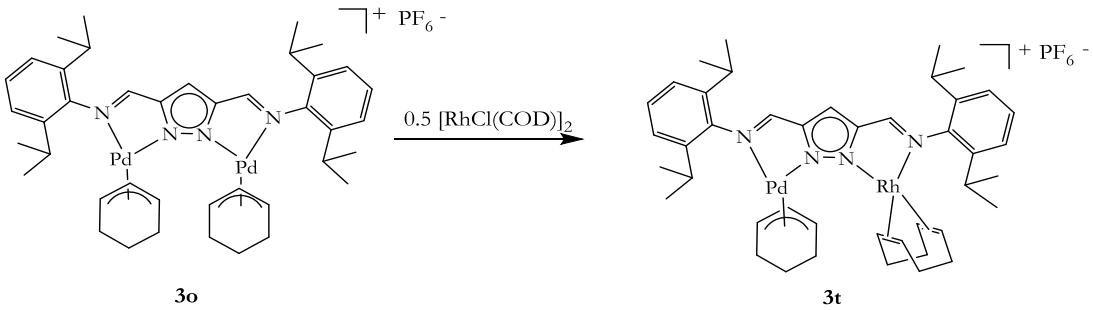

3o **3t**

To a CH_2Cl_2 solution (15 mL) of **3o** (150 mg, 0.15 mmol) was added with stirring ~0.5 mol equivalent) of $[RhCl(COD)]_2$ (30 mg, 0.06 mmol). After stirring overnight, what appears to be the formation of Pd(0) species was observed. The reaction mixture was filtered over celite to obtain a bright yellow-orange solution. Addition of hexane dropwise to the CH_2Cl_2 solution results in the precipitation of a bright orange solid. The solid was filtered and dried in vacuum for several minutes. Very fine needles were recrystallized from a CH_2Cl_2 solution of the complex by slow evaporation of the CH_2Cl_2 solution for several days.

Yield:	54.3 mg, 37%
Molecular formula:	$C_{43}H_{58}F_6N_4PPdRh$
Molecular weight:	985.3 g/mol.
HRMS (TOF-ESI):	Calcd. For: $C_{43}H_{58}N_4PdRh$ (839.2762); Found: 839.2764.
MS (ESI, CH_2Cl_2) m/z (%):	839 (100%) $[M\text{-}PF_6]^+$.
IR (ATR, cm^{-1}):	2957 (m); 1605 (s); 1586 (s); 1460 (m); 1439 (m); 1346 (m); 1300 (m); 1141 (m); 836 (vs); 558 (s).
^{1}H-NMR ($CDCl_3$) δ:	1.13 (d, $^3J_{HH}$ = 6.8 Hz, 6H, CH_3^{iPr}); 1.19 (d, $^3J_{HH}$ = 6.8 Hz, 6H, CH_3^{iPr}); 1.22 (d, $^3J_{HH}$ = 6.8 Hz, 6H, CH_3^{iPr}); 1.26 (d, $^3J_{HH}$ = 6.8 Hz, 3H, CH_3^{iPr}); 1.40 (d, $^3J_{HH}$ = 6.8 Hz, 3H, CH_3^{iPr}); 1.74-1.92 (m, 2H, $CH_2^{Cy(allyl)}$); 1.80 (br s, 2H, $CH_2^{Cy(allyl)}$); 2.08 (br s, 4H, CH_2^{COD}); 2.40 (br s, 2H, $CH_2^{Cy(allyl)}$); 2.54 (br s, 4H, CH_2^{COD}); 3.04 (sept, $^3J_{HH}$ = 6.8 Hz, 2H, CH^{iPr}); 3.29 (sept, $^3J_{HH}$ = 6.8 Hz, 2H, CH^{iPr}); 3.49 (br s, 2H, CH^{COD}); 4.16 (br s, 1H, $CH^{Cy(allyl)}$); 5.17 (br s, 2H, CH^{COD}); 5.49 (m, 1H, $CH^{Cy(allyl)}$); 5.68 (t, 1H, $CH^{Cy(allyl)}$); 5.75 (m, 1H, $CH^{Cy(allyl)}$); 7.13-7.36 (m, 6H, CH^{Ar}); 7.57 (s, 1H, CH^{Pz4}); 7.97 (s, 1H, CH=N); 8.22 (s, 1H, CH=N).

$^{13}C\{^{1}H\}$ ($CDCl_3$) δ:	19.8 ($CH_2^{Cy(allyl)}$); 22.3 (CH_3^{iPr}); 22.7 (CH_3^{iPr}); 25.7 (CH_3^{iPr}); 28.3 (CH^{iPr}); 28.5 (CH_3^{iPr}); 29.49 ($CH_2^{Cy(allyl)}$); 30.1 (CH_2^{COD}) 30.5 (CH_2^{COD}); 80.0 ($CH^{Cy(allyl)}$); 82.0 (CH^{COD}); 84.9 (CH^{COD}); 106.9 ($CH^{Cy(allyl)}$); 115.3 (CH^{Pz4}); 120.1; 123.8 (CH^{Ar}); 127.7 (CH^{Ar}); 128 (CH^{Ar}); 140.3 ($C^{Ar2/6}$); 141.5 ($C^{Ar2/6}$); 145.8 (C^{Ar}); 152.6 ($C^{Pz3/5}$); 153.9 ($C^{Pz3/5}$); 161.2 ($CH{=}N^{Pd}$); 163.7 ($CH{=}N^{Rh}$).
Elemental analysis:	Calcd. For $C_{44}H_{60}Cl_2F_6N_4PPdRh{\cdot}CH_2Cl_2$: (C) 49.38 (H) 5.65 (N) 5.24; Found: C (49.17) (H) 5.73 (N) 5.17.

11.5. 4 Synthesis of $[L^2Pd(\eta^3\text{-}C_6H_9)Rh(COD)]BAr^F{}_4$ (3u)

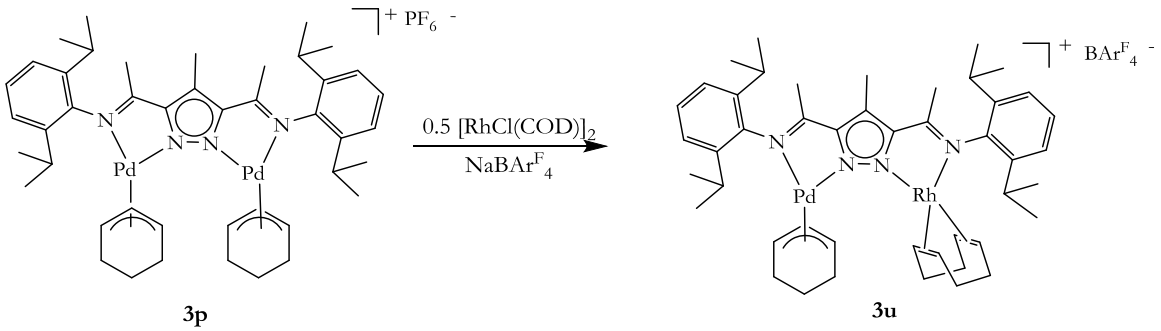

To a CH_2Cl_2 solution (15 mL) of **3p** (78.8 mg, 0.079 mmol) was added 0.5 mol equivalent of $[RhCl(COD)]_2$ (19.3 mg, 0.039 mmol) with stirring. After 2 h, a dark red solution was formed, accompanied by the formation of traces of Pd(0). The reaction was filtered over celite to obtain a bright red solution. A bright orange powder (74.0 mg) was obtained after evaporating the solution. The powder was divided into two fractions; the first fraction was dissolved in CH_2Cl_2, stirred over a mol equivalent $NaBAr^F{}_4$, and again filtered. The slow evaporation of a CH_2Cl_2/cyclohexane (10:1) solution (fraction 1) of the complex at room temperature gave the complex as bright orange prisms.

Yield:	74.0 mg, 94%
Molecular formula:	$C_{46}H_{64}F_6N_4PPdRh$
Molecular weight:	1027.3 g/mol.
HRMS (TOF-ESI):	Calcd. For $C_{46}H_{64}N_4PdRh$ (881.3232); Found: 881.3232.
MS (ESI, CH_2Cl_2) *m/z* (%):	881.9 (100) $[M\text{-}PF_6]^+$.

IR (ATR, cm^{-1}): 2967 (m); 2928 (m); 1613 (m); 1581 (m); 1456 (m); 1465 (m); 1345 (s); 1275 (vs); 1158 (vs); 1121 (vs); 888 (s); 841 (m); 717 (s); 450 (m).

^{1}H-NMR ($CDCl_3$) δ: 1.14-1.33 (m, 24H, CH_3^{iPr}); 1.55-1.63 (br s, 2H, $CH_2^{Cy(allyl)}$); 1.80 (br s, 2H, $CH_2^{Cy(allyl)}$); 2.08 (br s, 4H, CH_2^{COD}); 2.47 (br s, 2H, $CH_2^{Cy(allyl)}$); 2.26 (s, 3H, CH_3C=N); 2.28 (s, 3H, CH_3C=N); 2.33-2.47 (m, 4H, CH_2^{COD}); 2.59 (s, 3H, CH_3^{Pz4}); 2.90-3.36 (m, 4H, CH^{iPr}); 4.08 (br t, 2H, CH^{COD}); 5.08 (br t, 2H, CH^{COD}); 5.35-5.43 (m, 2H, $CH^{Cy(allyl)}$); 5.62 (m, 1H, $CH^{Cy(allyl)}$); 7.10-7.36 (m, 6H, CH^{Ar}).

^{13}C{^{1}H} ($CDCl_3$) δ: 11.7 (CH_3^{Pz4}); 20.4 ($CH_2^{Cy(allyl}$); 20.9 (CH_3C=N); 21.5 (CH_3C=N); 21.6 (CH_3^{iPr}); 23.5 (CH_3^{iPr}); 23.7 (CH_3^{iPr}); 23.9 (CH_3^{iPr}); 24.5 (CH_3^{iPr}); 24.8 (CH_3^{iPr}); 25.0; 28.2 (CH^{iPr}); 28.4 (CH^{iPr}); 28.5 (CH^{iPr}); 29.5 ($CH_2^{Cy(allyl)}$); 30.1 (CH_2^{COD}); 30.2 (CH_2^{COD}); 79.4 ($CH^{Cy(allyl)}$); 82.8 (CH^{COD}); 83.5 (CH^{COD}); 106.6 ($CH^{Cy(allyl}$); 124.0 (C^{Pz4}); 124.3 (CH^{Ar}); 127.4 (CH^{Ar}); 127.9 (CH^{Ar}); 138.8 ($C^{Cy(allyl)}$); 139.0 (C^{Ar1}); 140.3 ($C^{Ar2/6}$); 143.8 (C^{Ar}); 152.7 ($C^{Pz3/5}$); 170.6 (CH_3C=N^{Pd}); 173.6 (CH_3C=N^{Rh}).

11.5. 5 Synthesis of $[L^1Pd(\eta^3\text{-}C_4H_7)Rh(CO)_2]PF_6$ (3w)

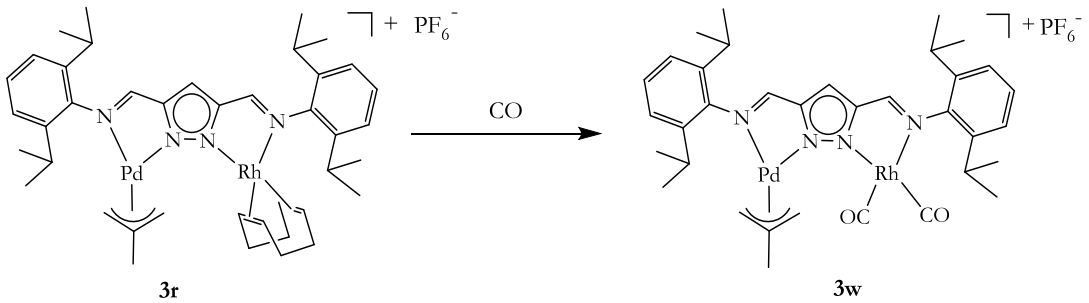

3r **3w**

Carbon monoxide (CO, 1 atm) was continuesly bubled through a CH_2Cl_2 solution (15 mL) of **3r** (30.0 mg, 0.035 mmol) for 30 min. This was followed by a change in colour of the solution from yellow to lemon green. The CH_2Cl_2 solution of the complex was kept in the fridge at -20 °C under an atmosphere of CO. Lemon green powdery material was harvested from the solution after several days.

Yield:	24.1 mg, 81%
Molecular formula:	$C_{35}H_{44}F_6N_4O_2PPdRh$
Molecular weight:	863.9 g/mol.
MS (ESI, CH_2Cl_2) m/z (%):	764.1 (100%) $[M+H-PF_6]^+$.
^{1}H-NMR ($CDCl_3$) δ:	0.98-1.40 (m, 24H, CH_3^{iPr}); 2.08 (s, 3H, $CH_3^{Me(allyl)}$); 2.67-3.27 (m, 4H, CH^{iPr}); 4.02 (m, 2H, $CH_2^{Me(allyl)}$); 4.28 (m, 2H, CH_2, $^{Me(allyl)}$) 7.10-7.40 (m, 6H, CH^{Ar}); 8.05 (s, 1H, CH^{Pz4}); 8.15 (s, 1H, CH=N); 8.16 (s, 1H, CH=N).
$^{13}C\{^1H\}$ ($CDCl_3$) δ:	22.8 (CH_3^{iPr}); 23.0 ($CH_3^{Me(allyl)}$); 24.6 (CH_3^{iPr}); 27.0 (CH^{iPr}); 28.6 (CH^{iPr}); 62.4 ($CH_2^{Me(allyl)}$); 108.0 117.5 (CH^{Pz}); 120.1 (CH^{Pz}); 122.8; 124.1 (CH^{Ar}); 126.5 (CH^{Ar}); 129.6 (CH^{Ar}); 134.5 ($C^{Me(allyl)}$); 134.9; 139.1 ($C^{Ar2/6}$); 139.6 ($C^{Ar2/6}$); 146.4 (C^{Ar}); 146.7 (C^{Ar}); 153.0 ($CC=N^{Pd}$); 154.7 ($CC=N^{Rh}$); 164.2 ($CH=N^{Pd}$); 164.4 ($CH=N^{Rh}$); CO-not observed.

11.5. 6 Synthesis of $[L^1Pd(\eta^3\text{-}C_6H_9)Rh(CO)_2]PF_6$ (3x)

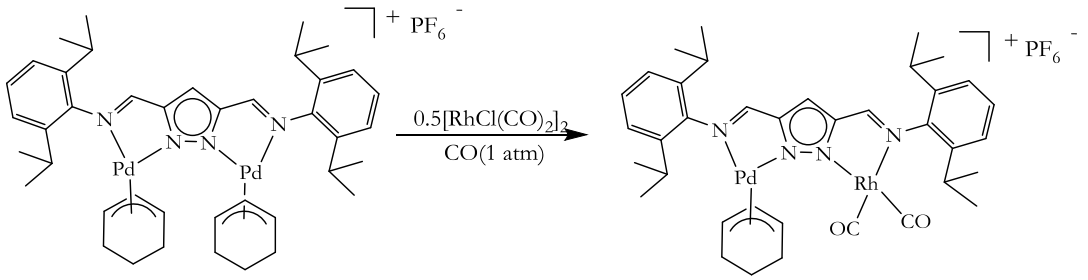

3o **3x**

To a CH_2Cl_2 solution (10 mL) of **3o** (34.0 mg, 0.035 mmol) was added 0.5 mol equivalent $[RhCl(CO)_2]_2$ (6.80 mg, 0.017 mmol) and the mixture stirred for 30 min under 1 atm CO atmosphere. After this period, what appears to be the formation of Pd(0) species was observed. The reaction mixture was filtered over celite to obtain a bright yellowish-orange solution. Addition of hexane dropwise to the CH_2Cl_2 solution results in the precipitation of a bright yellow solid. This was filtered and dried in vacuum for several hours.

Yield:	16 mg, 41%
Molecular formula:	$C_{37}H_{46}F_6N_4O_2PPdRh$

Molecular weight:	933.1 g/mol.
HRMS (TOF-ESI):	Calcd. For $C_{37}H_{46}N_4O_2PdRh$ (787.1718); Found: 787.1718.
MS (ESI, CH_2Cl_2) m/z (%):	817 (10%) $[M+CO-PF_6]^+$; 787 (100%) $[M-PF_6]^+$.
IR (ATR, cm^{-1}):	2970 (m); 2933 (m); 2877 (m); 2098 (vs); 2039 (vs); 1611 (m); 1577 (m); 1495 (m); 1357 (vs); 1275 (vs); 1050 (vs); 936 (m); 777 (m); 888 (m); 843 (m); 806 (m); 672 (m); 612 (m).
^{1}H-NMR ($CDCl_3$) δ:	1.04 (m, 2H, $CH_2^{Cy(allyl)}$); 1.08 (d, $^3J_{HH}$ = 6.8 Hz, 12H, CH_3^{iPr}); 1.22 (d, $^3J_{HH}$ = 6.8 Hz, 6H, CH_3^{iPr}); 1.36 (d, $^3J_{HH}$ = 6.8 Hz, 6H, CH_3^{iPr}); 1.81 (br s, 4H, $CH_2^{Cy(allyl)}$); 3.19 (m, 4H, CH^{iPr}); 5.24 (br s, 1H, $CH^{Cy(allyl)}$); 5.52 (br s, 1H, $CH^{Cy(allyl)}$); 5.70-5.73 (m, 1H, $CH^{Cy(allyl)}$); 7.24-7.40 (m, 6H, CH^{Ar}); 7.80 (s, 1H, CH^{Pz4}); 7.93 (s, 1H, CH=N); 8.31 (s, 1H, CH=N).
^{13}C{^{1}H} ($CDCl_3$) δ:	19.1 ($CH_2^{Cy(allyl)}$); 22.7 (CH_3^{iPr}); 24.4 (CH_3^{iPr}); 28.4 (CH^{iPr}) 28.7 (CH^{iPr}); 28.9 (CH^{iPr}); 79.8 (CH); 102.3 ($CH^{Cy(allyl)}$); 107.4 ($CH^{Cy(allyl)}$); 116.0 (CH); 116.5 (CH); 124.2 ($CH^{Ar3/5}$); 124.4 ($CH^{Ar3/5}$); 127.8 ($CH^{Ar3/5}$); 128.3 ($CH^{Ar3/5}$); 128.4 ($CH^{Ar3/5}$); 129.1 (CH^{Ar4}); 129.4 (CH^{Ar4}); 139.3 ($C^{Ar2/6}$); 139.5 ($C^{Ar2/6}$); 146.1 (C^{Ar}); 155.3 ($CC=N^{Rh}$); 161.7 ($CH=N^{Pd}$); 166.3 ($CH=N^{Rh}$); 179.5 (CO).

11.5. 7 Synthesis of $[L^2Pd(\eta^3\text{-}C_6H_9)Rh(CO)_2]BAr^F_4$ (3y)

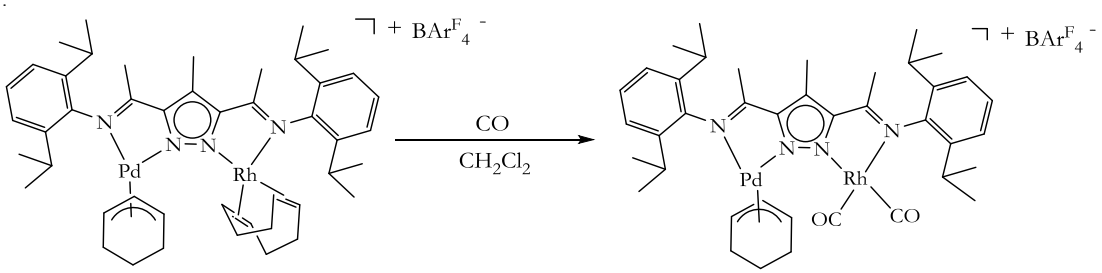

3u **3y**

Carbon monoxide (CO, 1 atm), was continuously bubbled through a CH_2Cl_2 solution (10 mL) of **3u** (14.0 mg, 8.0 μmol) in a schlenk flask for 20 minutes. The initial orange solution, gradually changed with time to a lemon green solution. This solution, however when exposed to the atmosphere, gradually reverts to orange. However, when kept under an atmosphere of CO, the

lemon green colour was persistent. A solution of the complex was kept in the referigerator for several days at -20 ºC. After this period, yellow crystalline solid material was isolated.

Yield:	6 mg, 44%
Molecular formula:	$C_{72}H_{64}BF_{24}N_4O_2RhPd$
Molecular weight:	1693.4 g/mol.
HRMS (TOF-ESI):	Calcd. For $C_{40}H_{52}N_4O_2PdRh$ (829.2189); Found: 829.2194.
MS (ESI, CH_2Cl_2) *m/z* (%):	829 (55%) $[M\text{-}BAr^F{}_4]^+$; 800 (5%)$[M\text{-}CO\text{-}BAr^F{}_4]^+$.
IR (ATR, cm^{-1}):	2931 (m); 2970 (m); 2093 (vs); 2032 (vs); 1611 (m); 1577 (m); 1465 (m); 1448 (m); 1354 (m); 1277 (vs); 1121 (vs); 901 (m); 840 (m); 685 (s); 670 (s).
^{1}H-NMR (CDCl3) δ:	1.04-1.06 (m, 2H, $CH_2{}^{Cy(allyl)}$); 1.07-1.39 (m, 24H, $CH_3{}^{iPr}$); 1.81 (m, 4H, $CH_2{}^{Cy(allyl)}$); 2.24 (s, 3H, CH_3C=N); 2.49 (s, 3H, $CH_3{}^{Pz4}$); 2.55 (s, 3H, CH_3C=N); 2.87-3.04 (m, 4H, CH^{iPr}); 4.30 (m, 2H, $CH^{Cy(allyl)}$); 5.62 (m, 1H, $CH^{Cy(allyl)}$); 7.27-7.31 (m, 6H, CH^{Ar}); 7.51 (s, 4H, CH^{BArF4}); 7.69 (s, 8H, CH^{BArF4}).
^{13}C{^{1}H} ($CDCl_3$) δ:	10.3 ($CH_3{}^{Pz4}$); 18.9 ($CH_2{}^{Cy(allyl)}$); 19.0 (*C*H_3C=N); 20.7 (*C*H_3C=N); 23.3 ($CH_3{}^{iPr}$); 23.6 ($CH_3{}^{iPr}$); 24.0 ($CH_3{}^{iPr}$); 24.1 (C^{CF3}); 24.6 (CF_3) 28.5 (CH^{iPr}); 28.6 (CH^{iPr}); 28.7 (CH^{iPr}); 28.8 (CH^{iPr}); 28.9 (CH^{iPr}); 29.8 ($CH_2{}^{Cy(allyl)}$); 79.6 ($CH^{Cy(allyl)}$); 80.0 ($CH^{Cy(allyl)}$); 107.0 (CH^{Ar}); 117.5 (CH^{BArF4}); 119.2; 122.7 (CH^{BArF4}); 122.8 (C^{Pz4}); 124.5 (CH^{Ar}); 124.6 (CH^{Ar}); 124.9 (CH^{Ar}); 125.0 (CH^{Ar}); 126.4 (CH^{BArF4}); 127.9 (CH^{Ar}); 128.7 (CH^{Ar}); 129.2 (CH^{Ar}); 134.9 (CH^{BArF4});138.5 (C^{Ar}); 138.6 (C^{Ar}); 138.7 (C^{Ar}); 138.8 (C^{Ar}); 138.9 (C^{Ar}); 142.8 (C^{Ar}); 143.7 (C^{Ar}); 160.8 (C^{Ar}); 162.1 (C^{Ar}); 162.8 (C^{Ar}); 170.7 (CH_3C=N^{Pd}); 175.5 (CH_3C=N^{Rh}).

11. 6 Homobimetallic rhodium complexes

11.6. 1 Synthesis of $[L^2Rh_2(CO)_4)]PF_6$ (3z1)

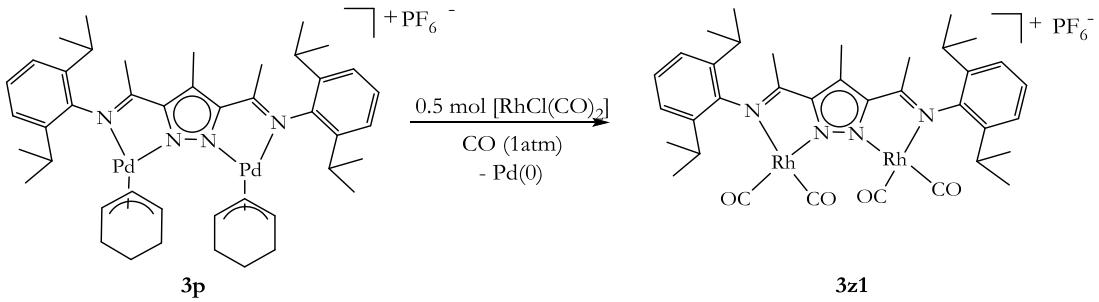

3p **3z1**

To a CH_2Cl_2 solution (10mL) of **3p** (10.0 mg, 0.01 mmol) was added 0.5 mol equivalent (1.90 mg, 0.05 mmol) of $[RhCl(CO)_2]_2$ with stirring under 1 atm of CO. A lemon green solution was formed after a few minutes. The formation of Pd(0) species is observed after 2 h. The reaction mixture was allowed to stir for 48 h, after this period, a black suspension was observed. This suspension when filtered over celite to yield a lemon green solution, which when evaporated, gives a lemon green powder.

Yield:	4.1 mg, 43%
Molecular formula:	$C_{36}H_{43}F_6N_4O_4PRh_2$
Molecular weight:	946.10 g/mol.
HRMS (TOF-ESI):	Calcd. For $C_{36}H_{43}N_4O4Rh_2$ (801.1394); Found: 801.1409.
MS (ESI, CH_2Cl_2) m/z (%):	801(100%)$[M\text{-}PF_6]^+$; 770(15%)$[M\text{-}CO\text{-}PF_6]^+$; 743 (25%) $[M\text{-}2CO\text{-}PF_6]$; 712 (35%)$[M\text{-}4CO+Na\text{-}PF_6]^+$.
IR (ATR, cm^{-1}):	2923 (s); 2963 (s); 2869 (s); 2475 (s); 1569 (vs); 1437 (vs); 1383 (m); 1365 (s); 1326 (s); 1254 (m); 1226 (m); 1098 (s); 1075 (s); 1038 (m); 803 (s); 777 (s).
^{1}H-NMR ($CDCl_3$) δ:	1.21 (d, $^3J_{HH}$ = 6.8 Hz, 12H, CH_3^{iPr}); 1.37 (d, $^3J_{HH}$ = 6.8 Hz, 12H, CH_3^{iPr}); 2.36 (s, 6H, CH_3C=N); 2.65 (s, 3H, CH_3^{Pz4}); 3. 08 (m, 4H, CH^{iPr}); 7.26-7.39 (m, 6H, CH^{Ar}).
$^{13}C\{^1H\}$ ($CDCl_3$) δ:	10.2 (CH_3^{Pz4}); 22.7 (CH_3C=N); 23.4 (CH_3C=N); 23.9 (CH_3^{iPr}); 25.2 (CH_3^{iPr}); 28.8 (CH^{iPr}); 124.8 (C^{Ar}) 126.4 ($C^{Pz3/5}$); 128.4 (C^{Ar}); 129.0 (C^{Ar}); 139.3 (C^{Ar}); 143.9 (C^{Ar}); 154.7 (CCH_3); 176.7 (CH_3C=N).

11.6. 2 Synthesis of $[L^2Rh_2(COD)_2]Cl$ ($3c_1$)

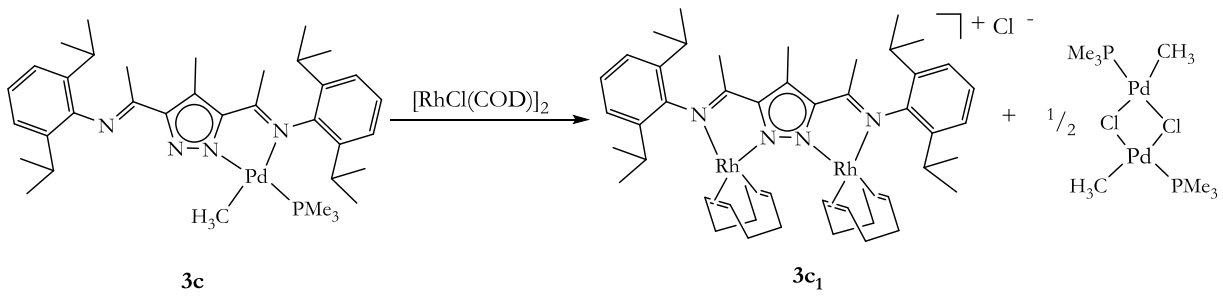

3c **$3c_1$**

To a CH_2Cl_2 solution (10 mL) of **3c** (100 mg, 0.15 mmol) was added 1 mol equivalent $[RhCl(COD)]_2$ (72.4 mg, 0.15 mmol) with stirring for 72 h. The bright yellow solution was filtered and the filtrate evaporated to obtain a yellow powder. The powder was washed with hexane (3x3 mL), and the solid dried in air. The solid was again dissolved in CH_2Cl_2 (2 mL) and slowly layered with hexane, precipitating a yellow solid in the process. The precipitate was filtered and dried in air.

Yield:	65 mg, 46%
Molecular formula:	$C_{48}H_{67}ClN_4Rh_2$
Molecular weight:	942.4 g/mol.
MS (ESI, CH_2Cl_2) m/z (%):	905 (30%) $[M\text{-}Cl]^+$; 695 (30%) $[M\text{-}Rh(COD)\text{-}Cl]^+$.
^{1}H-NMR ($CDCl_3$) δ:	1.23 (d, $^3J_{HH}$ = 6.8 Hz, 12H, CH_3^{iPr}); 1.32 (d, $^3J_{HH}$ = 6.8 Hz, 12H, CH_3^{iPr}); 2.36 (s, 6H, CH_3C=N); 2.65 (s, 3H, CH_3^{Pz4}); 2.33-2.52 (m, 8H, CH_2^{COD}); 3.10 (m, 4H, CH^{iPr}); 3.91 (br s, 8H, CH_2^{COD}); 4.24 (br s, 4H, CH^{COD}); 5.07 (br s, 4H, CH^{COD}); 7.16-7.39 (m, 6H, CH^{Ar}).
$^{13}C\{^1H\}$ ($CDCl_3$) δ:	11.40 (CH_3^{Pz4}); 18.8 (CH_3C=N); 19.4 (CH_3C=N); 22.3 (CH_3^{iPr}); 23.4 (CH_3^{iPr}); 23.8 (CH_3^{iPr}); 24.9 (CH_3^{iPr}); 28.0 (CH^{iPr}); 28.1 (CH^{iPr}); 30.0 (CH_2^{COD}); 30.6 (CH_2^{COD}); 81.7 (CH^{COD}); 81.8 (CH^{COD}); 83.5 (CH^{COD}); 83.6 (CH^{COD}); 120.9 (C^{Pz4}); 122.6 (CH^{Ar}) ; 122.7 (CH^{Ar}); 123.7 (CH^{Ar}); 126.7 (CH^{Ar}); 128.7 (C^{Ar}); 135.9 (C^{Ar}); 140.4 (C^{Ar}); 147.2 (C^{Ar}); 163.8 (C^{Pz}); 172.5 (CH_3C=N).

11.6. 3 Synthesis of $[L^2{}_2Rh_2(OAc)_2(MeOH)_2](PF_6)_2$ (4e)

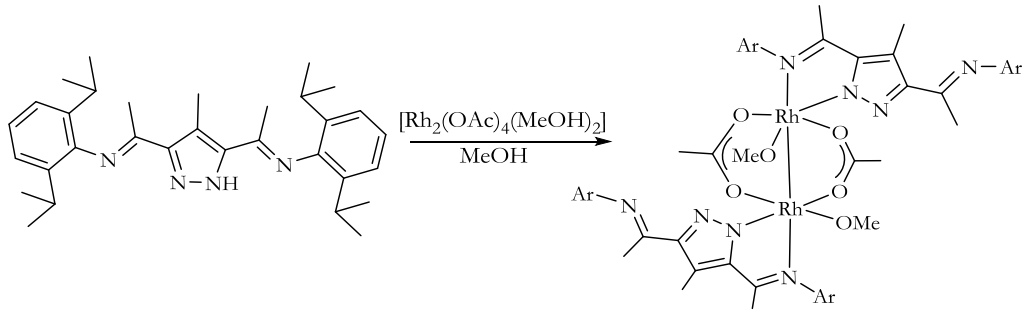

4e

To a methanolic solution (10 mL) of **HL²** (20.0 mg, 41.2 μmol) was added a 1.1 mol equivalent $[Rh_2(OAc)_4(MeOH)_2]$ (20.0 mg, 43.7 μmol) with stirring for 18h to form a dark red solution. The solution was filtered and allowed to slowly evaporate at room temperature for 48 h, after which the product was isolated as dark red crystalline solids.

Yield:	11 mg, 16%
Molecular formula:	$C_{70}H_{97}F_{12}N_8O_6P_2Rh_2$
Molecular weight:	1642.3 g/mol.
MS (ESI, CH_2Cl_2) *m/z* (%):	484 (100%) $[L]^+$
IR (ATR, cm^{-1}):	2959 (m); 2926 (m); 1637 (vs); 1583 (vs); 1375 (s); 1365 (s); 1436 (vs); 1383 (s); 1184 (s); 1097 (vs); 692 (vs); 510 (s); 497 (vs).
^{1}H-NMR ($CDCl_3$) δ:	0.98 (d, $^3J_{HH}$ = 6.8 Hz, 12H, $CH_3{}^{iPr}$); 1.02 (d, $^3J_{HH}$ = 6.8 Hz, 12H, $CH_3{}^{iPr}$); 1.19 (d, $^3J_{HH}$ = 6.8 Hz, 24H, $CH_3{}^{iPr}$); 1.35 (s, 3H, $CH_3{}^{OAc}$); 1.55 (s, 6H, $CH_3{}^{OAc}$); 2.03 (s, 6H, CH_3C=N); 2.52 (m, 4H, CH^{iPr}); 2.56 (s, 6H, CH_3C=N); 2.81 (s, 6H, $CH_3{}^{Pz4}$); 3.29 (m, 4H, CH^{iPr}); 7.00 (s, 6H, CH^{Ar}); 7.24 (s, 6H, CH^{Ar}).
^{13}C{^{1}H} ($CDCl_3$) δ:	11.6 ($CH_3{}^{Pz4}$); 20.2 (CH_3C=N): 21.2 (CH_3C=N); 23.8 ($CH_3{}^{iPr}$); 24.4 ($CH_3{}^{iPr}$); 24.6 ($CH_3{}^{iPr}$); 24.8 ($CH_3{}^{iPr}$); 27.7 (CH^{iPr}); 28.1 (CH^{iPr}); 121.4 (C^{Pz4}); 122.9 (CH^{Ar}); 123.4 (CH^{Ar}); 123.7 (CH^{Ar}); 125.3 (CH^{Ar}); 135.7 (C^{Ar}); 141.2 (C^{Ar}); 142.6 (C^{Ar}); 145.1 (CH^{Ar}); 148.4 (CH^{Ar}); 154.6 (CH^{Ar}); 158.7 (CH^{Ar}); 166.2 (CH_3C=N); 186.1 (C^{OAc}); 191.6 (C^{OAc}).

11. 7 Tetranuclear zinc(II) complexes

11.7. 1 Synthesis of $[L^1_2Zn_4(\mu\text{-}OAc)_6]$ (4a)

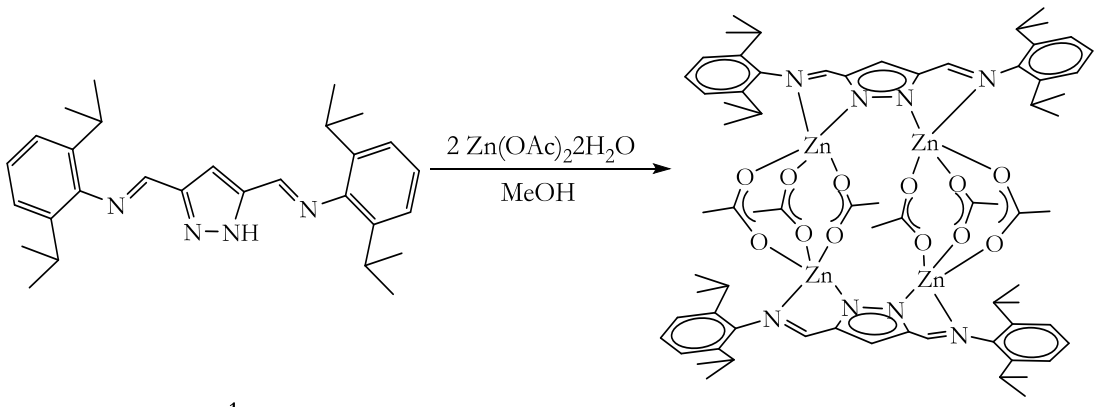

HL^1 **4a**

A Schlenk flask was equipped with a magnetic stirrer, evacuated, and filled with nitrogen. The flask was charged with $Zn(OAc)_2 \cdot 2H_2O$ (200 mg, 0.90 mmol) in MeOH (10 mL). The ligand, **HL^1** (200 mg, 0.45 mmol) was added to the reaction mixture and the mixture stirred at room temperature for 48 h. The solvent was evaporated, dissolved in CH_2Cl_2, and allowed to slowly evaporate at room temperature. The product was obtained as white crystalline solid. The solid was isolated and dried overnight in air.

Yield: 230 mg, 73 %

Molecular formula: $C_{70}H_{92}N_8O_{12}Zn_4$

Molecular weight: 1501.1 g/mol.

MS (ESI, CH_3OH) *m/z* (%):565 (40%) $[LZn(OAc)]^+$; 688 (60%) $[LZn_2(OAc)_2+2H]^+$; 947 (15%) $[L_2Zn\text{-}H]^+$; 1073 (8%) $[L_2Zn_2(OAc)]^+$.

IR (ATR, cm^{-1}): 2961 (m); 2929 (m); 2870 (m); 1585 (vs); 1439 (vs); 1385 (m); 1257 (m); 1188 (m); 1118 (m); 1061 (m); 875 (m); 799 (s); 756 (s); 618 (m); 481 (m).

^{1}H-NMR ($CDCl_3$) δ: 1.13-1.20 (m, 48H, CH_3^{iPr}); 1.84 (s, 18H, CH_3^{OAc}); 3.08 (m, 8H, CH^{iPr}); 7.15-7.18 (m, 14H, CH^{Pz}, CH^{Ar}); 8.23 (d, *J* = 7.7 Hz, 4H, CH=N).

$^{13}C\{^1H\}$ ($CDCl_3$) δ: 22.6 (CH_3^{iPr}); 23.9 (CH_3^{iPr}); 28.0 (CH^{iPr}); 118.7 (CH^{Ar}); 122.9 (CH^{Ar}); 123.1 (CH^{Ar}); 124.6 (CH^{Ar}); 125.3 (CH^{Ar}); 132.6 (C^{Ar}); 138.2 (C^{Ar}); 140.3 (C^{Ar}); 153.8 (C^{Pz}); imine (not observed); 180.3 (C^{OAc}).

Elemental analysis: Calcd. For $C_{70}H_{92}N_8O_{12}Zn_4 \cdot 0.5CH_2Cl_2$: (C) 54.93 (H) 6.08 (N) 7.27: Found: (C) 54.51 (H) 6.03 (N) 7.21.

Subsequent complexes were prepared in like manner.

11.7. 2 Synthesis of $[L^2{}_2Zn_4(\mu\text{-}OAc)_6]$ (4b)

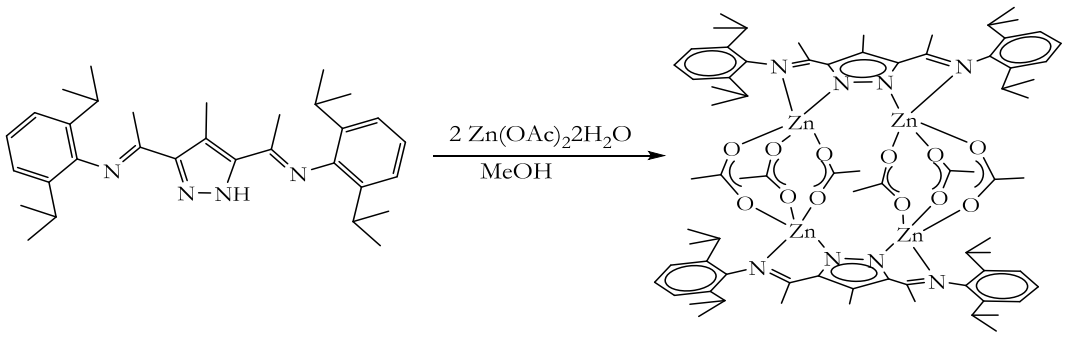

HL^2 **4b**

To a stirring methanolic solution (15 mL) of $Zn(OAc)_2{\cdot}2H_2O$ (180 mg, 0.83 mmol) was added 0.5 mol equivalent of the ligand, **HL^2** (200 mg, 0.41 mmol) with stirring for 48h. The product was isolated as a white crystalline solid from the slow evaporation of dichloromethane solution of the complex.

Yield:	230 mg, 73 %
Molecular formula:	$C_{76}H_{104}N_8O_{12}Zn_4$
Molecular weight:	1585.3 g/mol.
MS (ESI, CH_3OH) m/z (%):	1496 (10%) $[L_2Zn_4(OAc)_4MeOH]^+$; 1469 (100%) $[L_2Zn_4(OAc)_3(MeOH)_2]^+$; 731 (20%) $[LZn_2(OAc)_2]^+$.
IR (ATR, cm^{-1}):	2963 (m); 2928 (m); 2870 (m); 1603 (vs); 1430 (vs); 1365 (m); 1231 (m); 1190 (m); 1065 (m); 618 (m); 774 (s); 670 (m); 558 (m).
^{1}H-NMR ($CDCl_3$) δ:	1.06-1.14 (m, 48H, $CH_3{}^{iPr}$); 2.22 (s, 30H, $CH_3C{=}N$, CH_3O^{Ac}); 2.63 (s, 6H, $CH_3{}^{Pz4}$); 2.94 (m, 8H, CH^{iPr}); 7.08-7.14 (m, 12H, CH^{Ar}).
$^{13}C\{^1H\}$ ($CDCl_3$) δ:	12.1 ($CH_3{}^{Pz4}$); 20.3; 22.6; 23.9; 24.2; 28.0; 123.4 (C^{OAc}); 139.2; 147.7; 165.7; 179.9 (C^{OAc}).
Elemental analysis:	Calcd. For $C_{76}H_{104}N_8O_{12}Zn_4$: (C) 57.65 (H) 6.62 (N) 7.08; Found: (C) 57.34 (H) 5.39 (N) 7.35.

11.7. 3 Synthesis of $[L^3{}_2Zn_4(\mu\text{-}OAc)_6]$ (4c)

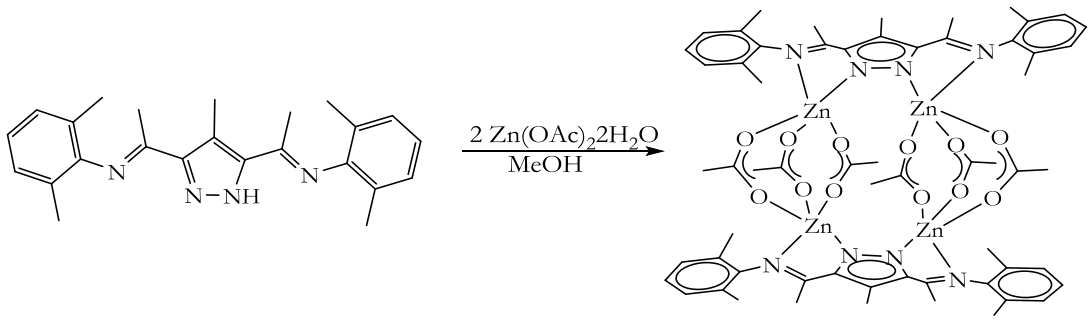

HL^3 **4c**

To a stirring methanolic solution (15 mL) of $Zn(OAc)_2{\cdot}2H_2O$ (270 mg, 1.23 mmol) was added 0.5 mol equivalent **HL^3** (200 mg, 0.63 mmol) with stirring for 48 h. The product was isolated as a white crystalline solid from the slow evaporation of a 50:50 mixture CH_2Cl_2/CH_3OH solution of the complex.

Yield:	300 mg, 72 %
Molecular formula:	$C_{60}H_{72}N_8O_{12}Zn_4$
Molecular weight:	1358.8 g/mol.
MS (ESI, CH_3OH) m/z (%):	1299 (10%) $[L_2Zn_4(OAc)_5]^+$; 934 (100%) $[L_2Zn(OAc)]^+$.
IR (ATR, cm^{-1}):	2922 (br); 1590 (vs); 1423 (vs); 1320 (s); 1201 (s); 1095 (m); 1065 (m); 1024 (m); 970 (m); 784 (m);767 (s); 666 (s); 618 (s); 569 (m).
^{1}H-NMR ($CDCl_3$) δ:	1.78 (s, 18H, CH_3^{OAc}); 2.12 (s, 24H, CH_3^{Ar}); 2.20 (s, 12H; $CH_3C{=}N$); 2.65 (s, 6H, CH_3^{Pz4}); 6.99-7.07 (m, 12H, CH^{Ar}).
$^{13}C\{^1H\}$ ($CDCl_3$) δ:	12.0 (CH_3^{Pz4}); 18.0 (CH_3^{Ar}); 18.8 ($CH_3^{Pz3/5}$); 22.3; 118.6 (C^{Ar}); 124.9 (C^{Ar}); 128.1 (CH^{Ar}); 129.1 (CH^{Ar}); 179.4 (C^{OAc}).
Elemental analysis:	Calcd. For $C_{60}H_{72}N_8O_{12}Zn_4{\cdot}CH_2Cl_2$: (C) 50.75 (H) 5.17 (N) 7.76; Found: (C) 50.71 (H) 5.39 (N) 7.92.

11.7. 4 Synthesis of $[L^4{}_2Zn_4(\mu\text{-}OAc)_6]$ (4d)

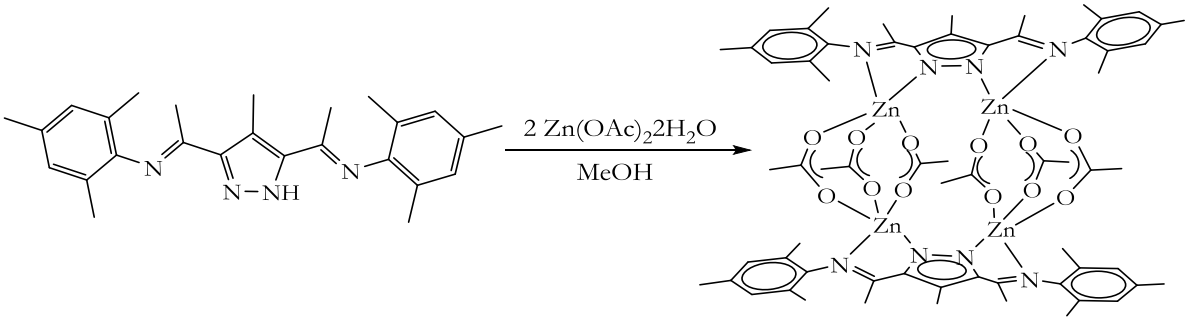

HL⁴ **4d**

To a stirring methanolic solution (10 mL) of $Zn(OAc)_2 \cdot 2H_2O$ [270 mg, 1.23 mmol] was added 0.5 mol equivalent of **HL⁴** (200 mg, 0.63 mmol) with stirring for 48 h. The product was isolated as a white crystalline solid from the slow evaporation of a methanolic solution of the complex.

Yield:	300 mg, 69%
Molecular formula:	$C_{64}H_{80}N_8O_{12}Zn_4$
Molecular weight:	1414.9 g/mol.
MS (ESI, CH_3OH) *m/z* (%):	991.4 (100%) $[L_2Zn_2(MeOH)_2+H]^+$.
IR (ATR, cm^{-1}):	2295 (br); 2916 (m); 1607 (vs); 1417 (vs); 1316 (s); 1210 (vs); 1031 (m); 851 (vs); 664 (vs).
^{1}H-NMR ($CDCl_3$) δ:	1.69 (s, 18H, $CH_3{}^{OAc}$); 2.09 (s, 24H, $CH_3{}^{Ar}$); 2.18 (s, 12H; CH_3C=N); 2.29 (s, 12H, $CH_3{}^{Ar}$); 2.62 (s, 6H, $CH_3{}^{Pz4}$); 6.87 (br s, 8H, CH^{Ar}).
$^{13}C\{^1H\}$ ($CDCl_3$) δ:	12.0 ($CH_3{}^{Pz4}$); 17.9 (CH_3); 18.7 (CH_3); 20.8 ($CH_3{}^{Ar}$); 22.3 ($CH_3{}^{OAc}$); 118.7 (CH^{Ar}); 128.7 (C^{Ar}); 139.9 (C^{Ar}); 165.8 (CH_3C=N) 179.5 (C^{OAc}).
Elemental analysis:	Calcd. For $C_{64}H_{80}N_8O_{12}Zn_4 \cdot CH_2Cl_2$: (C) 52.05 (H) 5.51 (N) 7.47; Found: (C) 52.34 (H) 5.81 (N) 7.67.

11. 8 Bis-cyclopentadienyl/indenyl/fluorenyl-tethered pyrazolyl ligands

11.8. 1 Synthesis of H_3L^5

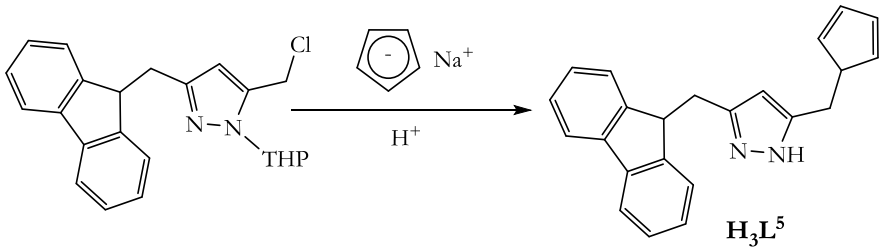

H_3L^5

To a stirring THF solution (15 mL) of NaCp (0.17 g, 2.61 mmol) cooled to -40ºC was added via cannula, a THF solution of 3-((9H-fluoren-9-yl)methyl)-5-(chloromethyl)-1-(tetrahydro-2H-pyran-2-yl)-1H-pyrazole (1.02 g, 2.7 mmol). The reaction was warmed up to room temperature and stirred overnight. A dark brown solution was formed. The solvent was evaporated, re-dissolved in CH_2Cl_2, and washed with H_2O (3x5 mL). The organic fraction was dried over $MgSO_4$ and evaporated to dry. The orange solid obtained was re-dissolved in C_2H_5OH, 5 mL ethanolic HCl added and reflux for several days to complete THP deprotection. The product was obtained as an orange solid.

Yield	890 mg, 81%
Molecular formula:	$C_{23}H_{20}N_2$
Molecular weight:	324.5 g/mol.
MS (EI) *m/z* (%):	324 (100%) $[M]^+$; 259 (55%) $[M\text{-}Cp]^+$.
IR (ATR, cm^{-1}):	2927 (br); 2949 (m); 1560 (w); 1533 (vs); 1419 (s);1255 (w); 1048 (m); 862 (s); 750 (m).
^{1}H-NMR ($CDCl_3$) δ:	3.15 (d, $^3J_{HH}$ = 6.9 Hz, 2H, CH_2, pyrazol-CH_2-Cp); 3.27 (d, J = 6.8.Hz, 2H, CH_2, pyrazol-CH_2-fluorene); 4.10 (t, $^3J_{HH}$ = 6.8 Hz, 1H, CH, H-1-Cp); 4.30 (t, $^3J_{HH}$ = 6.9 Hz, 1H, CH, H-9-fluorene); 5.96 (s, 1H, CH, H-4-pyrazol); 7.22-7.36 (m, 8H, CH, H-Ar); 7.70-7.74 (m, 4H, CH, H-Cp); NH-not observed.
$^{13}C\{^1H\}$ ($CDCl_3$) δ:	30.8 (CH_2, pyrazol-CH_2-fluorene); 32.1 (CH_2, pyrazol-CH_2-Cp); 47.1 (CH, C-9-fluorene); 60.5, 61.0 (CH, C-1-Cp); 120.0 (CH, C-4/C-5-fluorene); 124.1 (CH, C-1/C-8-fluorene); 127.2, 127.5 (CH, C-2/C-3/C-6/C-7-fluorene); 141.1 (C, C-4/fluorene); 146.3 (**C**H, C-2/C-3/C-4/C-5-Cp); 146.3 (C, C-3/C-5-pyrazol).

11.8. 2 Synthesis of H_3L^6

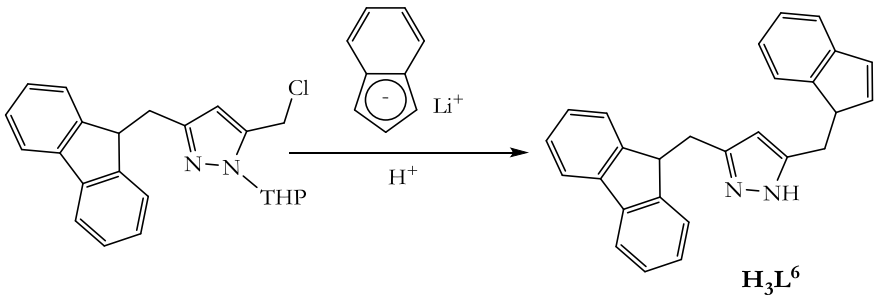

H_3L^6

A lithium salt solution of indene was prepared by treating indene (1 mL, 8.6 mmol) with (3.4 mL, 2.5 M BuLi, 8.5 mmol) at -65°C and allowed to warm up to room temperature over 18 h. To this red lithium salt solution was added dropwise 3-((9H-fluoren-9-yl)methyl)-5-(chloromethyl)-1-(tetrahydro-2H-pyran-2-yl)-1H-pyrazole (3.2 g, 8.4 mmol) with stirring for 18 h, after which the red colour was discharged. The reaction was quenched, followed by evaporation of all volatiles, which gave the THP protected product as a brown solid. This solid was dissolved in ethanol and 5 mL ethanolic HCl added. Complete deprotection was obtained after refluxing the ethanolic solution for several days. Addition of hexane to a concentrated CH_2Cl_2 solution of the ligand precipitates the ligand as an orange solid.

Yield:	2.8 g, 89%
Molecular formula:	$C_{27}H_{22}N_2$
Molecular weight:	374.5 g/mol.
MS (EI) m/z (%):	374 (100%) $[M]^+$.
IR (ATR, cm^{-1}):	2923 (br); 2957 (m); 1566 (w); 1533 (vs); 1424 (s);1255 (w); 1048 (m); 864 (s); 756 (m).
^{1}H-NMR ($CDCl_3$) δ:	3.19 (d, $^3J_{HH}$ = 7.0 Hz, 2H, CH_2, Pz-CH_2-fluorene); 3.36 (s, 2H, CH_2, H-1-indene); 3.87 (s, 2H, CH_2, pyrazol-CH_2-indene); 4.27 (t, 1H, $^3J_{HH}$ = 6.9 Hz, CH, H-9-fluorene); 5.84 (s, 1H, CH, H-4-pyrazol); 6.17 (s, 1H, CH, H-2-indene); 7.13-7.42 (m, 12H, CH, CH^{Ar}); 7.47 (d, $^3J_{HH}$ = 6.9 Hz, 1H, CH, H-4-indene); 7.71 (d, $^3J_{HH}$ =7.6 Hz, 2H, CH, H-4/H-5-fluorene).
^{13}C-NMR ($CDCl_3$) δ:	26.3 (CH_2, pyrazol-CH_2-indene); 30.9 (CH_2, pyrazol-CH_2-fluorene); 37.7 (CH_2, C-1-indene); 47.3 (CH, C-9-fluorene); 104.4 (CH, C-4-pyrazol); 119.3 (CH, C-Ar); 120.0 (CH, C-4/C-5-

fluorene); 123.7 (CH, C-4-indene); 124.5 (CH, C-Ar); 126.1 (CH, C-1/C-8-fluorene); 126.9 (CH, C-Ar); 127.0, 127.3 (CH, C-2/C-3/C-6/C-7-fluorene); 130.0 (CH, C-2-indene); 140.9 (C, C-3-indene); 141.4 (C, C-4-fluorene); 144.4, 144.7 (C, C-3/C-7-indene); 146.3 (C, C-3/C-5-pyrazol).

The synthesis of **HL**[7] and **HL**[8] have already been reported and would not be covered here.

11. 9 Synthesis of trimethylsilyl derivatives

H_3L^5: X = fluorenyl, Y = cyclopentadienyl
H_3L^6: X = fluorenyl, Y = indenyl
H_3L^7: X = fluorenyl, Y = fluorenyl
H_3L^8: X = indenyl, Y = indenyl

HL^9: X = fluorenyl, Y = indenyl
HL^{10}: X = fluorenyl, Y = fluorenyl
HL^{11}: X = indenyl, Y = indenyl

General procedure for preparation of precursors

A dry THF solution (20 mL) of 3-(fluoren-9-ylmethyl), 5-(inden-9-ylmethyl)-1*H*-pyrazol (HL^6) (0.59 g, 1.58 mmol, 1.00 Eq.) was cooled to –65°C. To this was added *n*-BuLi (2.5 M, 1.9 mL, 4.7 mmol, 3.0 Eq.), and the reaction gradually warmed to 0°C. A dark red solution was formed which was allowed to stir further for 14 h at room temperature. To the dark red solution was added TMSCl (0.66 g, 4.7 mmol, 3.0 Eq.) dropwise. The red lithium salt solution was immediately discharged to a colourless solution. The reaction was allowed to stir at room temperature overnight. The solution was evaporated, redissolved in toluene and the off-white solid of LiCl filtered. The toluene solution was evaporated, to yield the product as an off-white crystalline solid.

11.9. 1 Synthesis of L^9

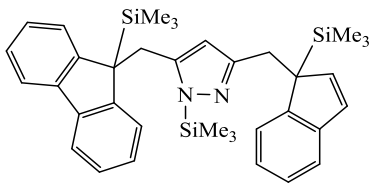

L^9

Using the general procedure, the product was obtained as an off-white crystalline solid.

Yield:	250 mg, 42 %
Molecular formula:	$C_{36}H_{46}N_2Si_3$
Molecular weight:	591.0 g/mol.
MS (EI) *m/z* (%):	590 (65%) $[M]^+$; 519 (100%) $[M\text{-}SiMe_3]^+$.
IR (ATR, cm^{-1}):	3033 (br); 2959 (s); 1581 (s); 1436 (vs); 1444 (vs) 1249 (m); 1010 (m); 817 (m) 725 (vs); 622 (vs).
^{1}H-NMR ($CDCl_3$) δ:	-0.30 (s, 9H, $SiMe_3$); -0.16 (s, 9H, $SiMe_3$); -0.12 (s, 9H, CH_3, $SiMe_3$); 2.37 (s, 2H, CH_2, pyrazol-CH_2-fluorene); 3.30 (s, 2H, CH_2, H-1-indene); 3.61 (s, 2H, CH_2, pyrazol-CH_2-indene); 3.68 (1H, CH, H-9-fluorene); 6.02 (s, 1H, CH, H-2-indene); 7.00-7.85 (m, 11H, CH^{Ar}).
^{13}C-NMR ($CDCl_3$) δ:	-6.02 (C-$SiMe_3$); -0.00 (N-$SiMe_3$); 19.5 (CH_2, pyrazol-CH_2-indene); 24.2 (CH_2, pyrazol-CH_2-fluorene); 26.2 (CH_2, C-1-indene); 42.6 (C, C-9-fluorene); 102.0 (CH, C-4-pyrazol); 117.2-126.3 (CH, C^{Ar}); 127.0, 129.7 (CH, C-2/C-3/C-6/C-7-fluorene); 130.0 (CH, C-2-indene); 138.4 (C, C-3-indene); 141.7 (C, C-4-fluorene); 144.0 (C, C-3/C-7-indene); 145.5 (C, C-3/C-5-pyrazole).

11.9. 2 Synthesis of L^{10}

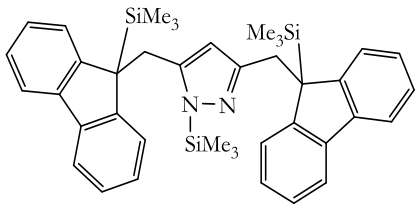

L^{10}

Following a similar synthetic procedure as done for the general procedure, using 3,5-Bis(fluoren-9-ylmethyl)-1*H*-pyrazol (HL^7) (0.50 g, 1.2 mmol, 1.00 Eq.) in dry THF (15 mL) with n-BuLi (2.5 M, 1.4 mL, 3.6 mmol, 3.0 Eq.) and TMSCl (0.49 g, 3.6 mmol, 3.0 Eq.). The product was obtained as a white crystalline solid.

Yield:	310 mg, 40%
Molecular formula:	$C_{40}H_{48}N_2Si_3$
Molecular weight:	641.1 g/mol.
MS (EI) *m/z* (%):	640 (100%) [M^+]; 568 (40%) [M-$SiMe_3$] $^+$.
IR (ATR, cm^{-1}):	3207 (m); 3039 (br); 3060 (s); 2955 (s); 1575 (s); 1437 (vs); 1447 (vs) 1249 (m); 1007 (m); 817 (m) 730 (vs); 623 (vs).
^{1}H-NMR ($CDCl_3$) δ:	-0.12, -0.28, -0.41 (s, 27H, CH_3, $SiMe_3$); 3.25 (s, 4H, CH_2, pyrazol-CH_2-fluorene); 3.35-3.90 (t, $^3J_{HH}$ = 7 Hz, 2H, CH, H-9-fluorene); 4.52 (s, 1H, CH^{Pz}); 7.05-7.83 (m, 14H, CH^{Ar}).
$^{13}C\{^1H\}$ ($CDCl_3$) δ:	-2.04, -4.06 (C, $SiMe_3$); 26.3 (CH_2, pyrazol-CH_2-fluorene); 47.7 (C, C-9-fluorene); 102.6 (CH, C-4-pyrazol); 120.0 (CH, C-4/C-5-fluorene); 123.0 (CH, C-1/C-8-fluorene); 125.8; 126.5 (CH, C-2/C-3/C-6/C-7-fluorene); 139.9 (C, C-4a/C-4b-fluorene); 146.1 (C, C-3/C-5-pyrazol).

11.9. 3 Synthesis of HL[11]

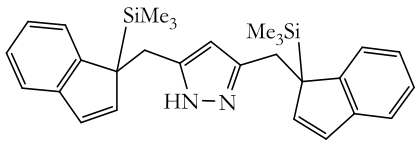

HL[11]

Following the general procedure a using a THF solution (20 mL) of 3,5-Bis(inden-9-ylmethyl)-1*H*-pyrazol (HL[8]) (0.54 g, 1,7 mmol, 1.00 Eq.), with n-BuLi (2.5 M, 2.0 mL, 5.0 mmol, 3.0 Eq.) and TMSCl (0.70 g, 5.0 mmol, 3.0 Eq.). The product was obtained as a light yellow powder

Yield:	260 mg, 33%
Molecular formula:	$C_{29}H_{36}N_2Si_2$
Molecular weight:	468.8 g/mol.
EI (MS) *m/z* (%):	468 (100%) $[M]^+$.
IR (ATR, cm^{-1}):	2929 (w); 2957 (m); 1566 (m); 1532 (s); 1424 (vs); 1255 (m); 1048 (m); 864 (vs); 756 (m).
^{1}H-NMR ($CDCl_3$) δ:	-0.08 (s, 18H, $SiMe_3$); 3.41 (s, 4H, CH_2, H-1-indene); 3.57 (s, 4H, CH_2, pyrazol-CH_2-indene); 3.73 (s, 1H, CH, H-4-pyrazol); 3.94 (s, 2H, CH, H-2-indene); 7.01-7.28 (m, 6H, CH^{Ar}); 7.51 (s, 2H, CH, H-4-indene).

11. 10 Heteroleptic N-Heterocyclic carbene and fluorenyl/indenyl pyrazolyl tethered derivatives

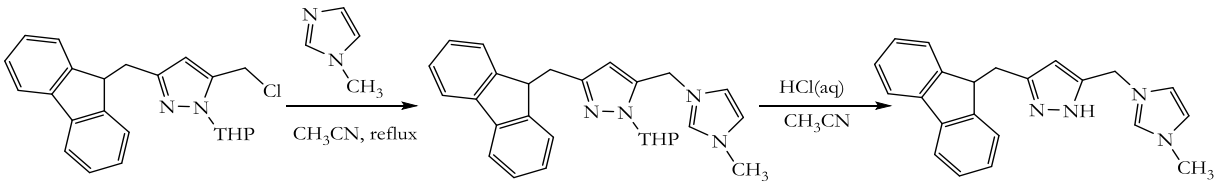

General procedure:

In a typical experiment, an acetonitrile solution (40 mL) of the mono substituted fluorenyl derivative 3-((9H-fluoren-9-yl)methyl)-5-(chloromethyl)-1-(tetrahydro-2H-pyran-2-yl)-1H-pyrazole (0.75 g, 2.0 mmol) was added 0.50 g of Na_2CO_3. To this mixture was added methyl imidazole (1 mL, 12.0 mmol) and the mixture was refluxed with stirring for 72 h. After this period, the volatile components were removed under vacuum to obtain a yellow oil residue. This oil was dissolved in 5 mL of CH_2Cl_2 and 40 mL of petroleum ether added dropwise to precipitate a yellow oil once again. The petroleum ether was decanted and the yellow oil dried under vacuum to obtain a yellow solid. The resulting solid was dried azeotropically with toluene and isolated as a white powder, rapidly forming oil on exposure to air. The THP protection was removed by adding 5 mL of ethanolic HCl and refluxing the solution in CH_3CN for 72 h. The analytically pure THP free product precipitates out of solution, filtered and dried under vacuum for several hours.

11.10. 1 Synthesis of H_3L^{12}

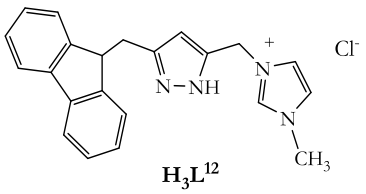

H_3L^{12}

Using the general synthetic procedure, the product was obtained as a white hygroscopic solid.

Yield: 150 mg, 85%

Molecular formula: $C_{22}H_{21}N_4Cl$

Molecular weight:	376.9 g/mol.
MS (ESI, DMSO) *m/z* (%):	383 (100%) $[M\text{-}Cl+K]^+$
EI:	340 (35%) $[M+H\text{-}Cl]^+$, 326 (100%) $[M\text{-}Me\text{-}Cl]^+$.
IR (ATR, cm^{-1}):	2922 (m); 1467 (m); 1344 (m); 1185(m); 1266 (s); 1003 (m); 751 (vs); 721 (m).
^1H(DMSO-d_6) δ:	3.16 (d, $^2J_{HH}$ = 6 Hz, 2H, CH_2); 3.87 (s, 3H, CH_3^{Imdz}); 4.33 (t, 1H, $^3J_{HH}$ = 6 Hz, CH^{Fluor}); 5.35 (s, 2H, Pz-CH_2-Imdz); 5.94 (s, 1H, CH^{Pz}); 7.2-7.87 (m, 10H, CH^{Ar}); 9.20 (s, 1H, CH^{Imdz})
$^{13}C\{^1H\}$ (DMSO-d_6) δ:	28.9 (Pz-CH_2-fluorene) 34.1 (N-CH_3); 45.9 (Pz-CH_2-Imdz); 46.3 (CH^{Fluor}); 103.3 (CH^{Pz4}); 124.5, 126.9, 127.3,136.5, 140.3, 143.2, 144.5 (C^{Pz5}), 146.0 (C^{Pz3}).
Elemental analysis :	Calcd. For $C_{22}H_{21}ClN_4 \cdot HCl$: (C) 63.93 (H) 5.36 (N) 13.55; Found: (C) 63.53 (H) 5.42 (N) 13.46.

11.10. 2 Synthesis of H_3L^{13}

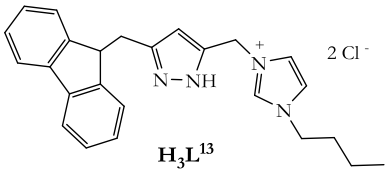

H_3L^{13}

Using the general procedure, 3-((9H-fluoren-9-yl)methyl)-5-(chloromethyl)-1-(tetrahydro-2H-pyran-2-yl)-1H pyrazole (3.0 g, 8.0 mmol) was treated with 1-butyl-1H-imidazole (1.5 g, 12.0 mmol) in acetonitrile under refluxing conditions. The product obtained as a yellow hygroscopic oil.

Yield:	2.1 g, 62 %
Molecular formula:	$C_{25}H_{28}N_4Cl_2$
Molecular weight:	455.3 g/mol.
MS (ESI, DMSO) *m/z* (%):	383 (100%) $[M\text{-}Cl]^+$.
IR (ATR, cm^{-1}):	3073 (m); 2933 (m); 2259 (m); 2251 (br); 1714 (br); 1594 (w); 1560 (s); 1447 (vs); 1287 (m); 1172 (s); 1158 (s); 1105 (m); 632 (m); 730 (vs); 754 (vs); 742 (s).

^{1}H-NMR (DMSO-d_6)	0.86 (t, $^{3}J_{HH}$ = 7.3 Hz, 3H, CH_3); 1.13-1.39 (m, 2H, CH_2); 1.63-1.88 (m, 2H, $CH_2^{n\text{-}Bu}$); 3.17 (d, $^{3}J_{HH}$ = 7.0 Hz, 2H, Pz-CH_2-fluorene); 4.19 (t, $^{3}J_{HH}$ = 7.1 Hz, 2H, CH_2); 4.34 (t, $^{3}J_{HH}$ = 6.7 Hz, 1H, CH^{Fluor}); 5.37 (s, 2H, Pz-CH_2-Imdz); 5.95 (s, 1H, CH^{Pz4}); 7.02-7.99 (m, 10H, H^{Imdz}- Ar^{H}); 7.84 (d, $^{3}J_{HH}$= 7.6 Hz, 2H, CH^{Fluor}); 9.41 (s, 1H, CH^{Imdz}).
^{13}C{^{1}H} (DMSO-d_6) δ	:13.2 (CH_3CH_2-); 18.1 ($CH_2CH_2CH_3$); 29.0 (fluorene-CH_2-Pz); 31.4 (-$CH_2CH_2CH_2$-); 45.9 (Pz-CH_2-Imdz); 46.3 (CH^{Fluor}); 48.6 (N-CH_2CH_2-); 103.4 (CH^{Pz4}); 120.0; 122.5 (CH^{Ar}); 124.5 (CH^{Ar}); 126.9 (CH^{Ar}); 127.3; 136.1 (CH^{Imdz}); 140.3; 143.4; 144.2 (C^{Pz5}); 146.0 (C^{Pz3}).
Elemental analysis :	Calcd. For $C_{25}H_{27}ClN_4 \cdot H_2O \cdot HCl$: (C) 64.65 (H) 6.29 (N) 12.06; Found: (C) 63.81 (H) 6.11 (N) 12.66.

11.10. 3 Synthesis of H_3L^{14}

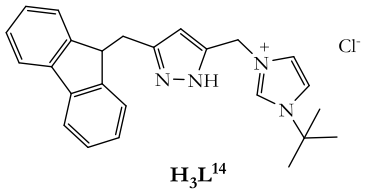

H_3L^{14}

Using 3-((9H-fluoren-9-yl)methyl)-5-(chloromethyl)-1-(tetrahydro-2H-pyran-2-yl)-1H pyrazole (4.0 g, 10.0 mmol) with 1-tert butyl-1H-imidazole (2.0 g, 15.0 mmol) in acetonitrile under refluxing for a week. The product obtained as a pale yellow solid.

Yield:	1.5 g, 30 %
Molecular formula:	$C_{25}H_{27}N_4Cl$
Molecular weight:	419.0 g/mol.
MS (ESI, DMSO) m/z (%):	383 (100%) $[M\text{-}Cl]^+$, 327 (27%) $[M\text{-}^{t}Bu\text{-}Cl]^+$, 259 (11%) [M-Imdz-Cl]$^+$.
IR (ATR, cm^{-1}):	3167 (br); 2983 (m); 1551 (m); 1449 (m); 1379 (s); 1232 (m); 1220 (s); 1127 (s); 829 (vs); 739 (vs) 557 (vs).

^{1}H-NMR (DMSO-d_6) δ: 1.59 (s, 9H, CH_3^{tBu}); 3.18 (d, $^{3}J_{HH}$ = 6.9 Hz, 2H, fluorene-CH_2-Pz); 4.34 (t, $^{3}J_{HH}$ = 6.9 Hz, 1H, fluorene-CH_2-Pz); 5.34 (s, 2H, Imdz-CH_2-Pz); 5.94 (s, 1H, CH^{Pz}); 7.20-7.40 (m, 6H, CH^{Fluor}); 7.67 (t, 1H, $^{4}J_{HH}$ = 1.8 Hz, CH^{Imdz}); 7.85 (d, $^{3}J_{HH}$ = 7.5 Hz, 2H, CH^{Fluor}); 8.06 (t, $^{4}J_{HH}$ = 1.8 Hz, 1H, CH^{Imdz}); 9.56 (t, $^{4}J_{HH}$ = 1.8 Hz, 1H, CH^{Imdz}); 15.08 (s, 1H, NH^{pz}).

^{13}C{^{1}H}(DMSO-d_6): 29.0 (CH_3^{tBu}); 29.1 (fluorene-CH_2-Pz); 46.0 (Imdz-CH_2-Pz); 46.4 (fluorene-CH_2-Pz); 54.9, 103.3 (CH^{Pz}); 120.0, 120.4, 122.5, 124.5, 126.9, 127.3, 133.3, 134.6 (CH^{Imdz}); 140.3, 143.2, 144.4, 145.3 C^{Pz5}), 146.1 (C^{Pz3}).

11.10. 4 Synthesis of H_3L^{15}

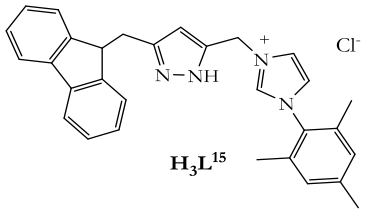

H_3L^{15}

Using 3-((9H-fluoren-9-yl)methyl)-5-(chloromethyl)-1-(tetrahydro-2H-pyran-2-yl)-1H pyrazole (2.0 g, 15.0 mmol) with 1-mesityl-1H-imidazole (1.5 g, 12.0 mmol) in acetonitrile under refluxing conditions for several days. Product was obtained as a white solid.

Yield: 4.81 g, 90 %

Molecular formula: $C_{30}H_{30}N_4Cl$

Molecular weight: 482.1 g/mol.

MS (ESI, DMSO) m/z (%): 445.1 (100%) $[M\text{-}Cl]^+$.

IR (ATR, cm^{-1}): 3429 (m); 2955 (m); 1572 (m); 1549 (m); 1447 (s); 1205 (vs); 1158 (m); 1005 (m); 870 (vs); 774 (vs); 759 (vs); 745 (vs); 731 (m).

^{1}H-NMR (DMSO-d_6) δ: 2.01 (s, 6H, CH_3); 2.34 (s, 3H, CH_3); 3.20 (d, $^{3}J_{HH}$ = 6.9 Hz, 2H, fluorene-CH_2-pz); 4.34 (t, 1H, CH^{Fluor}); 5.47 (s, 2H, Imdz-CH_2-Pz); 5.97 (s, 1H, CH^{Pz4}); 7.16 (s, 3H, CH^{Ar}); 7.25-7.39 (m, 8H, CH^{Ar}); 7.83 (d, $^{3}J_{HH}$ = 1.9 Hz, 1H, CH^{Imdz}); 7.95 (s, 1H, CH^{Imdz}); 9.56 (s, 1H, CH^{Imdz}); 13.01 (s, 1H, NH^{Pyz}).

$^{13}C\{^{1}H\}$ (DMSO-d_6) δ:	16.7 (o-CH_3^{Mes}); 20.4 (p-CH_3^{Mes}); 28.5 (fluorene-CH_2-Pz); 46.2 (fluorene-CH_2-Pz); 46.8 (Imdz-CH_2-Pz); 102.5 (CH^{pz}); 120.0, 123.2 (CH^{Ar}), 123.9 (CH^{Ar}), 124.5 (CH^{Ar}), 126.9 (CH^{Ar}), 127.3 (CH^{Ar}), 129.3 (CH^{Ar}), 131.2, 134.3, 137.5 (CH^{Imdz}); 140.3, 140.4, 145.4 (C^{Pz5}), 146.0 (C^{Pz3}).
Elemental analysis :	Calcd. For $C_{30}H_{29}ClN_4$: (C) 74.91 (H) 6.23 (N) 11.65; Found: (C) 74.30; (H) 5.97 (N) 11.66.

11.10. 5 Synthesis of H_3L^{16}

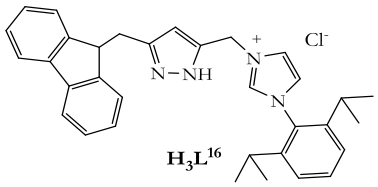

H_3L^{16}

Using 3-((9H-fluoren-9-yl)methyl)-5-(chloromethyl)-1-(tetrahydro-2H-pyran-2-yl)-1H-pyrazole (1.2 g, 3.1 mmol, 1 eq) and 1-(2,6-diisopropylphenyl)-1H-imidazole (1.0 g, 4.1 mmol, 1.3 eq) dissolved in acetonitrile (15 mL) and refluxed for 5 days. The solution was cooled to 90°C and ethanolic HCl added and refluxing continued. The reaction solution after cooling was added dropwide to diethyl ether in a beaker to precipitate the crude. The product was purified by the sublimation of unreacted imidazole precursor and obtained as a white solid.

Yield:	0.48 g, 25 %
Molecular formula:	$C_{33}H_{35}N_4Cl$
Molecular weight:	523.2 g/mol.
MS (ESI, DMSO) m/z (%):	487 (100%) $[M\text{-}Cl]^+$.
IR (ATR, cm^{-1}):	3430 (s); 3173 (m); 1480 (m); 1462 (m); 1378 (m); 1199 (m); 1126 (m); 826 (vs); 737 (vs); 558 (vs).
^{1}H-NMR ($CDCl_3$) δ	1.07 (d, $^{3}J_{HH}$ = 6.8 Hz, 6H, CH_3^{iPr}); 1.12 (d, $^{3}J_{HH}$ = 6.8 Hz, 6H, CH_3^{iPr}); 2.19 (sept, $^{3}J_{HH}$ = 6.8 Hz, 2H, CH^{iPr}); 3.28 (d, $^{3}J_{HH}$ = 6.5 Hz, 2H, fluorene-CH_2-Pz); 4.31 (t, $^{3}J_{HH}$ = 6.4 Hz, 2H, fluorene-CH_2-Imdz); 5.85 (s, 2H, Pz-CH_2-Imdz); 5.96 (s, 1H, CH^{Pz}); 7.05 (s, 1H, CH^{Ar}); 7.16-7.77 (m, 12H, CH^{Imdz}, CH^{Ar}); 10.18 (s, 1H, CH^{Imdz}).

$^{13}C\{^{1}H\}$ ($CDCl_3$) δ: 24.2 (CH_3^{iPr}); 24.3 (CH_3^{iPr}); 28.7 (CH^{Ar}); 46.9 (CH^{Ind}; 119.8 (CH^{Pz}); 120.1; 123.1 (CH^{Ar}); 123.7 (CH^{Ar}); 124.7 (CH^{Ar}); 127.1 (CH^{Ar}); 127.3 (CH^{Ar}); 128.5 (CH^{Ar}); 130.3; 131.9; 138.1 (CH^{Imdz}); 141.0; 145.4 (C^{Pz5}); 146.4 (C^{Pz3}).

Elemental analysis : Calcd. For $C_{33}H_{36}ClN_4$: (C) 75.86 (H) 6.70 (N) 10.72; Found: (C) 74.65 (H) 6.83 (N) 11.65.

11.10. 6 Synthesis of H_3L^{17}

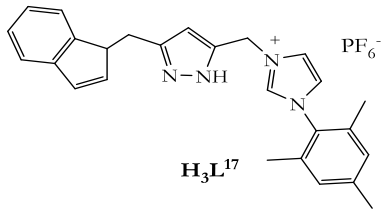

Using 3-((1H-inden-1-yl)methyl)-5-(chloromethyl)-1-(tetrahydro-2H-pyran-2-yl)-1H-pyrazole (1.2 g, 3.2 mmol, 1 Eq.) and 1-mesityl-1H-imidazole (0.6 g, 3.2 mmol, 1.0 Eq.) dissolved in acetonitrile (10 mL) under reflux for 5 days. A 28% aqueous ammonia solution (2 mL) was added and the mixture and the solution treated with NH_4PF_6 (0.6 g, 3.2 mmol, 1 Eq.). The reaction mixture was washed with water (3x5 mL) and the organic phase dried over $MgSO_4$. This was added dropwise to Et_2O to precipitate the solid. The precipitate was washed with Et_2O (3x3 mL) and dried in vacuum. The product was obtained as a colourless solid.

Yield: 0.10 g, 6%

Molecular formula: $C_{26}H_{26}N_4PF_6$

Molecular weight: 539.5 g/mol.

MS (ESI, DMSO) m/z (%): 395.1 (100%) $[M\text{-}PF_6]^+$, 233.2 (7%) $[M\text{-}Imdz]^+$, 187.1 (13%) $[Imdz]^+$.

IR (ATR, cm^{-1}): 3139 (m); 1551 (m); 1447 (m); 1162 (s); 1203 (s); 1030 (s); 840 (vs); 559 (s).

^{1}H-NMR (DMSO-d_6) δ: 2.03 (s, 6H, o-CH_3^{Mes}); 2.33 (s, 3H, p-CH_3^{Mes}); 2.86-2.97 (m, 2H, indene-CH_2-pz); 3.05-3.12 (m, 2H, CH); 5.56 (s, 2H, Imdz-CH_2-pz); 6.54 (s, 1H, Imdz-CH-pz); 6.93 (s, 1H, indene); 7.12-7.38 (m, 4H); 7.56-7.64 (m, 1H, indene); 7.95 (t, $^4J_{HH}$= 1.8 Hz, 1H, CH^{Imdz}); 8.10 (t, $^4J_{HH}$ = 1.8 Hz, 1H, CH^{Imdz}); 9.62 (s, 1H, CH^{Imdz}); 13.10 (s, 1H, NH^{pz}).

$^{13}C\{^{1}H\}$ (DMSO-d_6) δ: 16.9 (o-CH_3^{Mes}); 20.6 (p-CH_3^{Mes}); 29.9 (indene-CH_2-Pz); 30.0(indene-CH-Pz); 46.9 (Imdz-CH_2-Pz); 102.6 (CH^{ind}); 105.2 (CH^{Pz}); 120.1, 123.5 (CH^{Ar}), 123.9 (CH^{Ar}), 125.4 (CH^{Ar}), 126.8 (CH^{Ar}), 128.7, 129.2, 131.2, 134.2 (CH^{Imdz}); 137.82, 140.2, 140.7, 141.9, 147.3 (C^{Pz3}), 148.3, 152.5 (C^{Ar}); 155.8 (C^{Ar}).

Elemental analysis: Calcd. For $C_{33}H_{36}ClN_4$: C (78.99) H (6.58) N (12.70); Found: C (70.65) H (6.43) N (26.01).

11.10. 7 Synthesis of H_3L^{18}

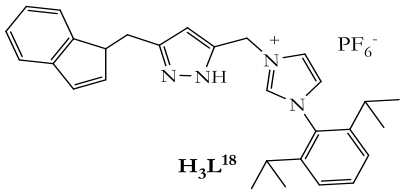

H_3L^{18}

Using 3-((1H-inden-1-yl)methyl)-5-(chloromethyl)-1-(tetrahydro-2H-pyran-2-yl)-1H-pyrazole (1.2 g, 3.2 mmol, 1 Eq.) and 1-(2,6-diisopropylphenyl)-1H-imidazole (0.6 g, 3.2 mmol, 1.0 Eq.) dissolved in acetonitrile (10 mL) with refluxing for 5 days. A 10% ammonia solution (2 mL) was added and the mixture treated with NH_4PF_6 (0.6 g, 3.2 mmol, 1 Eq.). The organic phase was washed with water (7 mL) and dried over $MgSO_4$. This solution was added dropwise to Et_2O. The product precipitated was filtered and dried in vacuum. The product was obtained as a colourless solid

Yield: 0.54 g, 36 %

Molecular formula: $C_{29}H_{33}N_4Cl$

Molecular weight: 473.1 g/mol.

IR (ATR, cm^{-1}): 2998 (s); 2962 (s); 1450 (vs); 1369 (m); 1108 (m); 1339 (m); 1186 (vs); 1003 (m); 730 (vs); 743 (vs).

^{1}H-NMR (DMSO-d_6) δ: 1.05-1.02 (m, 12H, CH_3^{iPr}); 2.88-2.97 (m, 2H, CH^{iPr}); 3.07-3.14 (m, 2H, Ind-CH_2-Pz); 3.93 (m, 1H, Ind-CH-Pz); 5.60 (s, 2H, Imdz-CH_2-Pz); 6.53 (s, 1H, CH^{Pz}); 6.94 (m, 1H, CH^{Imdz}); 7.20-7.70 (m, 8H, CH^{Imdz}, CH^{Ar}); 8.03-8.13 (m, 2H, CH^{Ar}); 9.62 (s, 1H, CH^{Imdz}); 13.03 (s, 1H, NH^{Pz}).

$^{13}C\{^{1}H\}$ (DMSO-d_6) δ: 23.8 (CH_3^{iPr}); 28.1 (CH^{iPr}); 29.9 (Ind-CH_2-pz); 37.3 (Ind-CH-pz); 47.0 (Imdz-CH_2-Pz); 104.86 (CH^{pz}); 120.2, 123.8 (CH^{Ar}), 124.5

(CH^{Ar}), 125.1 (CH^{Ar}), 125.5 (CH^{Ar}), 126.9 (CH^{Ar}), 130.5, 130.6, 131.5, 138.2 (CH^{Imdz}); 145.1 (C^{Pz3}).

11.10. 8 Synthesis of $[H_3L^{14}{}_2Rh_2(OAc)_4](PF_6)_2$ (4f)

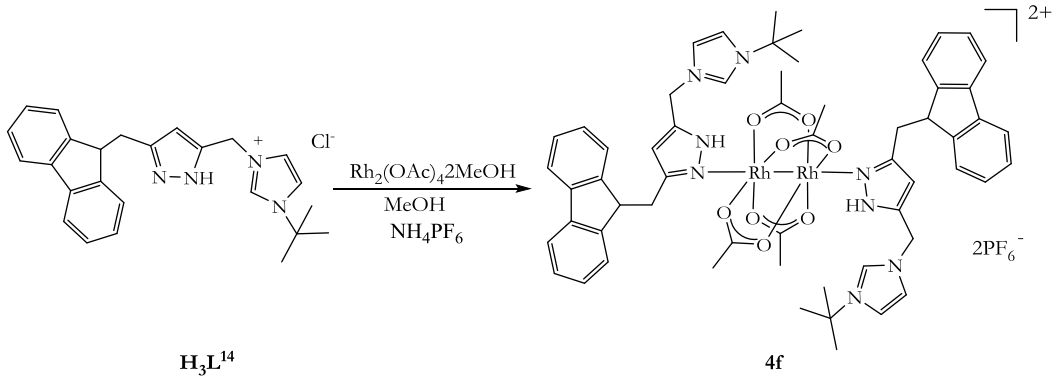

H_3L^{14} 4f

To a MeOH solution (10 mL) of $\mathbf{H_3L^{14}}$ (50 mg, 0.10 mmol) was added 0.5 mol equivalent of $Rh_2(OAc)_4{\cdot}2MeOH$ (26.5 mg, 0.05 mmol) with stirring. A pale blue solution was formed in 5 min. 2.0 mol equivalent NH_4PF_6 was added and the reaction was allowed to stir overnight. A purple suspension was formed was overnight, the precipitate was filtered and washed several times with methanol (3x3 mL) after which the product was dried in air to obtain the pure product. This product was sparingly soluble in both methanol and CH_2Cl_2 but dissolves in a 50:50 mixture of the two. Crystals of the product were obtained by the slow evaporation of 50:50 methanolic/CH_2Cl_2 solution of the complex at room temperature.

Yield:	40 mg, 63 %
Molecular formula:	$C_{58}H_{66}N_8O_8Rh_2$
Molecular weight:	1208.3 g/mol.
MS (ESI, MeOH) m/z (%):	825 (10%) $[LRh_2(OAc)_4]^+$; 382 (100%) $[L]^+$.
IR (ATR, cm^{-1}):	3173 (m); 2555 (m); 1588 (vs); 1572 (s); 1436 (vs); 1415 (vs); 13809 (m); 1205(m); 1130 (m); 908 (m); 841 (vs); 819 (vs); 746 (m).
^{1}H-NMR ($CDCl_3$) δ:	1.59 (s, 18H, $CH_3{}^{tBu}$); 1.80 (s, 12H, $CH_3{}^{OAc}$); 4.30 (t, 2H, CH^{Imdz}); 5.29 (s, 8H, CH_2); 5.91 (s, 2H, CH^{Pz}); 7.25-7.37 (m, 8H, CH^{Ar}); 7.63 (s, 2H, CH^{Imdz}); 7.83 (d, $^4J_{HH}$ = 1.2 Hz, 2H, CH^{Imdz}); 8.01 (s, 8H, CH^{Ar}); 9.34 (s, 2H, CH^{Imdz}); 12.78 (s, 2H, NH^{Pz}).

List of prepared complexes and ligands

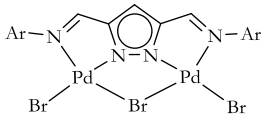

1b

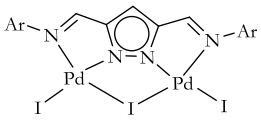

1c

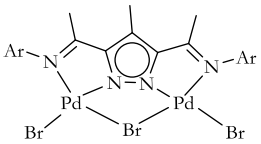

2b

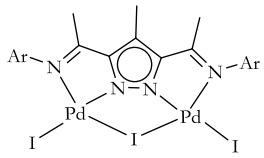

2c

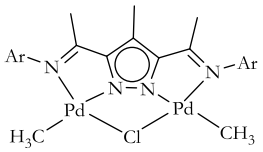

2f

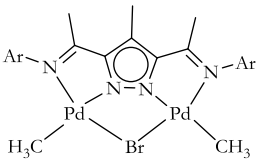

2g

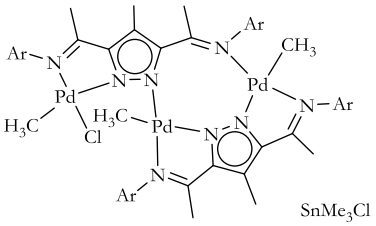

2h

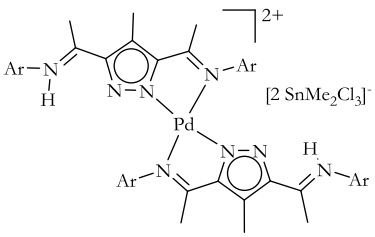

2i

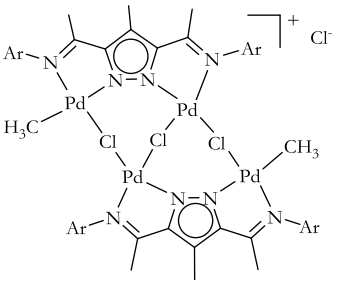

2d$_2$

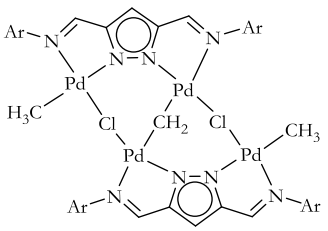

2k

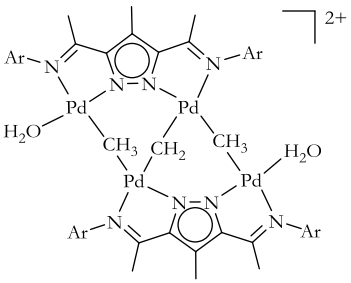

2l

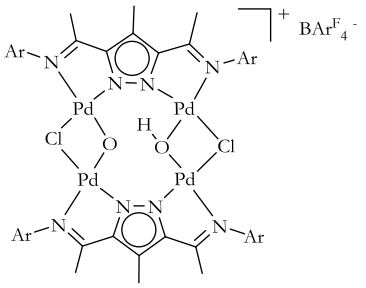

2p

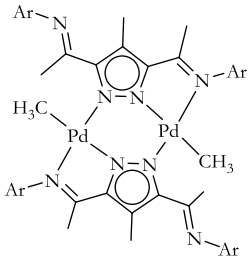

3a

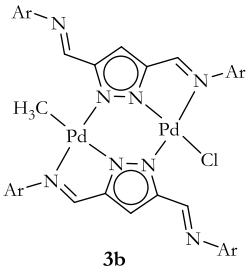

3b

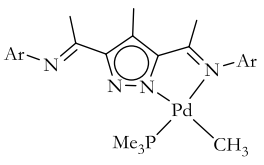

3c

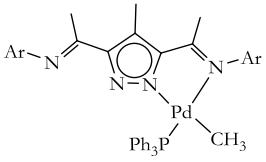

3d

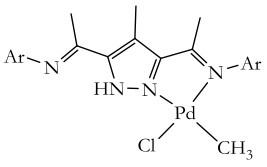

3e

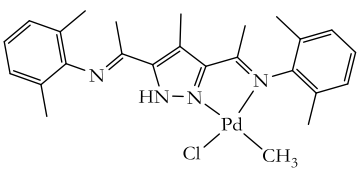

3f

Ar = 2,6-^{i}Pr$_2$-C$_6$H$_3$

List of prepared complexes and ligands

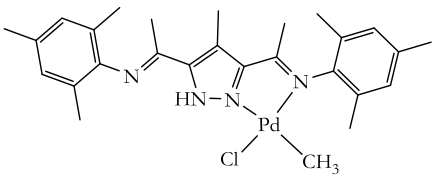

3g

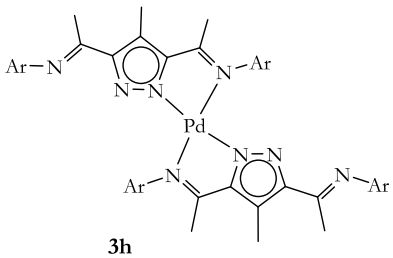

3h

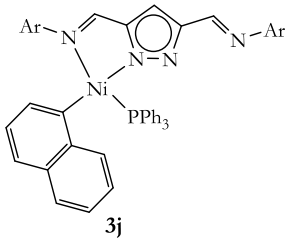

3j

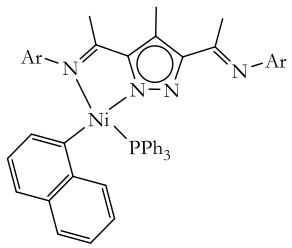

3k

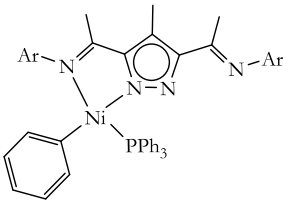

3l

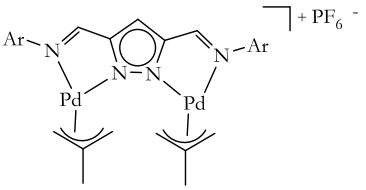

3m

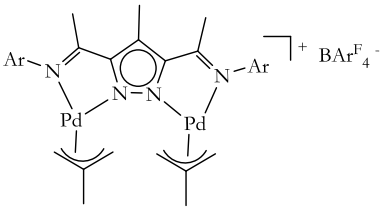

3n

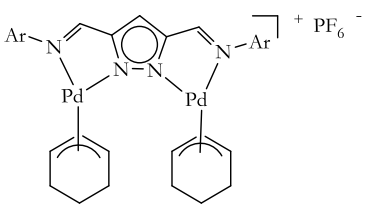

3o

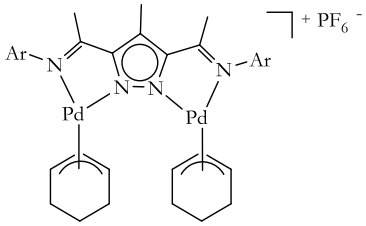

3p

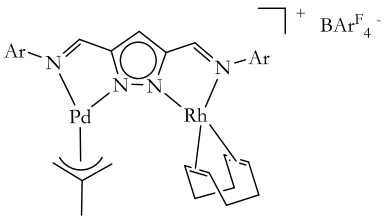

3r

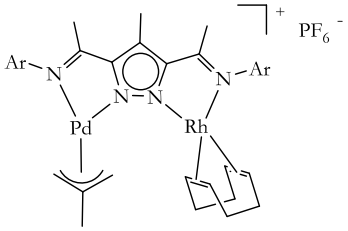

3s

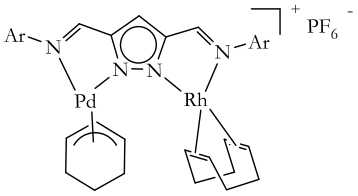

3t

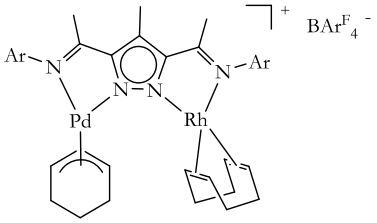

3u

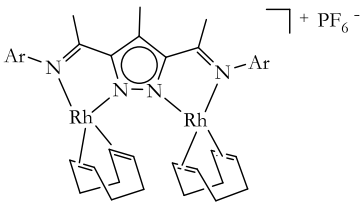

3v

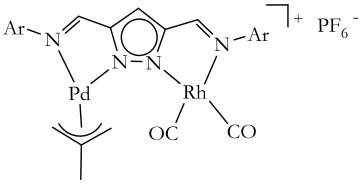

3w

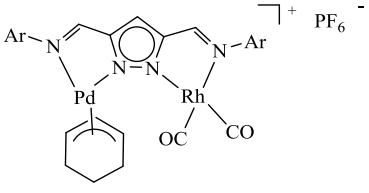

3x

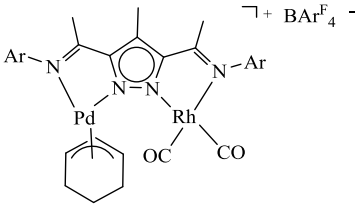

3y

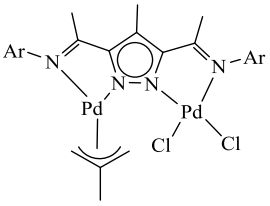

3z

Ar = 2,6-^{i}Pr$_2$-C$_6$H$_3$

List of prepared complexes and ligands

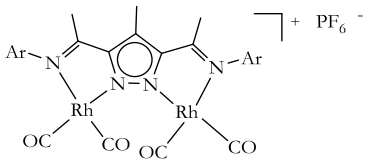

3z1

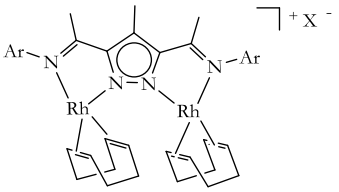

X = PF_6 (3v)
X =C1 ($3C_1$)

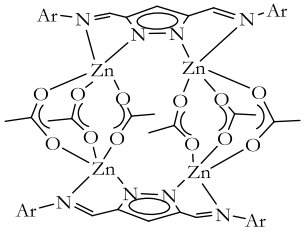

4a

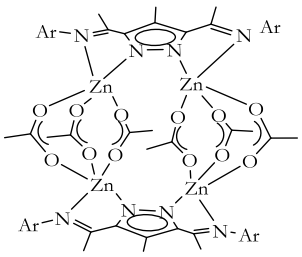

4b

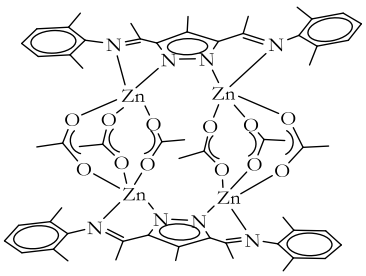

4c

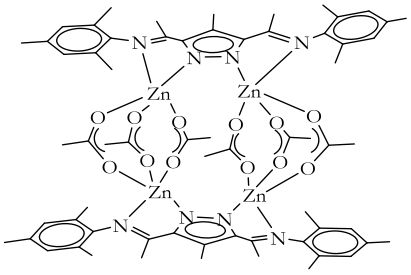

4d

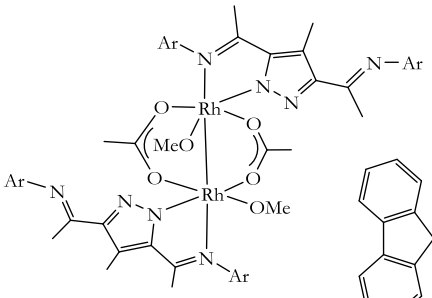

4e

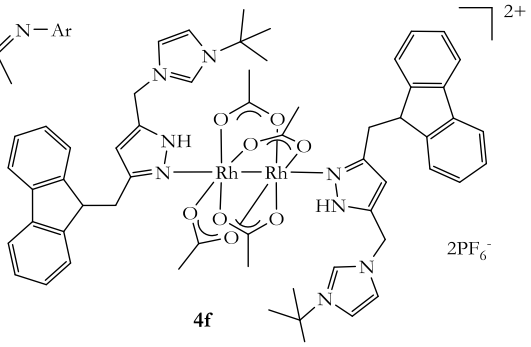

4f

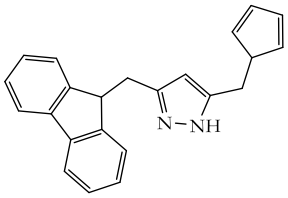

H_3L^5

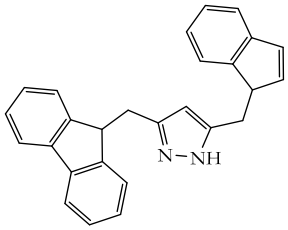

H_3L^6

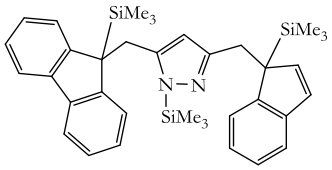

L^9

Ar = 2,6-^{i}Pr$_2$-C$_6$H$_3$

List of prepared complexes and ligands

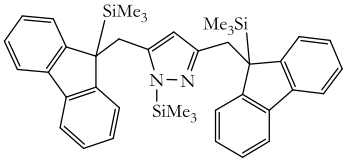

L[10]

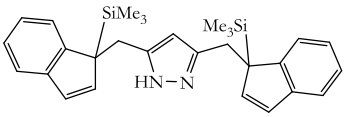

HL[11]

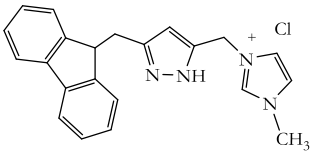

H$_3$L[12]

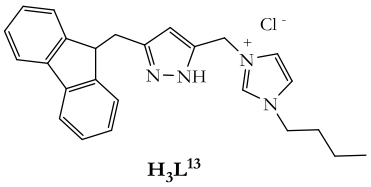

H$_3$L[13]

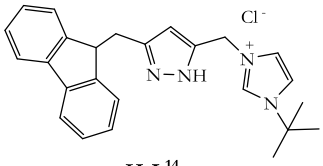

H$_3$L[14]

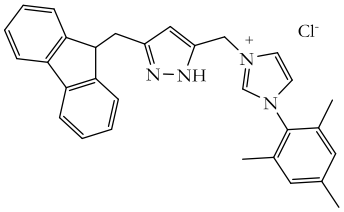

H$_3$L[15]

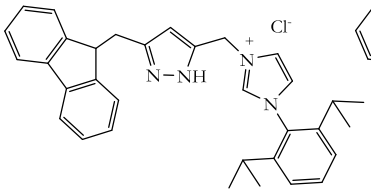

H$_3$L[16]

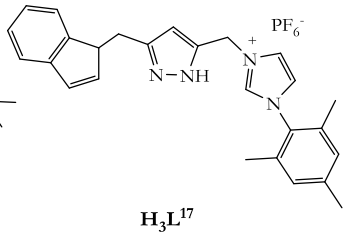

H$_3$L[17]

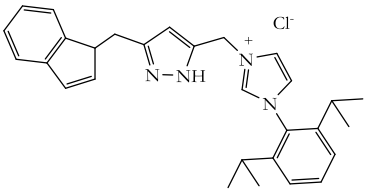

H$_3$L[18]

11. 11: Crystallographic Data

Label	**2h**	**2i**
Empirical formula	$C_{74}H_{114}Cl_2N_8OPd_3Sn$	$C_{70}H_{104}Cl_{10}N_8PdSn_2$
Formula weight	1640.52	1755.89
Temperature	133(2) K	133(2) K
Wavelength	0.71073 Å	0.71073 Å
Crystal system	Triclinic	Triclinic
Space group	*P* -1	*P* -1
Unit cell dimensions	a = 13.3849(9) Å α = 93.101(5)°	a = 10.2900(4) Å α = 111.722(3)°
	b = 15.8627(10) Å β = 91.417(5)°	b = 13.8960(6) Å β = 93.324(3)°
	c = 19.8753(13) Å γ = 94.222(5)°	c = 15.4928(6) Å γ = 99.462(3)°
Volume	4200.6(5) $Å^3$	2012.86(14) $Å^3$
Z	2	1
Density (calculated)	1.297 Mg/m^3	1.449 Mg/m^3
Absorption coefficient	1.031 mm^{-1}	1.212 mm^{-1}
F(000)	1688	896
Crystal size	0.29 x 0.21 x 0.11 mm^3	0.5 x 0.5 x 0.46 mm^3
Theta range for data collection	1.29 to 24.70°	1.61 to 26.76°
Index ranges	-13<=h<=15, -18<=k<=18, -23<=l<=23	-13<=h<=12, -17<=k<=17, -19<=l<=19
Reflections collected	44270	26484
Independent reflections	14097 [R(int) = 0.1318]	8535 [R(int) = 0.0372]
Completeness to theta =	98.5 %	99.6 %
Absorption correction	None	Numerical
Max. and min. transmission	0.9204 and 0.7503	0.6268 and 0.5395
Refinement method	Full-matrix least-squares on F^2	Full-matrix least-squares on F^2
Data / restraints / parameters	14097 / 0 / 830	8535 / 1 / 429
Goodness-of-fit on F^2	1.043	1.050
Final R indices [I>2sigma(I)]	R1 = 0.0583, wR2 = 0.1437	R1 = 0.0400, wR2 = 0.1048
R indices (all data)	R1 = 0.0722, wR2 = 0.1507	R1 = 0.0432, wR2 = 0.1068
Largest diff. peak and hole	1.635 and -1.019 $e.Å^{-3}$	1.058 and -2.045 $e.Å^{-3}$

Crystallographic Data

Label	**2k**	**3a**
Empirical formula	$C_{67}H_{96}Cl_2N_8Pd_4$	$C_{66}H_{92}N_8Pd_2$
Formula weight	1510.02	1210.28
Temperature	133(2) K	133(2) K
Wavelength	0.71073 Å	0.71073 Å
Crystal system	Monoclinic	Triclinic
Space group	*P* 21/c	*P* -1
Unit cell dimensions	a = 12.9287(5) Å α = 90°	a = 13.5729(6) Å α = 111.890(3)°
	b = 19.8561(4) Å β = 93.957(3)°	b = 22.2338(10) Å β = 92.033(3)°
	c = 30.0916(10) Å γ = 90°	c = 23.2797(10) Å γ = 90.035(4)°
Volume	7706.5(4) $Å^3$	6513.9(5) $Å^3$
Z	4	4
Density (calculated)	1.301 Mg/m^3	1.234 Mg/m^3
Absorption coefficient	1.027 mm^{-1}	0.595 mm^{-1}
F(000)	3088	2544
Crystal size	0.19x0.11x0.10 mm^3	0.21 x 0.07 x 0.06 mm^3
Theta range for data collection	1.23 to 25.65°	1.60 to 25.73°
Index ranges	-12<=h<=15, -24<=k<=24, -36<=l<=36	-16<=h<=14, -27<=k<=26, -28<=l<=28
Reflections collected	81720	68299
Independent reflections	14535 [R(int) = 0.0660]	24564 [R(int) = 0.1776]
Completeness to theta =	99.7%	98.8 %
Absorption correction	Numerical	Numerical
Max. and min. transmission	0.9047 and 0.7670	0.9284 and 0.7513
Refinement method	Full-matrix least-squares on F^2	Full-matrix least-squares on F^2
Data / restraints / parameters	14535 / 31 / 751	24564 / 0 / 1417
Goodness-of-fit on F^2	1.001	1.041
Final R indices [I>2sigma(I)]	R1 = 0.0408, wR2 = 0.0716	R1 = 0.0998, wR2 = 0.1461
R indices (all data)	R1 = 0.0668, wR2 = 0.0780	R1 = 0.1924, wR2 = 0.1725
Largest diff. peak and hole	0.532 and -0.515 $e.Å^{-3}$	0.985 and -0.900 $e.Å^{-3}$

Crystallographic Data

Label	**3b**	**3c**
Empirical formula	$C_{62}H_{84.5}ClN_8O_{0.75}Pd_2$	$C_{36.50}H_{56}ClN_4PPd$
Formula weight	1202.13	723.67
Temperature	133(2) K	133(2) K
Wavelength	0.71073 Å	0.71073 Å
Crystal system	Triclinic	Monoclinic
Space group	*P* -1	*P* 21/n
Unit cell dimensions	a = 12.3368(5) Å α = 67.294(3)°	a = 18.0042(8) Å α = 90°
	b = 16.8529(8) Å β = 78.181(3)°	b = 8.5291(2) Å β = 93.548(4)°
	c = 17.3280(7) Å γ = 82.082(4)°	c = 24.7195(11) Å γ = 90°
Volume	3246.1(2)Å^3	3788.6(3) Å^3
Z	2	4
Density (calculated)	1.230 Mg/m^3	1.269 Mg/m^3
Absorption coefficient	0.637 mm^{-1}	0.631 mm^{-1}
F(000)	1255	1424
Crystal size	0.44x0.25x0.18mm^3	0.5 x 0.16 x 0.12 mm^3
Theta range for data collection	1.29 to 25.63°	1.36 to 25.70°
Index ranges	-14<=h<=14,-20<=k<=18,-21<=l<=21	21<=h<=21, -9<=k<=10, -30<=l<=30
Reflections collected	34720	42713
Independent reflections	12217[R(int) =0.0615]	7178 [R(int) = 0.1011]
Completeness to theta =	99.6%	99.4%
Absorption correction	Numerical	Numerical
Max. and min. transmission	0.9003 and 0.7906	0.8795 and 0.5859
Refinement method	Full-matrix least-squares on F^2	Full-matrix least-squares on F^2
Data / restraints / parameters	12217/ 66 /694	7178 / 0 / 427
Goodness-of-fit on F^2	1.057	1.039
Final R indices [I>2sigma(I)]	R1 = 0.0553, wR2 = 0.1538	R1 = 0.0460, wR2 = 0.1181
R indices (all data)	R1 = 0.0704, wR2 = 0.1631	R1 = 0.0580, wR2 = 0.1240
Largest diff. peak and hole	1.534 and -1.284 e.Å^{-3}	1.036 and -0.793 e.Å^{-3}

Crystallographic Data

Label	**3h**	**3i**
Empirical formula	$C_{64}H_{86}N_8Pd$	$C_{112}H_{78}B_2F_{48}N_8Pd_2$
Formula weight	1073.81	2682.24
Temperature	133(2) K	133(2) K
Wavelength	0.71073 Å	0.71073 Å
Crystal system	Monoclinic	Triclinic
Space group	*P* 21/c	*P* -1
Unit cell dimensions	a = 8.7514(6) Å α = 90°	a = 13.0997(4) Å α = 73.881(3)°
	b = 21.3165(16) Å β = 101.921(6)°	b = 13.1432(4) Å β = 83.613(3)°
	c = 15.8556(12) Å γ = 90°	c = 17.5534(6) Å γ = 71.885(3)°
Volume	2894.1(4) $Å^3$	2758.46(15) $Å^3$
Z	2	1
Density (calculated)	1.232 Mg/m^3	1.615 Mg/m^3
Absorption coefficient	0.367 mm^{-1}	0.460 mm^{-1}
F(000)	1144	1340
Crystal size	0.26 x 0.09 x 0.07 mm^3	0.5 x 0.45 x 0.35 mm^3
Theta range for data collection	1.62 to 25.00°	1.64 to 26.72°
Index ranges	-10<=h<=9, -25<=k<=25, -18<=l<=18	-16<=h<=16, -16<=k<=16, -22<=l<=22
Reflections collected	28514	35344
Independent reflections	5099 [R(int) = 0.1933]	11696 [R(int) = 0.0390]
Completeness to theta =	100.0 %	99.8 %
Absorption correction	Numerical	Numerical
Max. and min. transmission	0.8981 and 0.5965	0.9166 and 0.7555
Refinement method	Full-matrix least-squares on F^2	Full-matrix least-squares on F^2
Data / restraints / parameters	5099 / 0 / 342	11696 / 42 / 772
Goodness-of-fit on F^2	1.073	1.037
Final R indices [I>2sigma(I)]	R1 = 0.0739, wR2 = 0.1108	R1 = 0.0522, wR2 = 0.1367
R indices (all data)	R1 = 0.1519, wR2 = 0.1355	R1 = 0.0590, wR2 = 0.1403
Largest diff. peak and hole	0.705 and -1.315 $e.Å^{-3}$	2.314 and -1.313 $e.Å^{-3}$

Crystallographic Data

Label	**3k**	**3l**
Empirical formula	$C_{60}H_{65}N_4NiP$	$C_{59}H_{66}N_4NiP$
Formula weight	931.84	920.84
Temperature	133(2) K	133(2) K
Wavelength	0.71073 Å	0.71073 Å
Crystal system	Monoclinic	Triclinic
Space group	*P* 21/c	*P*-1
Unit cell dimensions	a = 17.5591(9) Å α = 90°	a = 10.1233(10) Å α = 75.101(8)°
	b = 17.1847(6) Å β = 102.785(4)°	b = 12.8898(14) Å β = 88.306(8)°
	c = 17.4217(7) Å γ = 90°	c = 22.209(2) Å γ = 66.845(8) °
Volume	5126.6(4) $Å^3$	2566.6(5) $Å^3$
Z	4	2
Density (calculated)	1.207 Mg/m^3	1.192 Mg/m^3
Absorption coefficient	0.452 mm^{-1}	0.450 mm^{-1}
F(000)	1984	982
Crystal size	0.21 x 0.09 x 0.05 mm^3	0.22 x 0.06 x 0.02 mm^3
Theta range for data collection	1.68 to 25.00°	1.78 to 26.82°
Index ranges	-20<=h<=20, -20<=k<=20, -20<=l<=20	-12<=h<=12, -15<=k<=16, 0<=l<=28
Reflections collected	35756	10934
Independent reflections	8863 [R(int) = 0.1955]	10934 [R(int) = 0.0000]
Completeness to theta =	98.2 %	99.2%
Absorption correction	Numerical	Numerical
Max. and min. transmission	0.9659 and 0.7675	0.9201 and 0.6555
Refinement method	Full-matrix least-squares on F^2	Full-matrix least-squares on F^2
Data / restraints / parameters	8863 / 1 / 604	10934 / 0 / 575
Goodness-of-fit on F^2	1.130	0.743
Final R indices [I>2sigma(I)]	R1 = 0.1061, wR2 = 0.1524	R1 = 0.1173, wR2 = 0.1768
R indices (all data)	R1 = 0.1830, wR2 = 0.1755	R1 = 0.3334, wR2 = 0.2787
Largest diff. peak and hole	0.542 and -0.416 $e.Å^{-3}$	0.595 and -1.050 $e.Å^{-3}$

Crystallographic Data

Label	**3n**	**3p**
Empirical formula	$C_{84}H_{93}BF_{24}N_4Pd_2$	$C_{45}H_{63}Cl_2F_6N_4PPd_2$
Formula weight	1838.23	1088.6
Temperature	133(2) K	133(2) K
Wavelength	0.71073 Å	0.71073 Å
Crystal system	Monoclinic	Monoclinic
Space group	*P* 21/c	*P* 21/n
Unit cell dimensions	a = 16.0445(3) Å α = 90°	a = 8.3238(2) Å α = 90.0°
	b = 16.9736(2) Å β = 100.237(2)°	b = 25.4691 Å β = 94.485(2) °
	c = 31.7612(6) Å γ = 90°	c = 22.4117(5) Å γ = 90°
Volume	8511.9(2) Å^3	2758.46(15) Å^3
Z	4	4
Density (calculated)	1.434 Mg/m^3	1.527 Mg/m^3
Absorption coefficient	0.520 mm^{-1}	0.965 mm^{-1}
F(000)	3752	2224
Crystal size	0.50 x 0.48 x 0.32 mm^3	0.5x0.07x0.03 mm^3
Theta range for data collection	1.29 to 25.64°	1.21 to 25.63°
Index ranges	-19<=h<=19,-18<=k<=20,-38<=l<=38	-9<=h<=10, -30<=k<=30, -27<=l<=27
Reflections collected	97363	48499
Independent reflections	16051 [R(int) = 0.0706]	8898 [R(int) = 0.0874]
Completeness to theta =	99.7%	99.6%
Absorption correction	Numerical	Numerical
Max. and min. transmission	0.8988 and 0.8084	0.9702 and 0.7656
Refinement method	Full-matrix least-squares on F^2	Full-matrix least-squares on F^2
Data / restraints / parameters	16051 / 152 / 1054	8898 / 6 / 569
Goodness-of-fit on F^2	1.034	1.010
Final R indices [I>2sigma(I)]	R1 = 0.0642, wR2 = 0.1802	R1 = 0.0406, wR2 = 0.0713
R indices (all data)	R1 = 0.0753, wR2 = 0.1889	R1 = 0.0636, wR2 = 0.0766
Largest diff. peak and hole	2.571 and -1.101 e.Å^{-3}	0.915 and -0.609 e.Å^{-3}

Crystallographic Data

Label	**3q**	**3t**
Empirical formula	$C_{86}H_{96}Cl_8F_{12}N_8P_2Pd$	$C_{44}H_{60}Cl_2F_6N_4P$ Pd Rh
Formula weight	1705.47	1070.14
Temperature	133(2) K	133(2) K
Wavelength	0.71073 Å	0.71073 Å
Crystal system	Triclinic	Monoclinic
Space group	*P* -1	C c
Unit cell dimensions	a = 12.6945(11) Å α = 97.038(6)°	a = 22.5325(13) Å α = 90°
	b = 13.5645(11) Å β = 115.436(6)°	b = 13.2280(5) Å β = 110.444(4)°
	c = 14.6984(14) Å γ = 110.504(6)°	c = 16.6094(10) Å γ = 90°
Volume	1681.55(15) $Å^3$	4638.8(4)$Å^3$
Z	1	4
Density (calculated)	1.398 Mg/m^3	1.532 Mg/m^3
Absorption coefficient	0.603 mm^{-1}	0.953 mm^{-1}
F(000)	880	2184
Crystal size	0.39 x 0.32 x 0.28 mm^3	0.5x0.02x0.02 mm^3
Theta range for data collection	1.62 to 26.92°	1.82 to 25.67
Index ranges	-16<=h<=15,-17<=k<=15,-18<=l<=18	-27<=h<=27, -16<=k<=16, -18<=l<=20
Reflections collected	25795	22020
Independent reflections	8671[R(int) = 0.1243]	8081 [R(int)=0.0923]
Completeness to theta =	100.0%	99.4 %
Absorption correction	Numerical	Numerical
Max. and min. transmission	0.8693 and 0.5634	0.9854 and 0.7946
Refinement method	Full-matrix least-squares on F^2	Full-matrix least-squares on F^2
Data / restraints / parameters	8671 / 14 / 472	8081 / 2 / 541
Goodness-of-fit on F^2	1.004	1.005
Final R indices [I>2sigma(I)]	R1 = 0.0567, wR2 = 0.13290	R1=0.0513, wR2= 0.0826
R indices (all data)	R1 = 0.0823, wR2 = 0.1416	R1=0.0743, wR2=0.0894
Largest diff. peak and hole	0.905 and -0.910 $e.Å^{-3}$	0.632 and-0.771 $e.Å^{-3}$

Crystallographic Data

Label	**3u**	**3z**
Empirical formula	$C_{90}H_{100}BF_{24}N_4$ Pd Rh	$C_{37}H_{52}Cl_4N_4Pd_2$
Formula weight	1913.86	907.43
Temperature	133(2) K	133(2) K
Wavelength	0.71073 Å	0.71073 Å
Crystal system	Triclinic	Monoclinic
Space group	*P* -1	*P* 21/c
Unit cell dimensions	a = 12.6288(4) Å α = 99.524(3)°	a = 19.3381(17) Å α = 90°
	b = 13.3336(4) Å β = 98.920(3)°	b = 12.5436(8) Å β = 96.192(7)°
	c = 26.6732(9) Å γ = 91.400(3)°	c = 16.4910(14) Å γ = 90°
Volume	4370.2(2) $Å^3$	3976.9(5) $Å^3$
Z	2	4
Density (calculated)	1.454 Mg/m^3	1.516 M/m^3
Absorption coefficient	0.493 mm^{-1}	1.204 mm^{-1}
F(000)	1960	1848
Crystal size	0.23 x 0.19 x 0.07 mm^3	0.18 x 0.05 x 0.04 mm^3
Theta range for data collection	1.55 to 25.68°	1.94 to 25.50°
Index ranges	-15<=h<=15, -15<=k<=16, -32<=l<=32	-23<=h<=23, -15<=k<=15, -19<=l<=18
Reflections collected	51040	35252
Independent reflections	16476 [R(int) = 0.0790]	7206 [R(int) = 0.2064]
Completeness to theta =	99.2%	97.6 %
Absorption correction	Numerical	Numerical
Max. and min. transmission	0.9676 and 0.9006	0.9120 and 0.7257
Refinement method	Full-matrix least-squares on F^2	Full-matrix least-squares on F^2
Data / restraints / parameters	16476 / 57 / 1111	7206 / 6 / 444
Goodness-of-fit on F^2	1.035	0.920
Final R indices [I>2sigma(I)]	R1 = 0.0774, wR2 = 0.2030	R1 = 0.0719, wR2 = 0.0848
R indices (all data)	R1 = 0.1099, wR2 = 0.2241	R1 = 0.1597, wR2 = 0.1017
Largest diff. peak and hole	0.891 and -1.991 $e.Å^{-3}$	0.889 and -0.637 $e.Å^{-3}$

Crystallographic Data

Label	**4a**	**4b**
Empirical formula	$C_{75}H_{102}Cl_{10}N_8O_{12}Zn_4$	$C_{62}H_{76}Cl_4N_8O_{12}Zn_4$
Formula weight	1923.6	1528.59
Temperature	133(2)K	133(2) K
Wavelength	0.71073	0.71073 Å
Crystal system	Monoclinic	Triclinic
Space group	*P* 21/n	*P* -1
Unit cell dimensions	a = 20.0089(5) Å α = 90°	a = 10.5775(5) Å α = 96.820(4)°
	b = 11.1020(2) Å β = 98.483(2)°	b = 11.1996(5) Å β = 105.941(3) °
	c = 20.0964(2) Å γ = 90°	c = 16.0678(7) Å γ = 107.980(3)°
Volume	4415.35(19) $Å^3$	1697.22(13) $Å^3$
Z	2	1
Density (calculated)	1.447 Mg/m^3	1.496 Mg/m^3
Absorption coefficient	1.436 mm^{-1}	1.618 mm^{-1}
F(000)	1988	788
Crystal size	0.50 x 0.40 x 0.17 mm^3	0.50 x 0.50 x 0.20 mm^3
Theta range for data collection	1.34 to 26.77°	1.35 to 26.75°
Index ranges	-25<=h<=25, -14<=k<=14, -25<=l<=25	-13<=h<=11, -14<=k<=14, -20<=l<=20
Reflections collected	50548	22197
Independent reflections	9347 [R(int) = 0.0537]	7193 [R(int) = 0.1226]
Completeness to theta =	99.5%	99.5 %
Absorption correction	Numerical	Numerical
Max. and min. transmission	0.7788 and 0.4302	0.6414 and 0.3971
Refinement method	Full-matrix least-squares on F^2	Full-matrix least-squares on F^2
Data / restraints / parameters	9347 / 0 / 574	7193 / 0 / 416
Goodness-of-fit on F^2	1.009	1.036
Final R indices [I>2sigma(I)]	R1 = 0.0322, wR2 = 0.0741	R1 = 0.0509, wR2 = 0.1428
R indices (all data)	R1 = 0.0441, wR2 = 0.0778	R1 = 0.0565, wR2 = 0.1470
Largest diff. peak and hole	0.414 and -0.435 $e.Å^{-3}$	1.999 and -1.078 $e.Å^{-3}$

Crystallographic Data

Label	**4e**	**4f**
Empirical formula	$C_{72}H_{10}Cl_4N_8O_6Rh_2$	$C_{58.50}H_{68}F_{12}N_8\ O_{8.5}0P_2Rh_2$
Formula weight	1525.25	1514.97
Temperature	133(2)K	133(2) K
Wavelength	0.71073 Å	0.71073 Å
Crystal system	Monoclinic	Triclinic
Space group	*P* 21/c	*P* -1
Unit cell dimensions	a = 15.41(3) Å α = 90°	a = 10.1681(4) Å α = 79.585(3)°
	b = 38.29482) Å β = 116.87°	b = 12.1809(5) Å β = 77.163(3)°
	c = 14.671(3) Å γ = 90°	c = 13.6238(6) Å γ = 85.386(3)°
Volume	7538(3) $Å^3$	1616.69(12) $Å^3$
Z	4	1
Density (calculated)	1.344 Mg/m^3	1.556 Mg/m^3
Absorption coefficient	0.633	0.654 mm^{-1}
F(000)	3192	771
Crystal size	0.254 × 0.245 × 0.115 mm^3	0.28 x 0.18 x 0.08 mm^3
Theta range for data collection	1.61 to 25.63°	1.56 to 26.81°
Index ranges	-18<=h<=16, -46<=k<=46, -16<=l<=17	-12<=h<=12, -15<=k<=15, -17<=l<=17
Reflections collected	11178	20991
Independent reflections	14071 [R(int) = 0.0776]	6838 [R(int) = 0.0319]
Completeness to theta =	100%	98.7 %
Absorption correction	Numerical	Numerical
Max. and min. transmission	0.7075 and 0.8819	0.9390 and 0.8628
Refinement method	Full-matrix least-squares on F^2	Full-matrix least-squares on F^2
Data / restraints / parameters	14071 / 2 / 861	6838 / 117 / 459
Goodness-of-fit on F^2	0.960	1.001
Final R indices [I>2sigma(I)]	R1 = 0.0343, wR2 = 0.0750	R1 = 0.0403, wR2 = 0.0985
R indices (all data)	R1 = 0.0505, wR2 = 0.0791	R1 = 0.0541, wR2 = 0.1029
Largest diff. peak and hole	-0.493 and -0.706 e.$Å^{-3}$	1.182 and -0.946 e.$Å^{-3}$

Crystallographic Data

Label	**[HL^{10}]Cl**
Empirical formula	$C_{37}H_{41}ClN_2Si$
Formula weight	605.35
Temperature	133(2) K
Wavelength	0.71073 Å
Crystal system	Triclinic
Space group	*P*-1
Unit cell dimensions	a = 8.9189(5) Å α = 88.296(4)°
	b = 13.5893(7) Å β = 86.115(4)°
	c = 14.0794(7) Å γ = 81.066(4)°
Volume	1681.55(15) Å^3
Z	2
Density (calculated)	1.196 Mg/m^3
Absorption coefficient	0.213 mm^{-1}
F(000)	644
Crystal size	0.36 x 0.18 x 0.15 mm^3
Theta range for data collection	1.45 to 26.83°
Index ranges	-10<=h<=11, -17<=k<=17, -17<=l<=17
Reflections collected	21591
Independent reflections	7126 [R(int) = 0.0868]
Completeness to theta =	100.0%
Absorption correction	Numerical
Max. and min. transmission	0.9625 and 0.8080
Refinement method	Full-matrix least-squares on F^2
Data / restraints / parameters	7126 / 1 / 391
Goodness-of-fit on F^2	1.070
Final R indices [I>2sigma(I)]	R1 = 0.0488, wR2 = 0.1160
R indices (all data)	R1 = 0.0720, wR2 = 0.1233
Largest diff. peak and hole	0.341 and -0.341 e.Å^{-3}

11. 12: List of Abbreviations

Å	Angstrom
[cat]	catalyst
Ar	Aryl
BuLi	Butyl lithium
CH_2Cl_2	Dichloromethane
COD	Cyclooctadiene
DHP	Dihydropyran
DME	Dimethoxyether
DMSO	Dimethylsulfoxide
DSC	Differential Scanning Calorimetry
EI	Electron ionization
ESI	Electrospray ionization
Et_2O	Diethyl ether
EtOH	Ethanol
g	gram
GPC	Gel Permeation Chromatography
HR-MS	High Resolution Mass Spectroscopy
Hz	Hertz
^{i}Pr	Isopropyl
IR	Infrared
J	Coupling constant
KO^{t}Bu	Potassium tert-butoxide
L	Ligand
M	Molar
m/z	mass to charge ratio
M^+	Molecular ion
MALDI	Matrix-assisted laser desorption ionization
Me	Methyl
MeOH	Methanol
M_n	Number average molecular weight
MS	Mass spectroscopy
M_w	Weight average molecular weight

Abbreviations

n-Bu	normal-butyl
NMR	Nuclear Magnetic Resonance
$NaBAr^{F}_{4}$	Sodium tetrakis[3,5-bis(trifluoromethyl)phenyl]borate
OAc	Acetate
°C	Degree Celsius
Ph	Phenyl
ppm	parts per million
p-TSA	*para*- toluenesulfonic acid
Py	Pyridine
Pz	Pyrazolyl
TG	Thermogravimetry
THF	Tetrahydrofuran
THP	Tetrahydropyran
TMS	Trimethylsilylchloride
λ	wavelength [nm]

11. 13: References

1 C. E. Tinberg, S. J. Lippard, *Acc. Chem. Res*. **2011**, 44, 280.

2 N. Sträter, W. N. Libscomb, T. Klabunde, B. Krebs, *Angew. Chem. Int. Ed*. **1996**, 35, 2025.

3 J. Weston, *Chem. Rev*. **2005**, 105, 2151.

4 M. Shibasaki, Y. Yamamoto, *Multimetallic Catalysts in Organic Synthesis*; Wiley-VCH: Weinheim, Germany, 2004.

5 E. K. van den Beuken, B. L. Ferringa, *Tetrahedron* **1998**, 54, 12985.

6 B. Gabriele, R. Mancuso, G. Salerno, M. Costa, *Adv. Synth. Catal.* **2006**, 348, 1101.

7 A. Zanardi, R. Corberan, J. A. Mata, E. Peris, *Organometallics* **2008**, 27, 3570.

8 C. P. Casey, J. D. Audett, *Chem. Rev*. **1986**, 86, 339.

9 F. R. Lemke, D. J. Szalda, R. M. Bullock, *J. Am. Chem. Soc*. **1991**, 113, 8466.

10 J. R. Moss, L. G. Scott, *Coord. Chem. Rev*. **1984**, 60, 171.

11 N. D.Jones, B. R. James. *Adv. Synth. Catal.* **2002**, 344, 1126.

12 R. C. Matthews, D. K. Howell, W.-J. Peng, S. G. Train, W. D. Treleaven, G. G. Stanley, *Angew. Chem. Int. Ed. Engl.* **1996**, 35, 2253.

13 M. E. Broussard, B. Juma, S. G. Train, W.-J. Peng, S. A. Laneman, G. G. Stanley, *Science* **1993**, 260, 1784.

14 H. Li, T. J. Marks*, Proc. Natl. Acad. Sci.* USA **2006**, 103, 15295.

15 M. Delferro, T. J. Marks, *Chem. Rev*. **2011**, 111, 2450.

16 E. Solari, S. Antonijevic, S. Gauthier, R. Scopelliti, K. Severin, *Eur. J. Inorg. Chem*. **2007**, 367.

17 T. Weskamp, F. J. Kohl, W. A. Herrmann, *J. Organomet. Chem*. **1999**, 582, 362.

18 K. Severin, *Chem. Eur. J*. **2002**, 8, 1515.

19 Y. Borguet, X. Sauvage, G. Zaragoza, A. Demonceau, L. Delaude, *Organometallics* **2011**, 30, 2730.

20 S. Matsunaga, M. Shibasaki, *M. Bull. Chem. Soc. Jpn*. **2008**, 81, 60.

21 J. M. López-Valbuena, E. C Escudero-Adan, J. Benet-Buchholz, Z. Freixa, P.W.N.M. van Leeuwen, *Dalton Trans*. **2010**, 39,8560.

22 D. C. Powers, T. Ritter, *Acc. Chem. Res*. **2012**, 45, 840.

23 G. Natta, P. Pino, g. Mazzanti, U. Giannini, *J. Am. Chem. Soc*. **1957**, 79, 2975.

24 D. S. Breslow, N. R. Newburg, *J. Am. Chem. Soc*. **1957**, 79, 5072.

25 F. R. Wild, F. W. P. Zolnai, L. Huttner, G. H. H. Brintzinger, *J. Organomet. Chem*. **1982**, 232, 233.

26. J. A. Ewen, R. L. Jones, A. Razavi, J. Ferrara, *J. Am. Chem. Soc.* **1998**, 110, 6255.

27 H. Braunschweig, F. M. Breitling, *Coord. Chem. Rev.* **2006**, 250, 2691.

28 H. Makio, N. Kashiwa, T. Fujita, *Adv. Synth. Catal.* **2002**, 344, 5.

29 H. Makio, H. Terao, A. Iwashita, T. Fujita, *Chem. Rev*. **2011**, 111, 2363.

30 N. Guo, C. L. Stern, T. J. Marks, *J. Am. Chem. Soc.* **2008**, 130, 2246.

31 J. C. Flores, T. E. Ready, J. C. W. Chien, M. D. Rausch, *J. Organomet. Chem.* **1998**, 562, 11.

32 S. K. Kim, H. K. Kim, M. H. Lee, S. W. Yoon, Y. Han, S. Park, J. Lee, Y. Do, *Eur. J. Inorg. Chem*. **2007**, 537.

33 S. Amin, T. J. Marks, *J. Am. Chem. Soc*. **2007**, 129, 2938.

34 S. Amin, T. J. Marks, *J. Am. Chem. Soc*. **2006**, 128, 4506.

35 S. K. Kim, H. K. Kim, M. H. Lee, S. W. Yoon, Y. Han, S. Park, J. Lee, Y. Do, *Eur. J. Inorg. Chem*. **2007**, 537.

36 N. Guo, L. Li, T. J. Marks, *J. Am. Chem. Soc*. **2004,** 126, 6542.

37 R. W. Barnhart, G. C. Bazan, *J. Am. Chem. Soc*. **1998**, 120, 1082.

38 J. Huang, Z. Feng, H. Wang, Y. Qian, J. Sun, Y. Xu, W. Chen, G. Zheng, *J. Mol. Catal. A: Chem*. **2002**, 189, 187.

39 F. M. Bauers, S. Mecking, *Angew. Chem. Int. Ed.* **2001**, 40, 3020.

40 C. M. Wang, S. Friedrich, T. R. Youkin, R. T. Li, R. H. Grubbs, D. A. Bansleben, M. W. Day, *Organometallics* **1998**, 17, 3149.

41 G. J. P. Britovsek, V. C. Gibson, D. F. Wass, *Angew. Chem. Int. Ed.* **1999**, 38, 428.

42 Z. Guan, P. M. Cotts, E. F. McCord, S. J. McLain, *Science* **1999**, 283. 2059.

43 L. K. Johnson, S. Mecking, M. Brookhart, *J. Am. Chem. Soc*. **1996**, 118, 267.

44 D. P. Gates, S. A. Svejda, E. Onate, C. M. Killian, L. K. Johnson, P. S. White, M. Brookhart, *Macromolecules* **2000**, 33, 2320.

45 K. A. Ostoja Starzewski, J. Witte, *Angew. Chem. Int. Ed. Engl.* **1985**, 24, 599.

46 B. L. Small, M. Brookhart, A. M. A. Bennett, *J. Am. Chem. Soc.* **1998**, 120, 4049.

47 G. J. P. Britovsek, V. C. Gibson, B. S. Kimberly, P. J. Maddox, S. Mastroianni, S. J. McTavish, S. Redshaw, G. A. Solan, S. Strömberg, A. J. P. White, D. J. Williams, *J. Am. Chem. Soc*. **1999**, 121, 8728.

48 Z. Guan, W. J. Marshall, *Organometallics* **2002**, 21, 3850.

49 P. van Leeuwen, P. C. J. Kamer, J. N. H. Reek, P. Dierkes*, Chem. Rev*. **2000**, 100, 2741.

50 A. Tomov, J. P. Broyer, R. Spitz, *Macromol. Symp*. **2000**, 150, 53.

51 A. Held, F. M. Bauers, S. Mecking, *Chem. Commun*. **2000**, 301.

52 G. J. Domski, J. M. Rose, G. W. Coates, A. D. Bolig, M. Brookhart, *Prog. Polymer Sci*. **2007**, 32, 30.

53 S. D. Arthur, A. M. A. Bennett, M. S. Brookhart, E. B. Coughlin, J. Feldman, S. D. Ittel, L. K. Johnson, C. M. Killian; K. A. Kreutzer, E. F. McCord, S. J. McLain, A. Parthasarathy, L. Wang, Z.-Y Yang; **1999**, WO Patent 9623010 A2 960801.

54 P. B. MacKenzie, L. S. Moody, C. M. Killian, J. A. Ponasik, J. P. McDevitt, **1998**, WO Patent 9840374.

55 V. C. Gibson, C. Redshaw, G. A. Solan, *Chem. Rev*. **2007**, 107, 1745.

56 B.L. Small, M. Brookhart, *J. Am. Chem. Soc*. **1998**, 120, 7143.

57 A. M. A. Bennet, (Dupont) **1998**, WO Patent 98/27124.

58 F. Bauers, S. Mecking, *Macromolecules* **2001**, 34, 1165.

59 J. Sun, Y. Shan, Y. Xu, Y. Cui, H. Schumann, M. Hummert, *J. Polym. Sci., Part A: Polym. Chem*. **2004**, 42, 6071.

60 Y,-H Shan, J.-Q Sun, Y.-J Xu, Y-G. Cui, F. Lin, *J. Chin, Polym. Sci*. **2005**, 23, 301.

61 H. Makio, T. Fujita, *Acc. Chem. Res*. **2009**, 42, 1532.

62 A. Nakamura, T. Anselment, J. Claverie, B. Goodall, R. Jordan, S. Mecking, B. Rieger, A. Sen, P.W.N.M. van Leeuwen, K. Nozaki, *Acc. Chem. Res*. **2013**, *46*, 1439.

63 M. Arndt-Rosenau, **2006**, US 2006/0004218 A1.

64 A. Koppl, H. G. Alt, *J. Mol. Catal. A: Chem*. **2000**, 154, 45.

65 T. V. Laine, M. Klinga, M. Leskela, *Eur. J. Inorg. Chem*. **1999**, 959.

66 G. Ambrosi, M. Formica, V. Fusi, L. Giorgi, M. Micheloni, *Coord. Chem. Rev*. **2008**, 252, 1121.

67 B. A. Rodriguez, M. Delferro, T. J. Marks, *J. Am. Chem. Soc*. **2009**, 131, 5902.

68 H. Shen, B. R. Goodall, U.S. Pat. **2006**, 2006/0270811.

69 W. Dittrich, R.C. Schulz, *Angew. Makromol. Chemie*. **1971**, 15, 109.

70 X. Mi, Z. Ma, N. Cui, L. Wang, Y. Ke, Y. Hu, *J. Appl. Polym. Sci*. **2003**, 88, 3273.

71 E. Szuromi, H. Shen, B. L. Goodall, R. F. Jordan, *Organometallics* **2008**, 27, 402.

72 D. A. Barnes, G. M. Benedikt, B. L. Goodall, S. S. Huang, H. A. Kalamarides, S. Lenard, L. H. McIntosh II, K. T. Selvy, R. A. Shick, L. F. Rhodes, *Macromolecules* ***2003***, 36, 2623.

73 H.-K. Luo, H. Schumann, *J. Mol. Catal. A: Chem.* **2005**, 227, 153.

74 B. A. Rodriguez, M. Delferro, T. J. Marks, *J. Am. Chem. Soc.* **2009**, 131, 5902.

75 M. H. Klingele, S. Brooker, *Coord. Chem. Rev.* **2003**, 241, 119.

76 U. Beckmann, S. Brooker, *Coord. Chem. Rev.* **2003**, 245, 17.

77 S. Brooker, T. C. Davidson, S. J. Hay, R. J. Kelly, D. K. Kennepohl, P. G. Plieger, B. Moubaraki, K. S. Murray, E. Bill, E. Bothe, *Coord. Chem. Rev.* **2001**, 3, 216.

78 S. Brooker, *Eur. J. Inorg. Chem.* **2002**, 2535.

79 W. Kaim, *Coord. Chem. Rev.* **2002**, 230, 127.

80 S. Trofimenko, *Chem. Rev.* **1993**, 93, 943.

81 E. K. Van Den Beuken, B. L. Feringa, *Tetrahedron* **1998**, 54, 12985.

82 S. Trofimenko, *Progr. Inorg. Chem.* **1986**, 34, 115.

83 G. La Monica, G. A. Ardizzoia, *Progr. Inorg. Chem.* **1997**, 46, 151

84 S. Trofimenko, *Chem. Rev.* **1972**, 72, 497.

85 N. Kitajima, W. B. Tolman, *Prog. Inorg.Chem.* **1995**, 43, 419.

86 M. D. Ward, J. A. McCleverty and J. C. Jeffery, *Coord. Chem. Rev.* **2001**, 222, 251.

87 T. A. Kaden, *Coord. Chem. Rev.* **1999**, 190–192, 371.

88 C. Pettinari and C. Santini, in *Comprehensive Coordination Chemistry II*, ed. J. A. McCleverty and T. J. Meyer, Elsevier, Amsterdam, **2004**, vol. 1, ch. 1.10, pp. 159–210.

89 F. Mani, *Coord. Chem. Rev.* **1992**, 120, 325.

90 A. P. Sadimenko, S. S. Bason, *Coord. Chem. Rev.* **1996**, 147, 247.

91 G. La Monica, G. A. Ardizzoia, *Prog. Inorg. Chem.* **1997**, 46, 151.

92 T. N. Sorrell, D. L. Jameson, *Inorg. Chem.* **1982**, 21, 1014.

93 F. Paap, A. Erdonmez, W.L. Driessen, J. Reedijk, *Acta Crystallogr.* **1986**, C42, 783.

94 A. L. Spek, W. L. Driessen, W. G. R. Wiesmeijer, *Acta Crystallogr.* **1988**, C44, 1567.

95 F. Meyer, S. Beyreuther, K. Heinze, L. Zsolnia, *Chem. Ber./Receuil* **1997**, 130, 605.

96 T. N. Sorrell, V.A. Vankai, M.L. Garrity, *Inorg. Chem.* **1991**, 30, 207.

97 C. M. Hartshorn, P. J. Steel, *J. Chem. Soc. Chem. Commun.* **1997**, 541.

98 T. N. Sorrell, A. S. Borovik, C.-C. Shen, *Inorg. Chem.* **1986**, 25, 589.

99 S. Trofimenko, *J. Am. Chem. Soc.* **1967**, 89,3170.

100 S. Trofimenko, *J. Am. Chem. Soc.* **1969**, 91, 3183.

101 S. Trofimenko, *Accounts Chem. Res.* **1971**, 4, 17.

102 C. Pettinari, R. Pettinari, *Coord. Chem. Rev.* **2005**, 249, 525.

103 C. Pettinari, R. Pettinari, *Coord. Chem. Rev.* **2005**, 249, 663.

104 M. A. Halcrow, *Coord. Chem. Rev.* **2005**, 249, 2880.

105 X. Liu, J. A. McAllister, M. P. de Miranda, E. J. L. McInnes, C. A. Kilner, M. A. Halcrow, *Chem.–Eur. J.* **2004**, 10, 1827.

106 G. B. Deacon, A. Gitlits, B. W. Skelton and A. H. White, *Chem. Commun.* **1999**, 1213.

107 E. Sebe, I. A. Guzei, M. J. Heeg, L. M. Liable-Sands, A. L. Rheingold, C. H. Winter, *Eur. J. Inorg. Chem.* **2005**, 3955.

108 J. C. Roder, F. Meyer and H. Pritzkow, *Z. Naturforsch., B: Chem. Sci.* **2002**, 57, 773.

109 G. A. Ardizzoia, S. Cenini, G. La Monica, N. Masciocchi, A. Maspero, M. Moret, *Inorg. Chem.* **1998**, 37, 4284.

110 C. Mealli, C. S. Arcus, J. L. Wilkinson, T. J. Marks, J. A. Ibers, *J. Am. Chem. Soc.* **1976**, 98, 711.

111 G. B. Deacon, E. E. Delbridge, C. M. Forsyth, *Angew. Chem. Int. Ed.* **1999**, 38, 1766.

112 F. Breher. H. Rüegger, *Angew. Chem., Int. Ed.* **2005**, 44, 473.

113 G. B. Deacon, E. E. Delbridge, C. M. Forsyth, B. W. Skelton, A. H. White, *J. Chem. Soc., Dalton Trans.* **2000**, 745.

114 W. Burger, J. Strähle, *Z. Anorg. Allg. Chem.* **1985**, 529, 111.

115 K. R. Gust, J. E. Knox, M. J. Heeg, H. B. Schlegel, C. H. Winter, *Angew. Chem., Int. Ed.* **2002**, 41, 1591.

116 X. Liu, J. A. McAllister, M. P. de Miranda, E. J. L. McInnes, C. A. Kilner, M. A. Halcrow, *Chem.–Eur. J.* **2004**, 10, 1827.

117 S. L. Renard, I. Sylvestre, S. A. Barrett, C. A. Kilner, M. A. Halcrow, *Inorg. Chem.* **2006**, 45, 8711.

118 G. B. Deacon, E. E. Delbridge, C. M. Forsyth, B. W. Skelton,A. H. White, *J. Chem. Soc., Dalton Trans.* **2000**, 745.

119 G. B. Deacon, C. M. Forsyth, A. Gitlits, R. Harika, P. C. Junk, B. W.Skelton and A. H. White, *Angew. Chem., Int. Ed.* **2002**, 41, 3249.

120 M. A. Halcrow, *Dalton Trans.* **2009**, 2059.

121 F. Meyer, *Eur. J. Inorg. Chem.* **2006**, 3789

122 A. L. Gavrilova, B. Bosnich, *Chem. Rev.* **2004**, 104, 349.

123 R. Mukherjee, *Coord. Chem. Rev.* **2000**, 203, 151.

124 J. Klingele, S. Dechert, F. Meyer, *Coord. Chem. Rev.* **2009**, 253, 2698.

125 R. Fusco*, Chem. Heterocycl. Compd.* 1967, 22, 3.

126 G. Coispeau, J. Elguero, *Bull. Soc. Chim. Fr.* **1970**, 2717.

127 Y. Lin, S. A. Lang, Jnr. *J. Heterocycl. Chem.* **1977**, 14, 345.

128 M. Konrad, S. Wuthe, F. Meyer, E. Kaifer, *Eur. J. Inorg. Chem.* **2001**, 9, 2233.

129 C. Dubs, A. Inagaki, M. Akita, *Chem. Commun.* **2004**, 2760.

130 J. C. Röder, F. Meyer, R. F. Winter, E. Kaifer, *J. Organomet. Chem.* **2002**, 641, 113.

131 W. L. Driessen, R .A. G. D. Graaff, J. Ochocki, J. Reedijk, *Inorg. Chim. Acta* **1988**, 41, 150.

132 M. R. Malachowski, H. B. Huynh, L. J. Tomlinson, R. S. Kelly, J. W. Furbee, Jnr., *J. Chem. Soc. Dalton Trans.* **1995**, 31.

133 G. J. van Driel, W. L. Driessen, J. Reedijk, *Inorg. Chem.* **1985**, 24, 2919.

134 T. N. Sorrell, D. L. Jameson, *Inorg. Chem.* **1982**, 21, 1014.

135 S. Tanaka, C. Dubs, A. Inagaki, M. Akita, *Organometallics* **2004**, 23, 317.

136 C. Dubs, T. Yamamoto, A. Inakai, M. Akita, *Organometallics* **2006**, 25, 1344.

137 S. Tanaka, C. Dubs, A. Inagaki, M. Akita, *Organometallic*s **2005**, 24, 163.

138 S. A. Reindle, A. Poethig, M. Drees, B. Bechlars, E. Herdtweck, W. A. Herrmann, F. E. Kuehn, *Organometallics* **2013**, 32, 4082.

139 Y. Zhou, Z. Xi, W. Chen, D. Wang, *Organometallics* **2008**, 27, 5911.

140 Y. Zhou, W. Chen, *Organometallics* **2007**, 26, 2742.

141 J.C. Röder, F. Meyer, E. Kaifer, *Angew. Chem. Int. Ed.* **2002**, 41, 2304.

142 K. Shindo, Y. Mori, K. Motoda, H. Sakiyama, N. Matsumoto, H. Okawa, *Inorg. Chem.* **1992**, 31, 4987.

143 T. G. Schenk, J. M. Downs, C. R. C. Milne, P. B. Mackenzie, H. Boucher, J. Whelan, B. Bosnich, *Inorg. Chem.* **1985**, 24, 2334.

144 C. Dubs, T. Yamamoto, A. Inagaki, M. Akita, *Organometallics* **2006**, 25, 1359.

145 J. C. Röder, F. Meyer, H. Pritzkow, *Organometallics* **2001**, 20, 811.

146 F. Meyer, E. Kaifer, P. Kircher, K. Heinze, H. Pritzkow, *Chem. Eur. J.* **1999**, 5, 1617.

147 J. Ackermann, F. Meyer, E. Kaifer, H. Pritzkow*, Chem. Eur. J.* **2002**, 8, 247.

148 Y. Zhou, W. Chen, *Organometallics* **2007**, 26, 2742.

149 Y. Zhou, X. Zhang, W. Chen, H. Qiu, *J. Organomet. Chem.* **2008**, 693, 205

150 U. J. Scheele, M. Georgiou, M. John, S. Dechert, F. Meyer, *Organometallics* **2008**, 27, 5146.

151 G. Noël, J. C. Röder, S. Dechert, H. Pritzkow, L. Bolk, S. Mecking, F. Meyer, *Adv. Synth. Catal.* **2006**, 348, 887.

152 M.-C Moret, P. Chen, *Organometallics* **2008**, 27, 4903.

153 A. Sachse, V. Daebel, A. Lange, S. Demeshko, S. Dechert, F. Meyer, *Dalton Trans.* **2010**, 39, 3903.

154 A. Sachse, M. John, F. Meyer, *Angew. Chem. Int. Ed.* **2010**, 49, 1986.

155 J. C. Röder, F. Meyer, E. Kaifer, H. Pritzkow, *Eur. J. Inorg. Chem.* **2004**, 1646.

156 J. C. Röder, F. Meyer, H. Pritzkow, *Chem. Commun.* **2001**, 2176.

157 A. Sachse, G. Noël, S. Dechert, S. Demeshko, A. Honecker, A. Alfonsov, V. Kataev, F. Meyer, *Eur. J. Inorg. Chem.* **2008**, 5390.

158 A. Sachse, S. Demeshko, F. Meyer, *Dalton Trans.* **2009**, 37, 7756.

159 O. Dechy-Cabaret, B. Martin-Vaca, D. Bourissou, *Chem. Rev.* **2004**, 104, 6147.

160 O. Wolf, M. Crank, M. Patel, F. Marscheider-Weidemann, J. Schleich, B.Hüsing, G. Angerer, *Techno-economic Feasibility of Large scale Production of Bio-based Polymers in Europe*, Tech. rep. EUR 22103 EN, European Commission, **2005**.

161 S. Jacobsen, P. Degée, H. Fritz, P. Dubois, R. Jérôme, *Polym. Eng. Sci.* **1999**, 39, 1311.

162 A.-C. Albertsson, I. K. Varma, *Adv. Polym. Sci.* **2002**, 12, 1841.

163 A. -C. Albertsson, I. K. Varma, *Biomicromolecules* **2003**, 4, 1466.

164 M. Vert in *Biopolymers*, Vol. 4 (Eds.: A. Steinbüchel, Y. Doi), Wiley-VCH, Weinheim, **2002**. Pg. 179.

165 C. R. Hankermeyer, R. S. Tjeerdema, *Rev. Environ Contam Toxicol.* **1999**, 159, 1.

166 Y. Tokiwa, B. P. Calabia, *Biotechnol Lett.* **2004**, 26, 15, 1181.

167 R. W. Lenz, R. H. Marchessault, *Biomacromolecules*, **2005**, 6, 1.

168 X. Pang, X. Zhuang, Z. Tang, X. Chen, *Biotechnol J.* **2010**, 5, 1125.

169 R. Auras, B. Harte, S. Selke, *Macromol. Biosci.* **2004**, 4, 835.

170 R. H. Platel, L. M. Hodgson, C. K. Williams, *Polym. Rev.* **2008**, 48, 11.

171 K. Fukushima, Y. Kimura, *Polym. Int.* **2006**, 55, 626.

172 S. K. Ritter, *Chem. Eng. News* **2002**, 80, 19.

173 O. Dechy-Cabaret, B. Martin-Vaca, D. Bourissou, *Chem. Rev.* **2004**, 104, 6147.

174 W. Dittrich, R.C. Schulz, *Angew. Makromol. Chemie.* **1971**, 15, 109.

175 C. M. Thomas, *Chem. Soc. Rev.* **2010**, 39, 165.

176 H. R. Kricheldorf, M. Berl, N. Scharnagl, *Macromolecules* **1988**, 21. 286.

177 P. Dubois, R. Jérôme, P. Teyssié, *Makromol. Chem., Macromol. Symp.* **1991**, 42/43, 103.

178 M. H. Chisholm, M. J. Patmore, Z. Zhou, *Chem. Commun.* **2005**, 127.

179 N. E. Kamber, W. Jeong, R. M. Waymouth, R. C. Pratt, B. G. G. Lohmeijer, J. L. Hedrick, *Chem. Rev.* **2007**, 107, 5813.

180 C. K. Williams, *Chem. Soc. Rev.* **2007**, 36, 1573.

181 C. A. Wheaton, P. G. Hayes, B. J. Ireland, *Dalton Trans.* **2009**, 4832.

182 A. P. Dove, *Chem. Comm.* **2008**, 6446.

183 H. Chen, H. Tang, C. Lin, *Polymer* **2007**, 48, 2257.

184 D. J. Darensburg, W. Choi, C. P. Richers, *Macromolecules* **2007**, 40, 3521.

185 M. H. Chisholm, J. C. Gallucci, G. Yaman, *Inorg. Chem.* **2007**, 46, 8676.

186 H.-Y. Chen, J.-H, Huang, C.-C. Lin, *Macromolecules* **2007**, 40, 8855.

187 M.-L. Shueh, Y.-S. Wang, B.-H. Huang, C.-Y. Kuo, C.-C. Lin, *Macromolecules* **2004**, 37, 5155.

188 P. A. Cameron, D. Jhurry, V. C. Gibson, J. P. W. Andrew, D. J. Williams, S. Williams. *Macromol. Rapid Commun.* **1999**, 20, 616.

189 D. Pospiech, H. Komber, D. Jehnichen, L. Häussler, K. Eckstein, H. Scheibner, A. Janke, H. R. Kricheldorf, O. Petermann*, Biomacromolecules* **2005**, 6, 439.

190 M. H. Chisholm, J. C. Gallucci, C. Krempner, *Polyhedron* **2007**, 26, 4436.

191 B. J. O'Keefe, M. A. Hillmyer, W. B. Tolman, *J. Chem. Soc., Dalton Trans.* **2001**, 2215.

192 M. Okada, *Prog. Polym. Sci.* **2002**, 27, 87.

193 C. A. Wheaton, P. G. Hayes, B. J. Ireland, *Dalton Trans.* **2009**, 4832.

194 C. M. Thomas, *Chem. Soc. Rev.* **2010**, 39, 165.

195 M. Cheng, A. B. Attygalle, E. B. Lobkovsky, G. W. Coates, *J. Am.Chem. Soc.* **1999**, 121, 11583.

196 M. H. Chisholm, S. S. Iyer, M. E. Matison, D. G. McCollum, M. Pagel, *Chem. Commun.* **1997**, 1999.

197 M. H. Chisholm, N. W. Eilerts, J. C. Huffman, S. S. Iyer, M. Pacold, K. Phomphrai, *J. Am. Chem. Soc.* **2000**, 122, 11845.

198 M. H. Chisholm, J. C. Gallucci, K. Phomphrai, *Inorg. Chem.* **2002**, 41, 2785.

199 M. H. Chisholm, J. C. Gallucci, H. Zhen, J. C. Huffman, *Inorg. Chem.* **2001**, 40, 5051.

200 L. E. Breyfogle, C. K. Williams, V. G. Young-Jr., M. A. Hillmyer, W. B. Tolman, *Dalton Trans.* **2006**, 928.

201 M. S. Hill, P. B. Hitchcock, *J. Chem. Soc.*, *Dalton Trans.* **2002**, 4694.

202 T. R. Jensen, L. E. Breyfogle, M. A. Hillmyer, W. B. Tolman, *Chem. Commun.* **2004**, 2504.

203 A. J. Arduengo, H. V. Rasika, D. F. Davidson, R. L. Harlow, *J. Organomet. Chem.* **1993**, 462, 13.

204 M. D. Hannant, M. Schormann, M. Bochmann, *J. Chem. Soc., Dalton Trans.* **2002**, 4071.

205 B. M. Chamberlain, M. Cheng, D. R. Moore, T. M. Ovitt, E. B. Lobkovsky, G. W. Coates, *J. Am. Chem. Soc.* **2001**, 123, 3229.

206 A. P. Dove, V. C. Gibson, E. L. Marshall, A. J. P. White, D. J. Williams, *J. Chem. Soc., Dalton Trans.* **2004**, 570.

207 M. H. Chisholm, J. C. Gallucci, K. Phomphrai, *Inorg. Chem.* **2005**, 44, 8004.

208 C. K. Williams, L. E. Breyfogle, S. K. Choi, W. Nam, V. G. Young Jr., M. A Hillmyer, W. B. Tolman, *J. Am. Chem. Soc.* **2003**, 125, 11350.

209 J. Ejfler, S. Szafert, K. Mierzwicki, L. B. Jerzykiewicz, P. Sobota, *Dalton Trans.* **2008**, 6556.

210 C.-Y Sung, C,-Y Li, J,-K Su, T,-Y Chen, C,-H Lin, B,-T Ko, *Dalton Trans.* **2012**, 41, 953.

211 C. Zhang, Z.-X. Wang, *J. Organomet. Chem.* **2008**, 693, 3151.

212 Z. Zheng, G. Zhao, R. Fablet, M. Bouyayhi, C. M. Thomas, T. Roisnel, O. Casagrande, Jr. and J.-F, Carpentier, *New J. Chem.* **2008**, 32, 2279.

213 T. R. Jensen, L. e. Breyfogle, M. A. Hillmyer, W. B. Tolman, *Chem. Commun.* **2004**, 2504.

214 J. H. Jeong, Y. H. An, Y. K. Kang, Q. T. Nguyen, H. Lee, B. M. Novak, *Polyhedron* **2008**, 27, 319.

215 X,-Y Yu, C. Zhang, Z,-X Wang, *Organometallics* **2013**, 32, 3262.

216 A. Otero, J. Fernández-Baeza, L. F. Sánchez-Barba, J. Tejeda , M. Honrado, A. Garcés, A. Lara-Sánchez, A. M. Rodríguez, *Organometallics* **2012**, 31, 4191.

217 B. Lian, C. M. Thomas, O. L. Casagrande, Jr., C. W. Lehmann, T. Roisnel, J,-F. Carpentier, *Inorg. Chem.* **2007**, 46, 328.

218 T. G. Schenck, J. M. Downes, C. R. C. Milne, J. F. Sawyer, B. Bosnich, L. Miller, *Inorg. Chem.* **1985**, 24, 2338.

219 V. J. Arán, M. Kumar, J. Molina, L. Lamarque, P. Navaro, E. Garcia-España, J. A. Ramirez, S. V. Luis, B. Escuder, *J. Org. Chem.* **1999**, 64, 6135.

220 J. C. Röder, F. Meyer, M. Konrad, S. Sandhöfner, E. Kaifer, H. Pritzkow, *Eur. J. Org. Chem.* **2001**, 4479.

221 A. Sachse, Dissertation, Georg-August University, Göttingen **2009**.

222 A. J. Pöe, M. S. Vaidya*, J. Chem. Soc.* **1961**, 1023.

223 F. R. Hartley, *Nature Physical Science*, **1972**, 236, 75.

224 T. Hosokawa, C. Calvo, H. B. Lee, P. M. Maitlis, *J. Am. Chem. Soc.* **1973**, 95, 4914.

225 D. M. Roe, C. Calvo, N. Krishnarnachari, P. M. Maitlis, *J. Chem. Soc. Dalton Trans*. **1975**, 125.

226 M. M. Olmstead, H. Hope, L. S. Benner, A. L. Balch, *J. Am. Chem. Soc. Commun.* **1977**, 99, 5502.

227 R. G. Holloway, B. R. Penfold, R. Colton, M. J. McCormick, *J. Chem. Soc. Chem. Commun*. **1976**, 21, 1.

228 A. L. Balch, J. R. Boemn, H. Hope, M. M. Olmstead, *J. Am. Chem. Soc.* **1976**, 98, 7431.

229 C. P. Casey, J. D. Audett, *Chem. Rev.* **1986**, 86, 339.

230 W. A. Hermann, *Adv. Organomet. Chem*. **1982**, 20, 159.

231 R. J. Puddephatt, *Polyhedron* **1998**, 7, 767.

232 J. D. Egbert, A. Chartoire, A. M. Z. Slawin, S. P. Nolan *Organometallics* **2011**, 30, 4494.

233 M. L. Scheuermann, D. W. Boyce, K. A. Grice, W. Kaminsky, S. Stoll, W. B. Tolman, O. Swang, K. I. Goldberg, *Angew. Chem. Int. Ed.* **2014**, 53, 6492.

234 P. Zalleno, S. Tambarini, P. A. Vigato, *Coord. Chem. Rev*. **1987**, 77, 165.

235 C. Fraser, B. Bosnich, *Inorg. Chem*. **1994**, 33, 338.

236 J,-P Costes, A. Dupois, J,-P Laurent, *J. Chem. Soc., Dalton Trans*. **1998**, 735.

237 C. Popeney, Z. Guan, *Organometallics* **2005**, 24, 1145.

238 A. Bastero, A. Ruiz, C. Claver, B. Miliani, E. Zangrando, *Organometallics* **2002**, 21, 8520.

239 R. E. Rülke, J. M. Ernsting, A. L. Spek, C. J. Elsevier, P. W. N. M. van Leeuwen, K. Vrieze, *Eur. J. Inorg. Chem*. **1993**, 32,5769.

240 T. Pechmann, C. D. Brandt, H. Werner, *Chem. Eur. J*. **2004**, 10, 728.

241 A. Sataka, H. Koshino, T. Nakata, *J. Organomet. Chem.* **2000**, 595, 208.

242 K. W. Muir, J. A. Ibers, *Inorg. Chem.* **1965**, 4, 778.

243 N. A. Bailey, J. M. Jenkins, R. Mason, B. L. Shaw, *J. Chem. Soc. Chem. Commun.* **1965**, 237.

244 (a) M. Brookhart, M. L. H. Green, *J. Organomet. Chem.* **1983**, 250, 395.

245 R. H. Crabtree, *Angew. Chem. Chem. Int. Ed.* **1993**, 32, 789.

246 A. Martın, *J. Chem. Ed.* **1999**, 76, 578.

247 A. Albinati, P. S. Pregosin, F. Wombacher, *Inorg. Chem.* **1990**, 29, 1812.

248 C. M. Wehman-OoYevaar, D. M. Grove, H. Kooijman, P.van der Sluis, A. L. Spek, G. Van Koten, *J. Am. Chem. Soc.* **1992**, 114, 9916.

249 T. Kawamoto, I. Nagasawa, H. Kuma, Y. Kushi, *Inorg. Chem.* **1996**, 35, 2427.

250 T. W. Hambley*, Inorg. Chem.* **1998**, 37, 3767.

251 E. F. Connor, T. R. Younkin, J. I. Henderson, A. W. Waltman, R. H. Grubbs, *Chem. Commun.* **2003**, 2272.

252 M. S. W. Chan, L. Deng, T. Ziegler, *Organometallics* **2000**, 19, 2741.

253 J. S. Wang, K. Matyjaszewski, *J. Am. Chem. Soc.* **1995**, 117, 6514.

254 H. Uegaki, Y. Kotani, M. Kamigaito, M. Sawamoto, *Macromolecules* **1998**, 31, 6756.

255 C. Granel, Ph. Dubois, R. Jéróme, Ph. Teyssié, *Macromolecules* **1996**, 29, 8576.

256 K. Matyjaszewski, *Macromol. Symp.* **1998**, 134, 1 05-118.

257 D. A. Singleton, D. T. Nowlan III; N. Jahed, K. Matyjaszewski, *Macromolecules* **2003**, 36, 8609.

258 M. C. Volger, K. Vrieze, *J. Organomet. Chem.* **1966**, 6, 297.

259 S. Hansson, P.-O. Norrby, M. Sjögren,B. Åkermark, M. E. Cucciolito, F. Giordano, A. Vitagliano, *Organometallics* **1993**, 12, 4940.

260 A. Gogoll, J. Örnebro, H. Grennberg, J.-E. Bäckvall, *J. Am. Chem. Soc.* **1994**, 116, 3631-3632.

261 J. W. Faller, H. L. Stokes-Huby, M. A. Albrizzio, *Helv. Chim. Act.* **2001**, 84, 3031.

262 J. M. Canal, M. Gómez, F. Jiménez, M. Rocamora, G. Muller, E. Duñach, D. Franco, A. Jiménez, F. H. Cano*, Organometallics* **2000**, 19, 966.

263 A. Guerrero, F. A. Jalon, B. R. Manzano, A. Rodriguez, R. M. Claramunt, P. Cornago, V. Milata, J. Elguero*, Eur. J. Inorg. Chem***. 2004**, 549-556.

264 A. Bastero, A. F. Bella, F. Fernández, S. Jansat, C. Claver, M. Gómez, G. Muller, A. Ruiz, M.

Font-Bardía, X. Solans, *Eur. J. Inorg. Chem.* **2007**, 132.

265 N. B. O'Bryan, T. O. Maier, I. C. Paul, R. S. Drago, *J. Amer. Chem. Soc.* **1973**, 95, 6640.

266 P. Zannello, S Tambarini, P. A. Vigato, *Coord. Chem. Rev*. **1987**, 77, 165.

267 J,-P, Costes, A. Dupois, J,-P Laurent*, J. Chem. Soc. Dalton Trans*. **1998**, 735.

268 C. Dubs, T. Yamamoto, A. Inagaki, M. Akita, *Organometallics* **2006**, 25, 1359.

269 J. H. H. Ho, S. W. W. Choy, S. A. Macgregor, B. A. Messerle, *Organometallics* **2011**, 30, 5978.

270 X. Yu, Y. Yamamoto, N. Miyaura. *Synlett*. **2009**, 994.

271 K. Yoshida, M. Ogasawara, T. Hayashi, *J. Org. Chem*, **2003**, 68, 1901.

272 M. Kondo, T. Kochi, F. Kakiuchi, *J Am Chem Soc.* **2011**, 12;133,32.

273 C. I. Simionescu, V. Percec, *J. Polym.Sci*. **1980**, 18, 147.

274 (a). G. B. Deacon, R. J. Phillips, *Coord. Chem. Rev*. **1980**, 33, 227. (b) V. Zelenák, Z. Vargová,K.Györyová *Spectrochim. Acta A.* **2007**, 66, 262.

275 J. Lewinski, M. Kościelski, K. Suwała, I. Justyniak, *Angew. Chem. Int. Ed.* **2009**, *48*, 7017.

276 A. Otero, J. Fernández-Baeza, L. F. Sánchez-Barba, J. Tejeda, M. Honrado, A. Garcés, A. Lara-Sánchez, and M. Rodríguez, *Organometallics* **2012**, 31, 4191.

277 D. Brizzolara, H. J.Cantow, K. Diederichs, E. Keller, A. J. Dombk, *Macromolecules* **1996**, 29, 191.

278 W. H. Carothers, G. L. Dorough, F. J. van Natta, *J. Am. Chem. Soc*. **1932**, 54, 761.

279 K. A. M. Thakur, R. T. Kean, M. T. Zell, B. E. Padden, E. J. Munson, *Chem. Commun*. **1998**, 1913.

280 F. Douin, P. O. Oguadinma, T, J. J. Whitehorne, R. E. Prud'homme, F. Schaper, *Organometallics* **2010**, 29, 2139.

281 J. Baran, A. Duda, A. Kowalski, R. Szymanski, S. Penczek, *Macromol. Rapid Commun*. **1997**, 18, 325.

282 O. V. Sizova, L. V. Skripnikov, A. Y. Sokolov, O. O. Lyubimova, *J. Struct. Chem*. **2007**, 48, 28.

283 K. A. Kreisel, G. P. A. Yap, O. Dmitrenko, C. R. Landis, K. H. Theopold, *J. Am. Chem. Soc.* **2007**, 129. 14162.

284 F. A. Cotton, R. A. Walton, Multiple Bonds between Metal Atoms, Eds., Oxford University Press, Oxford, **1993**.

285 K. Das, K. M. Kadish, J. L. Bear, *Inorg. Chem*. **1978**, 17,930.

286 M. P. Doyle, *Chem Rev*. **1986**, 86, 919.

287 M. P. Doyle D. C Forbes, *Chem Rev*. **1998**, 98, 911.

288 H. M. L. Davies, R. E. J. Beckwith, *Chem Rev*. **2003**, 103, 2861.

289 J. Hansen, H. M. L. Davies, *Coord Chem Rev.* **2008**, 252, 545.

290 U. Siemeling, P. Jutzi, *J. Organomet. Chem*. **1995**, 500, 175.

291 K.-S. Son, R. M. Waymouth, *J. Polym. Sci. Part A: Polymer Chemistry* **2010**, 48, 1579.

292 K.-S. Son, F. Joge, R. M. Waymouth, *Macromolecules* **2008**, 41, 9663.

293 M. S. Blais, J. C. W. Chien, M. D. Rausch, *Organometallics* **1998**,17, 3775.

294 R. A. J. Postema *PCT Int. Appl.* **1997**, WO 9742231 A1 19971113.

295 V. J. Chebny, R. Rathore, *J. Am. Chem. Soc.* **2007**, 129, 8458.

296 A. J. Arduengo, *Acc. Chem. Res.* **1999**, 32, 913.

297 Arduengo, A. J., Harlow, R. L., Kline, M. *J. Am. Chem. Soc.* **1991**, 113, 361.

298 R. E. Douthwaite, M. L. H. Green, P. J. Silcock, P. J. Gomes, *J. Chem. Soc., Dalton Trans*. **2002**, 1386.

299 F. Glorious, Ed. *N-Heterocyclic Carbenes in Transition Metal Catalysis*; Topics in Organometallic Chemistry, Vol. 21, Springer-Verlag, Berlin/Heidelberg, **2007**.

300 P. L. Arnold, M. Rodden, K. M. Davis, A. C. Scarisbrick, A. J. Blake, C. Wilson, *Chem. Commun.* **2004**, 1612.

301 P. L. Arnold, M. Rodden, C. Wilson, *Chem. Commun.* **2005**, 1743.

302 A. J. Arduengo, F. Davidson, R. Krafczy, W. J. Marshall, M. Tamm, *Organometallics* **1998**, 17, 3375.

303 R. J. Baker, M. L. Cole, C. Jones, M. F. Mahon, *Chem. Soc.- Dalton Trans.* **2002**, 1992.

304 A. J. Arduengo, H. V. R. Dias, J. C. Calabrese, F. Davidson, *Inorg. Chem.* **1993**, 32, 1541.

305 C. Yao, C. Wu, B. Wang, D. Cui, *Organometallics* **2013**, 32, 2204.

306 C. Zhang, F. Luo, B. Cheng, B. Li, H. Song, S. Xu, B. Wang, *Dalton Trans.* **2009**, 35, 7230.

307 B. Wang, D. Cui, K. Lv, *Macromolecules* **2008**, 41, 1983.

308 B. Wang, D. Wang, D. Cui, W. Gao, T. Tang, X. Chen, X. Jing, *Organometallics* **2007**, 26, 3167.

309 S. Mihan, I. Nifant'ev, *PCT Int. Appl.* **2004**, WO 2004020479 A2 20040311.

310 S. P. Downing, A. A. Danopoulos, *Organometallics* **2006**, 25, 1337.

311 S. P. Downing, P. J. Pogorzelec, A. A. Danopoulos, D. J. Cole-Hamilton, *Eur. J. Inorg. Chem*. **2009**, 1816.

312 G. Aullo´n, L. Brammer, E. A. Bruton, A. G. Orpen *Chem.Commun*. **1998**, 653.

313 A. Bondi, *J. Phys. Chem.* **1964**, 68, 441.

314 C. B. Aakeröy, T. A. Evans, K. R. Seddon, I. Pálinkó, *New J. Chem.* **1999**, 23, 145.

315 T. Steiner, *Acta Cryst.* **1998**, B54, 546.

316 L. S. Boffa, B. M. Novak, *Chem. Rev.* **2000**, 100, 1479.

317 L. K. Johnson, S. Mecking, M. Brookhart, *J. Am. Chem. Soc.* **1996**, 118, 267.

318 S. Mecking, L. K. Johnson, L. Wang, M. Brookhart, *J. Am. Chem. Soc.* **1998**, 120, 888.

319 T. R. Younkin, E. F. Conner, J. I. Henderson, S. K. Friedrich, R. H. Grubbs, D. A. Bansleben, *Science* **2000**, 287, 460.

320 V. C. Gibson, A. Tomov, *Chem. Commun.* **2001**, 1964.

321 H. Li, C. L. Stern, T. J. Marks, *Macromolecules* **2005**, 38, 9015.

322 M. R. Salata, T. J. Marks, *Macromolecules* **2009**, 42, 1920.

323 L. McElwee-White, D. A. Dougherty, *J. Am. Chem. Soc.* **1984**, 106, 3466.

324 O. Meth-Cohn, E. Vourin, T. A. Modro, *J. Org. Chem.* **1989**, 54, 4822.

325 G. Giordano, R. H. Crabtree, *Inorg. Synth.* **1979**, 19, 218.

326 Y. Tatsuno, T. Yoshida, S. Otsuka, *Inorg. Synth.* **1988**, 28, 342.

327 S. Imaizumi, T. Matsuhisha, Y Senda, *J. Organomet. Chem.* **1985**, 280, 441.

328 M. Strohalm, D. Kavan, P. Novák , M. Volný, V. Havlíče: mMass 3: A Cross-Platform Software Environment for Precise Analysis of Mass Spectrometric Data. *Anal Chem.* **2010**, 82, 4648.

329 M. Strohalm, M. Hassman, B. Košata, M. Kodíček: mMass Data Miner: an Open Source Alternative for Mass Spectrometric Data Analysis. *Rapid Commun Mass Spec.* **2008**, 22, 905.

330 STOE & CIE GmbH, X-AREA, Darmstadt, **2002**.

331 STOE & CIE GmbH, X-RED, Darmstadt, **2002**.

332 G. M. Sheldrick, SHELXL-97 Program for Crystal Structure Refinement, University of Göttingen, **1997**.

333 G. M. Sheldrick, SHELXL-97 Program for Crystal Structure Solution, University of Göttingen, **1997**.

Posters and Presentations

Workshop at Heimvolkshochschule Maria spring – Poster presentation
29th June 2010

NiKaS 2010 – Poster presentation

21st and 22nd October 2010

Workshop at Haus Hessenkopf, Goslar – Poster presentation
24th-25th June 2011

Workshop at Haus Höhenblick, Braunfels – Poster presentation
27th - 29th June 2012
jointly held with Landesforschungsschwerpunkt NanoKat, TU Kaiserslautern

NiKaS 2012 - Poster presentation

18th and 19 th October 2012

Workshop LIKAT Rostock – Poster presentation
16th - 18th September 2013

Heidelberg forum for Molecular catalysis (HFMC 2013) – Poster presentation

28th June 2013

20th EuCheMS Conference on Organometallic Chemistry–Poster presentation

30 June 2013 - 04 July 2013

University of St. Andrews, Scotland.

Acknowledgements

My sincere appreciation and profound gratitude to my supervisor Prof. Dr. Franc Meyer for the wonderful opportunity he granted me to work with his group under his supervision and providing an enabling working environment during my Ph.D. study.

I also express my sincere gratitude and appreciation to the members of the thesis committee, Prof. Dr. P. Vana (IPC) and Prof. Dr. D. Stalke (IAC).

- CaSuS for Funding, without which is would have been impossible to pursue the Ph.D. research.
- Dr. Sebastian Dechert, for collecting and solving most X-ray structure data related to this work (not forgetting Nicole and Anne).

CaSuS cooperation partners:

- Sebastian Primpke (IPC), for collaborative work and help with GPC measurements and analysis.
- Dr. Christian Maass, for collaborative work and efforts in handling and collecting X-ray data and solving particularly difficult structures.
- Torben Böhnisch: For help and insightful suggestions into challenging problems as well as proof reading.

Administrative and supporting staff:

- Dr. Hanna Steininger (CaSuS coordinator), for the wonderful job in coordinating all CaSuS related activities.
- Frau Petra Unger
- Jorge Teichgräber, Andreas Schwarz
- Staff at the NMR and Analytical departments in the Inorganic institute.

Colleagues at A. K. Meyer for the enabling and fun filled working environment, most especially Jann Meyer, Felix Krätzschmar and Mike Schütze who worked on various aspects of this project

To my family and most especially Maria……I say Thank You